The epidermal growth factor receptor is a relevant host factor in the early stages of the Zika virus life cycle *in vitro*

Dissertation

To obtain the academic degree
Doctor in Science, Doctor philosophiae naturalis (Dr. phil. nat.)

Submitted to the
Department of Biochemistry, Chemistry and Pharmacy
Johann Wolfgang Goethe University
Frankfurt am Main – Germany

Presented by
Catarina Prazeres Sabino
Born in Lisbon, Portugal

Frankfurt am Main (2022)
(D30)

vom Fachbereich Biochemie, Chemie, Pharmazie (14) der
Johann Wolfgang Goethe-Universität als Dissertation angenommen.

Dekan: Prof. Dr. Clemens Glaubitz

Gutachter: Prof. Dr. Robert Tampé
Prof. Dr. Eberhard Hildt

Datum der Disputation:

Table of contents

Index of Figures

Index of Tables

Abbreviations

%	percent
°C	degree Celsius
µg	microgram
µL	microliter
µm	micrometer
µM	micromolar
3’	three prime
5’	five prime
aa	amino acid
A_{230}	absorbance at 230 nanometers
A_{260}	absorbance at 260 nanometers
A_{280}	absorbance at 280 nanometers
A-loop	activation loop
AAV6	adeno-associated virus serotype 6
ADE	antibody-dependent enhancement
AP2	adaptor protein complex 2
APS	ammonium persulfate
Arbovirus	arthropod-borne virus
ATP	adenosine triphosphate
BCA	bicinchoninic acid
BSA	bovine serum albumin
BSL-3	biosafety level 3

C	capsid
Ca^{2+}	calcium ion
$CaCl_2$	calcium chloride
cDNA	complementary DNA
CH_3CO_2K	potassium acetate
CHO	Chinese hamster ovary
cHP	capsid region hairpin
CIE	clathrin-independent endocytosis
CLSM	confocal laser scanning microscopy
CME	clathrin-mediated endocytosis
CRISPR	clustered regularly interspaced short palindromic repeats
CO_2	carbon dioxide
CS	cyclization sequence
CZS	congenital ZIKV syndrome
DI	domain I
DII	domain II
DII	domain III
DABCO	triethylenediamine
DAG	1,2-diacylglycerol
DAPI	4′,6-diamidino-2-phenylindole
DAR	downstream AUG region
DB-1	dumbbell 1
DB-2	dumbbell 2

DC-SIGN	dendritic cell-specific intracellular adhesion molecule-3-grabbing non-integrin
DE	Germany
DENV	dengue virus
DEPC	diethyl pyrocarbonate
DMEM	Dulbecco's Modified Eagle's Medium
DMSO	dimethyl sulfoxide
DNA	deoxyribonucleic acid
DNase	deoxyribonuclease
dNTP	deoxynucleoside triphosphate
dpi	days post-infection
dsRNA	double-stranded RNA
DTT	dithiothreitol
E	envelope
E. coli	*Escherichia coli*
EBV	Epstein-Barr virus
ECL	enhanced luminol-based chemiluminescence
EDTA	ethylenediaminetetraacetic acid
EEA1	early endosome antigen 1
EGF	epidermal growth factor
EGFR	epidermal growth factor receptor
eIF4E	eukaryotic translation initiation factor 4E
eIF4F	eukaryotic translation initiation factor 4F

ELISA	enzyme-linked immunosorbent assay
ER	endoplasmic reticulum
ErbB	avian erythroblastic leukemia viral oncogene B homolog
ERK	extracellular signal-regulated kinase
ESCRT	endosomal sorting complex required for transport
FBS	fetal bovine serum
FP	H/PF/2013 French Polynesia strain of Zika virus
fwd	forward
g	gram
Gab1	Grb2-associated binding protein 1
GAPDH	glyceraldehyde 3-phosphate dehydrogenase
gas6	growth-arrest-specific 6
GBS	Guillain-Barré syndrome
GDP	guanosine diphosphate
GTP	guanosine triphosphate
Grb2	growth factor receptor binding protein 2
GRP78	glucose-regulating protein 78
h	hour
HBV	hepatitis B virus
HCl	hydrogen chloride
HCMV	human cytomegalovirus
HCV	hepatitis C virus
HeBS	HEPES-buffered saline

HEPES	4-(2-hydroxyethyl)-1-piperazineethanesulfonic acid
HER	human EGF receptor
HF	host factors
HIV-1	human immunodeficiency virus 1
hpe	hours post-electroporation
hpi	hours post-infection
HPV16	human papillomavirus type 16
HRP	horseradish peroxidase
hRPL27	human ribosomal protein L27
Hsp70	heat shock protein 70
HSV-1	herpes simplex virus type 1
IAV	influenza A virus
IF	immunofluorescence
IgG	immunoglobulin G
IgM	immunoglobulin M
ILVs	intraluminal vesicles
IP_3	inositol 1,3,5-triphosphate
IRES	internal ribosomal entry site
JAK	Janus kinase
JEV	Japanese encephalitis virus
kb	kilobase pair
KCl	potassium chloride
KH_2PO_4	potassium dihydrogen phosphate

KO	knockout
L	liter
LB	lysogeny broth
M	molar
MβCD	methyl-β-cyclodextrin
MAP	microtubule-associated protein
MAPK	mitogen-activated protein kinase
MEK	mitogen-activated protein kinase kinase
Mg^{2+}	magnesium ion
Min	minute
mL	milliliter
mm	millimeter
mM	millimolar
$MnCl_2$	manganese(II) chloride
Mnk1	MAPK interacting protein kinase 1
MOI	multiplicity of infection
MOPS	3-morpholinopropane-1-sulfonic acid
mpi	minutes post-infection
mRNA	messenger RNA
MTase	methyltransferase
mTOR	major target of rapamycin
MVBs	multivesicular bodies
Na2HPO$_4$	disodium hydrogen phosphate

NaAc	sodium acetate
NaCl	sodium chloride
NCAM1	neuronal cell adhesion molecule
NCE	non-clathrin endocytosis
ng	nanogram
nm	nanometer
NS	non-structural protein
nt	nucleotide
ORF	open reading frame
p-loop	phosphate-binding loop
PBS	phosphate-buffered saline
PBST	phosphate-buffered saline with triton X-100
PCR	polymerase chain reaction
PDK1	3-phosphoinositol-dependent protein kinase 1
pfu	plaque-forming units
PI3K	phosphoinositide 3-kinase
PIP_2	phosphatidylinositol 4,5-biphosphate
PIP_3	phosphatidylinositol 3,4,5-triphosphate
PKC	protein kinase C
PLCγ	phospholipase C gamma
prM/M	precursor of membrane/membrane
PRNT	plaque reduction neutralization test
pros1	protein S

PS	phosphatidylserine
PTB	phosphotyrosine binding
PTK	protein tyrosine kinase
PVDF	polyvinylidene fluoride
qPCR	real-time PCR
$RbCl_2$	rubidium chloride
RC	replication complex
RdRp	RNA-dependent RNA polymerase
rev	reverse
RIPA	radioimmunoprecipitation assay buffer
RNA	ribonucleic acid
rpm	rotations per minute
RSV	respiratory syncytial virus
RTK	receptor tyrosine kinase
RT-qPCR	real-time quantitative reverse transcription PCR
RV	rhinovirus
s	second
SARS-CoV-1	severe acute respiratory syndrome coronavirus 1
SARS-CoV-2	severe acute respiratory syndrome coronavirus 2
SDS	sodium dodecyl sulfate
SDS-PAGE	sodium dodecyl sulfate–polyacrylamide gel electrophoresis
sfRNA	subgenomic flavivirus RNA molecule
SH2	Scr homology-2

shc	Src homology 2 domain-containing transforming protein
sHP-3′-SL	small hairpin 3′ stem-loop
sgRNA	single-guide RNA
sNS1	secreted NS1
SL-I	stem-loop I
SL-II	stem-loop II
SLA	stem-loop A
SLB	stem-loop B
SOS	son of sevenless protein 1
SPOV	Spondweni virus
STAT	signal transducer and activator of transcription
TAE	Tris acetate EDTA
TAM	Tyro3-AXL-MER
TBST	Tris-buffered saline with tween 20
TEMED	tetramethylethylenediamine
TFB1	transformation buffer 1
TFB2	transformation buffer 2
TGEV	transmissible gastroenteritis virus
TGFα	transforming growth factor α
TGN	trans-Golgi network
TIM	T cell immunoglobulin mucin
TK	tyrosine kinase
tMOC	threshold Mander's overlap coefficient

Tris	tris(hydroxymethyl)aminomethane
U	976 Uganda strain of Zika virus
U	enzyme unit
UAR	upstream AUG region
USA	United States of America
UTR	untranslated region
V	volt
v/v	volume per volume
VACV	vaccinia virus
VPs	viral particles
w/v	weight per volume
WB	Western blot
WNV	West Nile virus
YFV	yellow fever virus
XRN1	5′-3′ exoribonuclease 1
ZIKV	Zika virus
ZIKV-RLuc	ZIKV-*Renilla* Luciferase

1. Introduction

Viruses are obligate parasites as they require the host cell machinery for replication. The first step of the viral life cycle is the interaction of the viral components with cell surface molecules, either attachment factors and/or receptors, followed by the entry of the virus into the host cell. Thus, the development of antiviral drugs that can interfere with this step constitutes an attractive therapeutic approach. The present study focuses on the Zika virus (ZIKV), a mosquito-borne flavivirus that received public attention in 2016 due to the sudden escalation of cases of congenital malformations in newborns and other neurological complications connected to ZIKV infection. Even though some molecules have been described to participate in the ZIKV entry, this process is still enigmatic and requires further research. In this study, the role of the human epidermal growth factor receptor (EGFR) in the ZIKV life cycle, with emphasis on viral entry, was investigated.

1.1 Zika virus

1.1.1 Taxonomic classification

ZIKV is a re-emerging arthropod-borne virus (arbovirus) and taxonomically classified as a member of the genus *Flavivirus* within the *Flaviviridae* family. This family contains 89 virus species grouped into four genera: *Flavivirus*, *Hepacivirus*, *Pegivirus,* and *Pestivirus*. Besides the hepatitis C virus (HCV) from the genus *Hepacivirus*, the relevant human pathogens from the *Flaviviridae* family, which are responsible for morbidity and mortality worldwide, are comprised within the genus *Flavivirus*.[1,2] The 53 species that this genus is composed of can be categorized into four clusters: mosquito-borne, tick-borne, no-known vector, and insect-specific flaviviruses. Each cluster is further divided into clades that combine viruses that have at least 69% of nucleotide sequence identity. ZIKV is a mosquito-borne virus and together with Spondweni virus (SPOV) constitute the clade X.[3–5] Apart from SPOV, other phylogenetically related and of public health concern flaviviruses are dengue virus (DENV), Japanese encephalitis virus (JEV), West Nile virus (WNV), and yellow fever virus (YFV) **(Figure 1)**.[6,7]

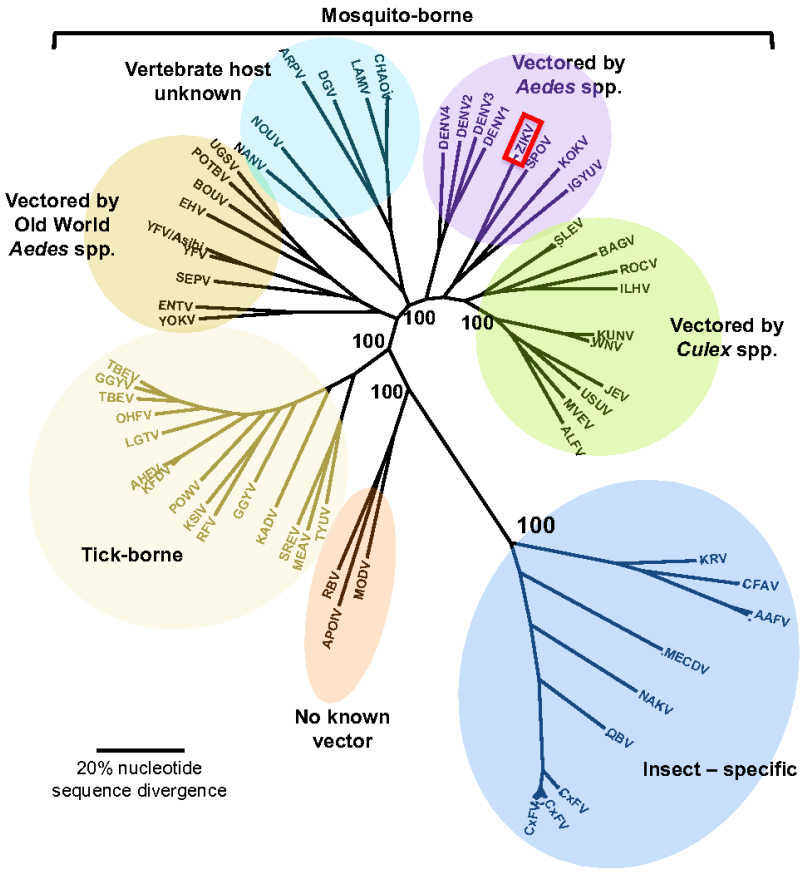

Figure 1 – Phylogenetic tree of the genus *Flavivirus*. ZIKV (highlighted in red), which is closely related to SPOV, belongs to the cluster of mosquito-borne flaviviruses vectored by mosquitoes of the Aedes species. Within the genus *Flavivirus* and besides the mosquito-borne cluster, viruses can be categorized into tick-borne, insect-specific, or no-known vectors, depending on their vector of transmission. The phylogenetic relationships were based on the analysis of conserved sequences in the RNA polymerase NS5. The scale indicates 20% nucleotide sequence divergence. Retrieved from Weaver et al., 2016.[8]

1.1.2 History and epidemiology

ZIKV and several other arboviruses were first discovered during a study on the YFV at the Uganda Virus Research Institute (previously named the Yellow Fever Research Institute) in Entebbe, Uganda.[8] Near this institute, in April 1947, in the Zika Forest, one of six rhesus monkeys (no. 766), which had been caged for research purposes, developed a fever. On the third day of fever, a blood sample was taken and the respective serum was injected intracerebrally or intraperitoneally into Swiss albino mice, and subcutaneously into another rhesus monkey. Only the mice that had been injected intracerebrally presented clinical signs and a transmissible pathogen was isolated from their brains. Later on, this pathogen was termed Zika virus according to the geographical origin of the isolate.[9] Shortly after, neutralizing antibodies against ZIKV were detected in the sera of residents of Uganda and the United Republic of Tanzania, indicating a possible human transmission.[10–12]

The first time that ZIKV was isolated from humans appears to be controversial. The virus was isolated from the serum of a 10-year-old girl in Nigeria in 1954. However, it

was reported that this isolated virus was more similar to SPOV than to ZIKV.[13–15] One decade later, a researcher from the Uganda Virus Research Institute reported that it was him who originally isolated ZIKV from his serum after becoming infected possibly while he was working in the Zika Forest.[13] In 1966, ZIKV was first isolated in the Asian continent, in Malaysia, from *Aedes aegypti* mosquitoes.[16] The first human cases of symptomatic ZIKV disease on this continent were reported only in 1977.[17] Nevertheless, serological tests performed in India, Malaysia, the Philippines, and Vietnam suggest the presence of the virus in the 1950s.[12,18–20]

During the first 60 years since ZIKV discovery, documented human cases were rare and exclusive to Africa and Southeast Asia without any major clinical signs being reported. That being said, it came as a surprise when a "dengue-like illness" outbreak was reported by local physicians in the State of Yap, in the Federated States of Micronesia in April 2007. Even though a few patients tested positive for DENV using an IgM kit, the physicians believed that this disease was not the same as the one from the two previous DENV outbreaks that occurred in Yap Island. In June 2007, ZIKV infection was confirmed in serum samples collected from patients in the acute phase of infection.[21,22]

During this entire time, ZIKV was disregarded by the scientific community due to the lack of large outbreaks and severe clinical manifestations. This changed when French Polynesia was hit by the largest outbreak that had been documented until that period. In October 2013, the first cases of ZIKV infection were reported.[23] The number of symptomatic patients kept growing and by the end of the outbreak, which lasted about six months, there were 32.000 estimated cases (11.5% of the population) of ZIKV infection. Besides the mild symptoms previously experienced in other outbreaks, 74 patients presented neurological and autoimmune complications. Among these, 42 were diagnosed with Guillain-Barré syndrome (GBS) (explained in chapter 1.1.3).[24–27] Rapidly, ZIKV reached other islands in the Pacific. [28–30]

Cases of rash associated with mild fever and arthralgia (joint pain) started to exponentially increase in the Northeast of Brazil at the end of 2014.[30–32] In March 2015, ZIKV infection was confirmed by the analysis of serum samples of acute-infected patients.[33,34] Within a few months, ZIKV had spread to at least 18 Brazilian states and between 440.000 and 1.300.000 infectious cases were estimated until then, as announced in December 2015 by the Ministry of Health.[35,36] Colombia reported the first case of ZIKV infection in October 2015 and by February 2016, cases of ZIKV transmission had been reported in 28 countries and territories in the American continent.[37–39] Moreover, numerous cases of ZIKV infection in non-endemic countries were stated due to travelers that carried the virus. Among these are most European

countries, several states of the United States of America, Canada, Japan, China, Australia, New Zealand, and others.[40–52]

Unlike the previous outbreaks in the Pacific, the epidemic in the Americas unveiled new neurological complications. Besides GBS, thousands of cases of microcephaly in newborns (explained in chapter 1.1.3) were connected to ZIKV infection.[36,53,54] Moreover, a retrospective study of the French Polynesia outbreak exposed various cases of microcephaly that had not been linked to ZIKV infection during the outbreak and before this epidemic.[55] The fast spread of ZIKV in the Americas and the increase in the number of ZIKV-associated cases of microcephaly led the World Health Organization to declare ZIKV infection a public health emergency of international concern on February 1st, 2016.[56] However, this only lasted 8 months due to the drastic reduction in the amount of ZIKV cases.[57] After this epidemic, only a few minor outbreaks were reported in Cuba, India, and Angola.[58–60] A representative overview of ZIKV spread worldwide is summarized in **Figure 2**.

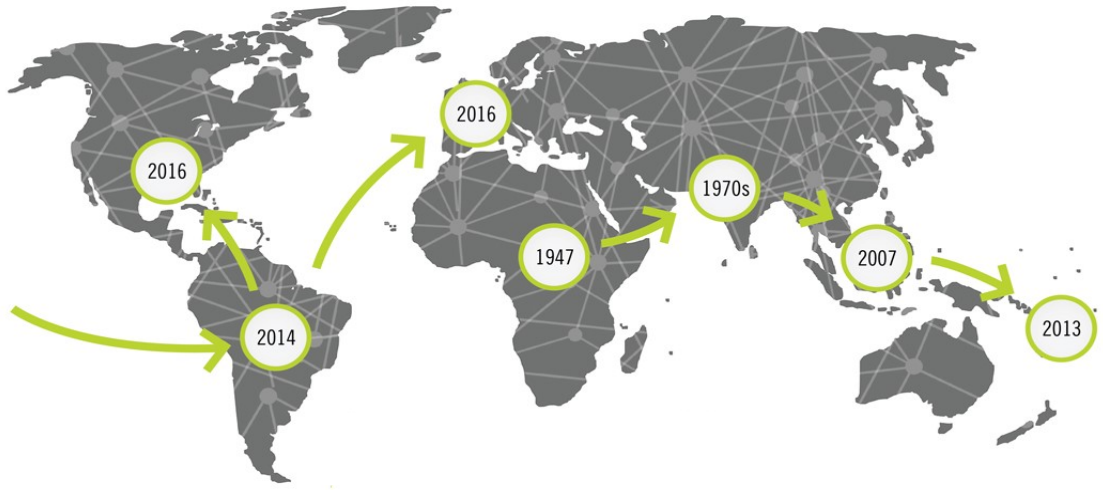

Figure 2 – Chronological map of ZIKV dissemination. ZIKV was discovered in the Zika Forest, in Uganda in 1947. The first human cases of ZIKV infection in the Asian continent were reported in 1977. The first outbreak occurred in the State of Yap, in the Federate States of Micronesia in 2007. ZIKV emerged in French Polynesia in 2013 where the largest outbreak until that time was documented. Shortly after, the first cases of ZIKV infection surged in Brazil in 2014. By 2016, ZIKV had rapidly spread all over the Americas with several cases appearing in non-endemic countries, including most European countries. Retrieved from Public Health Landscape website.[61]

1.1.3 Clinical manifestations

It is estimated that about 20-56% of ZIKV cases are symptomatic.[62,63] ZIKV infection is typically presented as mild fever, exanthema (rash), arthralgia, conjunctivitis, myalgia (muscle pain), and headache.[64,65] The incubation period of ZIKV is 3-14 days after the bite of an infected mosquito and the symptoms generally last in most cases from 2 to 7 days.[65] Besides these flu-like symptoms, neurological complications were linked to ZIKV infection. Approximately 75% of these complications in adults are GBS.[64] GBS is

an acute immune-mediated disease that affects the peripheral nervous system, leading to progressive muscle weakness and even paralysis.[66,67] Generally, the nerve damage is not permanent. However, persistent cases, which are approximately 20%, result in severe disability and respiratory failure with a mortality rate of 3-10%.[67–69] Further neurological complications connected to ZIKV infection are meningoencephalitis and acute myelitis, among others.[64,70,71] Pregnant women that are infected with ZIKV have an elevated chance of miscarriage, preterm birth, and stillbirth (fetal death before or during delivery).[72,73] Moreover, multiple congenital malformations in fetuses and newborns were associated with ZIKV infection during pregnancy. These malformations are referred to as congenital ZIKV syndrome (CZS) and are mainly neurological, musculoskeletal, ophthalmological, and auditory.[73–75] During the epidemic in the Americas, a drastic increase in the number of cases of microcephaly was reported.[76] Microcephaly is a neurological disorder in which the head size is smaller than what is expected for age, sex, and ethnicity **(Figure 3)**.[77] This condition can be correlated with an underdeveloped brain, impaired motor and cognitive functions, extracranial malformations, and facial distortion.[78] Apart from fatalities related to the CZS in newborns and fetal death during pregnancy, ZIKV mortality is rare with only a few reported cases.[79–82]

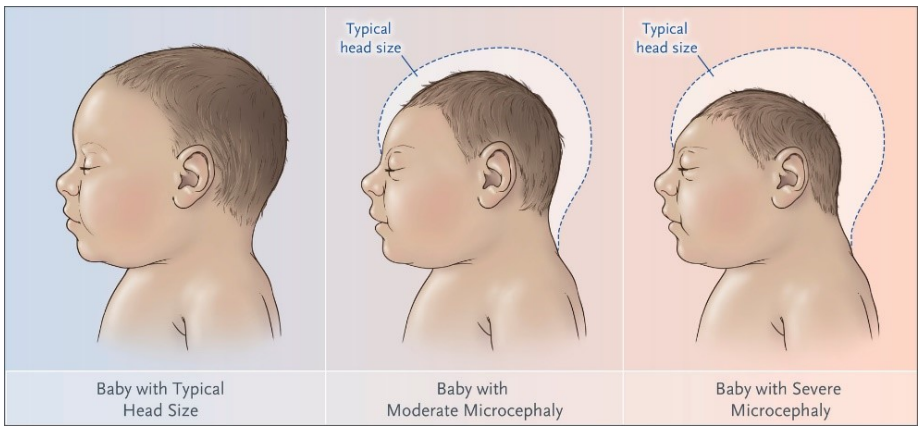

Figure 3 – Representative illustration of newborns with microcephaly. Microcephaly is a neurological condition in which the head size of a newborn is smaller than expected. This disorder can be moderate or severe and was linked to ZIKV infection. Retrieved from Petersen *et al.*, 2016.[83]

1.1.4 Viral evolution

Phylogenetic analyses disclose two major ZIKV lineages, the African and the Asian lineages that comprise innumerous viral strains **(Figure 4)**.[84,85] The African lineage is divided into the East African cluster, which contains the first isolated ZIKV strain (MR766) and its variants, and the West African cluster that covers all the West African strains, including the Nigeria strain.[86] The Asian lineage encompasses all strains from Southeast Asia, the Pacific, and the American cluster.[87] The ZIKV strains connected to human outbreaks share higher sequence homology with the mosquito strain P6-740

isolated in Malaysia in 1966 than the ones from the Nigerian cluster. This indicates that the strains responsible for the epidemic in the Americas and the birth defects evolved from this mosquito strain, belonging to the Asian lineage.[88] Yet, the ZIKV strains from these two lineages share approximately 88% and 96% nucleotide and amino acid sequence identity, respectively.[21,89] By contrast, the African lineage was rarely linked to human infection and was never detected outside the African continent nor connected to neurological disorders. The human outbreak and the CZS cases reported in Angola in 2016 were linked to the Asian lineage.[58] The reason behind the lack of association of human outbreaks with the African lineage remains unknown.

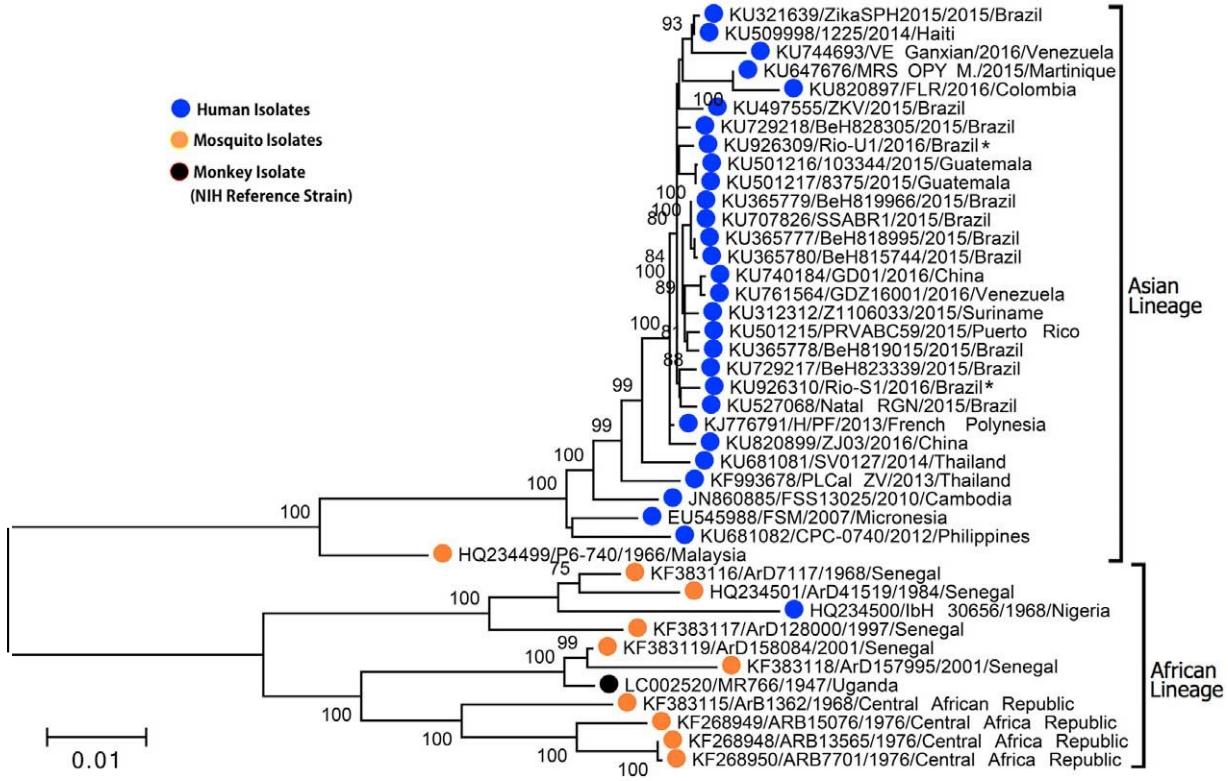

Figure 4 – Phylogenetic tree of ZIKV lineages. ZIKV strains are divided into African and Asian lineages. Not all ZIKV strains are represented in the illustration. Strains isolated from humans, mosquitoes, and monkeys are labeled in blue, orange, and black circles, respectively. The phylogenetic relationships were based on the analysis of the complete coding sequence of ZIKV strains. The scale indicates 1% nucleotide sequence divergence. Retrieved from Wang *et al.*, 2016.[88]

It has been suggested that genetic changes in the viral genome during ZIKV dissemination could have resulted in increased transmission by mosquitoes, infectivity, and human pathogenesis.[90,91] However, Aubry *et al.* revealed that the strains from the African lineage not only have higher transmissibility by mosquitoes but are also more lethal in immunocompromised adult mice than the strains from the Asian lineage.[92] These observations suggest that ZIKV re-emergence and evolution was not due to viral adaptation, but maybe because of arbitrary reunion of propitious epidemic conditions in the outbreak areas, namely increased air travel, immunologically naive human

populations, and high density of competent vectors.[92,93] Moreover, strains from both lineages were described to be capable to cross the placenta barrier and generate congenital malformations.[94,95] In fact, it was proposed that ZIKV strains from the Asian lineage might have become attenuated during viral evolution, increasing the number of birth defects instead of fetal deaths and consequently, explaining the absence of CZS cases linked to the African lineage.[92,96]

1.1.5 Viral transmission

As previously mentioned, ZIKV is an arbovirus and its main vector of transmission are the mosquitoes of the *Culicidae* family within the *Aedes* genus. The female mosquito is infected with ZIKV through the bite of an infected human or another mammal while the virus circulates in the bloodstream (viremia). After replication and spreading through the mosquito body until reaching the salivary glands, the virus present in the saliva of the mosquito is delivered into the dermis of the skin of the naive host during the blood-feeding.[97,98] ZIKV is transmitted between non-human primates and arboreal mosquitoes in a sylvatic cycle. Sporadically, ZIKV can be transmitted to humans by arboreal mosquitoes in forests. By contrast, in an urban cycle, humans are the primary host, and the transmission is carried out by urban mosquitoes, mainly *Aedes aegypti* and *Aedes albopictus*.[99] *Aedes aegypti* is the predominant vector of transmission in an urban environment as it is broadly distributed in Africa, America, Asia, and Oceania and has a superior vectorial capacity.[100,101] While *Aedes aegypti* propagates in tropical and subtropical conditions, *Aedes albopictus* thrives as well in temperate climates, including North America and Europe.[102] Besides these two mosquito species, *Aedes hensilli* and *Aedes polynesiensis* mosquitoes were linked to the outbreaks in the State of Yap and French Polynesia, respectively.[103–105]

Besides being transmitted by mosquitoes, ZIKV can also be spread directly human-to-human via body fluids. The most studied route of non-vector transmission is the maternal-fetal transmission due to the several cases of microcephaly and other congenital disorders associated with ZIKV infection. In this case, viral transmission occurs in the uterus through the placenta during pregnancy.[106,107] Perinatal transmission in which the newborn was most likely infected during childbirth was also reported.[108] Additionally, there is evidence of the presence of ZIKV infectious viral particles in breast milk, but viral transmission through this fluid has not been confirmed until now.[109] Another mode of transmission, which is not common among flaviviruses, is through sexual contact.[110] The majority of the reported cases of sexual transmission occurred from an infected male to a female.[111–113] This observation might be correlated to the fact that ZIKV shedding has a higher incidence and lasts longer in the testis and semen than in the vaginal tract and secretions.[114] Furthermore, viral transmission

through blood transfusion has been documented as well.[115–117] Other possible ways of ZIKV transmission with sporadic occurrence are organ transplantation, laboratory incidents, and animal bites.[118–121] A representative overview of the modes of ZIKV transmission is summarized in **Figure 5.**

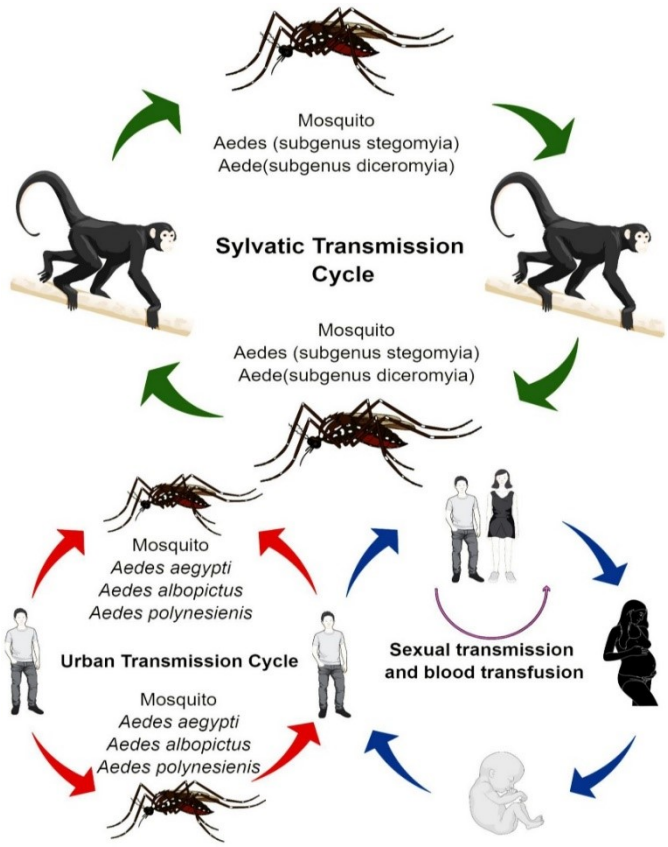

Figure 5 – Vector and non-vector borne routes of ZIKV transmission. In a sylvatic cycle, ZIKV is transmitted between non-human primates and arboreal mosquitoes, whereas in an urban cycle, the transmission occurs between humans and urban mosquitoes. ZIKV can also be transmitted human-to-human by sexual contact, blood transfusion, and from mother to child. Retrieved from Rather *et al.*, 2017.[122]

1.1.6 Diagnosis

Up to 80% of the infected patients are asymptomatic and for those who exhibit clinical signs, the symptoms are often non-specific and similar to other infections caused by different arboviruses.[123] In light of this, laboratory testing remains crucial for ZIKV diagnosis. The diagnosis can be performed based on both molecular and serological tests. Molecular tests consist of the direct detection of the genomic viral RNA mostly by real-time quantitative reverse transcription PCR (RT-qPCR).[124–126] Although this nucleic acid amplification test is highly sensitive and specific, it is only valid during the early phase of infection due to the short viremic period of ZIKV.[21] In most cases, ZIKV RNA can be detected in the serum up to 4 days after the symptoms appear, and as late as 11 days.[21,127] Considering that whole blood needs to be analyzed shortly after

collection and the inconsistency of saliva, urine is usually collected as a secondary specimen. In fact, ZIKV RNA can persist longer than 10 days in urine after the initial symptoms.[127,128] In children and newborns, as the blood collection tends to be more complicated, urine and saliva specimens are preferable.[129] In addition, cerebrospinal fluid, amniotic fluid, breast milk, semen, vaginal secretion, and tissues can be considered as specimens as well **(Figure 6)**.[128–134]

On the other hand, serological tests reside on the detection of viral antigen-specific antibodies (IgM or IgG) mainly by enzyme-linked immunosorbent assay (ELISA) or immunofluorescence assay.[21] IgM antibodies against ZIKV can be detected from day 5 to almost 12 weeks after the first clinical manifestations, while IgG appears just after IgM and can last a lifetime **(Figure 6)**.[135–137]

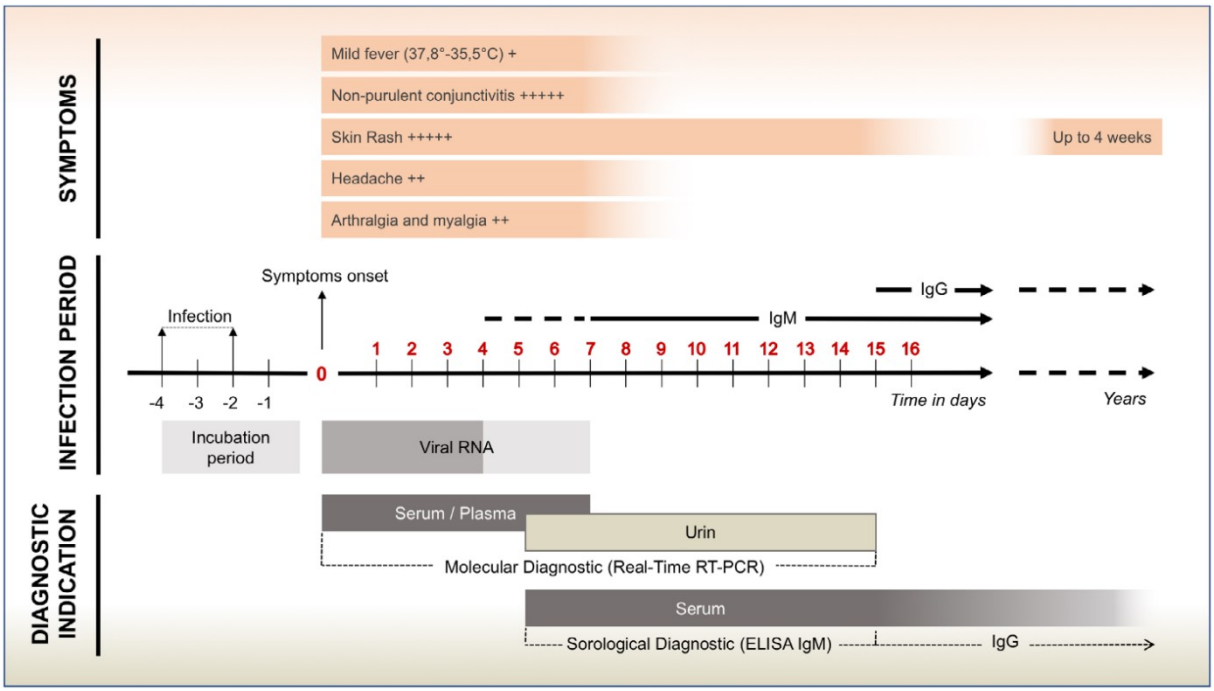

Figure 6 – Chronology of ZIKV infection and respective diagnostic indication. Diagnosis of ZIKV infection can be made based on molecular and/or serological tests depending on the day after the onset of the symptoms that the samples are collected. Molecular tests, such as RT-qPCR, are only adequate while ZIKV RNA can be detected in the serum/plasma, which in most cases is up to 4 days after the symptoms appear. A urine sample is usually collected additionally as ZIKV tends to persist longer than in blood. From day 5 up to 12 weeks after the onset of the symptoms IgM antibodies against ZIKV can be measured by ELISA from a serum sample, whereas IgG can be detected about a week later and can last several years. Retrieved from Jorge *et al.*, 2020.[138]

Nevertheless, the interpretation of these results can be challenging due to the cross-reactivity of the antibodies that exists in patients that were previously infected with other flaviviruses or vaccinated against these.[21,120,139] Therefore, positive results should be confirmed by plaque reduction neutralization test (PRNT). The plaque reduction neutralization assay can determine the virus-specific neutralizing antibody titer, but

requires extensive laboratory work partially because of the low throughput and longer time to obtain the results.[140,141] Hence, this assay can be disadvantageous for patient diagnosis during a large outbreak. Due to the cross-reactivity still existing in this serological assay, the PRNT should be performed in parallel against other flaviviruses that have a high prevalence in the region where the exposure occurred. In light of this, a positive result is considered when the $PRNT_{90}$ titer (dilution of the serum that is capable to reduce the number of plaques formed by a given virus by 90% in comparison to the free-serum control) against ZIKV is ≥10 and $PRNT_{90}$ titer against other flaviviruses tested is <10.[142,143]

1.1.7 Treatment and prevention

Until the present day, there is neither a specific antiviral treatment nor a preventive vaccine against ZIKV infection. As viral infection will eventually clear, the treatment is directed to relieving the symptoms. Infected patients are advised to rest, hydrate with fluids, take antihistamines and acetaminophen (paracetamol) for the pruritic rash and to mitigate the fever and pain, respectively.[144] If the symptoms aggravate, medical care should be sought. In the event of developing GBS, therapeutic plasma exchange or the administration of intravenous immunoglobulins can be used as treatment.[145]

The development of antiviral drugs generally relies on targeting the host cell by interfering with crucial steps of the viral life cycle and thereby, hampering the formation of new infectious viral particles and affecting the viral spread. Alternatively, these compounds can target the viral components, mainly focusing on the RNA polymerase (NS5) or the viral protease (NS2B-NS3) (see chapter 1.1.8.1). Both approaches require an extensive comprehension of the molecular and cellular mechanisms of ZIKV pathogenesis and the identification of important virus-host interactions. The development and the approval of novel compounds requires a long time and therefore, repurposing already existent licensed drugs which are used for other clinical indications to treat ZIKV infection is preferable.[146,147] Innumerous compounds including the antibiotic azithromycin, the antiparasitic drug nitazoxanide, the antimalaria drug chloroquine, the antiprotozoal drug emetine, and the antiviral drugs ribavirin and favipiravir have shown promising antiviral activity against ZIKV infection *in vitro*.[148–152] Still, only a few drugs have reached clinical trials, such as pinocembrin (post-entry process), galdesvir (viral polymerase inhibitor), ebselen (reactive oxygen species reductor), nordihydroguaiaretic acid (sterol regulatory element-binding proteins inhibitor), NITD008 (viral polymerase inhibitor), and 7-deaza-2'C-methyladenosine (viral polymerase inhibitor).[153–158] Currently, only galdesvir and ebselen have completed phase I of the clinical trials. The nordihydroguaiaretic acid and pinocembrin continue in phase I of the clinical trials, whereas NITD008 and 7-deaza-2'C-methyladenosine

were not approved. [159–161] Nevertheless, there is not sufficient information on the effects of any of these drugs on pregnant women due to their exclusion in clinical trials.

Due to the difficulties in the establishment of an effective and safe treatment, vector and personal preventive measures should be taken in ZIKV endemic countries. In the affected areas, the density of the viral vectors should be controlled by eliminating the breeding sites of mosquitoes and the human population should avoid mosquito bites by using insect repellents, long sleeves and pants, insect netting, and staying away from standing waters, for instance.[162,163] In addition, couples should practice abstinence or have protected sexual intercourse, including returning travelers.[164] To prevent the occurrence of microcephaly in fetuses or babies, pregnant women are not advised to travel to countries at risk and pregnancy should be avoided in high prevalence areas until the number of ZIKV cases undergoes a drastic reduction or complete eradication.[165]

Developing a preventive ZIKV vaccine as well as any other arbovirus vaccine is challenging due to the irregular emergence and ceasing of the epidemics. Moreover, for certain flaviviruses, including ZIKV and DENV, the antibody-dependent enhancement (ADE) phenomenon is problematic in the development of a safe vaccine. ADE occurs when the antibodies produced during an immune response bind to the virus without neutralizing its activity.[166,167] Subsequently, these antibodies can facilitate viral entry via Fc gamma receptors, increasing the immune response and illness severity.[168–170] Thus, the cross-reactivity of the flavivirus antibodies and the pre-existing immunity, which can be obtained either through previous flavivirus infection or vaccination, are a concerning issue in the production of a vaccine. As DENV and ZIKV are prevalent in the same areas, it has been implicated that ADE could be responsible for the neurological disorders associated with ZIKV infection.[171] Multiple candidate vaccines comprising live attenuated, purified inactivated, DNA, mRNA, virus-like particles, and viral vectors vaccines are in clinical trials.[172–175] However, the decline of ZIKV cases and the unpredictability of the outbreaks are hampering phase 2 and phase 3 of the clinical trials.

1.1.8 Molecular virology

1.1.8.1 Genome organization and functionality

ZIKV is a non-segmented, single-stranded, positive-sense RNA virus with a genome varying from 10398 to 11520 nucleotides (nt), depending on the strain and/or isolate. Nevertheless, the most predominant size of the genome is 10.8 kilobase pairs (kb).[176–178] The 5′ and 3′ ends of the genomic RNA contain two untranslated regions (UTR) that flank a single open reading frame (ORF). The 5′ UTR with around 100 nt holds a cap

structure composed of a guanosine residue that is connected to the 5′ end of the RNA through a 5′-5′ triphosphate bond.[179,180] This cap structure confers stability and protection to the viral RNA from degradation by exoribonucleases.[181] The cap is methylated at the nitrogen in position 7 of the guanosine, allowing the recognition by the initiation factor eIF4E and consequently, the translation of the viral genome.[182–184] Additionally, the cap structure is further methylated at the 2′-oxygen atom (2′-O) of the N1 ribose, yielding a cap-1 structure. This methylation is thought to shield the viral genome from being detected by the host cell sensors that stimulate the production of interferon genes to restrict viral translation.[185–187] The cap structure is followed by the conserved dinucleotide AG and two conserved stem-loop structures, SLA and SLB, which are separated by a poly(U) sequence **(Figure 7)**.[188,189] The SLA acts as the promoter for the viral genome replication by directly interacting with the viral polymerase NS5 and coordinates the addition of the cap structure in the nascent transcript.[190,191] Its presence is also required for both N-7 and 2′-O methylation of the cap structure.[192] The SLB is located near the ORF start codon and comprises the 5′ upstream AUG region (5′ UAR) sequence necessary for the interaction with the 3′ end of the viral genome.[193,194] Downstream the SLB, in the capsid coding region, the downstream AUG region (5′DAR) is another important element for the interaction of the 5′ with the 3′ end of the genome as well as the cyclization sequence (CS). In between these two regions lies the capsid region hairpin (cHP) that facilitates the positioning of the ribosome close to the start codon, enhancing viral translation **(Figure 7)**.[195,196] The 3′ UTR with approximately 400 nt lacks the poly(A) tail that is usually present in the host mRNA and terminates with the conserved dinucleotide CU sequence.[197,198] It is composed of two stem-loops (SL-I and SL-II), two dumbbells (DB-1 and DB-2), and a small hairpin 3′ stem-loop (sHP-3′-SL) **(Figure 7)**.[199] Except for the sHP-3′-SL, the exact function of these structures remains unknown. Nonetheless, they seem important for viral replication and translation. The sHP-3′-SL serves as a binding site to the poly(A)-binding protein and interacts with viral and other host proteins to control viral replication and translation.[200–202] Furthermore, the stem-loop structures are resistant to the host 5′-3′ exoribonuclease 1 (XRN1) activity. As a result, non-coding subgenomic flavivirus RNA molecules (sfRNAs) are generated by the degradation of uncapped viral RNA that stall at these structures **(Figure 8)**.[203,204] These sfRNAs are crucial for viral replication and antagonization of the interferon response.[205,206] Complementary sequences of the UAR, DAR, and CS can be found within the 3′ UTR. The base-pair interaction of the 5′UTR with the 3′UTR, namely 5′ CS-3′CS, 5′ UAR-3′ UAR, and 5′ DAR-3′ DAR, results in the cyclization of the viral genome **(Figure 7)**.[207] The cyclization allows

the viral polymerase NS5, which is bound to the SLA in the 5′ UTR, to reach the 3′ end of the viral genome that is vital for the initiation of the RNA synthesis.[207,208]

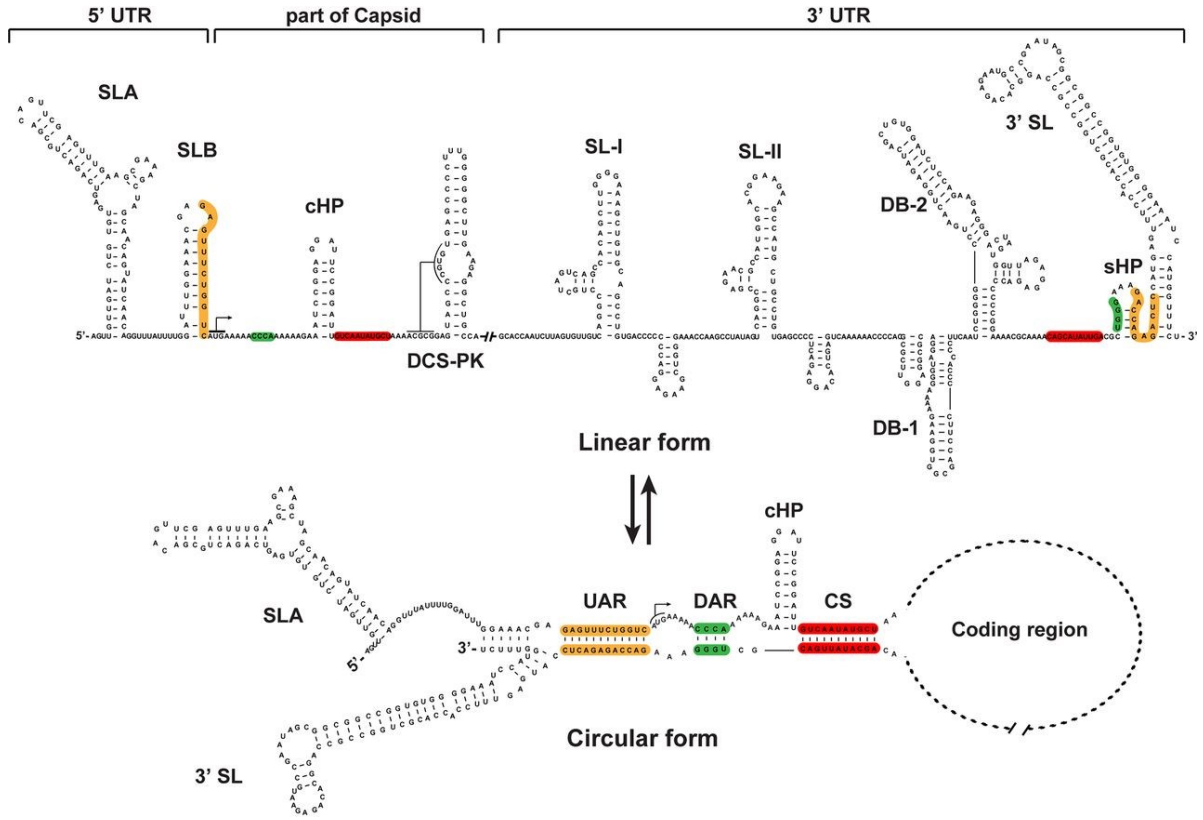

Figure 7 – Schematic representation of the linear and circular forms of the ZIKV genome. The ZIKV genome contains conserved RNA structures in the 5′ and 3′ untranslated regions (5′UTR and 3′UTR) that are specified in the representation. The 5′UTR comprises two stem-loops (SLA and SLB), a capsid region hairpin (cHP), and a cyclization sequence (CS) pseudoknot (DCS-PK), whereas the 3′UTR harbors two stem-loops (SL-I and SL-II), two dumbbells (DB-1 and DB-2), and a small hairpin 3′ stem-loop (sHP-3′-SL). The 5′ end can interact with the 3′ end of the genome through the upstream AUG region (UAR), downstream AUG region (DAR) and the CS marked in orange, green, and red, respectively. These interactions allow the cyclization of the viral genome. Retrieved from Li *et al.*, 2020.[207]

The ORF encodes a single large polyprotein of 3423 amino acid residues (aa). However, the polyprotein from the MR766 strain is shorter with 3419 aa, lacking a 4 aa N-glycosylation motif (VNDT) in the envelope region that is thought to be lost during cell culture passaging since its isolation.[177,178,209] The viral polyprotein is co- and post-translationally processed by cellular host and viral proteases into three structural and seven non-structural proteins. The structural proteins are located at the N-terminal end of the polyprotein and are comprised of the capsid (C), the precursor of membrane/membrane (prM/M), and the envelope (E) proteins, followed by the non-structural proteins (NS1, NS2A, NS2B, NS3, NS4A, NS4B, NS5) positioned at the C-terminal end **(Figure 8)**.[210] In the lumen of the endoplasmic reticulum (ER), the host signal peptidase splits the prM protein from the portion of the C protein that is integrated into the ER membrane (capsid anchor); the prM protein from the E protein;

the E protein from the NS1 protein; and NS4B protein from the hydrophobic region of NS4A protein (designated as 2k peptide). Meanwhile, on the cytoplasmic side, the viral serine protease (NS2B/NS3) cleaves the C/capsid anchor; the NS2A/NS2B; the NS2B/NS3; the NS3/NS4A; the NS4A/2k peptide, and the NS4B/NS5 junctions. In addition, an unknown host protease separates the NS1 protein from the NS2A protein. During the secretion of the viral particles, a furin protease resident in the trans-Golgi network (TGN) cleaves at the pr peptide and the M protein junction that is required for viral maturation **(Figure 8)**.[177,210]

The structural proteins, as the name indicates, structurally form the viral particle. The full-length C protein is composed of five helices (α1-α5) with the last helix (α5), denominated as the capsid anchor, anchoring the protein to the ER membrane.[211] The capsid anchor functions as a signal peptide that allows the translocation of the prM into the ER lumen. After cleavage by the viral protease (NS2B-NS3), the mature C protein, which is formed by the helices α1-α4, is released in the cytoplasm and associates with the viral genome. The mature C protein with about 11 kDa exists as a dimer and has an asymmetric charge distribution.[210,212] On the one side, it encompasses hydrophobic residues to interact with the viral lipid membrane. On the other side, it holds residues with a positive charge to interact with the negatively charged genomic RNA, acting as an RNA chaperone.[211,212] Besides integrating the viral nucleocapsid and ensuring the correct assembly of the viral particles, the C protein might shield the viral genome from host nucleases and RNA sensors after entering the host cells.[211,213] Additionally, it was shown to have a role in the development of neurological disorders associated with ZIKV infection.[214–216] The prM glycoprotein with around 26 kDa is subjected to cleavage by a furin protease in the TGN, generating the N-terminal pr peptide and the M protein. The latter is inserted into the viral lipid membrane. The prM interacts with the E protein to form heterodimers, assisting in its correct folding.[217–219] Both prM and E proteins have two transmembrane domains that serve as ER-retention signals and facilitate the formation of the lipid envelope of the viral particle.[220–222] The pr peptide covers approximately 12 aa of the fusion loop of the E protein, preventing the premature fusion of the viral particle within the cell. After cleavage, the fusion loop is exposed and the pr peptide is released to the extracellular environment, together with the viral particle.[223–225] The E protein is also a glycoprotein anchored to the membrane via its C-terminus.[226] With about 53 kDa it is constituted by four domains. The domain I (DI) connects the domain II (DII) and the domain III (DIII) by disulfide bridges. The DII is involved in the dimerization of the E protein and has a conserved amino acid sequence at the extremity of this domain that interacts with the host endosomal membrane during membrane fusion (fusion loop). The domain III exhibits an immunoglobulin-like structure and is responsible for the virus-host interactions

during attachment and entry. [227,228] The fourth domain is comprised of a stem anchor and two transmembrane regions, anchoring the E protein to the ER membrane.[229,230] As the major component of the surface of the viral particles, the E protein, mainly DII and DIII, is the principal target of neutralizing antibodies.[227,231]

The non-structural proteins are not part of the viral particle, but are crucial for the viral life cycle. The NS1 protein is a glycoprotein with approximately 46 kDa that exists in multiple forms. It is synthesized as a monomer and dimerizes within the ER lumen, inducing the reorganization of the ER membranes to form the sites of replication and assembly and integrating the replication complex (see chapter 1.1.8.2).[232,233] Additionally, the NS1 protein was associated with the suppression of interferon signaling.[234–236] Part of the dimeric NS1 protein undergoes maturation in the TGN, being secreted into the extracellular space as a hexameric lipoprotein (sNS1).[237–239] The sNS1 protein accumulates in the serum of patients during the acute phase of infection and thus, it is used as a diagnostic marker for viral infection.[240] Furthermore, the NS2A is a protein residing in the ER with a size of about 22 kDa and is important for viral replication as a member of the replication complex.[241] Besides being involved in viral replication, the NS2A protein has a central role in viral assembly. It binds to the 3'UTR of the newly synthesized viral RNA through its cytoplasmic loop and in addition recruits the uncleaved C-prM-E polyprotein and the viral protease (NS2B/NS3) to the assembly site, facilitating the formation of the nucleocapsid and the interaction with the remaining structural proteins.[242] The NS2A protein can also suppress the interferon response and was found to be correlated with ZIKV-induced neurovirulence.[234,243,244] The NS2B protein is also an ER-resident protein with approximately 14 kDa and is known as a cofactor of NS3. It interacts with the NS3 protein to form the viral protease, anchoring this to the ER membrane and activating its protease activity.[245–247] Moreover, the NS2B protein can also hamper the interferon response.[235,248] The NS3 protein with about 70 kDa has several functions. The N-terminal end comprises the serine protease domain that together with the NS2B protein cleaves the viral polyprotein on the cytoplasmic side. The C-terminal end harbors the RNA helicase and the nucleoside triphosphatase domains. The RNA helicase dissociates the double-stranded RNA (dsRNA) intermediate during the synthesis of the viral RNA, whereas the nucleoside triphosphatase provides the energy for the RNA helicase to dissociate the RNA strands.[246,249,250] Apart from playing a role in the maturation of the viral polyprotein and viral replication, the viral protease (NS2B/NS3) inhibits the interferon response and affects cytokinesis in neuronal cells, leading to a decrease in cell division and promoting cellular apoptosis.[248,251,252] It also impairs the formation of stress granules to prevent the ceasing of the host translation machinery that is vital for the synthesis of the viral proteins.[214] More recently, it was shown that the NS3 protein induces intracranial

calcification, a common fetal birth defect associated with ZIKV infection, and consequently, affects the brain development.[253] The NS4A and NS4B proteins are also ER-resident proteins, similar to the NS2A and NS2B proteins, with approximately 16 kDa and 27 kDa, respectively. The viral genome translates a hydrophobic segment denominated as the 2K peptide (2 kDa peptide) that is completely inserted in the ER membrane and located in between the NS4A and the NS4B proteins, functioning as a signal peptide for the NS4B protein.[210,254] Both NS4A and NS4B proteins are part of the replication complex. Nevertheless, the exact function during viral replication is not known. It was suggested that like other flaviviruses, these proteins induce autophagy to generate membrane structures to serve as replication sites. The NS4A and NS4B proteins were linked to microcephaly and other neurological disorders by dysregulating the Akt/major target of rapamycin (mTOR) signaling pathway and hampering neurogenesis.[255] Additionally, the NS4A protein impedes the interferon response and the formation of stress granules in a comparable manner as the viral protease NS2B-NS3.[214,256,257] The NS4B protein can also suppress the interferon response.[234,235] Lastly, the NS5 protein is the largest non-structural protein with about 103 kDa. The N-terminal end encloses the methyltransferase (MTase) domain responsible for the methylation of the viral RNA cap, while the C-terminal end contains the RNA-dependent RNA polymerase (RdRp) domain that catalyzes the viral RNA synthesizes.[258,259] The NS5 protein also antagonizes the interferon response by disrupting the Janus kinase/signal transducer and activator of transcription (JAK/STAT) signaling pathway and interacts with the NS3 protein to stimulate its helicase activity.[250,260–262] Even though the viral replication occurs in the cytoplasm, the NS5 protein was found mainly in the nucleus. This accumulation in the nucleus seems to protect the NS5 protein from cytoplasmic degradation, enabling its viral functions.[263]

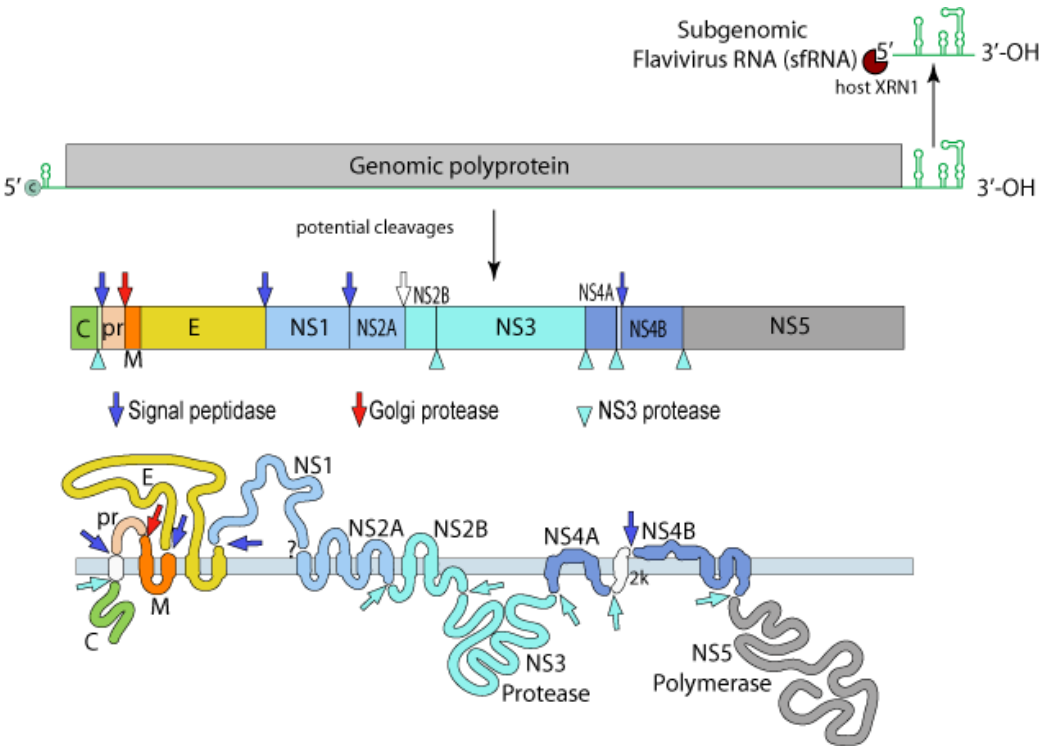

Figure 8 – Schematic representation of the ZIKV genome and respective viral polyprotein. The ZIKV genomic RNA comprises a single open reading frame (ORF) with two untranslated regions at the 5′ end and 3′ end of the genome. Non-coding subgenomic flavivirus RNA molecules (sfRNAs) are produced by the degradation of uncapped viral RNA by the host 5′-3′ exoribonuclease (XRN1) that stall at the stem-loop structures present at the 3′ end of the genome. The ORF encodes the viral polyprotein that is processed by host and viral proteases, originating three structural proteins (C, prM/M, and E) and seven non-structural proteins (NS1, NS2A, NS2B, NS3, NS4A, NS4B, NS5). All cleavage sites are indicated with arrows as well as the respective proteases. The predicted membrane topology of the viral polyprotein is represented on the bottom. Retrieved from ViralZone website.[264]

1.1.8.2 Structure of the viral particles

Similar to other flaviviruses, ZIKV particles are enveloped, ranging from 50 nm (mature form) to 60 nm (immature form) in diameter.[265–267] The surface of the immature viral particles consists of a host-derived lipid bilayer coated with 60 spikes. Each spike is formed by three copies of the prM protein and three copies of the E protein, yielding a total of 180 copies of each protein. After maturation, the 60 prM-E trimers are converted into 90 M-E dimers, flattening the surface of the virus and providing a smoother spherical appearance (**Figure 9A**). The M protein lies underneath the E protein layer. The E proteins are organized as dimers and displayed in raft configuration (**Figure 9C**). Each raft is made up of three dimers set out parallel to each other. In total, there are 30 rafts arranged in a herringbone pattern. Half of a raft represents an asymmetric unit with a total of 60 units in an icosahedral-like symmetry (**Figure 9B**) [229,266]. The inner core of 28-30 nm harbors the viral genome that is associated with 120 copies of the C protein (60 C dimers), creating the viral nucleocapsid.[211,268]

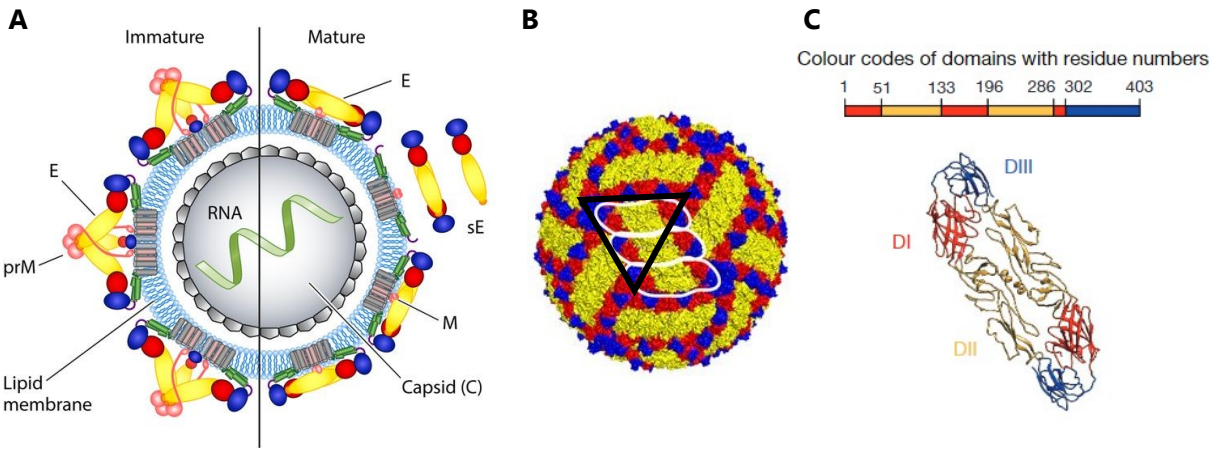

Figure 9 – Schematic representations of ZIKV viral particle. (A) Schematic representation of the immature (left) and mature (right) forms of the ZIKV viral particle. After maturation, the 60 prM-E trimers are reorganized into 90 M-E dimers, flattening the surface of the virus. **(B)** The viral particle has in total 30 rafts arranged in a herringbone pattern. Each raft is composed of three dimers set out parallel to each other (marked in white). Half of a raft represents an asymmetric unit (marked in black) with a total of 60 units in an icosahedral-like symmetry. **(C)** Representation of the nucleotide sequence of the E protein color-coded by domains (top). The E proteins are organized as dimers and each E protein possesses three domains: domain I (DI), domain II (DII), and domain III (DIII) that are represented in red, yellow, and blue, respectively. Retrieved and adapted from Kostyuchenko *et al.*, 2020, and Heinz and Stiasny, 2017.[229,269]

1.1.8.3 Viral life cycle

The ZIKV life cycle is still poorly studied and thus, it is presumed to resemble the life cycle of other flaviviruses. The cycle begins with the interaction of the E glycoprotein with multiple cell surface molecules that allow the attachment and the concentration of the viral particles at the cell surface before their contact with the receptors.[270] A variety of molecules were described to participate in this process. The binding of the viral particles to these attachment factors is relatively nonspecific and with low affinity. Glycosaminoglycans, such as heparan sulfate and chondroitin sulfate, were reported to be involved in ZIKV attachment.[271] Shortly after, these data were contradicted by Gao *et al.* which showed that heparan sulfate is required for DENV attachment, but not for ZIKV.[272] Concerning viral receptors, Hamel *et al.* identified the participation of the dendritic cell-specific intracellular adhesion molecule-3-grabbing non-integrin (DC-SIGN), the T cell immunoglobulin mucin (TIM)-1 and members of the Tyro3-AXL-MER (TAM) family of receptor tyrosine kinases (RTKs) in the ZIKV entry process, emphasizing AXL as a promising ZIKV receptor.[273] Besides the direct interaction of the E protein with the cell surface receptors, the entry of ZIKV and other flaviviruses was shown to occur as well through exposed phosphatidylserines (PS) present on the viral membrane in the case of the PS receptors, TIM and TAM. For the TAM receptors, the contact is made indirectly via the receptor ligands, for instance, the growth-arrest-specific 6 (gas6) and protein S (pros1).[274–276] However, there are conflicting data regarding the role of AXL

in ZIKV entry that seems to be cell type-specific. While AXL appears to be essential for viral infection in human endothelial cells, skin cells, and brain glial cells, it is not required in human neuronal progenitor cells, cerebral organoids, and mice lacking interferon receptors.[273,275–282] During the timeframe of the present study, other molecules were reported to play a role during ZIKV entry, including α2,3-linked sialic acid, heat shock protein 70 (Hsp70), integrin αvβ5, neuronal cell adhesion molecule (NCAM1), and glucose-regulating protein 78 (GRP78).[283–287] Still, the exact mechanism of how ZIKV enters the host cell involving all these receptors remains unknown. The viral attachment and entry into a host cell dictate to a certain extent the tropism and pathogenicity of a virus.[288] In a conventional situation, a virus binds with high affinity to a specific receptor, mimicking its ligand and tricking the host cell into taking up the virus. However, for certain viruses, such as the flaviviruses, viral entry is a far more complex process and usually involves several cellular attachment factors and receptors. These can function either simultaneously, independently of each other, sequentially, or in a cell-type-specific manner.[6,289] ZIKV enters the host cell by receptor-mediated endocytosis in clathrin-coated pits.[290] Nevertheless, recent evidence indicates that internalization can also occur in caveolin-coated pits.[291] After reaching the endosomal compartment, the acidic environment induces conformational changes of the E glycoprotein, triggering the fusion between the viral envelope and the endosomal membrane.[266,292] Consequently, the disintegration of the viral capsid (uncoating) leads to the release of the viral genome into the cytoplasm, concluding the entry process. The genomic RNA acts as mRNA and serves as the template for both translation and replication. As the viral particles lack the non-structural proteins and the viral replication is dependent on the RdRp activity of the NS5 protein, the translation of the viral genome takes place before the viral replication. The translation occurs at the ER surface and is thought to be driven by a cap-dependent mechanism.[210] Nonetheless, a recent study shows that ZIKV contains a short nucleotide sequence within the 5'UTR that functions as an internal ribosomal entry site (IRES).[293] The N-terminus of the nascent polyprotein harbors an ER-localization signal that immediately directs the ribosomes to translocate the viral polyprotein into the ER, resulting in its embedding in the ER membrane.[294] The polyprotein is cleaved co- and post-translationally into the structural and the non-structural proteins by both host and viral proteases (see chapter 1.1.8.1).[177,210] Mature C, NS3, and NS5 are soluble cytoplasmic proteins, whereas NS1 is expected to be a soluble ER luminal protein. Moreover, NS2A, NS2B, NS4A, and NS4B are ER-resident proteins, while prM and E are integral membrane proteins facing the ER lumen. Successively, the viral proteins induce the rearrangement of the ER membranes to form invaginations denominated as vesicle packets that will serve as the site for replication and assembly. Thus, allowing spatial compartmentalization between

these two events and protecting the replication machinery from cellular immune defense systems.[295–297] Subsequently, the replication complex assembles in these sites and coordinates the viral replication. The NS5 protein binds to the SLA in the 5′ UTR, which acts as a promoter, and interacts with the 3′ end of the genomic RNA due to the cyclization of the viral genome (see chapter 1.1.8.1). Hence, the RdRp domain of the NS5 protein transcribes a complementary negative-sense strand RNA, forming a dsRNA intermediate.[258,259] The helicase activity of the NS3 protein unwinds the dsRNA and the negative-sense strand RNA is used as a template for the synthesis of multiple copies of positive-sense strand RNA (asymmetric replication).[250] The cyclization of the viral genome is not required for the synthesis of the positive-sense strand RNA. Following viral replication, the negative-sense strand RNA can undergo a new cycle of RNA synthesis, whereas the positive-sense strand RNA is capped and methylated at the 5′ end as a result of the NS3 helicase and the NS5 MTase activities **(Figure 10)**.[210]

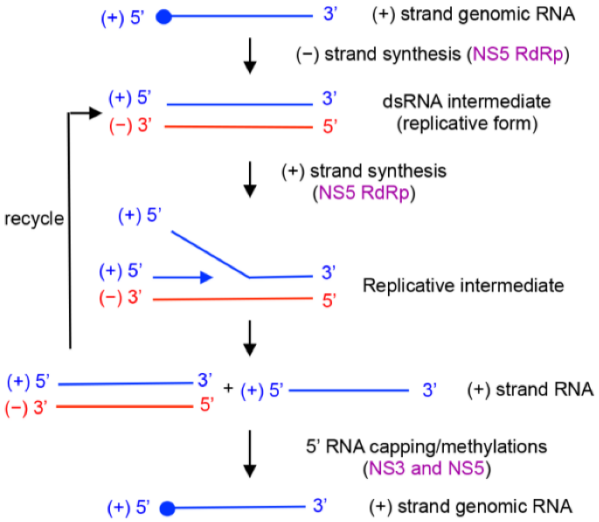

Figure 10 – Schematic representation of the synthesis of the ZIKV genomic RNA. The viral genome is a positive-sense strand RNA. The RNA-dependent RNA polymerase (RdRp) domain of the NS5 protein transcribes a complementary negative-sense strand RNA, generating a double-stranded RNA (dsRNA) intermediate. After the dissociation of the strands by the activity of the helicase domain of the NS3 protein, multiple copies of the positive-sense strand RNA are synthetized from the negative-sense strand RNA template (asymmetric replication). The formed dsRNA intermediate can be recycled for a new cycle of replication, whereas the positive-sense strand RNA is capped and methylated to originate the genomic RNA by the helicase domain of the NS3 protein and by the methyltransferase (MTase) domain of the NS5 protein, respectively. Retrieved and adapted from Klema *et al.*, 2015.[298]

After being capped and methylated, the newly synthesized genomic RNA is either translated or assembled to generate a new viral particle. The exact mechanism of ZIKV assembly is still not completely elucidated. Zhang *et al.* showed that after viral replication, the genomic RNA, the viral protease NS2B-NS3, and unprocessed C-prM-E complexes are escorted by the NS2A protein to the assembly sites, which are usually

at the opposite site of the pore of the replication vesicle. In these sites, the viral protease NS2B-NS3 and the host signal peptidase cleave the C-prM-E complex, releasing the C protein. Multiple copies of the mature C protein associate with the viral genome leading to its encapsidation. At this moment, the nucleocapsid buds into the ER lumen and consequently is wrapped by a lipid bilayer that contains the 60 trimers prM-E heterodimers.[242,295,299] Once assembled, the immature viral particle migrates using the secretory pathway, passing through the TGN. The low pH of the TGN environment induces conformational changes on the viral particles, uncovering the cleavage site of the pr peptide that is cleaved by a furin protease. The now mature viral particle leaves the host cell by exocytosis, inducing the dissociation of the pr peptide due to the neutral pH of the extracellular environment.[224,225,300] The released viral particles can then infect other cells and a new infection cycle starts. A summarized scheme of the viral life cycle is represented in **Figure 11**.

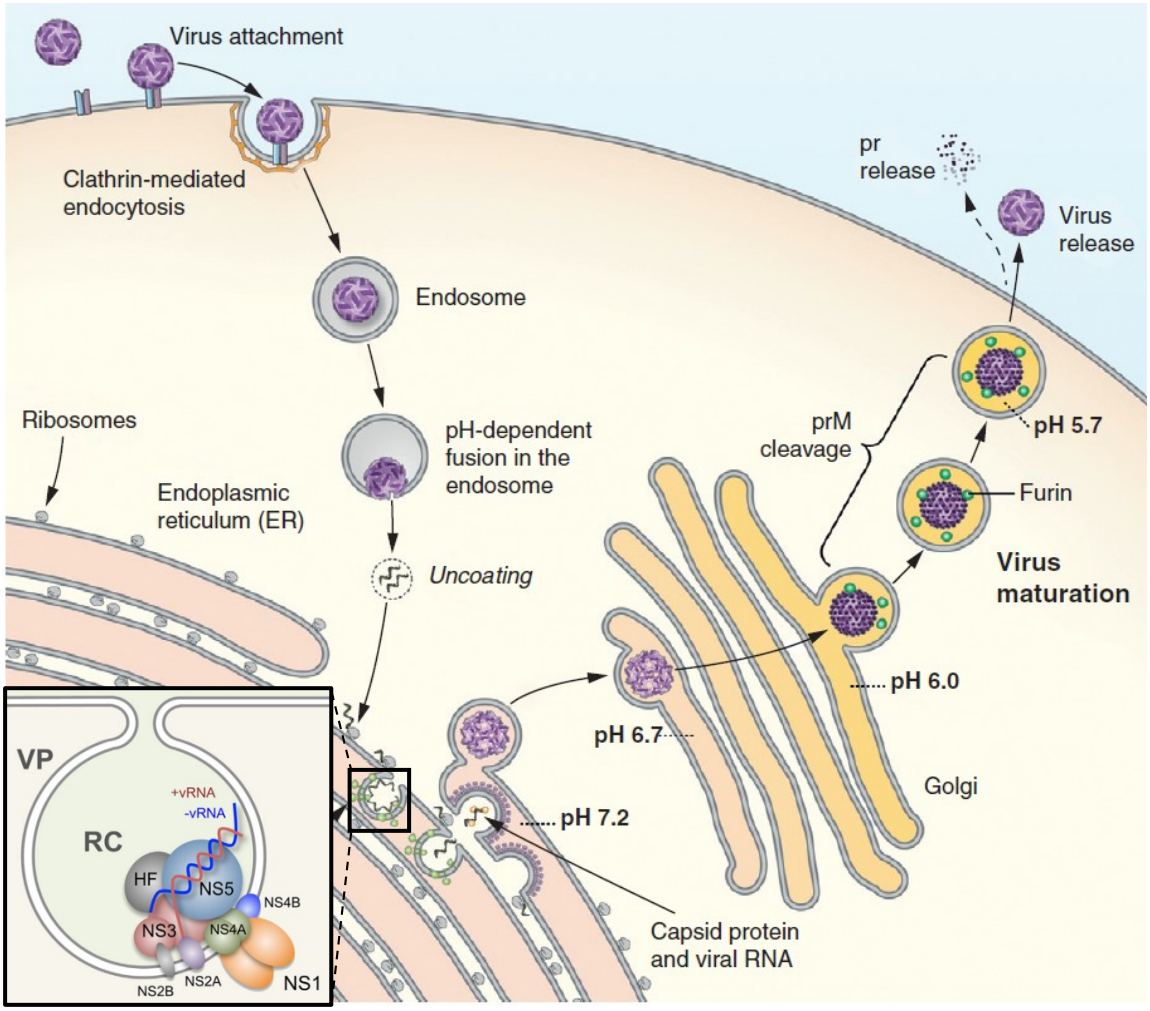

Figure 11 – Schematic representation of the life cycle of flaviviruses. The viral life cycle initiates with the attachment and the uptake of the viral particle by receptor-mediated endocytosis in clathrin-coated pits. In the endosomal compartment, the low environmental pH triggers conformational changes of the viral particle, allowing the fusion between the viral envelope and the endosomal membrane. As a result, the viral genomic RNA is released into the cytoplasm where is translated into structural and nonstructural

proteins. The viral proteins induce ER-invaginations called vesicle packets that will serve as replication and assembly sites. The replication complex (RC), formed by the viral non-structural proteins (NS1, NS2A, NS2B, NS3, NS4A, NS4B, and NS5) and host factors (HF) assembles in these sites to coordinate viral replication. After viral replication, the genomic RNA associates with the C protein and bud into the ER lumen, acquiring a lipid bilayer coated with multiple E-prM heterodimers. Following assembly, the immature viral particle moves through the secretory pathway and undergoes maturation in the TGN, where a furin protease splits the pr peptide from the M protein due to pH-induced conformational changes. The infectious viral particle leaves the cell by exocytosis and the pr peptide is released from the viral particle. Retrieved and adapted from Pierson and Diamond, 2012, and Muller and Young, 2013.[301,302]

1.2 Epidermal growth factor receptor

1.2.1 Classification and structure

The human epidermal growth factor receptor (EGFR) is one of the four members of the ErbB/HER family within the superfamily of the receptor tyrosine kinases (RTKs).[303,304] The family name has its origin in the name of the avian erythroblastic leukemia viral oncogene B (*erbb)* that encodes an aberrant homolog of the human EGF receptor (HER).[305,306] Besides the EGFR, also known as HER1 or ErbB1, the ErbB/HER family comprises the ErbB2 (HER2 or Neu), the ErbB3 (HER3), and the ErbB4 (HER4). Despite the human *erbb* genes being located in different chromosomes, the four molecules encoded by these possess similar structures.[307–309]

The *egfr* sequence is highly conserved among different species. The human *egfr* is approximately 245 kb long and encodes a 1210 aa EGFR precursor protein that undergoes maturation.[310] EGFR is a 170 kDa glycoprotein with 1186 aa residues that is composed of an N-terminal extracellular ligand-binding domain (the ectodomain), a single transmembrane domain, an intracellular juxtamembrane domain, a tyrosine kinase domain, and a C-terminal regulatory domain (**Figure 12**). The latter three domains are referred to as the endodomain.[311] The extracellular segment is heavily N-glycosylated at about 12 sites and comprises four subdomains: domain I (aa 1-165), domain II (aa 165-310), domain III (aa 310-480), and domain IV (aa 480-620), also denominated as L1, CR1, L2, and CR2 domains, respectively.[311,312] The domains I and III participate in ligand binding (L1 and L2), whereas the homologous domains II and IV contain cysteine-rich motifs (CR1 and CR2) that are involved in disulfide bond formation during receptor dimerization (**Figure 12**).[311] The extracellular region is connected to the intracellular juxtamembrane domain by a single transmembrane helix of about 23 aa residues, anchoring the receptor to the plasma membrane.[312] The juxtamembrane segment with 42 aa residues regulates the receptor downregulation, sorting, signal specificity, and RTK activity.[313–319] Moreover, this domain appears to be necessary for receptor dimerization and efficient ligand-induced receptor

internalization.[320,321] The juxtamembrane region is followed by the tyrosine kinase (TK) domain. The TK domain is vital for the activation of the receptor as it catalyzes the transfer of a γ-phosphate of adenosine triphosphate (ATP) to the hydroxyl-group of a tyrosine residue and consequently, activating downstream signaling cascades. This domain possesses a bilobate structure with a smaller N-lobe and a larger C-lobe, separated by a catalytic cleft where ATP binds (**Figure 12**).[322] The N-lobe contains the glycine-rich phosphate-binding loop (P-loop) that interacts with the phosphates of the ATP, whereas the C-lobe holds the activation loop (A-loop) that binds to the magnesium ion, which promotes ATP binding, and acts as a platform for docking the substrate peptide.[322–324] Lastly, the C-terminal domain is a long tail segment, harboring multiple tyrosine residues that, when phosphorylated by the TK domain, function as binding sites for adaptor molecules and signaling proteins that transmit the signal further downstream.[325,326] The proximal segment (first part) of the C-tail is associated with autoinhibitory effects that regulate the TK activity of the receptor.[327,328] Within this segment, an α-helix, denominated as AP2 helix due to its interaction with the clathrin adaptor protein complex 2 (AP2), mediates EGFR internalization and downregulation.[329] This domain also contains threonine and serine residues that are linked to receptor downregulation.[330]

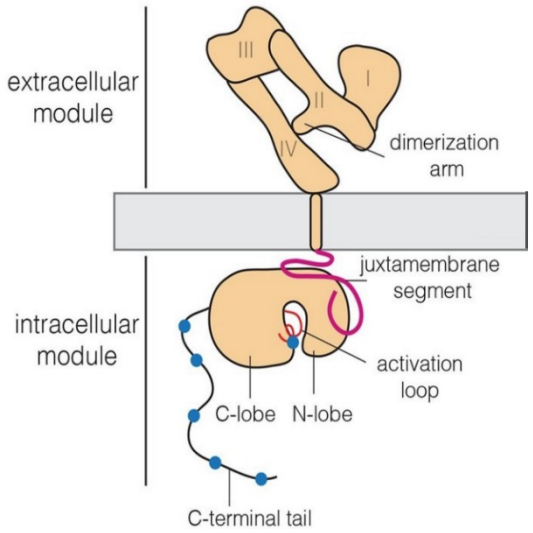

Figure 12 – Schematic representation of the EGFR structure. EGFR is a transmembrane protein with an N-terminal extracellular ligand-binding domain that is divided into four subdomains (domain I to IV). The domains I and III participate in ligand binding, whereas domains II and IV are involved in disulfide bond formation during receptor dimerization. The EGFR is anchored to the plasma membrane by a single transmembrane domain. The intracellular part of the receptor comprises the juxtamembrane domain, the tyrosine kinase domain, and the C-tail domain. The tyrosine kinase domain has a bilobate structure with a smaller N-lobe and a larger C-lobe, forming a catalytic cleft where ATP binds. The C-lobe harbors the activation loop that binds to the magnesium ion, which is required for ATP binding, and functions as a docking site for the substrate peptide. The C-terminal tail possesses several tyrosine residues that

can be phosphorylated and serve as docking sites for signaling molecules and consequently, activating downstream signaling cascades. Retrieved and adapted from Huang *et al.*, 2016.[331]

1.2.2 Activation

EGFR and the other members of the ErbB/HER family are activated upon ligand binding. ErbB ligands can be divided into three groups based on their relative affinity to the ErbB/HER receptor. The first group is comprised of ligands that bind exclusively to EGFR, including the canonical ligand EGF, transforming growth factor α (TGFα), amphiregulin, and epigen.[332–335] The second group includes heparin-binding EGF-like growth factor, betacellulin, and epiregulin, which can bind to EGFR and Erb4.[336–338] The last group covers the neuroregulins that bind to Erb3 and Erb4 or exclusively to Erb4.[339–341] More recently, angiogenin and connective tissue growth factor were identified as EGFR ligands, whereas prolidase as the only ligand of the ErbB2 receptor that was acknowledged until now.[342–344] ErbB ligands are synthesized as type I transmembrane precursor proteins, similar to EGFR, and the extracellular domain is subjected to cleavage by metalloproteases at the plasma membrane, releasing functional soluble growth factors.[345,346] These growth factors share an EGF-like motif with six conserved cysteine residues that are involved in the receptor binding, creating three intramolecular disulfide bridges with the domain.[347,348] In the absence of ligand binding, EGFR is mainly present as a monomer at highly ordered portions of the plasma membrane called lipid rafts, which are rich in cholesterol and sphingolipids.[349,350] A minor amount of EGFR dimers also exists, but ligand binding is required for the activation of downstream signaling cascades.[351,352] Monomeric EGFR adopts a tethered conformation in which domain II interacts with domain IV, sequestering the dimerization loop and auto-inhibiting the receptor (**Figure 13**).[353] Upon ligand binding to both domains I and III, the ectodomain is reorganized and the dimerization loop in the domain II is exposed, leading to a stable extended conformation. The uncovered dimerization loop can then interact with the dimerization loop of another ligand-bound receptor, forming a 2:2 ligand:receptor dimer with the ligands facing outwards from the dimer interface (**Figure 13**).[354,355] EGFR can homodimerize or heterodimerize with other ErbB receptors, but the ErbB2 is the preferred dimerization partner due to its constant extended conformation, allowing dimerization in the absence of ligand.[356,357] The domain IV also contributes to EGFR dimerization, but less than the domain II.[358] These interactions cause the rotation of the transmembrane domains, parallel to the plane of the plasma membrane.[359] Consequently, the intracellular symmetric inactive kinase dimer is dissociated and reoriented, forming an asymmetric active kinase dimer. In this asymmetric dimer configuration, the C-lobe of one monomer (activator kinase) interacts with the N-lobe of the other monomer (receiver kinase), activating it allosterically and inducing conformational changes in the N-lobe of the receiver kinase

(**Figure 13**). These conformational changes promote the "open configuration" of the A-loop, enabling the binding of ATP and substrate.[360] The interaction between activator and receiver kinases is stabilized by the C-terminal juxtamembrane segment of the receiver kinase that binds to the C-lobe of the activator kinase.[361,362] EGFR TK activation leads to autophosphorylation and transphosphorylation of the tyrosine residues in the C-terminal tails of the dimer.[363,364] Certain tyrosine residues are phosphorylated by other kinases, namely c-Src and protein kinase C (PKC).[365,366] These phosphorylated residues serve as docking sites for adaptor proteins that have Scr homology-2 (SH2) or phosphotyrosine binding (PTB) domains.[367,368] These proteins can then recruit other signaling molecules that will be phosphorylated and transduce EGFR-mediated signals.[369] Lipid rafts can assist in EGFR signaling transduction, acting as platforms to facilitate the crosstalk between signaling molecules.[370] However, upon activation, EGFR leaves these sites to be internalized.[371,372]

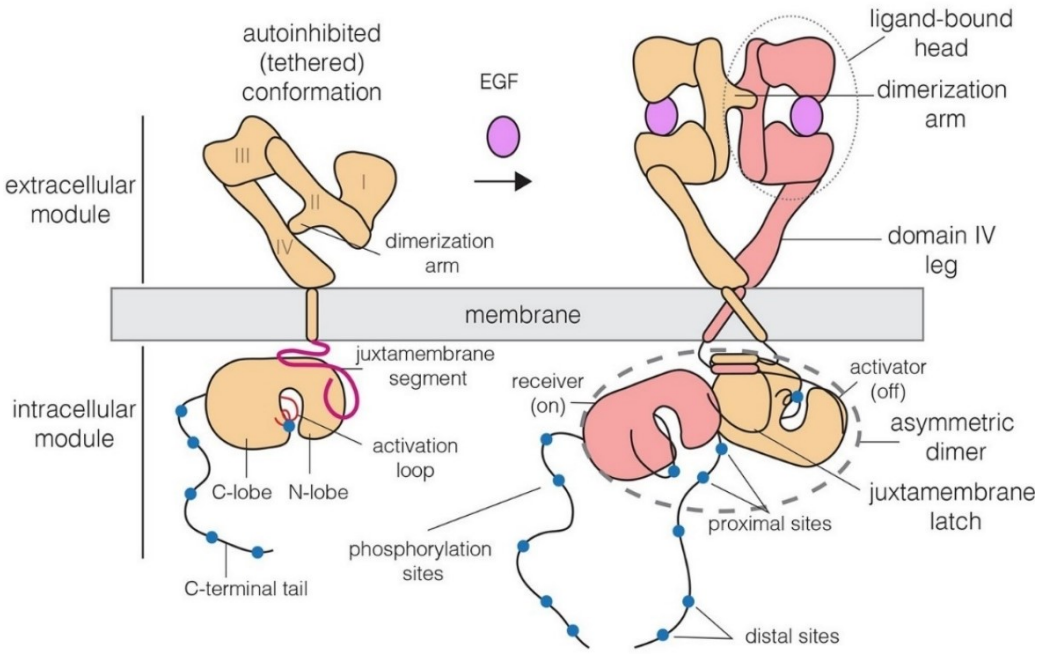

Figure 13 – Schematic representation of EGFR dimerization and activation. Upon ligand binding to domains I and III, such as EGF, the ectodomain undergoes conformational changes, which uncover the dimerization arm, promoting EGFR dimerization. EGFR dimerization causes the rotation of the transmembrane domain and allows the interaction of the C-lobe of the activator kinase (in yellow) with the N-lobe of the receiver kinase (in red), allosterically activating it. Activation of the EGFR tyrosine kinase results in the autophosphorylation and transphosphorylation of the tyrosine residues in the C-terminal tail (in blue), which act as docking sites for adaptor and signaling proteins. Retrieved and adapted from Huang *et al.*, 2016.[331]

1.2.3 Signaling pathways

Depending on the phosphorylation pattern of EGFR, different signal transduction pathways are activated, including the Ras/Raf/mitogen-activated protein kinase kinase (MEK)/ extracellular signal-regulated kinase (ERK) (hereafter referred to as MAPK/ERK) pathway, the phosphoinositide 3-kinase/Akt (PI3K/Akt) pathway, the phospholipase C gamma/protein kinase C (PLCγ/PKC) pathway, and the JAK/STAT pathway (**Figure 14**). Overall, these pathways regulate cell growth, proliferation, differentiation, migration, survival, angiogenesis, cytoskeleton organization, metabolism, immune and inflammatory response.[373–377]

The MAPK/ERK pathway is initiated with the recruitment and binding of the growth factor receptor-binding protein 2 (Grb2) directly to the phosphorylated tyrosine residues (Y1068 and Y1086) in the C-terminal tail of EGFR via its SH2 domain or indirectly through the adaptor Src homology 2 domain-containing transforming protein (Shc). Shc binds to the phosphorylated tyrosine residues of EGFR (Y1173 and Y1148) via its PTB domain or (Y1173) its SH2 domain and is phosphorylated, allowing the binding of Grb2.[378,379] Sequentially, Grb2 interacts via its SH3 domains with the Son of Sevenless protein 1 (SOS), a guanine nucleotide exchange factor, forming a complex.[380] The formation of this complex facilitates SOS in exchanging guanosine diphosphate (GDP) for guanosine triphosphate (GTP) in Ras, a small GTPase anchored to the plasma membrane, resulting in Ras activation.[381,382] Subsequently, Ras-GTP promotes the activation of the serine/threonine kinase c-Raf that phosphorylates and activates MEK1 and MEK2.[383,384] MEK activation further phosphorylates and activates ERK1 and ERK2.[385,386] Once activated, ERK1 and ERK2 can phosphorylate cytoplasmic proteins. Additionally, they can translocate to the nucleus, where they are responsible for phosphorylating and activating multiple transcription factors.[387]

Furthermore, activation of the PI3K/Akt pathway occurs with the indirect binding of the p85 regulatory subunit of the PI3K to the phosphorylated tyrosine residues in the C-terminal tail of EGFR through the adaptor Grb2-associated binding protein 1 (Gab1), which in turn binds to the adaptor protein Grb2 and the latter to EGFR.[388,389] The bound p85 regulatory subunit recruits the p110 catalytic subunit, forming the fully active PI3K.[390] The p110 catalytic subunit of PI3K can also be activated by binding to Ras-GTP.[391,392] Once activated, the p110 catalytic subunit of PI3K phosphorylates the phosphatidylinositol 4,5-biphosphate (PIP_2) present in the plasma membrane, producing the second messenger phosphatidylinositol 3,4,5-triphosphate (PIP_3).[393,394] Consecutively, Akt, also known as protein kinase B, and the upstream 3-phosphoinositol-dependent protein kinase 1 (PDK1) are recruited to the plasma

membrane and bind to PIP_3.[395] PDK1 phosphorylates and activates Akt that in turn phosphorylates several proteins, activating or inhibiting them.[396]

Moreover, the PLCγ directly interacts with the phosphorylated tyrosine residues (Y992 and Y1173) in the C-terminal tail of EGFR and hydrolyzes PIP_2, generating inositol 1,3,5-triphosphate (IP_3) and 1,2-diacylglycerol (DAG), two second messengers.[397,398] First, IP_3 induces the release of calcium ions (Ca^{2+}) from the ER.[399] Ca^{2+} together with DAG can activate the classical PKC isoforms, which are responsible for phosphorylating several proteins crucial in multiple biological functions.[400]

STAT proteins can bind directly to the phosphorylated tyrosine residues (Y954 and Y974) in the C-terminal tail of EGFR and become activated through phosphorylation by the EGFR TK domain.[401,402] However, STAT proteins can also be activated downstream of EGFR by c-Src and JAKs.[403,404]

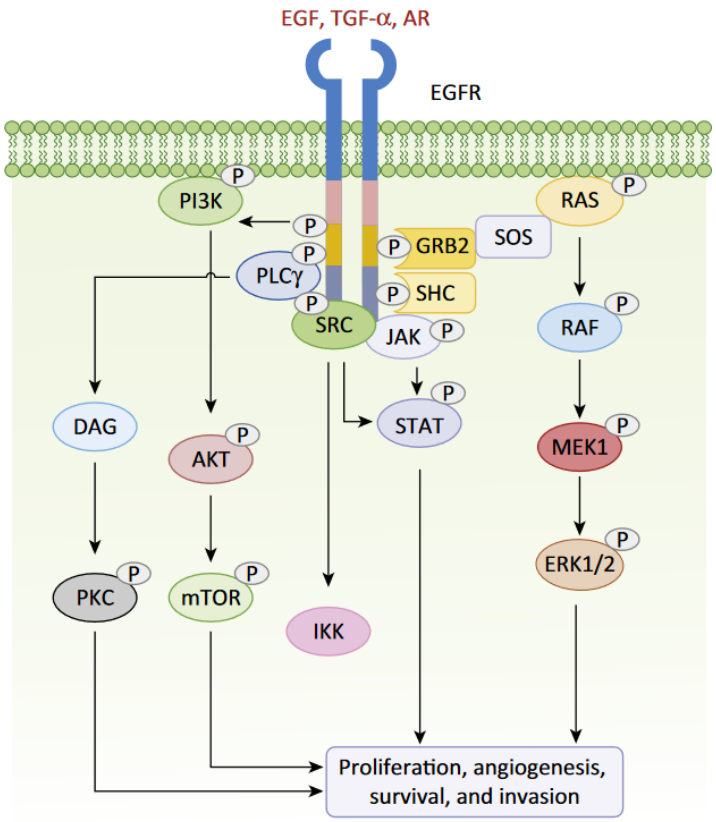

Figure 14 – Schematic representation of the different signaling transduction pathways activated upon EGFR activation. Upon ligand binding, such as EGF, transforming growth factor α (TGFα), and amphiregulin (AR), several tyrosine residues of the C-terminal tail of EGFR are phosphorylated by the TK domain of EGFR or by other kinases (Src and PKC), serving as docking sites for adaptor proteins, namely Grb2, Shc, PI3K, and PLCγ. Subsequently, these proteins can recruit other signaling molecules that will be phosphorylated and transduce EGFR-mediated signals. EGFR activation leads to the activation of the following downstream signaling cascades: the Ras/Raf/MEK/ERK (MAPK/ERK), the PLCγ/DAG/PKC, the PI3K/AKT/mTOR, and the SRC/JAK/STAT pathways. These pathways control important cellular functions, including cell proliferation, angiogenesis, survival, and invasion/migration. Retrieved from Shostak and Chariot, 2016.[405]

1.2.4 Internalization and endocytic sorting

Following activation, EGFR can be internalized by either clathrin-mediated endocytosis (CME) or clathrin-independent endocytosis (CIE) depending on the ligand, its concentration, and the number of receptors activated **(Figure 15)**.[406,407] In the presence of a lower concentration of ligand (<1-2 ng/mL), activated EGFR is recruited by the AP2 adaptor complex to cluster in clathrin-coated pits and is internalized by CME.[408–410] By contrast, higher concentrations of ligand (≥ 10 ng/mL) favor ubiquitination and CIE of EGFR.[411] Consequently, ubiquitinated EGFR is targeted to lysosomal degradation, eliminating the exceeding amounts of activated receptors and counteracting excessive signaling within the cell.[412] EGFR is ubiquitinated at multiple lysine residues of the TK domain by the E3 ubiquitin-ligase Cbl that can directly bind to the phosphorylated tyrosine residue Y1045 of EGFR or indirectly by forming a complex with Grb2 (Y1068 or Y1086).[413–415] Once internalized, EGFR reaches the early endosomes where it is sorted. Ubiquitinated EGFR is recognized by the endosomal sorting complex required for transport (ESCRT) machinery and directed into the intraluminal vesicles of multivesicular bodies (MVBs).[416] Then, MVBs fuse with lysosomes, resulting in EGFR degradation by the hydrolytic enzymes from the lysosome.[417] Unlike the ubiquitinated EGFR, the non-ubiquitinated, which is the case of EGFR internalized by CME, is recycled back to the cell surface.[418] CME seems to prolong EGFR signaling.[419] Nevertheless, in both cases EGFR is dephosphorylated by tyrosine protein phosphatases that inactivate the receptor before it is transported to the plasma membrane or degraded.[420,421] Moreover, the intensity and the duration of the signal and the type of ligand can also influence the fate of EGFR.[420,421] EGF-EGFR interaction is stable to endure the lower pH in the endosomes, enabling the receptor to be degraded. However, TGFα dissociates under these conditions and undergoes deubiquitination, escaping from lysosomal degradation and being recycled back to the plasma membrane.[422,423]

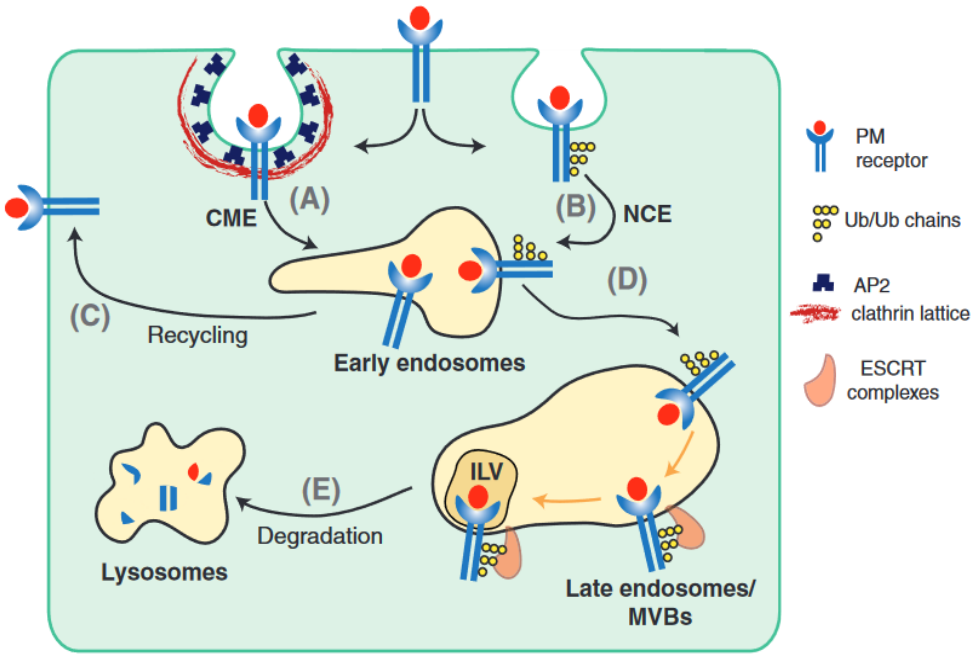

Figure 15 – Schematic representation of EGFR endocytic sorting. (A) With a low concentration of EGF, EGFR interacts with the adaptor protein complex 2 (AP2), promoting EGFR internalization by clathrin-mediated endocytosis (CME). **(B)** With a high concentration of EGF, EGFR is ubiquitinated (Ub), favoring EGFR internalization non-clathrin endocytosis (NCE). **(C)** In the early endosomes, EGFR is sorted. Non-ubiquitinated EGFR is recycled back to the cell surface. **(D)** Ubiquitinated EGFR is directed to intraluminal vesicles (ILVs) of the multivesicular bodies (MVBs) by the endosomal sorting complex required for transport (ESCRT) machinery. **(E)** MVBs fuse with lysosomes leading to the degradation of EGFR by lysosomal hydrolytic enzymes. Retrieved and adapted from Conte and Sigismund, 2016.[424]

1.2.5 The role of EGFR in the life cycle of viruses

EGFR regulates several crucial cellular processes as mentioned before. Therefore, it is an appealing host factor for viruses to exploit through direct binding by mimicking EGFR ligands or indirectly. Multiple viruses manipulate the EGFR-mediated endocytosis or the EGFR-mediated signaling to enter the host cells, to facilitate viral replication, or even to antagonize the host antiviral responses.[6]

The plasma membrane and the actin cortex, which lay beneath the plasma membrane, are major barriers to virus entry. Nevertheless, viruses have found different ways to overcome these, namely by pH-independent fusion at the plasma membrane together with the modulation of EGFR signaling to reorganize the actin cortex, or by triggering receptor-mediated endocytosis. Human cytomegalovirus (HCMV) enters the host cells by pH-independent fusion at the cell surface and directly interacts with EGFR, activating PI3K-dependent RhoA and cofilin, and consequently, causing the reorganization of the actin filaments.[425–427] Similar effect was described for herpes simplex virus type 1 (HSV-1), and Epstein-Barr virus (EBV).[428–430] However, most viruses enter the host cell by receptor-mediated endocytosis as it allows them to have direct transport to the replication sites, minimizing the exposure to immune surveillance molecules.[431]

Innumerous viruses rely on EGFR activation and endocytosis for viral entry. HCV activates EGFR and downstream signaling cascades via the tetraspanin CD81 and is co-internalized with the CD81-EGFR receptor complex.[432] In the case of the influenza A virus (IAV), EGFR is activated and promotes the IAV uptake due to the incapacity of the receptors sialic acids in transmitting signals across the plasma membrane.[433] EGFR is also a co-receptor for the flavivirus JEV, human papillomavirus type 16 (HPV16), vaccinia virus (VACV), respiratory syncytial virus (RSV), hepatitis B virus (HBV), transmissible gastroenteritis virus (TGEV), adeno-associated virus serotype 6 (AAV6), among others.[434–440] Besides viral entry, EGFR-mediated signaling cascades were described to facilitate viral replication and pathogenesis by inducing angiogenesis, protein synthesis, cytoskeleton reorganization, cell motility, and survival. This holds true for HCMV, EBV, human immunodeficiency virus 1 (HIV-1), severe acute respiratory syndrome coronavirus 1 (SARS-CoV-1), and more recently, for SARS-CoV-2.[429,441–444] Moreover, IAV-, rhinovirus (RV)-, HCV-, and RSV-induced activation of EGFR and downstream signaling cascades can promote inflammation and antagonize host antiviral responses by activating STAT proteins, stimulating the release of inflammatory mediators and reducing interferon production.[445–449]

Viruses modulate EGFR signaling through the expression of viral or host proteins that alter *egfr* expression. On the one hand, the HBV X protein and the EBV lysosomal-associated membrane protein 1 increase *egfr* expression.[450,451] On the other hand, adenovirus E1A protein decreases *egfr* expression to promote host apoptosis, whereas HCMV activates a transcriptional repressor of *egfr* to obligate the infected cell to respond only to virus-mediated signals, optimizing viral production.[452,453] Additionally, viruses control EGFR signaling by interfering with the degradation and recycling of EGFR. HIV-1, HPV16, and HCV diminish EGFR degradation to prolong EGFR-mediated signaling.[454–456] Other viruses, such as adenovirus and HSV-1, contribute to EGFR degradation.[457,458]

2. Aim of the study

The ZIKV life cycle is poorly understood and characterized. Understanding the viral life cycle and uncovering novel virus-host interactions are essential to the development of a specific antiviral therapy. Previous research work on the identification of suitable cell culture models to study ZIKV infection revealed that the Chinese hamster ovary (CHO) cells do not support viral infection.[459] Given the absence of both ZIKV infection and endogenous EGFR in these cells, this study aimed to investigate the relevance of EGFR and of EGFR-dependent signaling for the ZIKV life cycle *in vitro*.

3. Materials

3.1 Cells

3.1.1 Bacterial cells

Table 1 – Bacterial strain used in this study, the respective genotype and source.

Bacterial strain	Genotype	Source
Escherichia coli (E.coli) K12 strain DH5α	F^- Φ80*lac*ZΔM15 Δ(*lac*ZYA-*arg*F) U169 *rec*A1 *end*A1 *hsd*R17(r_k^-, m_k^+) *pho*A *sup*E44 *thi*-1 *gyr*A96 *rel*A1 λ^-	Invitrogen, Carlsbad, USA

3.1.2 Eukaryotic cells

Table 2 – Eukaryotic cells required for this study, the respective description and origin. All cell lines were obtained from ATCC (Manassas, USA).

Cell line	Description	Origin
A549	Adenocarcinoma human alveolar basal epithelial cells	Giard *et al.*, 1962 [460]
CHO	Epithelial Chinese hamster ovary cells	Kao and Puck, 1968 [461]
Vero	African green monkey kidney cells	Yasumura and Kawakita, 1962 [462]

3.1.3 Stable cells

Table 3 – Stable cells used in this study, the respective description, antibiotic concentration for cell selection and source.

Cell line	Description	Selection	Source
A549-Off-target #1	A549 cells generated by CRISPR/Cas9 system using non-specific single guide RNA that serves as control for EGFR knockout, clone no. 1	Puromycin [1.5 µg/mL]	Generated during this work

Cell line	Description	Selection	Source
A549-Off-target #2	A549 cells generated by CRISPR/Cas9 system using non-specific single guide RNA that serves as control for EGFR knockout, clone no. 2	Puromycin [1.5 µg/mL]	Generated during this work
A549-EGFR KO sgRNA 1 #5	A549 cells generated by CRISPR/Cas9 system using single guide RNA 1 that have EGFR knocked out, clone no. 5	Puromycin [1.5 µg/mL]	Generated during this work
A549-EGFR KO sgRNA 1 #16	A549 cells generated by CRISPR/Cas9 system using single guide RNA 1 that have EGFR knocked out, clone no. 16	Puromycin [1.5 µg/mL]	Generated during this work
A549-EGFR KO sgRNA 2 #8	A549 cells generated by CRISPR/Cas9 system using single guide RNA 2 that have EGFR knocked out, clone no. 8	Puromycin [1.5 µg/mL]	Generated during this work
A549-EGFR KO sgRNA 2 #10	A549 cells generated by CRISPR/Cas9 system using single guide RNA 2 that have EGFR knocked out, clone no. 10	Puromycin [1.5 µg/mL]	Generated during this work
A549-ZIKV RLuc*	A549 cells electroporated with *in vitro* transcribed capped ZIKV-*Renilla* Luciferase (ZIKV-RLuc) RNA and cultivated until a quasi-stable expression of the luciferase activity was obtained	No selection	Generated during this work
CHO-EGFR #22.2	CHO cells that stably overexpress EGFR, clone no. 22.2	G418 [0.5 mg/mL]	Friedrich *et al.*, 2013 [463]
CHO-EGFR #45	CHO cells that stably overexpress EGFR, clone no. 45	G418 [0.5 mg/mL]	Friedrich *et al.*, 2013 [463]

* Since no selection was performed this cell line is only considered quasi-stable

3.2 Tissue

Table 4 – Tissue required for this study and the respective origin.

Tissue	Origin
Liver	Golden Syrian hamster

3.3 ZIKV strains

Table 5 – ZIKV strains used in this study and the respective source.

Strain	Source
976 Uganda	European Virus Archive Global (EVAg), Marseille, FR
H/PF/2013 French Polynesia	European Virus Archive Global (EVAg), Marseille, FR
FSS13025 Cambodia	Shan *et al.*, 2017 [464]

3.4 Plasmids

Table 6 – Plasmids required for this study, the respective description and source.

Plasmid	Description	Source
pACYC177 ZIKV-RLuc	*Renilla* luciferase reporter ZIKV construct. Full-length ZIKV with the *Renilla* luciferase gene inserted downstream at the 76th nucleotide of the viral capsid gene	Shan *et al.*, 2017 [464]
pSpCas9(BB)-2A-Puro (PX459) V2.0 #62988	CRISPR/Cas9 cloning vector	Addgene, Massachusetts, USA; Ran *et al.*, 2013 [465]
PX459-Off Target	CRISPR/Cas9 cloning vector coding for a non-specific single guide RNA	Dr. Fabian Elgner, Paul-Ehrlich-Institut

Plasmid	Description	Source
PX459-EGFR sgRNA1	CRISPR/Cas9 cloning vector coding for an EGFR single guide RNA 1	Matthias Dusemund, Paul-Ehrlich-Institut
PX459-EGFR sgRNA2	CRISPR/Cas9 cloning vector coding for an EGFR single guide RNA 2	Matthias Dusemund, Paul-Ehrlich-Institut

3.5 Oligonucleotides

3.5.1 Cloning

Table 7 – Oligonucleotides used in cloning and the respective sequence in the 5′ → 3′ direction. Oligonucleotides were synthesized by Biomers.net (Ulm, DE).

Oligonucleotide	Sequence (5′→ 3′)
sgRNA_off-target_fwd	cac cgc act acc aga gct aac tca
sgRNA_off-target_rev	aaa ctg agt tag ctc tgg tag tgc
sgRNA_EGFR_1_fwd	cac cgt gag ctt gtt act cgt gcc t
sgRNA_EGFR_1_rev	aaa cag gca cga gta aca agc tca c
sgRNA_EGFR_2_fwd	cac cga gta aca agc tca cgc agt
sgRNA_EGFR_2_rev	aaa cac tgc gtg agc ttg tta ctc

3.5.2 Polymerase chain reaction (PCR)

Table 8 – Oligonucleotides used in PCR and the respective sequence in the 5′ → 3′ direction. Oligonucleotides were synthesized by Eurofins Genomics (Ebersberg, DE).

Oligonucleotide	Sequence (5′ → 3′)
EGFR_seq_4_fwd	att ttt tgc cta ctg gag ctc tta cag g
EGFR_seq_4_rev	ata ggc aaa tgg tgc aaa gca ggg

3.5.3 Real-time PCR (qPCR)

Table 9 – Oligonucleotides used in qPCR and the respective sequence in the 5′ → 3′ direction. Oligonucleotides were synthesized by Biomers.net (Ulm, DE).

Oligonucleotide	Sequence (5′→ 3′)
EGFR_fwd	tgg tta tgt cct cat tgc
EGFR_rev	aga taa gac tgc taa ggc
GAPDH_fwd	gac ccc ttc att gac ctc aac
GAPDH_rev	tgg act gtg gtc atg agt cc
hRPL27_fwd	aaa gct gtc atc gtg aag aac
hRPL27_rev	gct gct act ttg cgg ggg tag
ZIKV_fwd	aga tcc cgg ctg aaa cac tg
ZIKV_rev	ttg caa ggt cca tct gtc cc

3.5.4 Sequencing

Table 10 – Oligonucleotides used in sequencing and the respective sequence in the 5′ → 3′ direction. Oligonucleotides were synthesized by Biomers.net (Ulm, DE) or by Eurofins Genomics (Ebersberg, DE).

Oligonucleotide	Sequence (5′ → 3′)
Human U6 SeqF_Insert	act atc ata tgc tta ccg taa c
EGFR_seq_4_fwd*	att ttt tgc cta ctg gag ctc tta cag g
EGFR_seq_4_rev*	ata ggc aaa tgg tgc aaa gca ggg

* Same as used in PCR

3.6 Molecular weight markers

3.6.1 DNA markers

Table 11 – DNA markers used in this study and the respective manufacturer.

DNA marker	Manufacturer
GeneRuler 1 kb DNA Ladder	Thermo Fisher Scientific, Waltham, USA
GeneRuler 1 kb Plus DNA Ladder	Thermo Fisher Scientific, Waltham, USA

3.6.2 Protein markers

Table 12 – Protein markers used in this study and the respective manufacturer.

Protein marker	Manufacturer
PageRuler™ Prestained Protein Ladder	Thermo Fisher Scientific, Waltham, USA
PageRuler™ Plus Prestained Protein Ladder	Thermo Fisher Scientific, Waltham, USA

3.7 Antibodies

3.7.1 Primary antibodies

Table 13 – Primary antibodies required in this study and the respective species, clonality, dilution used in Western blot (WB) or immunofluorescence (IF) and manufacturer.

Antibody	Species	Clonality	Dilution (WB/IF)	Manufacturer
Anti-AXL (C89E7) #8661	Rabbit	Monoclonal	1:1000/ -	Cell Signaling Technology, Danvers, USA
Anti-β-Actin A5316	Mouse	Monoclonal	1:10000 /-	Sigma-Aldrich, St.Louis, USA

Antibody	Species	Clonality	Dilution (WB/IF)	Manufacturer
Anti-EEA1	Rabbit	Monoclonal	-/1:200	Thermo Fisher Scientific, Waltham, USA
Anti-EGFR (528) sc-120	Mouse	Monoclonal	-/1:50	Santa Cruz Biotechnology, Dallas, USA
Anti-EGFR [EP38Y] (ab52894)	Rabbit	Monoclonal	1:3000/ 1:250	Abcam, Cambridge, UK
Anti-ERK1/2 (137F5) #4695	Rabbit	Monoclonal	1:1000/ -	Cell Signaling Technology, Danvers, USA
Anti-Flavivirus Group Antigen clone D1-4G2-4-15	Mouse	Monoclonal	-/1:300	Merck Millipore, Darmstadt, DE
Anti-phospho-EGFR (Tyr1068) #2234	Rabbit	Polyclonal	1:1000/ -	Cell Signaling Technology, Danvers, USA
Anti-phospho-ERK1/2 (Thr202/Tyr204) #9106	Mouse	Monoclonal	1:1000/ -	Cell Signaling Technology, Danvers, USA
Anti-ZIKV E (K87)	Rabbit	Monoclonal	1:500/-	Dr. Sami Akhras, Paul-Ehrlich-Institut [466]

3.7.2 Secondary antibodies

Table 14 – Secondary antibodies required in this study and the respective species, clonality, dilution used in Western blot (WB) or immunofluorescence (IF) and manufacturer.

Antibody	Species	Clonality	Dilution (WB/IF)	Manufacturer
Anti-mouse IgG HRP	Sheep	Polyclonal	1:2000/-	Cytiva, Marlborough, USA
Anti-rabbit IgG HRP	Donkey	Polyclonal	1:2000/-	Cytiva, Marlborough, USA
Anti-mouse IRDye®680RD	Donkey	Polyclonal	1:5000/-	LI-COR Biosciences, Lincoln, USA
Anti-mouse IRDye®800CW	Donkey	Polyclonal	1:5000/-	LI-COR Biosciences, Lincoln, USA
Anti-rabbit IRDye®680RD	Donkey	Polyclonal	1:5000/-	LI-COR Biosciences, Lincoln, USA
Anti-rabbit IRDye®800CW	Donkey	Polyclonal	1:5000/-	LI-COR Biosciences, Lincoln, USA
Anti-mouse IgG-Alexa 488	Donkey	Polyclonal	-/1:1000	Invitrogen, Carlsbad, USA
Anti-mouse IgG-Alexa 546	Donkey	Polyclonal	-/1:1000	Invitrogen, Carlsbad, USA
Anti-rabbit IgG-Alexa 488	Donkey	Polyclonal	-/1:1000	Invitrogen, Carlsbad, USA
Anti-rabbit IgG-Alexa 546	Donkey	Polyclonal	-/1:1000	Invitrogen, Carlsbad, USA

3.8 Fluorescent dyes

Table 15 – Fluorescent dyes used in this study, the respective dilution used and manufacturer.

Fluorescent dye	Dilution	Manufacturer
DAPI (stock 100 µg/mL)	1:300	CARL ROTH GmbH + Co. KG, Karlsruhe, DE
Phalloidin-Atto 633 (stock 20 µM)	1:400	Sigma-Aldrich, St.Louis, USA

3.9 Inhibitors

3.9.1 Kinase inhibitors

Table 16 – Kinase inhibitors used in this study, the respective concentration used, target and manufacturer.

Inhibitor	Concentration	Target	Manufacturer
Erlotinib	25 µM	EGFR	Selleckchem, Houston, USA
Sorafenib	2 µM	Raf	Bayer, Leverkusen, DE
PD98059	50 µM	MEK	Merck Millipore, Darmstadt, DE

3.9.2 Lysosomal inhibitors

Table 17 – Lysosomal inhibitors required in this study, the respective concentration used, target and manufacturer.

Inhibitor	Concentration	Target	Manufacturer
Chloroquine	25 µM	Endosomal and lysosomal acidification	Sigma-Aldrich, St.Louis, USA

3.9.3 Phosphatase inhibitors

Table 18 – Phosphatase inhibitors required in this study, the respective dilution used, target and manufacturer.

Inhibitor	Dilution	Target	Manufacturer
Halt™ Phosphatase Inhibitor Cocktail (100x)	1:100	Serine/threonine and protein tyrosine phosphatases	Thermo Fisher Scientific, Waltham, USA
Phosphatase cocktail inhibitor 2	1:500	ATPases, alkaline, protein tyrosine, acid and phosphoprotein phosphatases	Sigma-Aldrich, St.Louis, USA

3.9.4 Protease inhibitors

Table 19 – Protease inhibitors used in this study, the respective concentration used, target and manufacturer.

Inhibitor	Concentration	Target	Manufacturer
Aprotinin	10 µg/mL	Serine proteases	AppliChem GmbH, Darmstadt, DE
EDTA	2.5 mM	Metalloproteases	Paul-Ehrlich-Institut facilities, Langen, DE
Halt™ Protease Inhibitor Cocktail, EDTA free (100x)	1x	Aspartic acid, cysteine and serine proteases	Thermo Fisher Scientific, Waltham, USA
Leupeptin	25 µg/mL	Serine and cysteine proteases	AppliChem GmbH, Darmstadt, DE

Inhibitor	Concentration	Target	Manufacturer
Pepstatin	20 µg/mL	Acidic and aspartic proteases	AppliChem GmbH, Darmstadt, DE
PMSF	1 mM	Serine proteases	AppliChem GmbH, Darmstadt, DE

3.9.5 Protein synthesis inhibitors

Table 20 – Protein synthesis inhibitors required in this study, the respective concentration used, target and manufacturer.

Inhibitor	Concentration	Target	Manufacturer
Cycloheximide	20 µg/mL	Protein synthesis	Sigma-Aldrich, St.Louis, USA

3.10 Reagents for cell culture

Table 21 – Reagents used in cell culture and the respective manufacturer.

Reagent	Manufacturer
Dulbecco's Modified Eagle's Medium (DMEM) high glucose (4.5 g/L glucose)	Sigma-Aldrich, St.Louis, USA
Fetal bovine serum (FBS superior)	Bio & Sell GmbH, Feucht, DE
G418 (Geneticin)	Merck Millipore, Darmstadt, DE
L-glutamine	Bio & Sell GmbH, Feucht, DE
Phosphate buffered saline (PBS) without Ca^{2+} and Mg^{2+}	Paul-Ehrlich-Institut facilities, Langen, DE
Penicillin/streptomycin	Paul-Ehrlich-Institut facilities, Langen, DE
Puromycin dihydrochloride	Sigma-Aldrich, St.Louis, USA
Trypsin/EDTA (0.05% Trypsin)	Paul-Ehrlich-Institut facilities, Langen, DE

3.11 Kits

Table 22 – Commercial kits required in this study and the respective manufacturer.

Kit	Manufacturer
DNeasy Blood & Tissue kit	QIAGEN, Hilden, DE
Gaussia-GLOW Juice Luciferase Assay kit	PJK GmbH, Kleinblittersdorf, DE
Maxima™ SYBR™ Green qPCR Master Mix (2x)	Thermo Fisher Scientific, Waltham, USA
Pierce™ BCA Protein Assay Kit	Thermo Fisher Scientific, Waltham, USA
PTK reagent kit	PamGene International BV, Den Bosch, NL
QIAGEN Plasmid Maxi Kit	QIAGEN, Hilden, DE
QIAprep Spin Miniprep Kit	QIAGEN, Hilden, DE
QIAquick PCR Purification Kit	QIAGEN, Hilden, DE
T7-Scribe Standard RNA IVT Kit	CELLSCRIPT, Wisconsin, USA

3.12 Enzymes

Table 23 – Enzymes used in this study and the respective manufacturer.

Enzyme	Manufacturer
ClaI	New England Biolabs GmbH, Frankfurt am Main, DE
T4 PNK	New England Biolabs GmbH, Frankfurt am Main, DE
FastDigest BbsI	Thermo Fisher Scientific, Waltham, USA
Q5 Hot Start DNA Polymerase	New England Biolabs GmbH, Frankfurt am Main, DE

Enzyme	Manufacturer
RevertAid H Minus Reverse Transcriptase	Thermo Fisher Scientific, Waltham, USA
RQ1 RNase-free DNase	Promega GmbH, Walldorf, DE
T7 DNA ligase	New England Biolabs GmbH, Frankfurt am Main, DE

3.13 Fine chemicals and reagents

Table 24 – Fine chemicals and reagents required in this study and the respective manufacturer.

Product	Manufacturer
3´-0-Me-m7G(5')ppp(5')G RNA Cap Structure Analog	New England Biolabs GmbH, Frankfurt am Main, DE
6-aminohexanoic acid	CARL ROTH GmbH + Co. KG, Karlsruhe, DE
Acetic acid	CARL ROTH GmbH + Co. KG, Karlsruhe, DE
Acetone	CARL ROTH GmbH + Co. KG, Karlsruhe, DE
Agarose LE	Genaxxon bioscience GmbH, Ulm, DE
Ampicillin	CARL ROTH GmbH + Co. KG, Karlsruhe, DE
APS	CARL ROTH GmbH + Co. KG, Karlsruhe, DE
ATP	Thermo Fisher Scientific, Waltham, USA
β-mercaptoethanol	CARL ROTH GmbH + Co. KG, Karlsruhe, DE
BSA fraction V	CARL ROTH GmbH + Co. KG, Karlsruhe, DE
Bradford reagent	Sigma-Aldrich, St.Louis, USA
Bromophenol blue	Sigma-Aldrich, St.Louis, USA
Butanol	CARL ROTH GmbH + Co. KG, Karlsruhe, DE

Product	Manufacturer
Calcium chloride	CARL ROTH GmbH + Co. KG, Karlsruhe, DE
Chloroform	CARL ROTH GmbH + Co. KG, Karlsruhe, DE
Crystal violet	Sigma-Aldrich, St.Louis, USA
DABCO	Merck Millipore, Darmstadt, DE
DEPC	CARL ROTH GmbH + Co. KG, Karlsruhe, DE
DMSO	Genaxxon bioscience GmbH, Ulm, DE
dNTPs mix (10 mM each)	Thermo Fisher Scientific, Waltham, USA
DTT	Biomol GmbH, Hamburg, DE
EDTA	CARL ROTH GmbH + Co. KG, Karlsruhe, DE
EGF	Sigma-Aldrich, St.Louis, USA
Ethanol (pure)	CARL ROTH GmbH + Co. KG, Karlsruhe, DE
Ethidium bromide	AppliChem GmbH, Darmstadt, DE
Formaldehyde (37.5%)	CARL ROTH GmbH + Co. KG, Karlsruhe, DE
Glycerol	GERBU Biotechnik GmbH, Heidelberg, DE
HEPES	CARL ROTH GmbH + Co. KG, Karlsruhe, DE
Hydrochloric acid	CARL ROTH GmbH + Co. KG, Karlsruhe, DE
Isopropanol	CARL ROTH GmbH + Co. KG, Karlsruhe, DE
Immobilon® Forte Western HRP substrate	Merck Millipore, Darmstadt, DE
Immobilon™ Western HRP substrate	Merck Millipore, Darmstadt, DE
Methyl-β-cyclodextrin	Sigma-Aldrich, St.Louis, USA
Methanol	CARL ROTH GmbH + Co. KG, Karlsruhe, DE

Product	Manufacturer
Mowiol 4-88	Sigma-Aldrich, St.Louis, USA
peqGOLD Trifast	Peqlab Biotechnologie GmbH, Erlangen, DE
Phenol	AppliChem GmbH, Darmstadt, DE
PrestoBlue™ cell viability reagent	Thermo Fisher Scientific, Waltham, USA
Random hexamer primer	Thermo Fisher Scientific, Waltham, USA
Roti 40 acrylamide/bisacrylamide (29:1)	CARL ROTH GmbH + Co. KG, Karlsruhe, DE
Roti®-block (10x)	CARL ROTH GmbH + Co. KG, Karlsruhe, DE
RQ1 DNase Stop Solution	Promega GmbH, Walldorf, DE
SDS	CARL ROTH GmbH + Co. KG, Karlsruhe, DE
SeaPlaque™ agarose	Lonza Group AG, Basel, CH
Skim milk powder	CARL ROTH GmbH + Co. KG, Karlsruhe, DE
Sodium acetate	CARL ROTH GmbH + Co. KG, Karlsruhe, DE
Sodium chloride	CARL ROTH GmbH + Co. KG, Karlsruhe, DE
Sodium hydroxide	CARL ROTH GmbH + Co. KG, Karlsruhe, DE
Sodium deoxycholate	CARL ROTH GmbH + Co. KG, Karlsruhe, DE
TEMED	AppliChem GmbH, Darmstadt, DE
Tris	CARL ROTH GmbH + Co. KG, Karlsruhe, DE
Triton X-100	Sigma-Aldrich, St.Louis, USA
Tween 20	CARL ROTH GmbH + Co. KG, Karlsruhe, DE

3.14 Buffers, media and solutions

3.14.1 Buffers

Table 25 – Buffers required in this study and the respective composition. All buffers were prepared with ultrapure water unless indicated otherwise.

Buffer	Composition
Anode buffer I	20% Ethanol (v/v) 300 mM Tris base
Anode buffer II	20% Ethanol (v/v) 25 mM Tris base
Cathode buffer	20% Ethanol (v/v) 40 mM 6-aminohexanoic acid
HEPES buffered saline (HeBS 2x) from Paul-Ehrlich-Institut facilities	50 mM HEPES 280 mM NaCl 1.5 mM Na_2HPO_4 pH 7.05
Luciferase lysis buffer (1x)	50% Luciferase lysis-juice 2x (v/v) see chapter 3.10
PBS without Ca^{2+} and Mg^{2+} from Paul-Ehrlich-Institut facilities	137 mM NaCl 2.7 mM KCl 1.8 mM KH_2PO_4 10 mM Na_2HPO_4 pH 7.1
PBST	0.5% Triton X-100 (v/v) in PBS
Radioimmunoprecipitation assay (RIPA) buffer	50 mM Tris-HCl pH 7.2 150 mM NaCl 0.1% SDS (w/v) 1% Sodium deoxycholate (w/v) 1% Triton X-100 (v/v)

Buffer	Composition
SDS running buffer (10x) from Paul-Ehrlich-Institut facilities	250 mM Tris base 2 M Glycine 1% SDS (w/v) pH 8.3
SDS loading buffer (4x)	4% SDS (w/v) 125 mM Tris-HCl pH 6.8 10% Glycerol (v/v) 10% β-Mercaptoethanol (v/v) 0.02% Bromophenol blue (w/v)
Separating gel buffer	1.5 M Tris base 0.4% SDS (w/v) pH 8.8
Stacking gel buffer	0.5 M Tris 0.4% SDS (w/v) pH 6.7
TAE buffer (50x) from Paul-Ehrlich-Institut facilities	2 M Tris base 1 M NaAc 50 mM EDTA pH 8
TBST from Paul-Ehrlich-Institut facilities	50 mM Tris 150 mM NaCl 0.05 or 0.1% Tween 20 (v/v) pH 7.8
TFB1 buffer	100 mM $RbCl_2$ 30 mM CH_3CO_2K 10 mM $CaCl_2$ 50 mM $MnCl_2$ 15% Glycerol (v/v) pH 5.8 adjusted with acetic acid

Buffer	Composition
TFB2 buffer	10 mM MOPS 10 mM $RbCl_2$ 75 mM $CaCl_2$ 15% Glycerol (v/v) pH 6.8 adjusted with acetic acid

3.14.2 Commercial buffers

Table 26 – Commercial buffers required in this study and the respective manufacturer.

Buffer	Manufacturer
Cell lysis buffer (10x)	Cell Signaling Technology, Danvers, USA
CutSmart® buffer (10x)	New England Biolabs GmbH, Frankfurt am Main, DE
DNA Gel Loading Dye buffer (6x)	Thermo Fisher Scientific, Waltham, USA
FastDigest buffer (10x)	Thermo Fisher Scientific, Waltham, USA
M-PER™ Mammalian Extraction Buffer	Thermo Fisher Scientific, Waltham, USA
NEBuffer 2 (10x)	New England Biolabs GmbH, Frankfurt am Main, DE
Q5 reaction buffer (5x)	New England Biolabs GmbH, Frankfurt am Main, DE
Reverse Transcriptase reaction buffer (5x)	Thermo Fisher Scientific, Waltham, USA
RQ1 DNase reaction buffer (10x)	Promega GmbH, Walldorf, DE
T4 ligation buffer (10x)	New England Biolabs GmbH, Frankfurt am Main, DE

3.14.3 Media

Table 27 – Media used in this study and the respective composition.

Medium	Composition
Freezing medium	70% growth medium (v/v) 20% FBS superior (v/v) 10% DMSO (v/v)
Growth medium for A549, A549-ZIKVRLuc, CHO, and Vero cells	DMEM high glucose (4.5 g/L) 10% FBS superior (v/v) 1% Penicillin/Streptomycin (v/v) 2 mM L-glutamine
Growth medium for CHO-EGFR #22.2 and #45 cells	DMEM high glucose (4.5 g/L) 10% FBS superior (v/v) 1% Penicillin/Streptomycin (v/v) 2 mM L-glutamine 0.5 mg/mL G418
Growth medium for A549-Off-target #1, A549-Off-target #2, A549-EGFR KO sgRNA1 #5, A549-EGFR KO sgRNA1 #15, A549-EGFR KO sgRNA2 #8, and A549-EGFR KO sgRNA2 #10	DMEM high glucose (4.5 g/L) 10% FBS superior (v/v) 1% Penicillin/Streptomycin (v/v) 2 mM L-glutamine 1.5 µg/mL puromycin
Lysogeny broth medium (LB) from Paul-Ehrlich-Institut facilities	1% Tryptone (w/v) 0.5% Yeast extract (w/v) 1% NaCl (w/v) pH 7.0
Mounting medium	10% Mowiol 4-88 (w/v) 25% Glycerol (v/v) 2.5% DABCO (w/v) 100 mM Tris-HCl pH 8.5

3.14.4 Solutions

Table 28 – Solutions required in this study and the respective composition. All solutions were prepared with ultrapure water unless indicated otherwise.

Solution	Composition
DEPC-H_2O	0.1% DEPC (v/v)
Crystal violet	0.1% Crystal violet (w/v) in 20% ethanol (v/v)
SeaPlaque™ agarose	4% SeaPlaque™ agarose (w/v)
Sodium acetate	3 M NaAc pH 5.2 adjusted with acetic acid
Penicilillin/Streptomycin (100x)	10.000 U/mL Penicillin 10 mg/mL Streptomycin

3.15 Consumables

Table 29 – Consumables used in this study and the respective manufacturer.

Product	Manufacturer
Cell culture flasks (T25, T75, T175)	Greiner Bio-One GmbH, Frickenhausen, DE
Cell culture plates (6-well plates)	Sarstedt AG, Nümbrecht, DE
Cell culture plates (12-, 24-, 96-well plates)	Greiner Bio-One GmbH, Frickenhausen, DE
Cell scrapers	A. Hartenstein GmbH, Würzburg, DE
CryoPure tubes (2 mL)	Sarstedt AG, Nümbrecht, DE
Falcon tubes (15 mL, 50 mL)	Greiner Bio-One GmbH, Frickenhausen, DE
Fixer type F 1-2	C & L GmbH, Planegg, DE
FrameStar® 96 PCR Plate for LC480	GeneON, Ludwigshafen, DE

Product	Manufacturer
Developer type E 1-3	C & L GmbH, Planegg, DE
Electroporation cuvettes (4 mm)	VWR International GmbH, Darmstadt, DE
Gel-Loading pipet tips	Corning Inc., Corning, USA
Graduated pipettes (2 mL, 5 mL, 10 mL, 25 mL)	Greiner Bio-One GmbH, Frickenhausen, DE
Glass beads 4 mm	CARL ROTH GmbH + Co. KG, Karlsruhe, DE
Hyperfilm ECL	Cytiva Europe GmbH, Freiburg, DE
Microscope coverslips (18 mm)	CARL ROTH GmbH + Co. KG, Karlsruhe, DE
Microscope slides SuperFrost® Plus	Thermo Fisher Scientific, Waltham, USA
Omnifix®-F Syringes (1, 5, 10, 20 mL)	B.Braun, Melsungen, DE
Protein tyrosine kinase PamChip®	PamGene International BV, Den Bosch, NL
Parafilm	Bemis, Bonn, DE
PCR reaction tubes	Sarstedt AG, Nümbrecht, DE
Phase Lock Gel Heavy (2 mL)	5 PRIME GmbH, Hamburg, DE
Pipette tips (10 µL, 100 µL, 300 µL, 1000 µL)	Sarstedt AG, Nümbrecht, DE
Pipette tips with filter (10 µL, 100 µL, 300 µL, 1000 µL)	Sarstedt AG, Nümbrecht, DE
Reaction tubes (1.5 mL, 2 mL)	Sarstedt AG, Nümbrecht, DE
RotiLabo® syringe filters (0.22 µm)	CARL ROTH GmbH + Co. KG, Karlsruhe, DE
Sterican® single-use hypodermic needles	B.Braun, Melsungen, DE

Product	Manufacturer
Transfer membrane ROTI® PVDF 0.45 µm	CARL ROTH GmbH + Co. KG, Karlsruhe, DE
Whatman paper 3 mm	VWR International GmbH, Darmstadt, DE

3.16 Devices

Table 30 – Devices required in this study and the respective manufacturer.

Device	Manufacturer
Accu-jet® pro pipette controller	BRAND GMBH + CO KG, Wertheim, DE
AGFA Curix 60 X-ray film processor	Agfa Healthcare GmbH, Mortsel, BE
Avanti J-26 XPI centrifuge	Beckman Coulter, Brea, USA
Axiovert 40C inverted phase-contrast microscope	Carl Zeiss, Oberkochen, DE
Bacterial incubator Innova 44	New Brunswick Scientific Co., Inc., Edison, USA
CO2 incubator Heracell™ 150i	Thermo Fisher Scientific, Waltham, USA
CO2 incubator Heraeus® BBD6220	Thermo Fisher Scientific, Waltham, USA
Confocal laser scanning microscope LSM 510	Zeiss, Oberkochen, DE
Confocal laser scanning microscope Leica TCS SP8	Leica Camera AG, Wetzlar, DE
Eclipse Ti	Nikon, Minato City, JP
Electrophoresis power supply EPS 301	Cytiva, Marlborough, USA
Gene Pulser Xcell electroporation system	Bio-Rad Laboratories, Hercules, USA

Device	Manufacturer
Hemocytometer	CARL ROTH GmbH + Co. KG, Karlsruhe, DE
Heraeus Fresco™ 17 microcentrifuge	Thermo Fisher Scientific, Waltham, USA
Heraeus™ Multifuge™ X1 centrifuge	Thermo Fisher Scientific, Waltham, USA
Heraeus™ Multifuge™ 1S-R centrifuge	Thermo Fisher Scientific, Waltham, USA
Heraeus™ Multifuge™ X3 FR centrifuge	Thermo Fisher Scientific, Waltham, USA
Hypercassette™	Cytiva, Marlborough, USA
Horizontal electrophoresis system HE33	Cytiva, Marlborough, USA
ImageQuant800 CCD Imager	Cytiva, Marlborough, USA
Infinite M1000 microplate reader	Tecan, Männedorf, CH
Intas gel documentation system	Intas Science Imaging Instruments GmbH, Göttingen, DE
LightCycler® 480 Instrument II	Roche, Basel, CH
Mini centrifuge Rotilabo®	CARL ROTH GmbH + Co. KG, Karlsruhe, DE
Mr. Frosty™ Freezing Container	Thermo Fisher Scientific, Waltham, USA
NanoDrop™ One C	Thermo Fisher Scientific, Waltham, USA
Odyssey® CLx Imaging System	LI-COR Biosciences, Lincoln, USA
Orion II LB 965 Microplate Luminometer	Berthold Technologies GmbH & Co. KG, Bad Wildbad, DE
Pipettes Research	Eppendorf AG, Hamburg
PamStation®12 System	PamGene International BV, Den Bosch, NL

Device	Manufacturer
Promax 1020 platform shaker	Heidolph Instruments GmbH & Co. KG, Schwabach, DE
RCT Classic magnetic stirrer heater	IKA®, Staufen, DE
S20 – SevenEasyTM pH meter	Mettler Toledo, Columbus, USA
Sartorius balance LP 6000 200S	Sartorius, Göttingen, DE
SONOPULS HD 2200 sonicator	Bandelin, Berlin, DE
Sorvall SLA1500 fixed angle rotor	Thermo Fisher Scientific, Waltham, USA
Standard incubator B 28	BINDER GmbH, Tuttlingen, DE
Standard power pack P25	Biometra, Göttingen, DE
SterilGard®III Advance	The Baker Company, Maine, DE
Stuart roller mixer SRT9	Bibby Scientific, Stone, UK
TE77 ECL semi-dry transfer unit	Cytiva, Marlborough, USA
Thermocycler	VWR International GmbH, Darmstadt, DE
Thermomixer compact	Eppendorf, Hamburg, DE
Triple Wide Mini vertical electrophoresis system	VWR International GmbH, Darmstadt, DE
UV transilluminator UVT2020	Intas Science Imaging Instruments GmbH, Göttingen, DE
VACUSAFE™ Vacuum Aspiration System	INTEGRA Biosciences Deutschland GmbH, Biebertal, DE
Vortex-Genie® 2	Scientific Industries, New York, DE
Water bath WBU 45	Memmert GmbH + Co.KG, Schwabach, DE

3.17 Software

Table 31 – Software required in this study and the respective manufacturer.

Software	Manufacturer
BioNavigator	PamGene International BV, Den Bosch, NL
Evolve12	PamGene International BV, Den Bosch, NL
Fiji (Image J)	Open source
Graph Pad Prism 8.4.2	GraphPad Software, La Jolla, USA
i-control 1.8	Tecan, Männedorf, CH
ImageQuantTL	Cytiva, Marlborough, USA
Image Studio	LI-COR Biosciences, Lincoln, USA
Image Studio Lite 5.2.5	LI-COR Biosciences, Lincoln, USA
INTAS GDS	Intas Science Imaging Instruments GmbH, Göttingen, DE
LAS X	Leica Camera AG, Wetzlar, DE
Light Cycler 480 Software version 1.5	Roche, Basel, CH
Mendeley	Mendeley, London, UK
MS Office	Microsoft, Redmond, USA
Simplicity 4.2	Berthold Technologies GmbH & Co. KG, Bad Wildbad, DE
SnapGene viewer	GSL Biotech, Chicago, USA
ZEN 2012 black edition	Zeiss, Oberkochen, DE
ZEN 2012 blue edition	Zeiss, Oberkochen, DE

4. Methods

4.1 Cell Biology

4.1.1 Bacterial cells

4.1.1.1 Cultivation and selection of transformed *E. coli*

In this study, *E. coli* K12 strain DH5α cells were used. Transformed bacteria were selected by the addition of 100 µg/mL ampicillin (w/v) to the LB medium. Single colonies of transformed bacteria carrying the desired plasmid were picked from the LB agar plates (see chapter 4.2.2), transferred into 2-5 mL of LB medium and cultivated for about 8 h at 37°C to generate a small bacterial culture. To produce overnight cultures of bacteria, LB medium was inoculated with transformed bacteria from a glycerol stock or with a small bacterial culture and cultivated aerobically for 16 h at 37°C in Erlenmeyer flasks with continuous shaking (150-200 rpm) in a bacterial incubator.

4.1.1.2 Preservation of transformed *E. coli*

To preserve transformed cells for a long duration, glycerol stocks were created. For this purpose, 10 mL of an overnight culture were centrifuged at 4.500 x g for 10 min at 4°C and the bacterial pellet was resuspended in 300 µL LB medium with ampicillin. Subsequently, the resuspended pellet was mixed with 700 µL of 100% glycerol (v/v) and stored in a cryotube at -80°C.

4.1.1.3 Harvest of transformed *E. coli*

To harvest transformed cells for plasmid DNA isolation, 5 (using QIAprep Spin Miniprep Kit) or 250 mL (using QIAGEN Plasmid Maxi Kit) of an overnight culture were centrifuged at 6.000 x g for 15 min at 4°C. The pellet was directly processed as described in chapter 4.2.3.

4.1.2 Mammalian cells

4.1.2.1 Cultivation and passaging

All cell culture procedures were performed in biosafety cabinets with vertical laminar flow following aseptic techniques, which included the use of sterile equipment, reagents and media. Cells were grown in DMEM supplemented with 10% FBS superior (v/v), 1% penicillin/streptomycin (v/v), and 2 mM L-glutamine in an incubator at 37°C with a content of 5% CO_2 and 90% relative humidity. Stably transfected cells were selected by adding either 1.5 µg/mL puromycin or 0.5 mg/mL G418 to the growth media. Adherent cells were passaged 2-3 times a week when cells reached 60%-90% confluency. During this process, the cells were gently washed with PBS and detached from the cell culture flasks or well-plates with a trypsin/EDTA solution for 5 min at 37°C.

The proteolytic activity of the trypsin was inactivated by the addition of 3 volumes of pre-warmed growth medium. Cells were resuspended and seeded in fresh growth medium at an appropriate split ratio (1:2-1:20) to maintain a propitious cell viability and growth rate. To perform the experiments, resuspended cells were counted using a hemocytometer and seeded consistently in well-plates or Petri-dishes at an adequate density.

4.1.2.2 Cryopreservation

For long-term storage of cultured cells, cryopreservation was performed. In light of this, cells with a low passage number and a 90% confluency were subjected to trypsinization, as described in 4.1.2.1. Resuspended cells were centrifuged for 5 min at 200 x g at 4°C and the cell pellet was washed with PBS. After repeating the same centrifugation step, the cell pellet was resuspended in a suitable amount of freezing medium, which has DMSO as a cryoprotective agent, and aliquoted into cryotubes. Consecutively, the cryotubes were placed into a cryo-freezing container with isopropanol and stored overnight at -80°C, allowing a slowly freezing process with a temperature reduction of about 1°C per minute. The following day, the cryotubes were transferred to the liquid nitrogen tank where they are stored at -170°C. When desired, cells were thawed by placing the cryovial in a water bath at 37°C for 1 min and transferred to a T75 flask for adhering. On the following day, the medium was changed.

4.1.2.3 Infection with ZIKV

All infection procedures and the maintenance of infectious cells were performed in a biosafety level 3 (BSL-3) facility. In this study, cells were infected with either H/PF/2013 French Polynesia or 976 Uganda strains of ZIKV, hereafter referred to as the French Polynesia (FP) and the Uganda (U) strains. These strains represent the two types of pathogenesis linked to ZIKV infection. The Uganda strain is associated with a mild condition, while the French Polynesia strain with neurological disorders. To infect cells systematically with the same amount of virus, virus stocks were prepared and the virus titer was determined as described in chapter 4.1.2.4 and chapter 4.1.2.5, respectively. In this study, cells were either infected with a multiplicity of infection (MOI) of 0.1, 1, 10, 20, and 50 depending on the goal of the experiment. MOI is the ratio of infectious viral particles added per cell. However, this does not reflect the exact number of viruses that will actually enter each cell.

4.1.2.4 Production of virus stocks from cell culture supernatant

ZIKV was propagated in Vero cells due to their high permissiveness derived from the lack of interferon response upon viral infection.[467,468] In this respective, multiple T175 flasks with $4x10^6$ seeded cells were infected with either the French Polynesia or the Uganda strain with a MOI of 0.1. Supernatants were collected at 2, and 5 days post-infection (dpi). For each batch of supernatants, dead cells and cell debris resultant from viral infection were removed by a centrifugation step at 4.500 x g for 10 min at 4°C. Afterwards, the supernatants that belonged to the same batch were pooled, aliquoted and stored at -80°C. The viral titers of each batch were determined by plaque forming assay as described in chapter 4.1.2.5.

4.1.2.5 Virus titration

The amount of virus was titrated by plaque forming assay (hereafter designated as plaque assay). To determine the intracellular virus titer by plaque assay, cells were trypsinized with 200 µL of trypsin solution at 37°C. After 3-5 min incubation, the protease activity was neutralized with 800 µL of growth medium. Cells were collected into reaction tubes and lysed through three freeze-thaw cycles at -80°C and 37°C, respectively. Subsequently, the cell suspension was centrifuged for 10 min at 5000 x g at 4°C to obtain a clear supernatant for the assay. To titrate the virus stocks, one aliquot was thawed and directly used.

To perform the plaque assay, $3x10^5$ Vero cells seeded in each well of a 6-well plate were infected with 100 µL of 10-fold dilutions (10^{-1} to 10^{-6} and one dilution per well) of supernatant. Meanwhile, the SeaPlaque™ agarose solution was boiled in a microwave and cooled in a water-bath at 65°C. After 2 h of infection at 37°C, the medium was removed, including the unbound infectious viral particles, and cells were overlayed with a 1:10 dilution of the agarose solution in pre-warmed growth medium. The agarose layer was solidified after incubation at room temperature for 15 min to prevent viral diffusion through the medium, but not affect cell-to-cell infection. To allow the visualization of plaques, cells were incubated for 4 days at 37°C. Afterwards, cells were fixed with 3.7% formaldehyde (v/v) in PBS for 20 min at 37°C. After removing the agarose overlay together with the fixation solution, cells were stained with approximately 500 µL of crystal violet solution for 15 min. Then, cells were washed once with water and the plaques in each dilution were counted. Only the wells containing more than 5 and less than 120 plaques were used to calculate the viral titers. The viral titers are expressed in plaque-forming units per mL (pfu/mL) and calculated as follow:

$$Viral\ titer\ (\frac{pfu}{mL}) = \frac{number\ of\ plaques}{dilution\ x\ inoculum\ (0.1\,mL)}$$

4.1.2.6 Binding, entry, and post-entry assays

In the binding assay, cells and the viral inoculum were pre-chilled at 4°C for 30 min. Afterwards, the cells were infected with the desired MOI at 4°C for 1 h, washed twice with PBS and lysed as described in chapter 4.1.2.15. In the entry assay, the cells were infected with the desired MOI at 37°C for 1 h, washed once with PBS and trypsinized with 200 µL of trypsin/EDTA solution for 3-5 min at 37°C to remove attached virus that are not fully internalized. 800 µL were added to each well to neutralize the trypsin activity and the cell suspension was collected into reaction tubes. Subsequently, the cells were pelleted for 10 min at 5000 x g at 4°C, washed once with PBS and centrifuged once more for 10 min at 5000 x g at 4°C. The cell pellet was lysed as described in chapter 4.1.2.15. For the post-entry assay, cells were infected with the desired MOI at 37°C for 3 h. Trypsinization and cell lysis were performed in the same manner as described for the entry assay. The successful removal of attached viruses from the cell surface was controlled by the quantification of the viral genomes by qPCR of infected cells at 4°C and subjected to trypsinization.

4.1.2.7 Electroporation

Resuspended A549, CHO, CHO-EGFR-1808 #22.2, and CHO-EGFR-1808 #45, obtained as described in chapter 4.1.2.1., were washed with ice-cold PBS and centrifuged for 5 min at 200 x g at 4°C. After performing this step twice and counting the cells using a hemocytometer, the concentration of cells was adjusted to $5x10^6$ cells/mL with PBS. Then, 800 µL of the cell suspension were mixed with 10 µg of *in vitro* transcribed RNA (see chapter 4.2.6) and placed into a 4 mm cuvette. Directly, cells were electrically pulsed a single time at 300 V and 950 µF using the Gene Pulser Xcell. After a 10 min room temperature recovery, electroporated cells were diluted in 12 mL growth medium and seeded into a T75 flask or in well-plates at an appropriate density. About 4 to 6 hours post-electroporation (hpe), when cells were adherent, the medium was changed to remove dead cells and cell debris derived from the electroporation procedure. Stable A549-ZIKV *Renilla* luciferase (A549-ZIKVRLuc) cells were generated by continuous cultivation of electroporated cells until a quasi-stable luciferase expression was achieved. Cells were cultivated in cell culture plates for 24 h before the onset of treatment (see chapter 4.1.2.14).

4.1.2.8 Transfection with calcium phosphate

A549 cells used for the generation of monoclonal EGFR knockout (KO) cells (see chapter 4.1.2.9) were transfected with calcium phosphate.[469] For this purpose, 1 µg of the desired plasmid DNA was initially diluted in ultrapure water to a final volume of 50 µL. Subsequently, the diluted DNA was mixed with 5.6 µL of 2.5 M of calcium chloride. Afterwards, the DNA-calcium chloride mixture was added drop-wise to 55.6 µL of 2x

HeBS buffer, allowing the formation of calcium phosphate-DNA co-precipitate. After 20 min incubation at room temperature, the mixture was dispersed onto the cells seeded in 6-well plates. Before transfection, the growth medium was replaced by medium containing 25 µM chloroquine to prevent lysosomal degradation of the exogenous DNA. On the following day, the chloroquine was removed by changing the growth medium.

4.1.2.9 Generation of monoclonal EGFR KO cells

At 48 hours post-transfection (48 hpi), cells transfected (see chapter 4.1.2.8) with plasmids containing either one of the sgRNA or the off-target sequence were selected with 1.5 µg/mL puromycin until the formation of resistant cell colonies (approximately two weeks). To pick cell colonies, a phase-contrast microscope was placed into a biosafety cabinet with vertical laminar flow and cell colonies were gently scraped with 10 µL trypsin solution and transferred to a 24-well plate containing growth medium. Each clone was expanded and the achievement of monoclonal EGFR KO cells was confirmed by Western blot, indirect immunofluorescence, and DNA sequencing.

4.1.2.10 EGF stimulation

To stimulate the cells with EGF, a 1:100 dilution in growth medium was primarily prepared. Then, the cells were stimulated for 30 min at 37°C with the chosen concentration of EGF also prepared in growth medium.

4.1.2.11 Cell viability assay

To choose an appropriate concentration for each inhibitor that does not affect the cell viability, the metabolic activity of treated cells was determined using the PrestoBlue™ Cell Viability reagent according to the manufacturer's instructions. In short, A549 cells were seeded in 96-well plates with $1x10^4$ cells per well and on the following day, cells were treated with a wide range of concentrations of each substance. At the desired time, the medium was removed and cells were incubated with 100 µL of PrestoBlue™ Cell Viability reagent diluted 1:10 in growth medium for 1 h at 37°C. The reagent contains resazurin that is metabolically reduced into a fluorescent compound by viable cells. The fluorescence was measured in the Infinite M1000 (excitation wavelength: 560 nm, 10 nm bandwidth; emission wavelength: 590 nm, 10 nm bandwidth). Cells treated with 2% of Triton X-100 were used as positive control. The fluorescence of the reagent was also measured to remove the background signal from all the measured values.

4.1.2.12 Determination of EGFR half-life

To determine the half-life of EGFR in ZIKV-infected cells, A549 cells were infected with either the French Polynesia or the Uganda strain (MOI=1). After 16 hpi, cells were serum-starved for 2 h to maximize the amount of EGFR at the cell surface. Subsequently, cells were co-treated with 20 µg/mL of cycloheximide and 100 ng/mL of EGF to inhibit protein translation and target EGFR for degradation, respectively. After 15, 30, 45, 60, 90, and 120 min of treatment, RIPA lysates were prepared as described in chapter 4.1.2.15 and analyzed by Western Blot. Untreated cells served as control (t=0 min). The half-life of EGFR was calculated based on an exponential decay non-linear regression analysis, y(0)=1 and plateau of y=0, using the Graph Pad Prism.

4.1.2.13 Cholesterol depletion from the plasma membrane

To selectively deplete cholesterol from the plasma membrane, methyl-beta-cyclodextrin (MβCD) was used. For this purpose, A549 cells were serum-starved for 24 h and subsequently treated with MβCD diluted in growth medium free of serum for 1 h at 37°C. Afterwards, cells were washed twice with PBS and either infected with ZIKV or treated with EGF.

4.1.2.14 Inhibition of the kinase activity of EGFR and respective MAPK/ERK signaling cascade

The kinase activity of EGFR and subsequent MAPK/ERK signaling cascade was inhibited with Erlotinib (EGFR inhibitor), Sorafenib (Raf inhibitor), and PD98059 (MEK inhibitor). A549 and A549-ZIKVRLuc cells were treated with 25 µM Erlotinib, 2 µM Sorafenib, and 50 µM PD98059 in growth medium at 37°C during the desired time. As a vehicle control, cells were treated with the correspondent amount of DMSO.

4.1.2.15 Cell lysis

At the desired time, medium was removed and cells were washed once with PBS. Different cell lysis methods were performed depending on the purpose of the experiment. For indirect immunofluorescence, cells were fixed with 3.7% formaldehyde (v/v) in PBS for 20 min at room temperature, followed by a washing step with PBS. The fixed cells were stored at 4°C until required. For the isolation of total RNA by guanidinium thiocyanate-phenol-chloroform extraction, cells or pelleted cells were lysed with 400 µL of peqGOLD Trifast™ reagent and stored at -80°C until the RNA isolation was performed. For the luciferase assay, cells were lysed with 200 µL of luciferase lysis buffer, centrifuged at 17.000 x g for 5 min and stored at -20°C until required for the assay. For Western blot, cells were lysed with 200 µL of pre-chilled RIPA buffer freshly supplemented with protease inhibitors for 10 min on ice and subsequently sonicated 10 sec using 20% power. After 10 min centrifugation at 17.000

x g and at 4°C, cell lysates were stored at -20°C until required for Bradford assay. However, for Western blot of phosphoproteins, the cells were lysed with 200 µL of pre-chilled cell lysis buffer (1x) freshly supplemented with protease inhibitors and phosphatase cocktail inhibitor 2. For the determination of the protein tyrosine kinase activity using the PamChip® peptide tyrosine kinase microarray system, cells were lysed with 200 µL pre-chilled M-PER™ Mammalian Extraction Buffer freshly supplemented with Halt™ Protease Inhibitor Cocktail (1x) and Halt™ Phosphatase Inhibitor Cocktail (1x) for 15 min on ice, followed by two centrifugations for 15 min at 17.000 x g and at 4°C. The last supernatant was divided in 20 µL aliquots and immediately stored at -80°C until required for the protein quantification using the Pierce™ BCA Protein Assay Kit.

4.1.2.16 Tissue homogenization

The liver of a golden Syrian hamster was kindly provided by Dr. Aileen Ebenig from the Division of Veterinary Medicine from the Paul-Ehrlich-Institut. The liver was rinsed a few times in PBS to remove the remaining blood. Afterwards, 100 mg of liver tissue was transferred to a douncer homogenizer and 2 mL pre-chilled RIPA buffer freshly supplemented with protease inhibitors were added. After a few manual strokes until tissue homogenization was achieved, the homogenate was incubated on ice for 10 min and subsequently centrifuged for 5000 x g for 10 min. 80 µL of the supernatant were used for Western blot analysis.

4.2 Molecular biology

4.2.1 Preparation of chemically competent *E. coli*

To produce chemically competent DH5α cells, 100 mL of LB medium without antibiotic were inoculated with 100 µL of bacterial cells in an Erlenmeyer flask and incubated overnight at 37°C in a bacterial incubator with continuous shaking (150-200 rpm). On the following day, 200 mL of pre-warmed LB medium without antibiotics were inoculated with 5 mL of the overnight culture and incubated at 37°C until reaching an optical density at 600 nm (OD_{600}) of 0.3-0.4. After 10 min incubation on ice, the bacterial culture was centrifuged for 10 min at 4.500 x g at 4°C. Afterwards, the pellet was resuspended in 80 mL of ice-cold transformation buffer 1 (TFB1) and subsequently incubated on ice for 15 min. Then, the bacterial cells were centrifuged again at 4.500 x g at 4°C for 10 min and the pellet was resuspended in 8 mL in TFB2. After 15 min incubation on ice, the cell suspension was divided into 100 µL aliquots and directly frozen using liquid nitrogen. The chemically competent cells were stored at -80°C.

4.2.2 Transformation of competent *E. coli*

To transform competent DH5α cells, a complete ligation mixture or 50-100 ng of plasmid DNA diluted in 10 µL of ultrapure water were added to one aliquot of chemically competent cells (see chapter 4.2.1). After 30 min incubation on ice, the uptake of DNA by the competent cells was carried out by heat shock at 42°C for 45 seconds and subsequently incubation on ice for 5 min. To enable the expression of the ampicillin resistance gene, 500 µL of pre-warmed LB medium without antibiotic was added to the transformed cells, following incubation for 1 h at 37°C with constant agitation at 700 rpm. Afterwards, the transformed cells were plated on a LB agar plate containing 100 µg/mL ampicillin (w/v) and incubated overnight at 37°C, allowing the selection of successfully transformed cells.

4.2.3 Isolation of plasmid DNA

The isolation of plasmid DNA from transformed cells was performed using the QIAprep Spin Miniprep Kit or the QIAGEN Plasmid Maxi kit according to the instructions of the manufacturer. The principle of the isolation is described in Birnboim and Doly.[470] Briefly, the pelleted bacteria (see chapter 4.1.1.3) were lysed with an alkaline lysis buffer containing SDS and sodium hydroxide. After neutralization, the solution was centrifuged to pellet precipitated proteins, chromosomal DNA, and cell debris. The plasmid DNA in the supernatant was purified using silica columns. In the case of the QIAGEN Plasmid Maxi kit, the plasmid DNA was precipitated with isopropanol, and subsequently washed with 70% ethanol, air-dried and dissolved in ultrapure water. The plasmid DNA was stored at -20°C.

4.2.4 Determination of the concentration of nucleic acids

The concentration of DNA or RNA in solutions was determined spectrophotometrically by measuring the absorbance of each sample at a wavelength of 260 nm (A_{260}) using the NanoDrop™ One^{c}. This is possible due to the presence of conjugated double bonds in purine and pyrimidine bases of the nucleic acids. The concentration of the nucleic acids is obtained using the Beer-Lambert law.[471] Additionally, the absorbance at 230 nm (A_{230}) and 280 nm (A_{280}) is measured as well by the device to detect contaminations of proteins or solvent residues derived from the extraction procedure. Samples are considered pure when $A_{260/280}$ and $A_{260/230}$ are between 1.8-2.0 and 2.0-2.2, respectively.

4.2.5 Restriction endonuclease digestion

To linearize circular plasmids, restriction endonuclease digestion was performed. In light of this, 40 µg of pACYC177 ZIKV-RLuc were linearized with 40 U of ClaI in 1x CutSmart® buffer. Ultrapure water was used to adjust the final volume of the reaction to 50 µL. The enzymatic reaction occurred at 37°C for 2 h.

4.2.6 *In vitro* run-off T7 transcription

To generate ZIKV-*Renilla* luciferase genomic RNA for electroporation, *in vitro* run-off T7 transcription was performed using the T7 Scribe™ Standard RNA IVT Kit following the manufacturer's instructions. Briefly, 4 µg of linearized plasmid DNA (see chapter 4.2.5) were mixed with 1x T7-Scribe™ Transcription Buffer, 2 µL T7-Scribe™ Enzyme solution, 20 U of ScriptGuard™ RNase Inhibitor, 10 mM DTT, 7.5 mM ATP, 7.5 mM CTP, 7.5 mM UTP, 1.5 mM GTP, and 6 mM 3´-0-Me-m7G(5')ppp(5')G RNA Cap Structure Analog. The ratio of cap analog: GTP used was 4:1. Ultrapure water was used to adjust the final volume to 20 µL. The enzymatic reaction took place at 37°C for 4 h. Afterwards, to degrade the template DNA 1 U RNase-Free DNase I was added to the reaction and incubated at 37°C for 15 min. Then, the *in vitro* transcribed RNA was purified by phenol-chloroform extraction and the RNA was stored at -80°C in 10 µg aliquots. The quality of the RNA was analyzed by agarose gel electrophoresis.

4.2.7 Agarose gel electrophoresis

The integrity of *in vitro* transcribed RNA (see chapter 4.2.6), PCR products (see chapter 4.2.14), and restriction endonuclease digestion products (see chapter 4.2.5) were analyzed by agarose gel electrophoresis. For this purpose, 0.7-2% LE agarose (w/v) was dissolved in 1x TAE buffer by heating in a microwave. Following the addition of 0.1 µg/mL ethidium bromide, the solution was poured into a horizontal gel electrophoresis chamber. The ethidium bromide intercalates into the nucleic acids and becomes fluorescent under UV light, emitting orange-red light at 590 nm.[472] After solidification, the agarose gel was covered with 1x TAE buffer and the samples, previously mixed with 1x DNA Gel Loading Dye buffer, were loaded onto the gel. The nucleic acids were separated at 90-120 V, visualized with a UV-transilluminator (254 nm/365 nm) and imaged using the INTAS Imaging system.

4.2.8 Phenol-chloroform extraction

To purify linearized plasmid DNA (see chapter 4.2.5) and *in vitro* transcribed RNA (see chapter 4.2.6) from aqueous solutions, phenol-chloroform extraction was performed. For this purpose, 40 µL (1/10 volume) of the sodium acetate solution were added to each sample and DEPC-H_2O was used to adjust the volume to a total of 400 µL. After the addition of 400 µL (1 volume) of phenol, samples were mixed by inversion and

centrifuged for 5 min. The upper phase was transferred to a fresh reaction tube and 400 µL (1 volume) of chloroform were added and mixed by vortexing. After transferring the samples to Phase Lock Gel tubes and a 5 min centrifugation, the upper phase was collected into a new reaction tube. The DNA and RNA present in the upper phase were precipitated by the addition of 1 mL (2.5 volumes) of ethanol and 280 µL (7/10 volume) of isopropanol, respectively. After 30 min centrifugation, the nucleic acid pellet was washed with 500 µL of 70% ethanol, air dried, and resuspended in 10-40 µL of DEPC-H_2O, depending on the size of the pellet. All centrifugation steps were performed at 17.000 x g and 4°C.

4.2.9 Guanidinium thiocyanate-phenol-chloroform extraction

Total RNA was isolated from cells using the peqGOLD Trifast™ reagent based on the method described by Chomczynski and Sacchi.[473] This reagent contains guanidinium thiocyanate and acidic phenol. Guanidinium thiocyanate is a chaotropic agent that denatures proteins, including endogenous RNases, whereas the presence of the acidic phenol leads to DNA denaturation, allowing the separation between DNA and RNA. After homogenization, 80 µL of chloroform were added to each sample, followed by vortexing and 5 min incubation at room temperature. Then, the samples were transferred to Phase Lock Gel tubes and centrifuged for another 5 min. The Phase Lock Gel tubes hold a gel that acts as a barrier and facilitates the collection of the upper phase, eliminating the contamination of the remaining phases. The RNA present in the upper phase was recovered by precipitation with 200 µL of isopropanol. After vigorous vortexing and 10 min incubation at room temperature, samples were centrifuged for 30 min. The RNA pellet was then washed with 500 µL of 75% ethanol, air-dried and resuspended in 10-15 µL of DEPC-H_2O. All centrifugation steps were performed at 17.000 x g and 4°C.

4.2.10 cDNA synthesis

To remove possible DNA contaminations resultant from the RNA isolation procedure, the samples were digested with DNase I. For this purpose, 4 µg of total RNA were incubated with 1 µL of RQ1 RNase-free DNase I, 1.1 µL of the corresponding 10x reaction buffer, and adjusted with DEPC-H_2O to a final volume of 11 µL. The digestion occurred at 37°C for 1 h. Later, the enzyme was inactivated with 1 µL of RQ1 DNase Stop Solution, followed by incubation at 65°C for 10 min. To initiate reverse transcription, 1 µL of random hexamer primer was added to each sample and subsequently incubated for 5 min at 65°C. After cooling samples on ice to allow the annealing of the primers, 4 µL of 5x reaction buffer, 2 µL of dNTP mix (10 mM each), and 1 µL of RevertAid H Minus Reverse Transcriptase (200 U) were added. Then, samples were incubated for 10 min at room temperature, enabling the extension of the

primers before 1 h incubation at 42°C. Enzyme inactivation was achieved by 10 min incubation at 70°C. The cDNA samples were stored at -20°C.

4.2.11 Real-time PCR (qPCR)

To detect and quantify specific viral genomes and intracellular transcripts, qPCR was performed using the Maxima™ SYBR™ Green 2x qPCR Master Mix and the LightCycler® 480 system. During the elongation step of the PCR, the SYBR Green dye binds to each new copy of dsDNA. Upon binding, this dye emits a fluorescence signal which is directly proportional to the amount of the target sequence amplified after each cycle. When the fluorescence signal overcomes the threshold level after a certain cycle, this cycle number is registered as a C_t (cycle threshold) value.[474] A quantitative analysis of the specific transcripts was achieved by calculating the n-fold expression using the $2^{-\Delta\Delta C_t}$ method.[475] GAPDH and hRPL27 were used as housekeeping genes. For each reaction, 3 µL of cDNA diluted 1:10 were mixed with 5 µL of Maxima™ SYBR™ Green 2x qPCR Master Mix, 0.25 µL of each oligonucleotide (initial concentration of 10 µM), 1.5 µL nuclease-free ultrapure water into a FrameStar®96 PCR plate with a final volume of 10 µL. Before placing into the LightCycler® 480 Instrument II, the plate was briefly centrifuged at 2000 x g. The qPCR program used is described in table 32.

Table 32 – Description of the qPCR program used.

Program	Temperature (°C)	Hold (s)	Ramp rate (°C/s)	Cycles
Initial denaturation	95	600	4.4	1
Denaturation	95	15	4.4	45
Annealing	56	30	2.2	
Elongation	72	30	4.4	
Melting	95	60	4.4	1
	56	30	2.2	
	97	-	0.1	
Cooling	37	30	2.2	

4.2.12 Cloning sgRNAs into PX459 plasmid

Single-guide RNAs (sgRNAs) sequences complementary to part of the EGFR DNA sequence were obtained from GenScript database and from those, oligonucleotides were designed by adding two overhangs required for cloning – forward oligonucleotide 5' CACCG and reverse oligonucleotide 5'AAAC (see chapter 3.5.1).[476] After being synthetized, 10 µM of each pair of oligonucleotides were phosphorylated with 5 U of T4 Polynucleotide Kinase (T4 PNK) in 1x T4 Ligation buffer. The volume of the reaction was adjusted with ultrapure water to a final volume of 10 µL and the reaction occurred at 37°C for 30 min. Subsequently, the phosphorylated oligonucleotides were annealed in a thermocycler at 95°C for 5 min, followed by cooling down to 25°C at 5°C/min. Afterwards, in a unique digestion-ligation reaction, 100 ng of the pSpCas9(BB)-2A-Puro (PX459) V2.0 plasmid encoding for Cas9 were digested with 1 µL of FastDigest *BbsI*, 1x FastDigest buffer and 2 µL of the phosphorylated and annealed oligonucleotides previously diluted 1:250 and were ligated to the PX459 plasmid with 0.5 µL T7 DNA ligase, 1 µL DTT (1mM final concentration), and 1 µL ATP (1 mM final concentration). The reaction was adjusted with ultrapure water with a final volume of 20 µL. In a thermocycler, the ligation reaction was incubated for 5 min at 37°C, followed by 5 min at 23 °C. This cycle was repeated 6x. Competent *E.coli* was transformed with the final ligation product (see chapter 4.2.2).

4.2.13 Extraction of genomic DNA

To confirm the achievement of monoclonal A549-EGFR KO cells, the genomic DNA of generated EGFR KO cells was extracted using the DNeasy Blood & Tissue kit according to the instructions of the manufacturer. 100 ng of genomic DNA were amplified by PCR and the purified PCR products (see chapter 4.2.15) were analyzed by DNA sequencing.

4.2.14 PCR

To amplify EGFR DNA fragments, 100 ng of genomic DNA extracted from cells (see chapter 4.2.13) were amplified with 0.5 µM of the appropriate oligonucleotides, 200 µM of dNTPs, 1x Q5 reaction buffer, 0.02 U/µL Q5 Hot Start DNA polymerase. The volume of the reaction was adjusted with ultrapure water to a final volume of 50 µL and the reaction occurred in a thermocycler as described in table 33. 10 µL of the PCR product was analyzed by agarose gel electrophoresis.

Table 33 – Description of the PCR program used.

Program	Temperature (°C)	Time (s)	Cycles
Initial denaturation	98	30	1
Denaturation	98	5	35
Annealing	50-72	10	
Elongation	72	20-60	
Final elongation	72	120-300	1
Hold	4	-	

4.2.15 PCR purification

After performing PCR and agarose gel electrophoresis analysis, the remaining PCR products were purified with the PCR purification Kit according to the instructions of the manufacturer.

4.2.16 DNA sequencing

To verify the DNA sequence of the monoclonal EGFR KO cell clones, 1.5 µL of the purified PCR products were mixed with 6 µL of the appropriate oligonucleotide diluted 1:10 (initial concentration of 10 µM) and 7.5 µL of ultrapure water in a reaction tube to obtain a final volume of 15 µL. The reaction tubes were sent for sequencing. The nucleotide sequence was determined by capillary electrophoresis by Eurofins Genomics and the raw sequence data were aligned and analyzed with Snap Gene Viewer software.

4.3 Protein biochemistry

4.3.1 Protein quantification by Bradford assay

To be able to compare different samples, the total protein concentration in cell lysates was determined using the Bradford reagent. In an acidic environment, the basic and the aromatic amino acids residues of the proteins bind to the Coomassie Brilliant G250 dye that is present in this reagent. The formation of the protein-dye complex results in a shift of the maximum absorption of the dye from 465 to 595 nm, which can be spectrophotometrically measured.[477] To perform this assay, 5 µL of each cell lysate were incubated with 100 µL of Bradford reagent in 96-well plates for 5 min at room

temperature. Afterwards, the absorbance was measured in the Infinite M1000. The protein amount was calculated using a standard curve generated with BSA.

4.3.2 Protein quantification with Pierce™ BCA Protein Assay Kit

As recommended by PamGene International BV, the total protein concentration in cell lysates analyzed by the PamChip® peptide tyrosine kinase microarray system was determined using the Pierce™ BCA Protein Assay Kit, according to the manufacturer's instructions. Under alkaline conditions, peptides or proteins containing three or more amino acid residues reduce the Cu^{2+} ions from the copper(II) sulfate to Cu^{+} that is present in the reagent provided in the kit. The Cu^{+} ions formed in the biuret reaction react with the bicinchoninic acid, which is also present in the reagent, resulting in a purple complex that can be detected at 562 nm.[478] The absorbance was measured in the Infinite 1000 and the protein amount was calculated using a standard curve generated with BSA.

4.3.3 Polyacrylamide gel electrophoresis

To separate proteins present in cell lysates based on their molecular weight, sodium dodecyl sulfate-polyacrylamide gel electrophoresis (SDS-PAGE) was performed using the Laemmli system.[479] For this purpose, equal amounts of protein (75-100 µg) were denatured and negatively charged by mixing with 1x SDS loading buffer and heated for 10 min at 95°C. After cooling, the samples and 4 µL of protein marker were loaded onto SDS-PAGE gels submerged in 1x SDS running buffer and the proteins were separated in a vertical chamber at 80-140 V. The SDS-PAGE gels were prepared with an acrylamide and bisacrylamide solution (29:1) and the polymerization was achieved with a 10% (w/v) ammonium persulfate (APS) solution and TEMED. Based on the molecular weight of proteins of interest, 8% or 10% of acrylamide/bisacrylamide were used for the separating gels and overlaid with stacking gels of 4%.

4.3.4 Luciferase assay

The luciferase activity of electroporated cells with *in vitro* transcribed ZIKV-*Renilla* luciferase RNA was determined using the Gaussia-GLOW Juice Kit according to the instructions of the manufacturer. The luciferase gene is inserted into the viral capsid coding sequence. Thus, the luciferase activity directly correlates with the rate of viral replication. In brief, 40 µL of cleared lysate were mixed with 20 µL of Gaussia GLOW-Juice containing coelenterazine, the luminescent substrate of the *Renilla* luciferase. The bioluminescence was measured with the Orion II microplate luminometer. The luciferase values were normalized to the protein concentration of the corresponding lysate.

4.4 Immunological methods

4.4.1 Western blot

To enable the detection of proteins of interest, proteins separated by SDS-PAGE were transferred onto a methanol-activated PVDF membrane in a semi-dry blotter with a discontinuous buffer system, as illustrated in Figure 16. The transfer occurred for 1 h with an electric field of 1.3 mA/cm^2.[480] After transfer, the membrane was blocked for 1 h at room temperature to prevent unspecific binding. The blocking solution alternated between 10% skim milk (w/v) in TBST (0.05% Tween 20) and 1x Roti®-Block solution, depending on the antibodies used. Subsequently, the membrane was incubated either overnight at 4°C or for 1 h at room temperature with primary antibodies diluted in the respective blocking solution. After washing 3x for 10 min with TBST (0.05% Tween 20), the membrane was incubated for 1 h at room temperature with secondary antibodies either conjugated with fluorescent dyes or horseradish peroxidase (HRP) diluted in the respective blocking solution. Afterwards, the membrane was washed 3x for 10 min with TBST (0.05% Tween 20) before detection. The incubation with the antibodies conjugated with fluorescent dyes was performed in a dark environment and also the following washing steps. When secondary antibodies conjugated with fluorescent dyes were used, the fluorescence was detected using the Odyssey® CLx Imaging System and the signal intensity was quantified using the Image Studio Lite software. In the case of the secondary antibodies conjugated with HRP, proteins were detected by using an enhanced luminol-based chemiluminescence (ECL) substrate that reacts with the HRP, emitting light at 428 nm.[481] This light signal was then captured with an x-ray film or using the Image Quant 800 CCD imager and the signal intensity was quantified using the ImageQuantTL software.

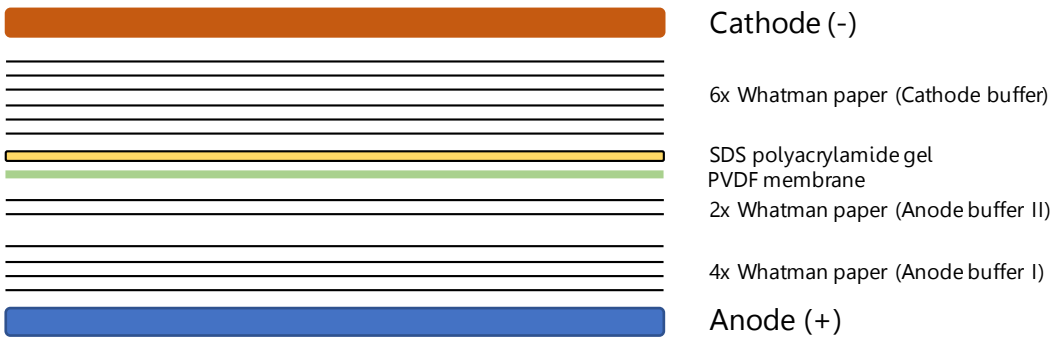

Figure 16 – Schematic representation of a semi-dry Western blot transfer system. In a semi-dry Western blot transfer system, the SDS polyacrylamide gel and the PVDF membrane are sandwiched between two stacks of Whatman paper and placed horizontally between two electrodes. The Whatman papers are soaked in the indicated buffers and the excess moisture and trapped air bubbles are removed during the assembling of the sandwich.

4.4.2 Western blot of phosphoproteins

To detect phosphoproteins, the procedure was the same as described in chapters 4.3.3 and 4.4.1 with the following exceptions. The separation of the proteins by SDS-PAGE occurred at 4°C and the buffers used in the transfer were pre-chilled before usage. Moreover, the membrane was blocked with 5% BSA (w/v) in TBST (0.1% Tween 20) at 4°C for 1 h and the washing steps were performed with ice-cold TBST (0.1% Tween 20). Both primary and secondary antibodies were diluted in ice-cold TBST (0.1% Tween 20) and the incubation with primary antibodies was carried out overnight at 4°C exclusively. Only secondary antibodies conjugated with HRP were used.

4.4.3 Indirect immunofluorescence

Subcellular localization and distribution of the proteins of interest were analyzed by indirect immunofluorescence and confocal laser scanning microscopy. For this purpose, cells were grown on 18 mm coverslips in 12 well-plates. At the desired time, cells were washed with PBS and fixed with a formaldehyde solution as described in chapter 4.1.2.15. The following steps were performed at room temperature and after each step, the cells were washed 3x 5min with PBS in a shaker. After fixation, cells were permeabilized with PBST for 10 min and blocked with 1% BSA (w/v) in PBS for 30 min. Primary and secondary antibodies diluted in PBS were incubated with the cells for 1 h in a humidified chamber and in case of the secondary antibodies, protected from light. Fluorescent dyes were incubated together with the secondary antibodies. Finally, the coverslips were mounted on microscope slides SuperFrost® Plus with mounting medium containing mowiol.

4.4.4 Protein tyrosine kinase (PTK) activity with PamChip®peptide tyrosine kinase microarray system

The kinase activity of EGFR was analyzed using the PamChip®peptide tyrosine kinase microarray system on the PamStation®12 instrument. The PTK PamChip® microarray comprises 196 individual peptide sequences 13 aa long that are immobilized on a porous membrane and act as a tyrosine kinase substrate. Cells were lysed as described in chapter 4.1.2.15 and the protein concentration was quantified with Pierce™ BCA Protein Assay Kit (see chapter 4.3.1). Per array, 5 µg of protein were mixed with a freshly prepared PTK Basic mix containing 4 µL of PK wash buffer (10x), 0.4 µL of BSA (100x), 0.4 µL DTT, 4 µL of 4 mM ATP solution, 4 µL PTK additive and 0.6 µL anti-phosphotyrosine FITC-conjugated antibody (clone PY20). The final volume was adjusted to 40 µL with ultrapure water. First, the arrays were blocked with 30 µL of a 2% BSA solution for 30 cycles (30 min), following a washing step with PK wash buffer. Afterwards, 40 µL of the sample (PTK Basic mix mixed with 5 µg of protein) were applied to the array and pumped back and forward through the porous membrane for 60

cycles. The activity of the kinases present in the cell lysates is detected by the binding of the fluorescently labeled anti-phosphotyrosine antibody. Based on the peptides that are phosphorylated, a prediction of the differentially activated upstream kinases was performed using the BioNavigator software and integrated databases. In this case, only EGFR was considered. The normalized kinase statistic was calculated using the BioNavigator Analysis software tool and indicates the difference of activity between the analyzed infected samples and the uninfected control.

4.5 Microscopy

4.5.1 Confocal laser scanning microscopy (CLSM)

Subcellular localization and distribution of the proteins of interest were analyzed by indirect immunofluorescence using a confocal laser scanning microscope (LSM 510 Meta or the TCS SP8) and respective imaging software. A confocal laser scanning microscope enables the detection of fluorescent-labeled proteins in a defined plane of the cell as well as a three-dimensional reconstruction of the cell. The presence of a pinhole prevents that the light emitted from a different plane reaches the detector, allowing the visualization of only a specific plane of the cell. A three-dimensional reconstruction of the cell can be obtained by assembling several images of multiple plans of the cell (z-stack imaging). The colocalization of two proteins was quantified by calculating the threshold Mander's overlap coefficient (tMOC) using the Fiji (Image J) software and a tMOC of 1 indicates a total overlapping between the analyzed proteins.

4.6 Statistical analysis

The results are presented as the mean value of at least three biological replicates ($n \geq 3$) unless stated otherwise. The error bars represent the corresponding standard deviation. In the graphs with the y-axis indicated as relative amount or number, the data was normalized and the fold change relative to the control group is represented. Hence, the control group is 1 and no standard deviation is shown. The statistical significance of the results was analyzed by two-tailed unpaired student's t-test or in the case of multiple comparisons, by multiple t-test with a Holm-Sidak correction using the Graph Pad Prism software. The level of statistical significance indicated in the graphs are expressed with asterisks (*) that correspond to the following p-value (p): ns = not significant $p > 0.05$; * $p \leq 0.05$; ** $p \leq 0.01$; *** $p \leq 0.001$; **** $p \leq 0.0001$.

5. Results

5.1 CHO cells neither support ZIKV infection nor express EGFR

From all the investigated cell lines by Himmelsbach and Hildt, the CHO cells were the only cell line that was not capable to support ZIKV infection.[459] These cells lack endogenous EGFR.[482] To confirm these findings, these cells were infected with either the French Polynesia or the Uganda strain with a multiplicity of infection of 1 (MOI 1) and analyzed at 48 hours post-infection (hpi) by Western blot and confocal laser scanning microscopy (CLSM). A549 cells were used as positive control, as they are permissive to ZIKV infection and express EGFR.[483] Viral infection was assessed by using a specific antibody against the ZIKV envelope (E) visible in green, whereas EGFR was visualized in red. In contrast to A549 cells, neither ZIKV envelope nor EGFR could be detected in CHO cells **(Figure 17 A and B)**.

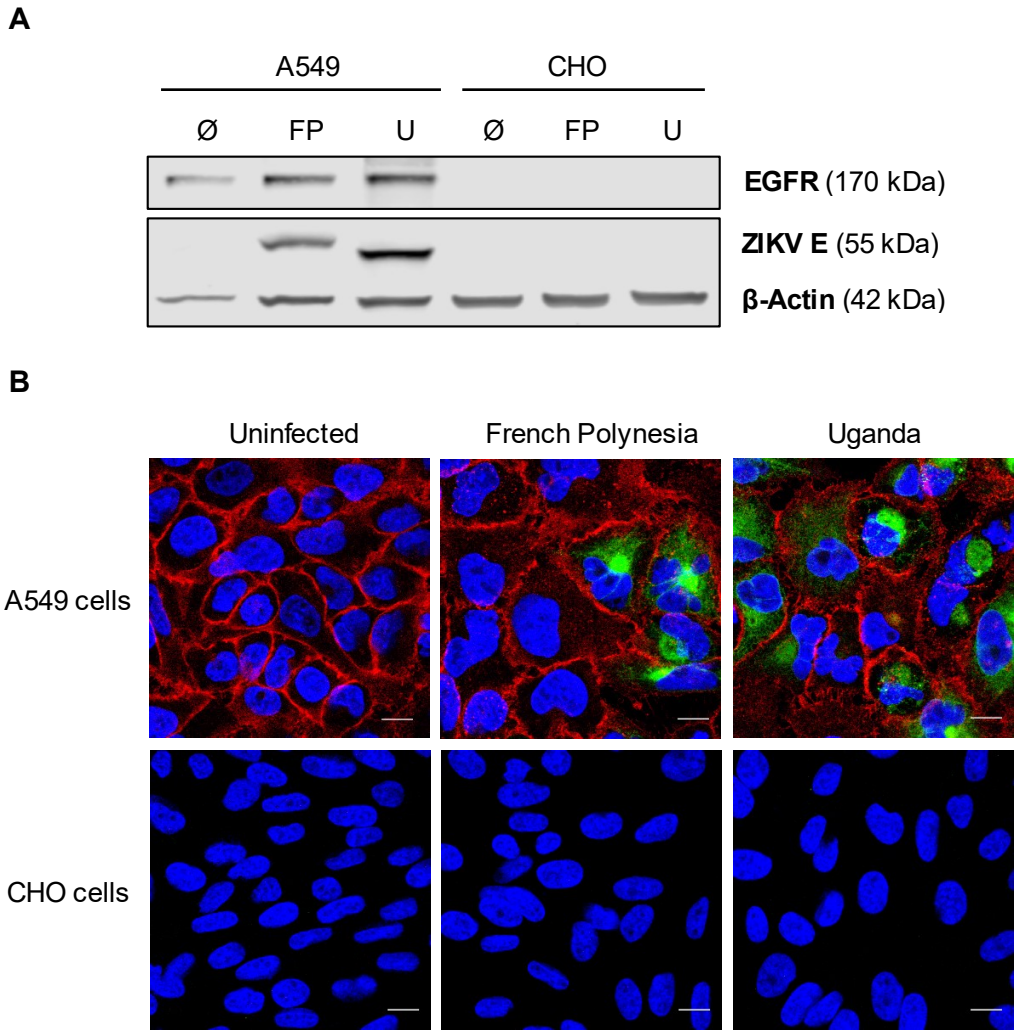

Figure 17 – CHO cells neither support ZIKV infection nor express EGFR. (A) Representative Western blot of EGFR and ZIKV envelope (E) in cell lysates of A549- and CHO-infected cells with either the French Polynesia (FP) or the Uganda (U) strain with MOI 1 and analyzed at 48 hours post-infection (hpi). A549 cells were used as positive control for ZIKV infection and EGFR expression, whereas uninfected cells (Ø)

were used as negative control for ZIKV infection. Detection of β-Actin served as the loading control. **(B)** CLSM analysis of A549- and CHO-infected cells with either the French Polynesia or the Uganda strain with MOI 1 and analyzed at 48 hpi. A549 cells were used as positive control for ZIKV infection and EGFR expression, while uninfected cells served as negative control for ZIKV infection. Nuclei were stained with DAPI in blue, EGFR and ZIKV E were visualized with specific antibodies in red and green, respectively. The scale bar represents 10 µm.

Even though the EGFR-specific antibody used recognizes a sequence that is conserved between human and hamster, the possibility that the EGFR-specific antibody does not interact with hamster EGFR was investigated. In light of this, the liver tissue of a Syrian golden hamster was homogenized and the EGFR protein level was analyzed by Western blot. EGFR could be detected in hamster liver tissue, but to a lesser extent than in A549 cells, demonstrating that hamster EGFR is recognized by this antibody **(Figure 18)**.

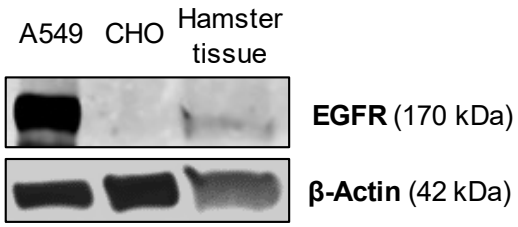

Figure 18 – EGFR antibody recognizes hamster EGFR. Representative Western blot of EGFR in cell lysates of A549 and CHO cells as well as of EGFR in homogenized hamster liver tissue. A549 and CHO cells were used as positive and negative control for EGFR expression, respectively. Detection of β-Actin served as loading control.

These data confirm that CHO cells neither support ZIKV infection nor express endogenous EGFR.

5.2 ZIKV entry is affected in CHO cells

To investigate which step of the viral life cycle is not supported in CHO cells, binding, entry, and post-entry assays were performed and the number of ZIKV genomes was quantified by qPCR. In the binding assay, the relative number of attached viral genomes did not differ between A549 and CHO cells for both ZIKV strains **(Figure 19 A)**. On the contrary, the entry assay revealed a significant decrease in the relative number of internalized ZIKV genomes in CHO cells in comparison to the A549 cells **(Figure 19 B)**. The same outcome could be observed in the post-entry assay **(Figure 19 C)**. Overall, a higher relative number of ZIKV genomes was measured for the Uganda strain in the entry and especially in the post-entry assay. These results suggest that ZIKV entry is the step of the viral life cycle that is not sustained in CHO cells.

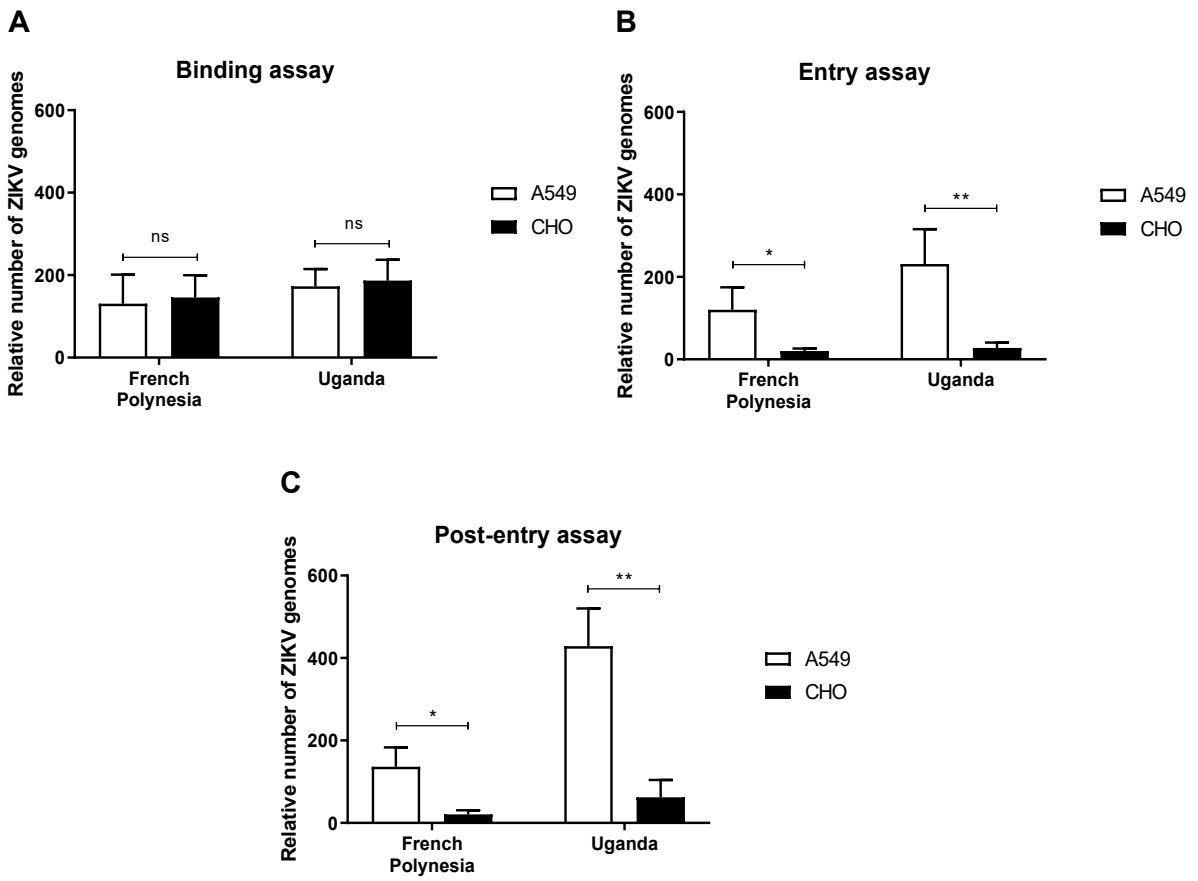

Figure 19 – ZIKV entry is affected in CHO cells. (A) Relative number of attached viral genomes of A549- and CHO-infected cells with the French Polynesia or the Uganda strain with MOI 1. The number of genomes was quantified by qPCR and normalized to the number of GAPDH transcripts after performing a binding assay. Uninfected cells of the respective cell line served as negative control and were used as the control group for the calculation of the fold change. **(B)** Relative number of internalized viral genomes of A549- and CHO-infected cells with the French Polynesia or the Uganda strain with MOI 1. The number of genomes was quantified by qPCR and normalized to the number of GAPDH transcripts after performing an entry assay. Uninfected cells of the respective cell line served as negative control and were used as the control group for the calculation of the fold change. **(C)** Relative number of replicated viral genomes of A549- and CHO-infected cells with the French Polynesia or the Uganda strain. The number of genomes was quantified by qPCR and normalized to the number of GAPDH transcripts after performing a post-entry assay. Uninfected cells of the respective cell line served as negative control and were used as the control group for the calculation of the fold change. ns = not significant $p > 0.05$; * $p \leq 0.05$; ** $p \leq 0.01$.

5.3 EGFR is expressed in most ZIKV permissive cell lines unlike AXL

As ZIKV entry is compromised in CHO cells and these cells lack endogenous EGFR, the relevance of EGFR for the ZIKV life cycle, with special emphasis on the viral entry, was investigated. To evaluate whether EGFR can be considered an essential host factor for the ZIKV life cycle, the protein level of EGFR and AXL, one of the first described ZIKV receptors, was analyzed by Western blot in ZIKV permissive cell lines reported by Himmelsbach and Hildt.[459] EGFR could be detected in all the analyzed cell lines, except

for the CHO and the HepG2/C3A cells. On the other hand, AXL was only detected in A549, HaCaT, HepG2/C3A, COS-7, and Vero cells **(Figure 20)**. These observations indicate that EGFR is expressed in the majority of ZIKV permissive cell lines contrary to AXL, highlighting EGFR as a potential host factor relevant for the ZIKV life cycle.

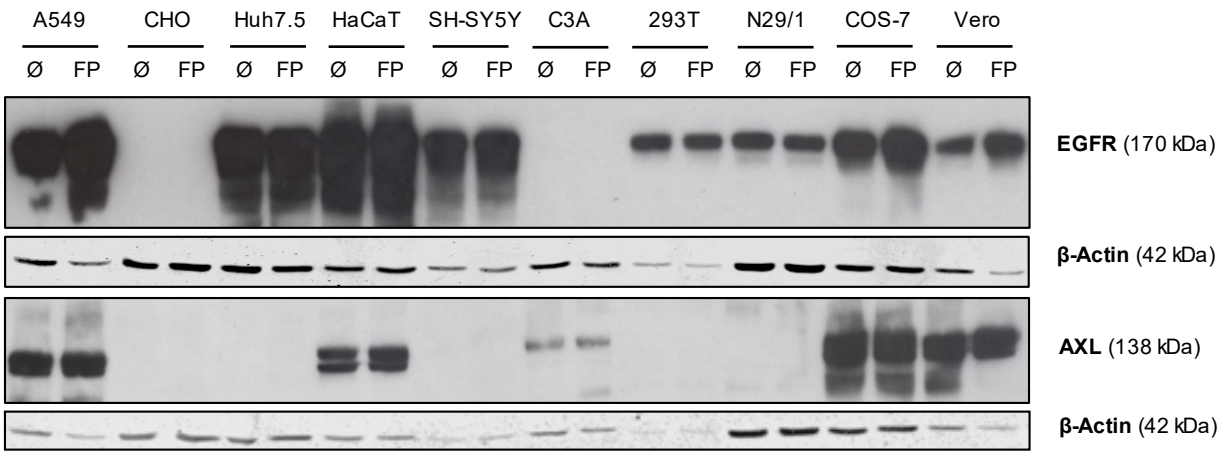

Figure 20 – EGFR expression is common to most ZIKV permissive cell lines contrary to AXL expression. Representative Western blot of EGFR and AXL in cell lysates of several cell lines infected with the French Polynesia (FP) strain with MOI 0.1 or that remained uninfected (Ø) and analyzed at 48 hpi. The lysates were the same as the ones used by Himmelsbach and Hildt.[459] A549 and CHO cells were used as positive and negative controls for EGFR expression, respectively. Detection of β-Actin served as loading control. The data is representative of n=1.

5.4 CHO cells overexpressing EGFR are not permissive to ZIKV infection, but EGFR overexpression in CHO cells augments viral entry

As previously mentioned, ZIKV entry is affected in CHO cells. To investigate whether the overexpression of EGFR in CHO cells can render these cells permissive to viral infection, CHO cells stably overexpressing EGFR were required. Two different cell clones expressing different amounts of EGFR were used in this study, CHO-EGFR #22.2 and CHO-EGFR #45. Initially, the functionality of EGFR molecules in these stable cells was investigated. For this purpose, CHO-EGFR #22.2 and CHO-EGFR #45 cells were stimulated with EGF, the canonical ligand of EGFR, and the phosphorylation levels of EGFR (p-EGFR) and downstream ERK (p-ERK 1/2) were analyzed by Western blot and quantified. A549 and CHO cells served as positive and negative control for EGFR functionality, respectively. Elevated levels of phosphorylated EGFR (p-EGFR) and ERK (p-ERK 1/2) were detected in CHO cells stably overexpressing EGFR upon EGF stimulation, but to a lesser extent than in A549 cells **(Figure 21 A)**. Furthermore, densitometric quantification of the intensity of the signals unveiled a dose-dependent augmentation of phosphorylated EGFR (p-EGFR) and ERK (p-ERK 1/2) for A549 cells **(Figure 21 B and F)**. This effect was not so pronounced in CHO cells overexpressing EGFR with the exception of phosphorylated EGFR (p-EGFR) in CHO-EGFR #22.2 cells

(Figure 21 D, E, H and I). As estimated, phosphorylated EGFR (p-EGFR) and downstream ERK (p-ERK 1/2) could not be observed in CHO cells upon EGF stimulation since they lack endogenous EGFR **(Figure 21 C and G)**. The results demonstrate that EGFR and respective MAPK/ERK pathway can be activated in CHO-EGFR #22.2 and CHO-EGFR #45 cells, suggesting that EGFR molecules are functional in these stable cells.

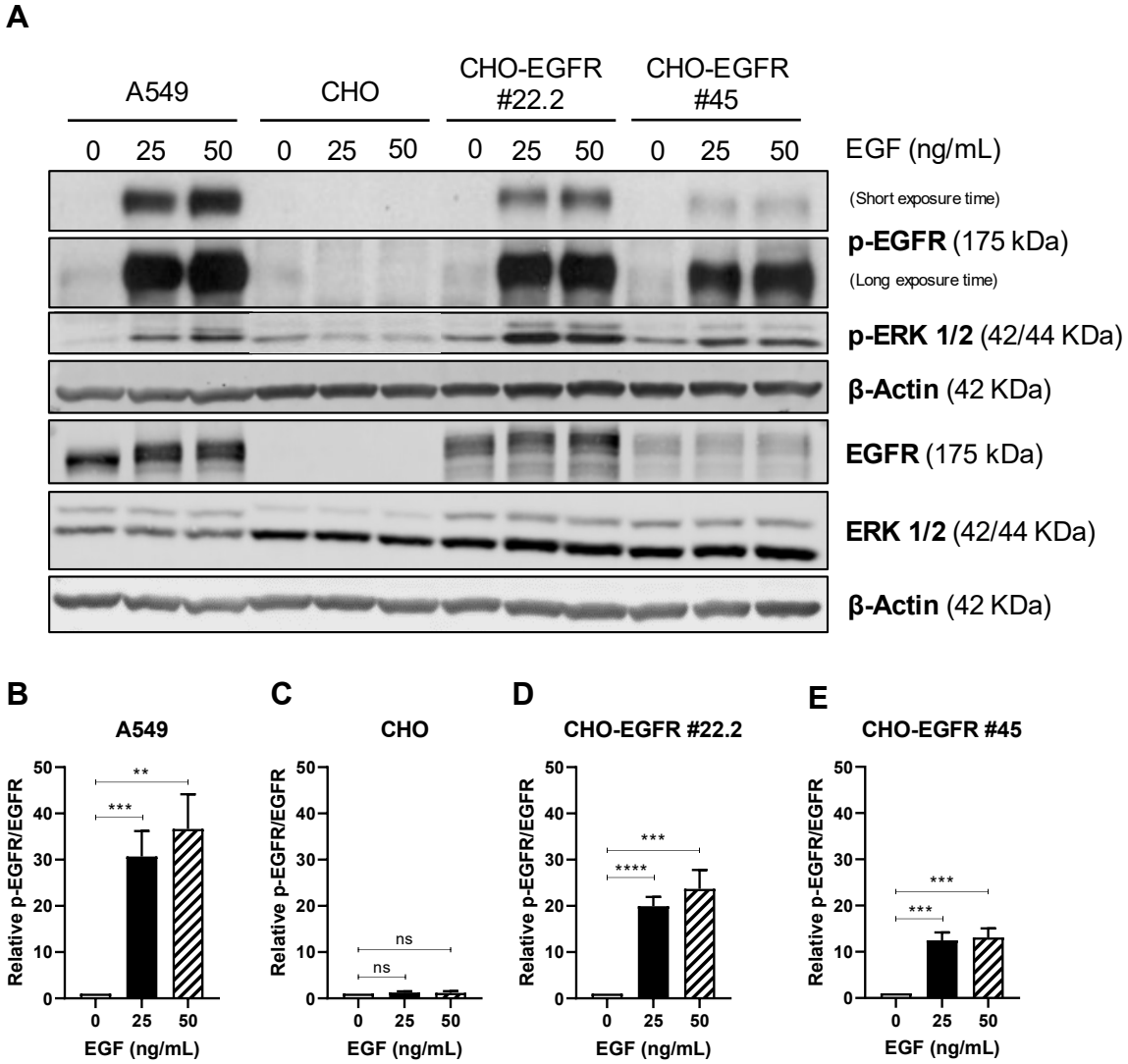

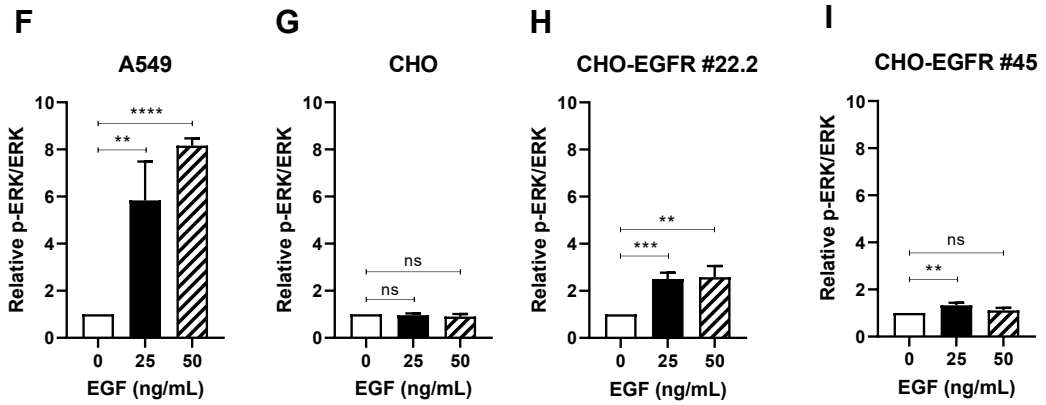

Figure 21 – Activation of EGFR and respective MAPK/ERK pathway in CHO cells stably overexpressing EGFR. (A) Representative Western blot and **(B - I)** respective densitometric quantification of **(B - E)** p-EGFR/total EGFR and **(F - I)** p-ERK/total ERK amount in cell lysates of **(B, F)** A549, **(C, G)** CHO, **(D, H)** CHO-EGFR #22.2, and **(E, I)** CHO-EGFR #45 cells that were stimulated with 25, and 50 ng/mL of EGF for 30 min. Detection of β-Actin served as loading control. The amount of p-EGFR and p-ERK was first normalized to the respective amount of β-Actin, followed by normalization to the total amount of EGFR and ERK, respectively. Unstimulated cells were used as negative control and control group for the calculation of the fold change. ns = not significant $p > 0.05$; ** $p \leq 0.01$; *** $p \leq 0.001$; **** $p \leq 0.0001$.

To further corroborate these data, the subcellular localization and distribution of EGFR were analyzed by CLSM using an EGFR-specific antibody visible in red. Likewise, A549 and CHO cells were used as positive and negative control for EGFR functionality, respectively. Similar to A549, the CHO cells stably overexpressing EGFR stimulated with EGF displayed intracellular EGFR, characterized by the delocalization of EGFR from the plasma membrane and the formation of dot-like structures. However, the degree of internalized EGFR in CHO cells stably overexpressing EGFR was less pronounced than in A549 cells **(Figure 22)**.

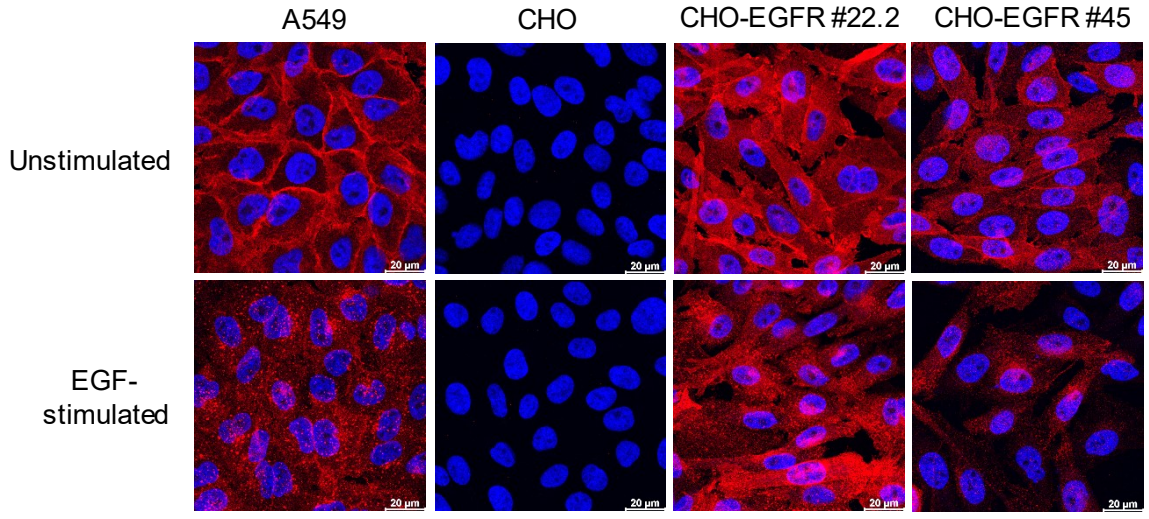

Figure 22 – EGFR internalization in CHO cells stably overexpressing EGFR upon EGF stimulation. CLSM analysis of A549, CHO, CHO-EGFR #22.2, and CHO-EGFR #45 cells stimulated with 100 ng/mL of

EGF for 30 min. Unstimulated cells were used as negative control. A549 and CHO cells served as positive and negative control for EGFR expression, respectively. Nuclei were stained with DAPI in blue and EGFR was visualized with a specific antibody in red. The scale bar represents 20 µm.

Taken together, these data demonstrate that EGFR in CHO cells stably overexpressing EGFR is functional.

After confirmation of the functionality of EGFR in CHO stably overexpressing EGFR, these cells were infected with MOI 50 and the number of ZIKV-infected cells was analyzed at 24 hpi by CLSM using a ZIKV envelope-specific antibody visualized in green. The protein level of EGFR was controlled using an EGFR-specific antibody visible in red. Likewise, A549 and CHO were used as positive and negative control for viral infection, respectively. Unlike for A549 cells, no ZIKV envelope could be detected in CHO-EGFR #22.2 cells nor in CHO-EGFR #45 cells **(Figure 23)**. These results indicate that overexpression of EGFR in CHO cells is not sufficient for the establishment of ZIKV infection.

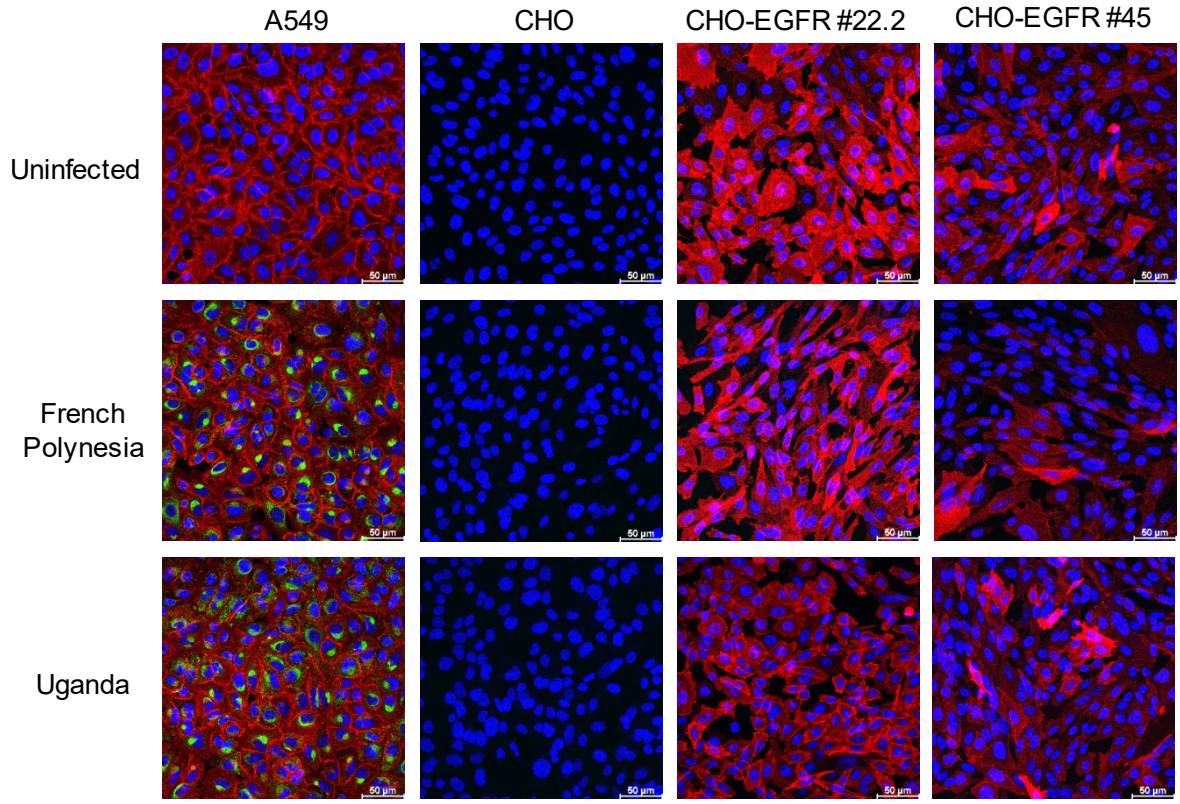

Figure 23 – CHO cells stably overexpressing EGFR cells do not sustain ZIKV infection similar to CHO cells. CLSM analysis of A549-, CHO-, CHO-EGFR #22.2-, and CHO-EGFR #45-infected cells with either the French Polynesia or the Uganda strain with MOI 50 and analyzed at 24 hpi. A549 and CHO cells were used as positive and negative control for ZIKV infection and EGFR expression, respectively. Nuclei were stained with DAPI in blue, EGFR and ZIKV E protein were visualized with specific antibodies in red and green, respectively. The scale bar represents 50 µm.

As ZIKV infection was unsuccessful in CHO cells stably overexpressing EGFR, the permissiveness of these cells as well as of the CHO cells was questioned. In light of this, CHO, CHO-EGFR #22.2, and CHO-EGFR #45 cells were electroporated with *in vitro* transcribed capped ZIKV-*Renilla* luciferase RNA and the number of ZIKV-infected cells was analyzed at 96 hours-post electroporation (hpe) by CLSM using a ZIKV envelope-specific antibody visible in green. In contrast to A549 cells, no ZIKV-infected cells could be observed in CHO cells nor in CHO cells stably overexpressing EGFR **(Figure 24 A)**. Moreover, the luciferase activity at 24, 48, 72, and 96 hours post-electroporation was determined by a luciferase assay. As the *Renilla* luciferase reporter is inserted into the viral genome, the luciferase activity directly correlates with the replication level. Even though luciferase activity could be measured at 24 hpe in CHO cells and CHO cells stably overexpressing EGFR, which reflects the initial translation of the electroporated ZIKV-*Renilla* luciferase RNA, this activity declined with time due to the absence of viral replication. Contrariwise, an increase in the luciferase activity over the analyzed time could be discerned for A549 cells. These data demonstrate that CHO cells as well as CHO cells stably overexpressing EGFR do not support ZIKV replication.

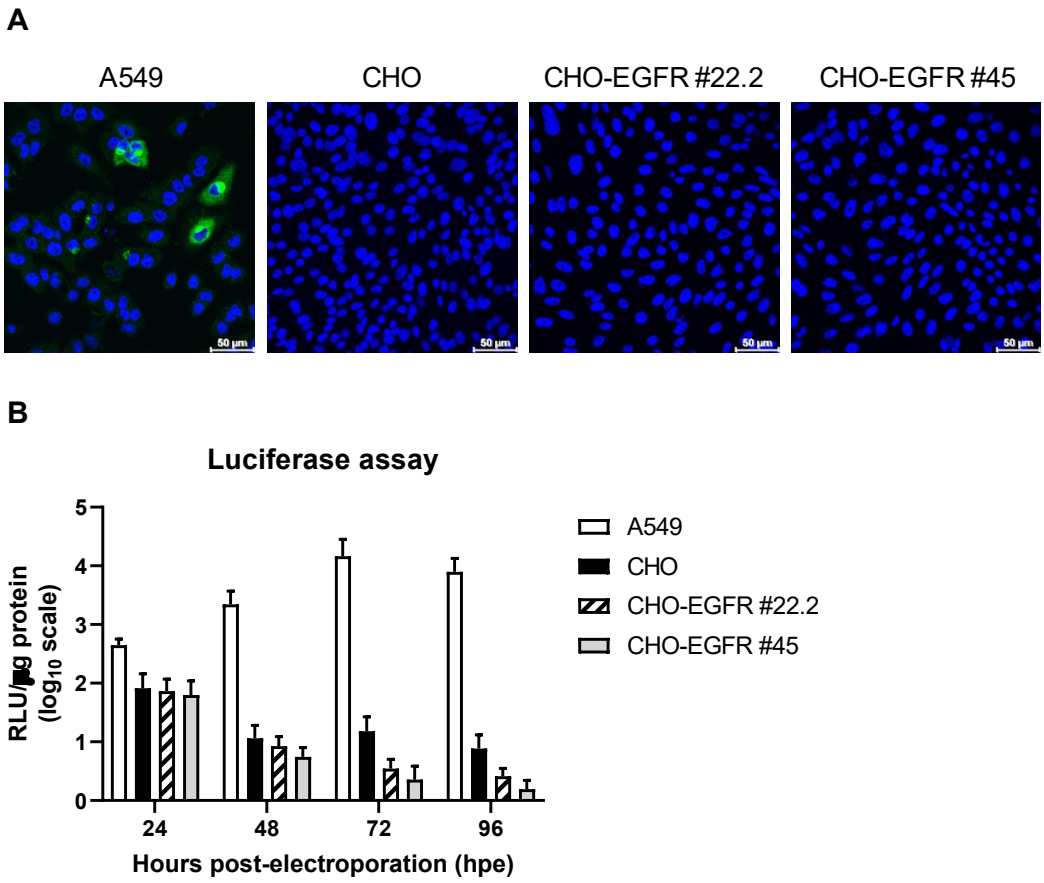

Figure 24 – CHO cells and CHO cells stably overexpressing EGFR fail to replicate ZIKV. (A) CLSM analysis of A549-, CHO-, CHO-EGFR #22.2-, and CHO-EGFR #45-electroporated cells with *in vitro* transcribed capped ZIKV-*Renilla* luciferase RNA and analyzed at 96 hours post-electroporation (hpe). A549 cells were used as positive control for viral replication. Nuclei were stained with DAPI in blue and

ZIKV E protein was visualized with a specific antibody in green. The scale bar represents 50 µm. **(B)** Luciferase activity of A549-, CHO-, CHO-EGFR #22.2-, and CHO-EGFR #45-electroporated cells with *in vitro* transcribed capped ZIKV-*Renilla* luciferase RNA and analyzed at 24, 48, 72, and 96 hpe. A549 cells served as positive control for viral replication. The luciferase activity is expressed in relative light units (RLU) per µg of protein. The results are presented on a $\log_{10}$ scale.

Even though EGFR overexpression in CHO cells did not render these cells permissive to ZIKV infection, ZIKV entry in CHO cells stably overexpressing EGFR was investigated. For this purpose, an entry assay was performed and the number of ZIKV genomes in CHO-EGFR #22.2 and CHO-EGFR #45 cells was determined by qPCR and compared to CHO cells. The entry assay revealed a decrease in the relative number of internalized ZIKV genomes in CHO cells stably overexpressing EGFR relatively to CHO cells for both viral strains **(Figure 25 A)**. To investigate whether the overexpression of EGFR in CHO cells could have an impact on ZIKV attachment to the cell surface and this way explain the observed decline in viral entry, a binding assay was performed and the number of ZIKV genomes was determined by qPCR. Similar to the entry assay, the binding assay displayed a reduction in the relative number of attached ZIKV genomes in CHO cells stably overexpressing EGFR **(Figure 25 B)**, suggesting that the decrease in the viral entry could stem from an inadequate binding of ZIKV to the cell surface. Thus, to better assess ZIKV entry in CHO cells stably overexpressing EGFR, the number of internalized viral genomes was corrected with the corresponding number of attached viral genomes. An increment in the relative number of internalized ZIKV genomes could be discerned in CHO cells stably overexpressing EGFR in comparison to CHO cells **(Figure 25 C)**.

Taken together, these results show that CHO cells as well as CHO cells overexpressing EGFR are not permissive to ZIKV infection since they are incapable to replicate ZIKV. Nonetheless, EGFR overexpression in CHO cells increases viral entry, implicating EGFR in the ZIKV entry process.

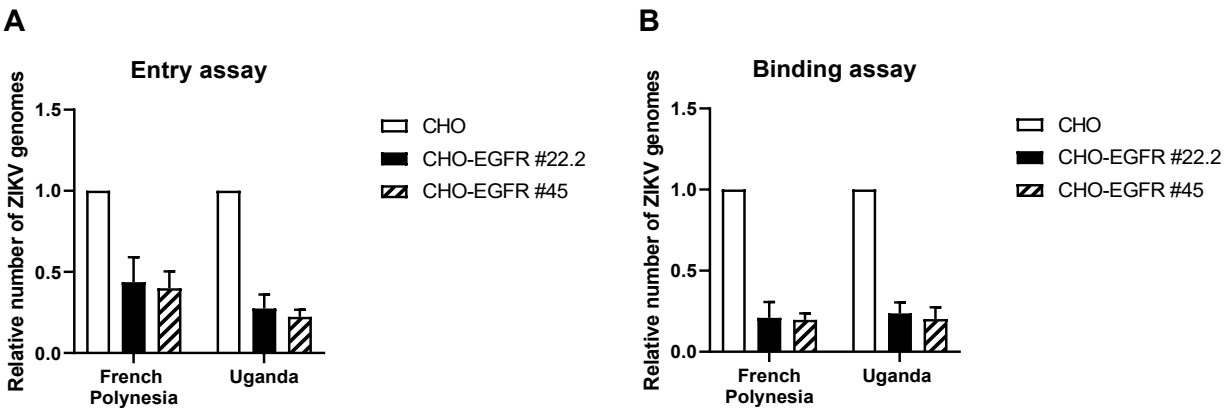

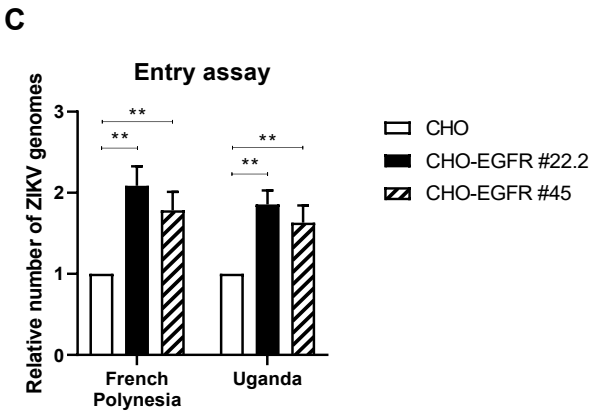

Figure 25 – ZIKV entry is increased in CHO cells stably overexpressing EGFR. (A) Relative number of internalized viral genomes of CHO-, CHO-EGFR #22.2-, and CHO-EGFR #45-infected cells with the French Polynesia or the Uganda strain with MOI 10. The number of genomes was quantified by qPCR and normalized to the number of GAPDH transcripts after performing an entry assay. CHO cells served as the control group for the calculation of the fold change. **(B)** Relative number of attached viral genomes of CHO-, CHO-EGFR #22.2-, and CHO-EGFR #45-infected cells with the French Polynesia or the Uganda strain with MOI 10. The number of genomes was quantified by qPCR and normalized to the number of GAPDH transcripts after performing a binding assay. CHO cells served as the control group for the calculation of the fold change. **(C)** Relative number of internalized viral genomes of CHO-, CHO-EGFR #22.2-, and CHO-EGFR #45-infected cells with the French Polynesia or the Uganda strain corrected to the number of attached viral genomes. CHO cells served as the control group for the calculation of the fold change. ** $p \leq 0.01$.

5.5. ZIKV infection increases the EGFR mRNA level but decreases the EGFR protein amount

To further characterize the relevance of EGFR during ZIKV infection, the EGFR mRNA level and protein amount were analyzed in ZIKV-infected cells. For this purpose, A549 cells were infected with either the French Polynesia or the Uganda strain using a low or a high MOI and analyzed at 1, 3, 6, 9, 12, 24, and 48 hpi. To verify the establishment of ZIKV infection, the number of viral genomes was quantified by qPCR. With the course of infection, a constant rise in the relative number of ZIKV genomes was measured for both viral strains and MOI, indicating that the infection was successful **(Figure 26 A and B)**.

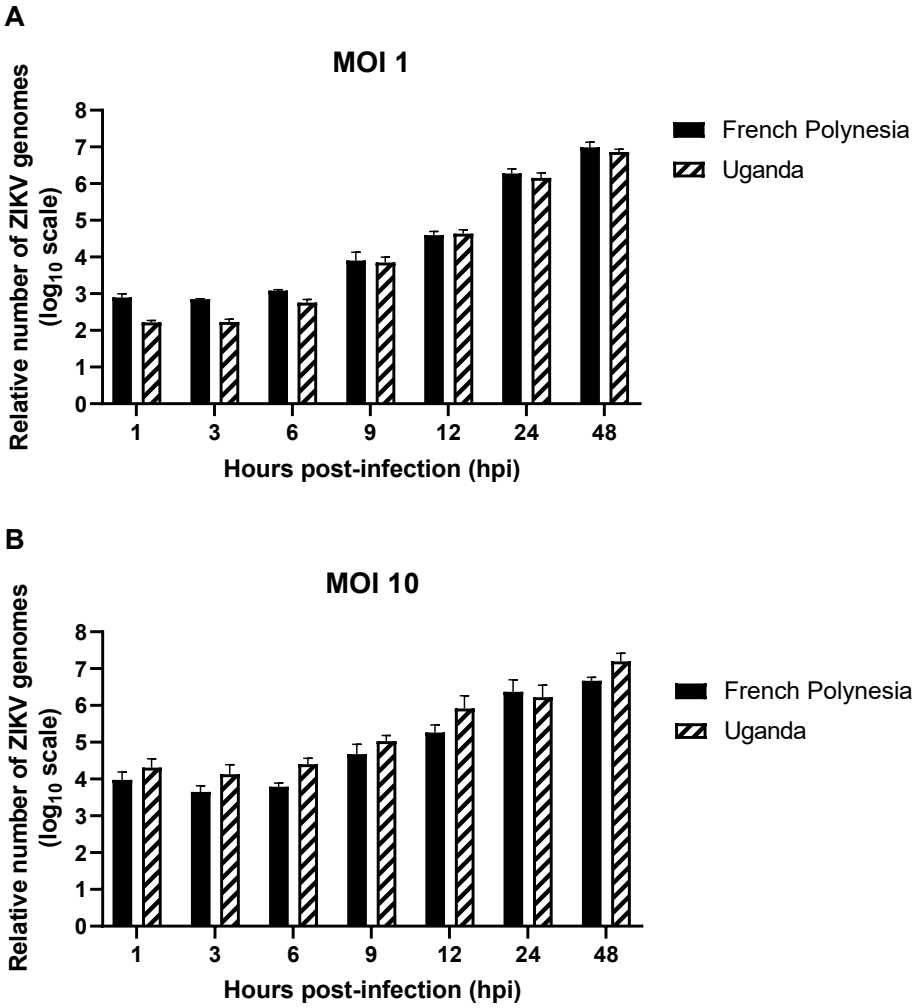

Figure 26 – Relative number of ZIKV genomes throughout infection. (A) Relative number of viral genomes of A549-infected cells with French Polynesia or the Uganda strain with MOI 1 and analyzed at the indicated times. The number of genomes was quantified by qPCR and normalized to the number of hRPL27 transcripts. Uninfected cells served as negative control and as the control group for the calculation of the fold change. The results are presented on a $\log_{10}$ scale. **(B)** Relative number of viral genomes of A549-infected cells with French Polynesia or the Uganda strain with MOI 10 and analyzed at the indicated times. The number of genomes was quantified by qPCR and normalized to the number of hRPL27 transcripts. Uninfected cells served as negative control and control group for the calculation of the fold change. The results are presented on a $\log_{10}$ scale.

The number of EGFR specific transcripts was determined as well by qPCR. In general, a gradual increase of the relative EGFR mRNA level accompanied the progress of the infection. In cells infected with a low MOI (MOI 1), a considerable rise in the EGFR mRNA level could be observed at 24 hpi for both ZIKV strains when compared with the uninfected control. Nevertheless, for the French Polynesia strain, at 3 and 12 hpi a significant increase in the mRNA level was measured **(Figure 27 A)**. With MOI 10, elevated EGFR mRNA levels could be discerned as earlier as 3 and 6 hpi for the Uganda and French Polynesia strain, respectively **(Figure 27 B)**. Taken together, these data indicate an increased *egfr* expression with ZIKV infection.

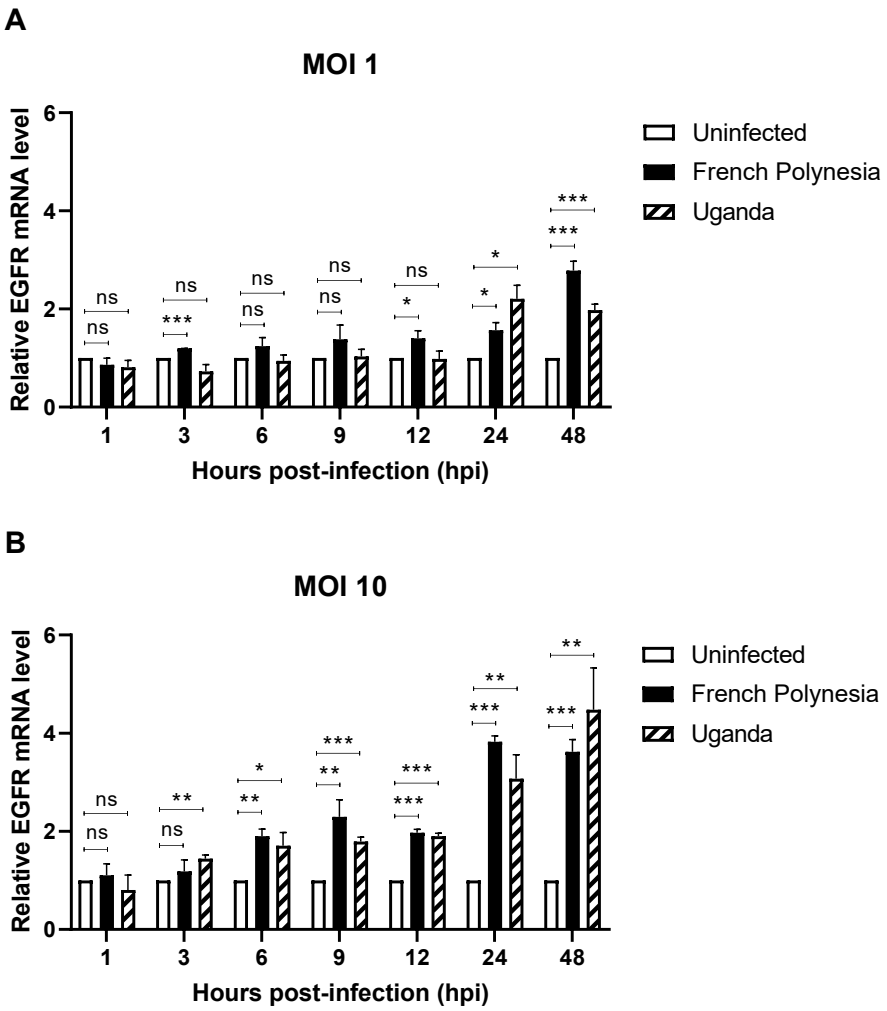

Figure 27 – Increase of EGFR mRNA level with ZIKV infection. (A) Relative EGFR mRNA level of A549-infected cells with French Polynesia or the Uganda strain with MOI 1 and analyzed at the indicated times. The number of EGFR transcripts was quantified by qPCR and normalized to the number of hRPL27 transcripts. Uninfected cells served as negative control and as the control group for the calculation of the fold change. **(B)** Relative EGFR mRNA level of A549 cells infected with French Polynesia or the Uganda strain with MOI 10 and analyzed at the indicated times. The number of EGFR transcripts was quantified by qPCR and normalized to the number of hRPL27 transcripts. Uninfected cells served as negative control and as control group for the calculation of the fold change. ns = not significant $p>0.05$; * $p\leq0.05$; ** $p\leq0.01$; *** $p\leq0.001$.

On the other hand, Western blot analysis revealed a reduction of the EGFR protein amount at 48 hpi for both MOI with lower levels for the Uganda strain **(Figure 28 A)**. Nonetheless, the densitometric quantification of the intensity of the signals showed a significant increment of the EGFR amount in ZIKV-infected cells with higher MOI at 9 and 24 hpi for the French Polynesia, and at 9 and 12 hpi for the Uganda strain **(Figure 28 B and C)**. The results indicate that ZIKV diminishes the EGFR protein amount at later times of infection.

A

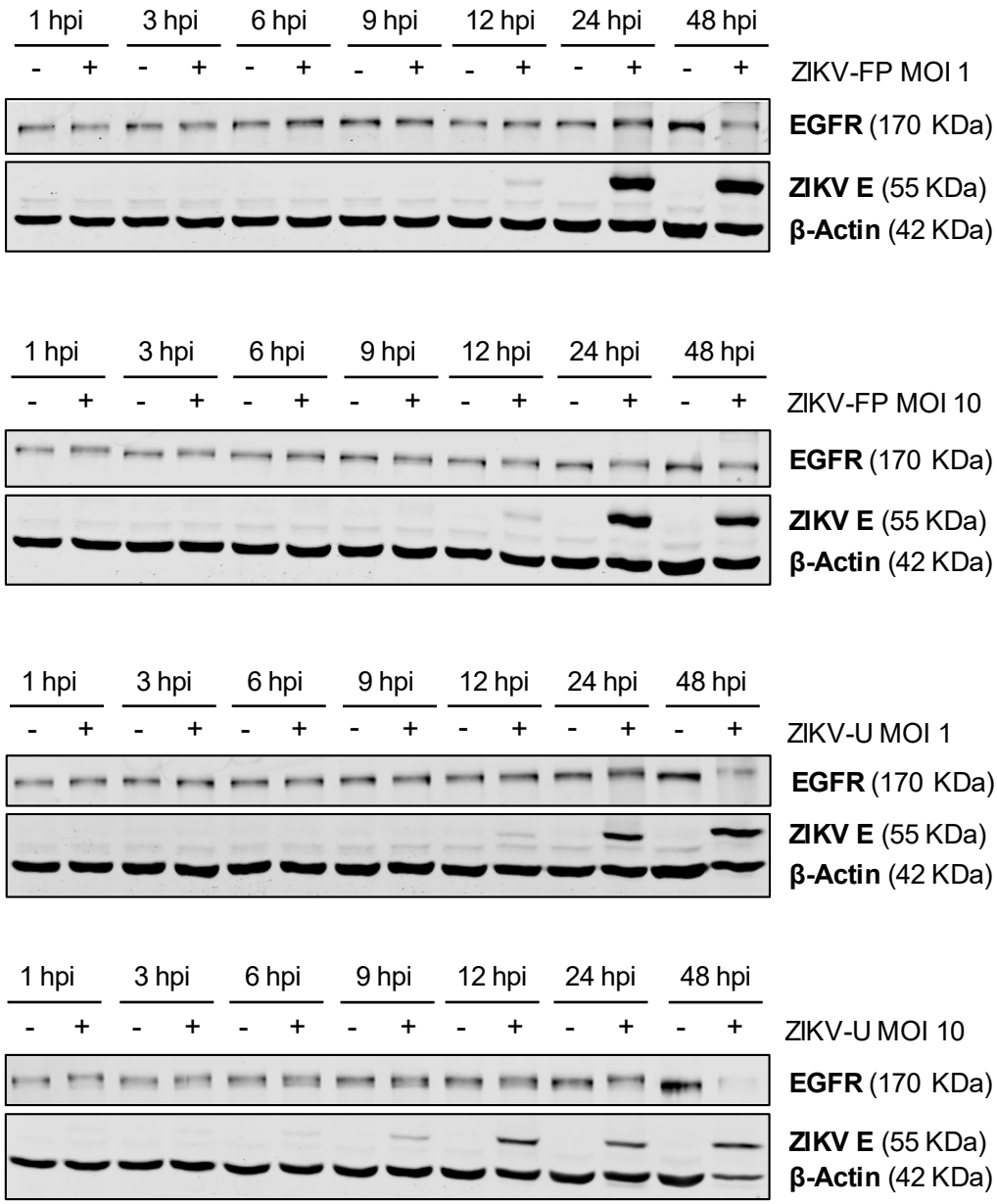
1 hpi
3 hpi
6 hpi
9 hpi
12 hpi
24 hpi
48 hpi
- + - + - + - + - + - + - +
ZIKV-FP MOI 1
EGFR (170 KDa)
ZIKV E (55 KDa)
β-Actin (42 KDa)
1 hpi
3 hpi
6 hpi
9 hpi
12 hpi
24 hpi
48 hpi
- + - + - + - + - + - + - +
ZIKV-FP MOI 10
EGFR (170 KDa)
ZIKV E (55 KDa)
β-Actin (42 KDa)
1 hpi
3 hpi
6 hpi
9 hpi
12 hpi
24 hpi
48 hpi
- + - + - + - + - + - + - +
ZIKV-U MOI 1
EGFR (170 KDa)
ZIKV E (55 KDa)
β-Actin (42 KDa)
1 hpi
3 hpi
6 hpi
9 hpi
12 hpi
24 hpi
48 hpi
- + - + - + - + - + - + - +
ZIKV-U MOI 10
EGFR (170 KDa)
ZIKV E (55 KDa)
β-Actin (42 KDa)

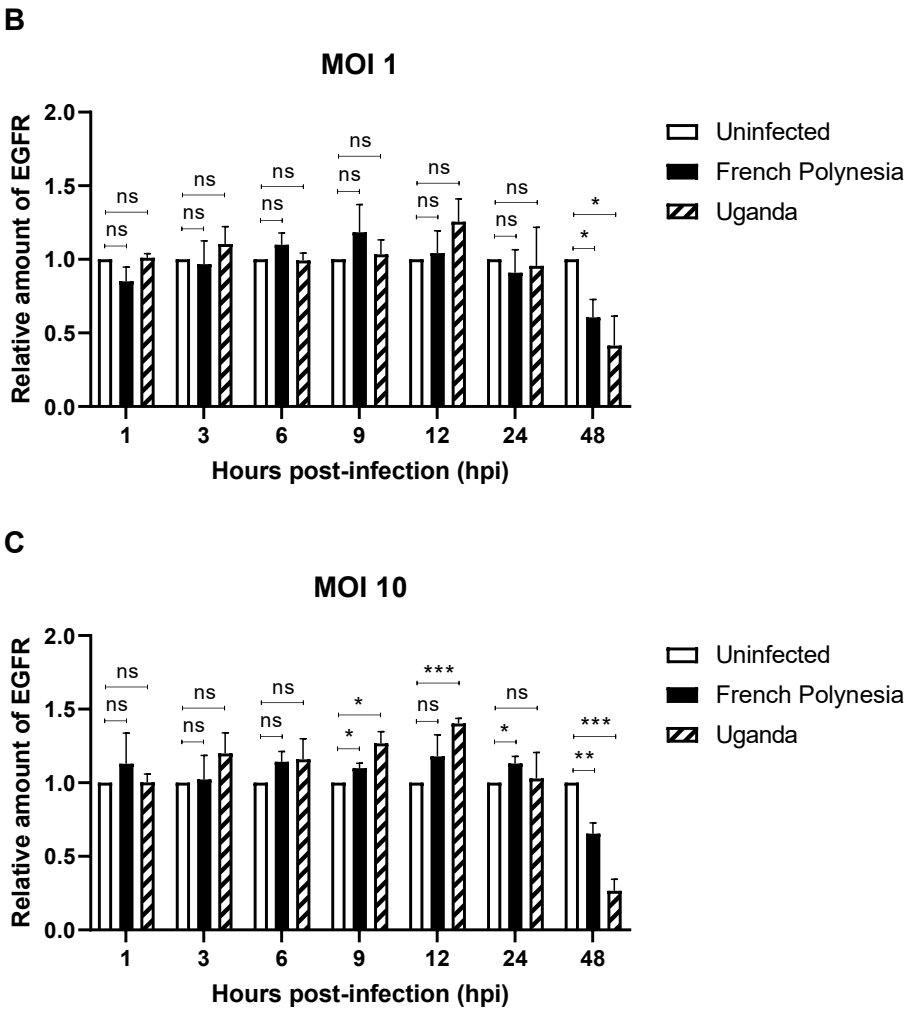

Figure 28 – Decrease of EGFR amount at later times of ZIKV infection. (A) Representative Western blot of EGFR and ZIKV envelope (E) and **(B, C)** respective densitometric quantification of EGFR in cell lysates of A549-infected cells with either the French Polynesia (FP) or the Uganda (U) strain with MOI 1 or MOI 10 and analyzed at the indicated times. Detection of β-Actin served as loading control. Uninfected cells (Ø) were used as negative control for ZIKV infection and as control group for the calculation of the fold change. ns = not significant $p > 0.05$; * $p \leq 0.05$; ** $p \leq 0.01$; *** $p \leq 0.001$.

5.6. ZIKV triggers EGFR internalization

Moreover, the subcellular localization and distribution of EGFR throughout infection were analyzed by CLSM using the same conditions as described before. The progression of viral infection was controlled by using a ZIKV envelope-specific antibody visualized in green. In uninfected cells, EGFR was predominantly localized at the periphery of the cells, as visible in red. This is in agreement with the expected localization of EGFR at the plasma membrane. However, in infected cells with a higher MOI, a partial amount of EGFR was delocalized from the plasma membrane as discernible by the appearance of dot-like structures at 1 hpi for both ZIKV strains. The same could be perceived at 9 and 12 hpi, but to a lesser extent. Furthermore, the EGFR dot-like structures were more pronounced at 24 and 48 hpi for both low and high MOI

(Figure 29). These findings suggest that ZIKV infection changes the EGFR subcellular localization and distribution.

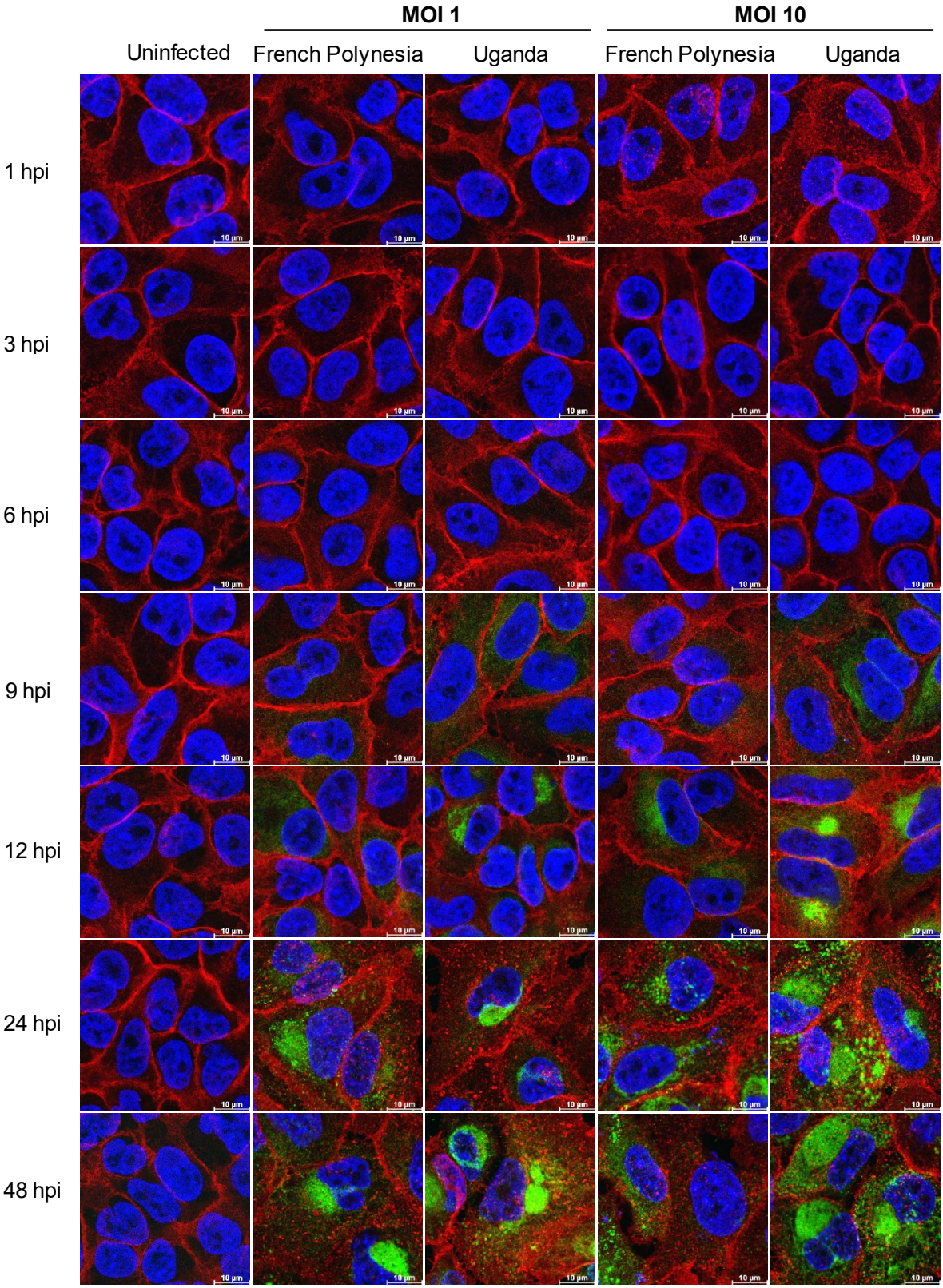

Figure 29 – ZIKV infection alters EGFR subcellular localization and distribution. CLSM analysis of A549-infected cells with either the French Polynesia or the Uganda strain with MOI 1 or MOI 10 and analyzed at the indicated times. Uninfected cells were used as negative control for ZIKV infection. Nuclei

were stained with DAPI in blue, EGFR and ZIKV E protein were visualized with specific antibodies in red and green, respectively. The scale bar represents 10 µm.

To investigate whether the previous observation of the appearance of EGFR dot-like structures corresponds to internalized EGFR, A549 cells were infected with the French Polynesia or the Uganda strain with MOI 1 and analyzed by CLSM at 16 hpi. As positive control, cells were stimulated with EGF. EGFR delocalization from the plasma membrane and formation of dot-like structures was visible in green in EGF-stimulated as well as in ZIKV-infected cells **(Figure 30 A)**. Internalized EGFR was assessed by the colocalization of EGFR with the early endosome antigen 1 (EEA1), an effector protein that is localized only in early endosomes, visualized in red. The colocalization of EGFR with EEA1 is visible in yellow and was quantified by calculating the threshold Mander's overlap coefficient (tMOC), in which 1 represents a total overlap of EGFR with EEA1 and 0 the opposite. Low tMOC values were obtained for uninfected cells, indicating that EGFR and EEA1 weakly colocalize. Contrariwise, an elevated colocalization of EGFR with EEA1 was observed in EGF-stimulated and ZIKV-infected cells, as shown by the high tMOC values **(Figure 30 B)**. Taken together, these data indicate that EGFR is internalized in ZIKV-infected cells.

A

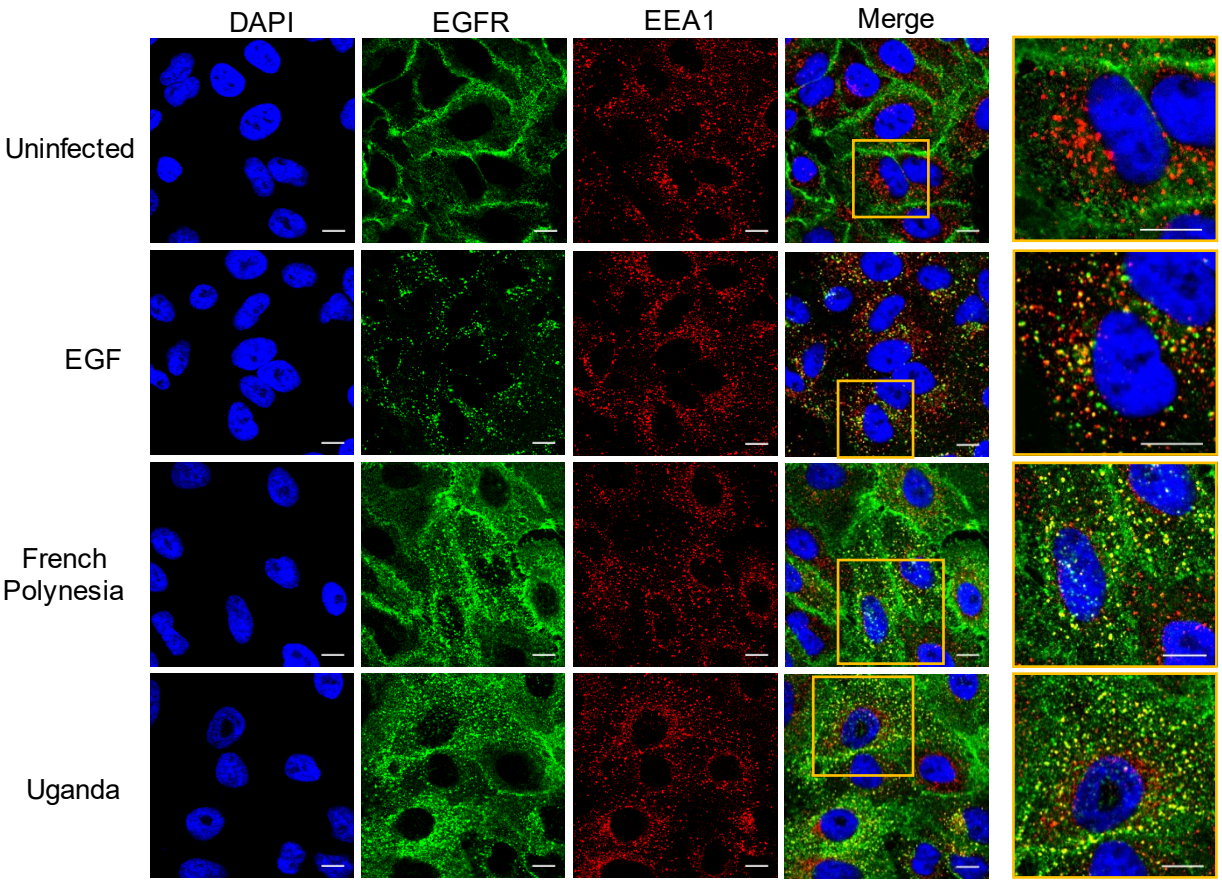

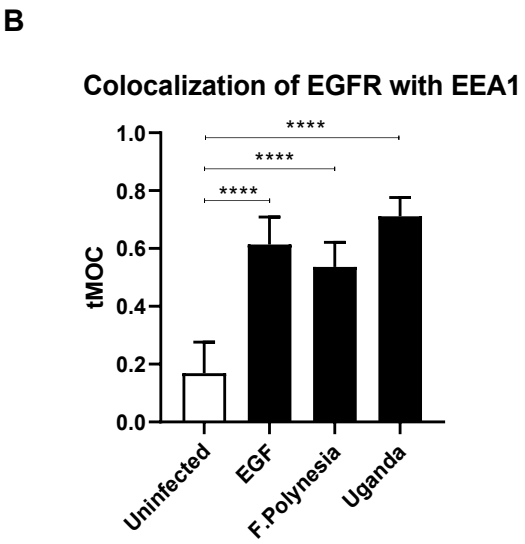

Figure 30 – EGFR colocalizes with EEA1 in ZIKV-infected cells. (A) CLSM analysis of A549-infected cells with either the French Polynesia or the Uganda strain with MOI 1 and analyzed at 16 hpi. Uninfected and EGF-stimulated cells (50 ng/mL EGF) were used as negative and positive control, respectively. Nuclei were stained with DAPI in blue, EGFR and EEA1 were visualized with specific antibodies in green and red, respectively. The yellow square indicates the area that was amplified. The scale bar represents 5 µm. **(B)** The colocalization of EGFR (green signal) with EEA1 (red signal) was quantified by the threshold of Mander's overlap coefficient (tMOC), in which 1 represents a total overlap and 0 the opposite. Quantification is based on at least 6 cells. **** $p \leq 0.0001$.

As the delocalization of EGFR from the cell surface was perceptible at 1 hpi with high MOI **(Figure 29)**, the subcellular localization and distribution of EGFR visible in green were analyzed by CLSM at early stages of infection – 5, 10, 30, 60, and 120 minutes post-infection (mpi). A549 cells were infected with either the French Polynesia or the Uganda strain with MOI 20 at 4°C to synchronize the infection, and subsequently shifted to 37°C to initiate endocytosis. EGFR subcellular localization and distribution in uninfected cells remained the same over time. By contrast, intracellular EGFR was recognized in ZIKV-infected cells at 30 mpi and to a lesser extent at 60 mpi by the formation of dot-like structures **(Figure 31 A)**. To corroborate the previous results, z-stack imaging of ZIKV-infected cells at 30 mpi was performed. The filaments of actin were stained with a Phalloidin-dye conjugate visualized in cyan, underlining the borders of the cells. A significant amount of intracellular EGFR, visualized in red and highlighted by the yellow arrows, was observed in infected cells in comparison to uninfected cells **(Figure 31 B)**. Taken together, these results indicate that EGFR is rapidly internalized during ZIKV entry into the host cell.

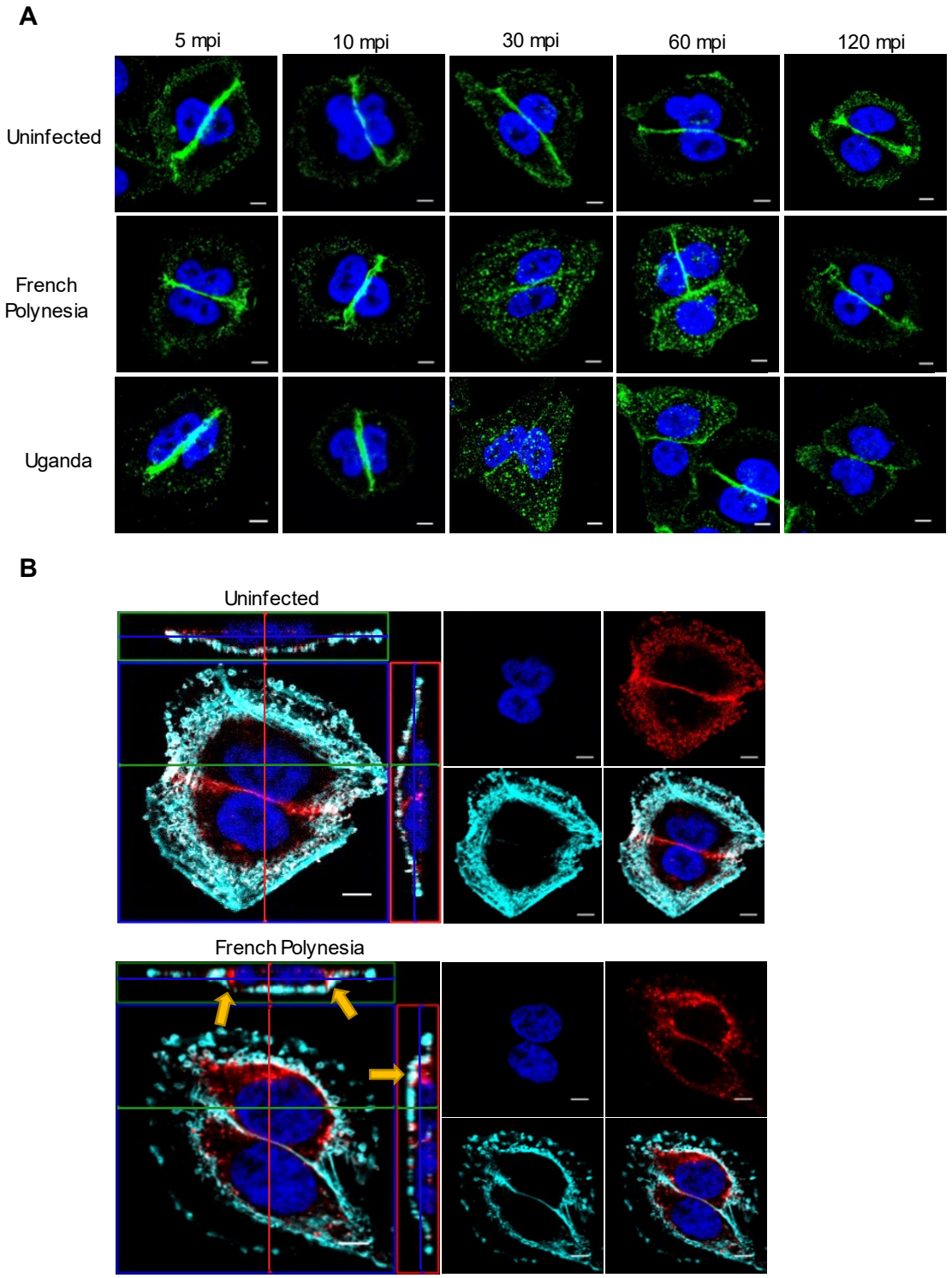

Figure 31 – EGFR is internalized in ZIKV-infected cells. (A) CLSM analysis of A549-infected cells with either the French Polynesia or the Uganda strain with MOI 20 and analyzed at 5, 10, 30, 60, and 120 min post-infection (mpi). Infection was synchronized at 4°C. Uninfected cells were used as negative control. Nuclei were stained with DAPI in blue and EGFR was visualized with a specific antibody in green. The scale bar represents 5 µm. **(B)** Z-stack imaging of A549-infected cells with the French Polynesia strain with MOI 20 and analyzed at 30 mpi. The yellow arrows highlight the intracellular EGFR. Uninfected cells were used as negative control. Nuclei and F-actin were stained with DAPI (blue) and Phalloidin-Atto 633 (cyan), whereas EGFR was visualized with a specific antibody in red. The scale bar represents 5 µm.

5.7. ZIKV activates EGFR and downstream MAPK/ERK signaling cascade

Activation of EGFR and respective signaling cascades results in receptor internalization. To investigate whether ZIKV-dependent internalization of EGFR reflects receptor activation during viral entry, A549 cells were infected with MOI 10 with either the French Polynesia or the Uganda strain and analyzed by Western blot at 5, 10, 15, 30, 60, and 120 mpi. Activation of EGFR and respective MAPK/ERK signaling cascade in ZIKV-infected cells was assessed by the degree of phosphorylation of EGFR at the tyrosine residue 1068 (p-EGFR) and of downstream ERK at the threonine residue 202 and the tyrosine residue 204 (p-ERK 1/2). An elevation of the levels of phosphorylated EGFR and ERK (p-EGFR and p-ERK 1/2) was visible at early times of infection for both ZIKV strains when compared to the uninfected control **(Figure 32 A)**. Quantitative analysis revealed increased amounts of phosphorylated EGFR (p-EGFR) at 5, 10, and 15 mpi in ZIKV-infected cells **(Figure 32 B and C)**. Overall, a higher level of phosphorylation of EGFR (p-EGFR) was detected for the Uganda strain **(Figure 32 C)**. Concerning ERK activation, elevated amounts of phosphorylated ERK (p-ERK 1/2) were also discerned at 5, 10, and 15 min for both strains **(Figure 32 D and E)**. Additionally, increased levels of phosphorylated ERK (p-ERK 1/2) were noticeable at 30 mpi exclusively in cells infected with the French Polynesia strain **(Figure 32 D)**.

A

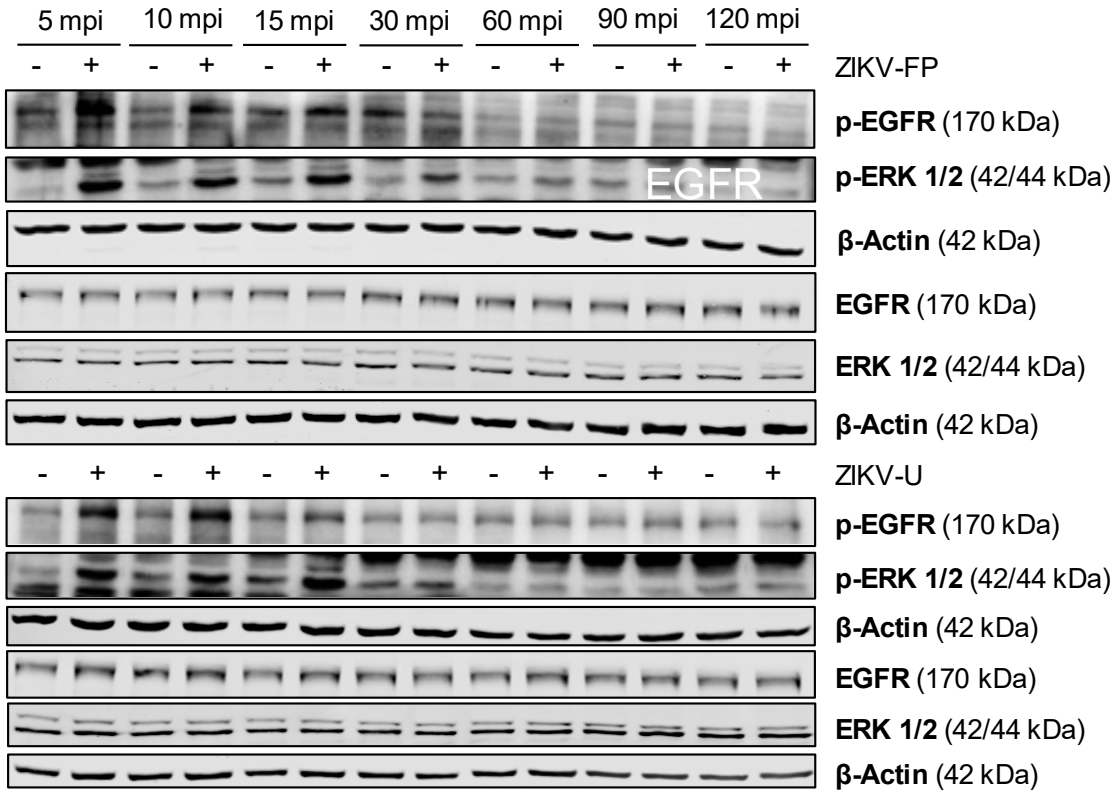

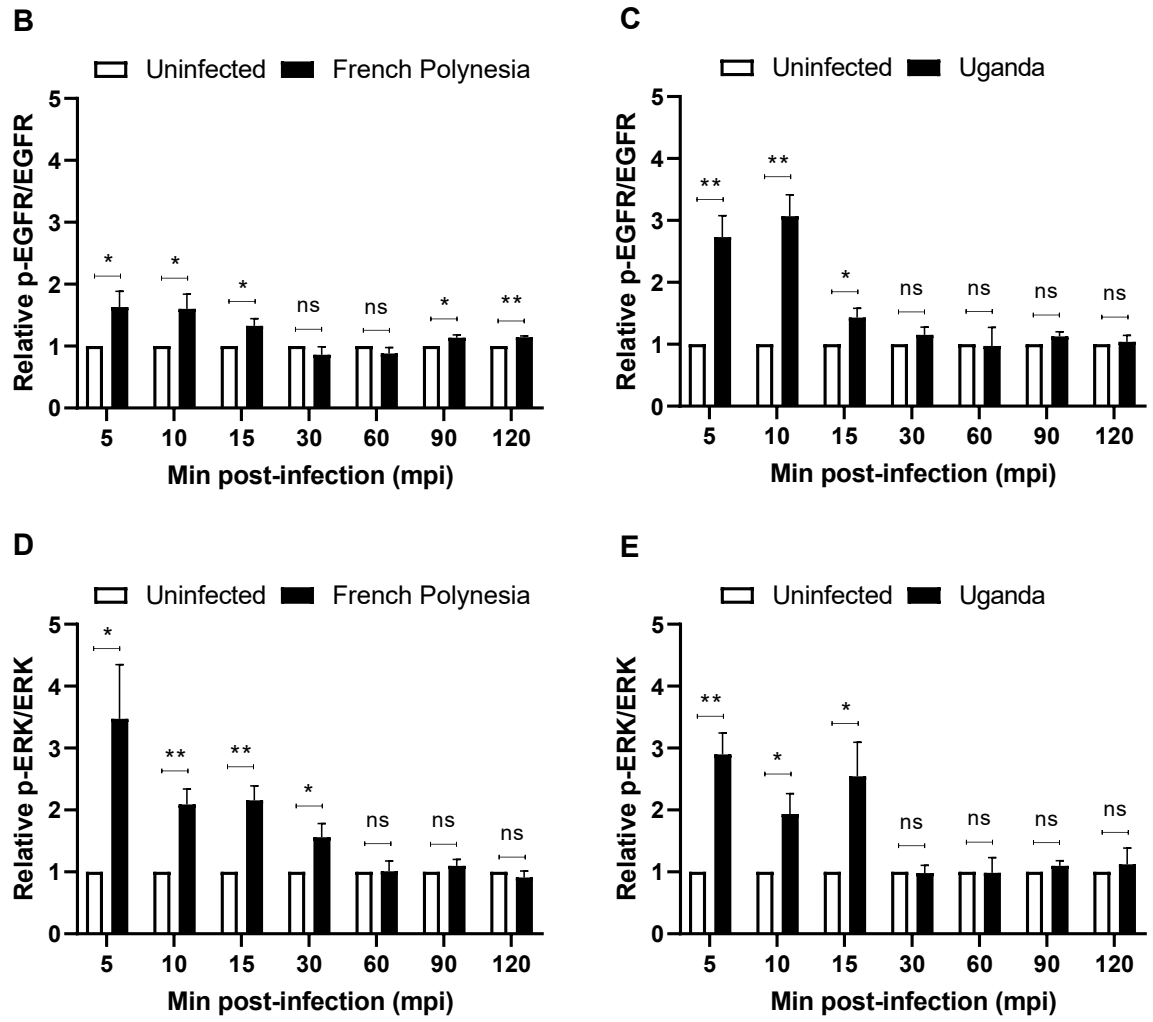

Figure 32 – Activation of EGFR and downstream ERK in ZIKV-infected cells. (A) Representative Western blot and **(B - E)** respective densitometric quantification of **(B, C)** p-EGFR/total EGFR and **(D, E)** p-ERK/total ERK in cell lysates of A549-infected cells with either the French Polynesia (FP) or the Uganda strain (U) with MOI 10 and analyzed at the indicated times. Detection of β-Actin served as loading control. The amounts of p-EGFR and p-ERK were first normalized to the respective amounts of β-Actin, followed by normalization to the total amount of EGFR and ERK, respectively. Uninfected cells (Ø) were used as negative control and as control group for the calculation of the fold change. ns = not significant $p > 0.05$; * $p \leq 0.05$; ** $p \leq 0.01$.

To further confirm these results and investigate whether the degree of activation is dependent on the number of infectious viral particles, A549 cells were infected with either MOI 10 or MOI 30 and at 15 mpi the EGFR kinase activity was analyzed using the PamChip® Peptide Microarray system. The normalized kinase statistic was calculated using the BioNavigator analysis software tool and represents the difference of activity between the analyzed infected samples and the uninfected control. The kinase activity of EGFR was increased in infected cells for both strains in comparison to uninfected cells, as shown by the positive values of the normalized kinase statistic. In general, the normalized kinase statistic was slightly augmented for the Uganda strain. In addition,

the normalized kinase statistic was higher with MOI 30 than with MOI 10, indicating a MOI-dependent activation of EGFR **(Figure 33)**.

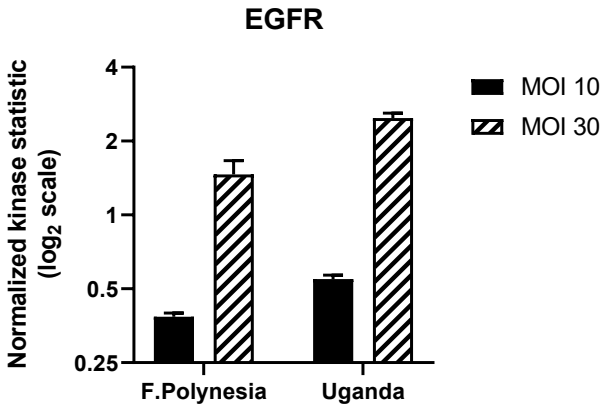

Figure 33 – EGFR kinase activity is increased in ZIKV-infected cells and is MOI-dependent. Kinase activity of EGFR in cell lysates of A549-infected cells with either the French Polynesia or the Uganda strain with MOI 10 or MOI 30 and analyzed at 15 mpi using the PamChip® Peptide Microarray system. The normalized kinase statistic was calculated by the BioNavigator anaylsis software and represents the difference of activity between the analyzed infected samples and the uninfected control group. The data were log_2 transformed by the BioNavigator analysis software. The plotted data is relative to n=6 and n=2 for MOI 10 and MOI 30, respectively.

These data indicate that ZIKV activates EGFR and subsequent MAPK/ERK signaling cascade in the early stages of infection.

5.8. ZIKV-French Polynesia strain delays EGFR degradation

Internalized EGFR is either recycled back to the cell surface or degraded in lysosomes. To investigate whether ZIKV infection affects EGFR half-life, A549 cells were infected with MOI 1 with either the French Polynesia or the Uganda strain. At 16 hpi, cells were serum-starved for 2 h to maximize the amount of EGFR at the cell surface, followed by co-treatment with EGF and cycloheximide to target EGFR for degradation and to prevent *de novo* protein synthesis, respectively. EGFR amount was analyzed by Western blot at 0, 15, 30, 60, 90, 120 min after treatment. The half-life was calculated using the one-phase exponential decay equation. In uninfected cells, after the addition of EGF, the EGFR half-life was approximately 53 min. Similar results were obtained in Uganda-infected cells with a half-life of about 55 min. However, the amount of EGFR was consistent throughout the time points investigated in French Polynesia-infected cells, as observed by the blot and respective quantitative analysis, with a half-life approximately three times longer ($t_{1/2}$=~169 min) **(Figure 34 A and B)**. These results suggest that the half-life of EGFR is prolonged in French-Polynesia infected cells when compared with uninfected cells or Uganda-infected cells.

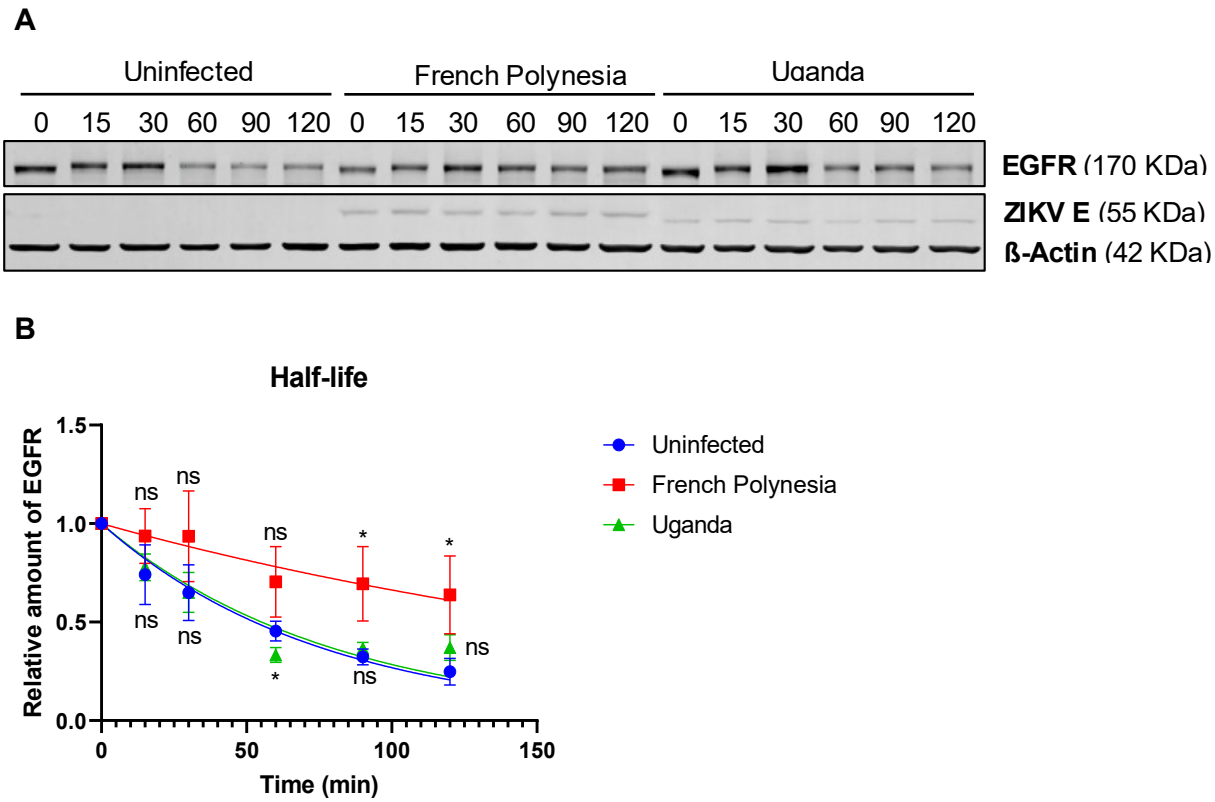

Figure 34 – Delayed degradation of EGFR in French-Polynesia-infected cells, but not in Uganda-infected cells. (A) Representative Western blot and **(B)** respective densitometric quantification of EGFR in cell lysates of A549-infected cells with either the French Polynesia or the Uganda strain with MOI 1 for 16 h, co-treated with 20 µg/mL cycloheximide and 100 ng/mL EGF and analyzed at 0, 15, 30, 60, 90, and 120 min after the beginning of the treatment. Detection of β-Actin served as loading control. t=0 of each condition was used as the control group for the calculation of the fold change. The half-life of EGFR was calculated based on an exponential decay non-linear regression analysis, y(0)=1 and plateau of y=0. ns = not significant $p > 0.05$; * $p \leq 0.05$.

5.9. Inhibition of EGFR and the respective MAPK/ERK signaling cascade diminishes ZIKV infection

To investigate whether EGFR activation and subsequent activation of downstream signaling cascades, in this case the MAPK/ERK pathway, is important for ZIKV infection, selective inhibitors namely Erlotinib (EGFR inhibitor), Sorafenib (Raf inhibitor) and PD98059 (MEK inhibitor) were used. Primarily, to avoid side effects derived from cell toxicity, the optimal working concentration of each compound was determined by cell viability assays. In light of this, a broad range of concentrations was chosen based on the available literature to treat A549 cells during 24 h. Except for Sorafenib, the concentrations tested were well tolerated by the cells **(Figure 35)**. Based on previous studies and the cell viability assays, further experiments were performed with 25 µM Erlotinib, 2 µM Sorafenib, and 50 µM PD98059.[484,485]

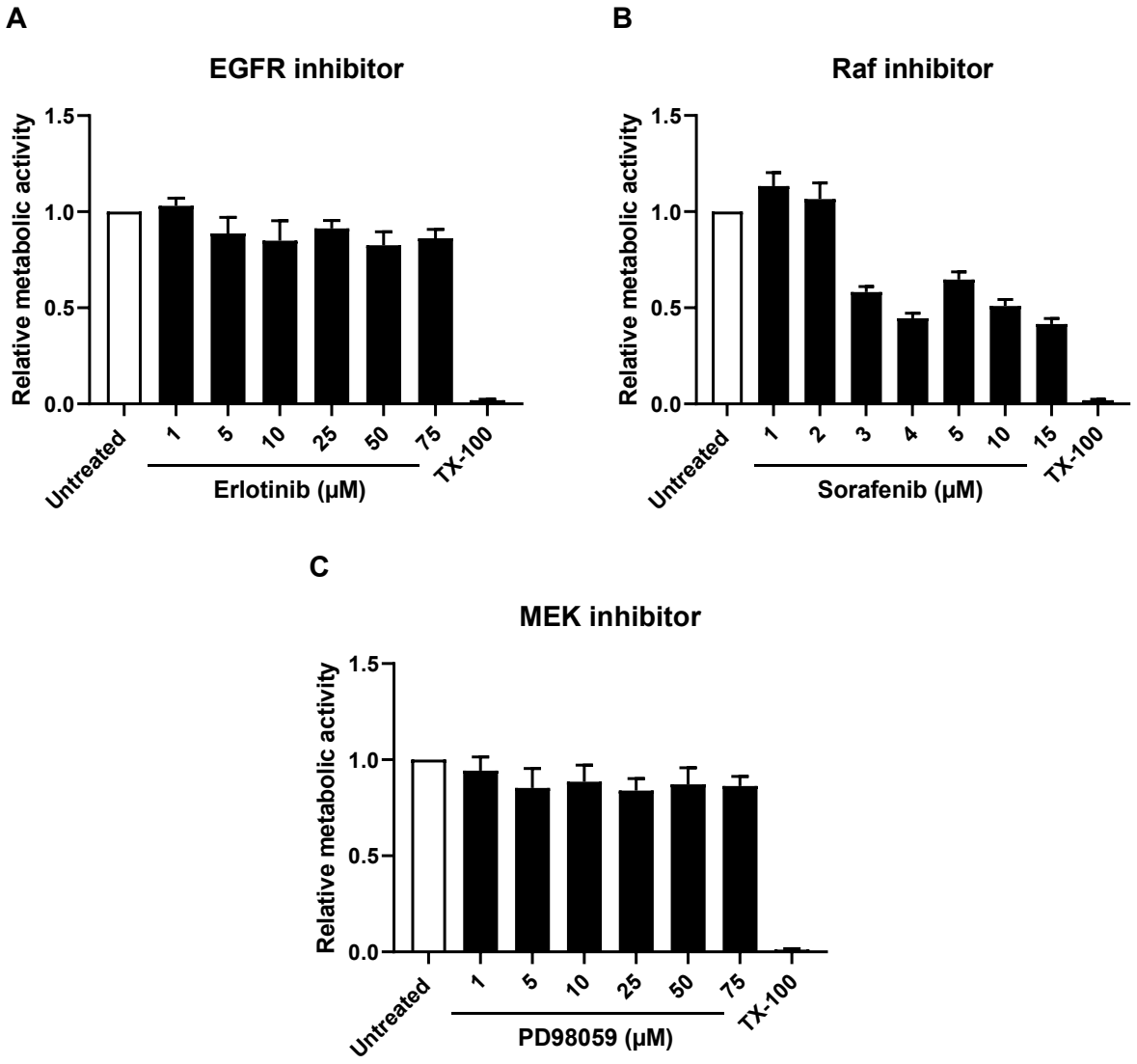

Figure 35 – Cell viability assays after treatment with inhibitors of EGFR and the respective MAPK/ERK signaling cascade. (A - C) Relative metabolic activity of **(A)** Erlotinib-, **(B)** Sorafenib-, and **(C)** PD98059-treated cells determined using the PrestoBlue™ Cell Viability Reagent. The treatment lasted 24 h. Cells treated with 2% Triton X-100 (TX-100) served as positive control. Untreated cells were used and negative control and as control group for the calculation of the fold change.

Following the determination of the optimal working concentrations, A549 cells were pre-treated for 2 h with Erlotinib, Sorafenib, and PD98059 and infected with MOI 1 with either the French Polynesia or the Uganda strain for 4 h. After a short trypsinization step to remove attached but not fully internalized infectious viral particles, cells were cultivated in the presence of the inhibitors and the number of ZIKV genomes was quantified by qPCR at 24 hpi. A significant reduction of the relative number of ZIKV genomes for both strains could be observed in Erlotinib-, Sorafenib-, and PD98059-treated cells in comparison to the DMSO-treated cells **(Figure 36 A-C)**.

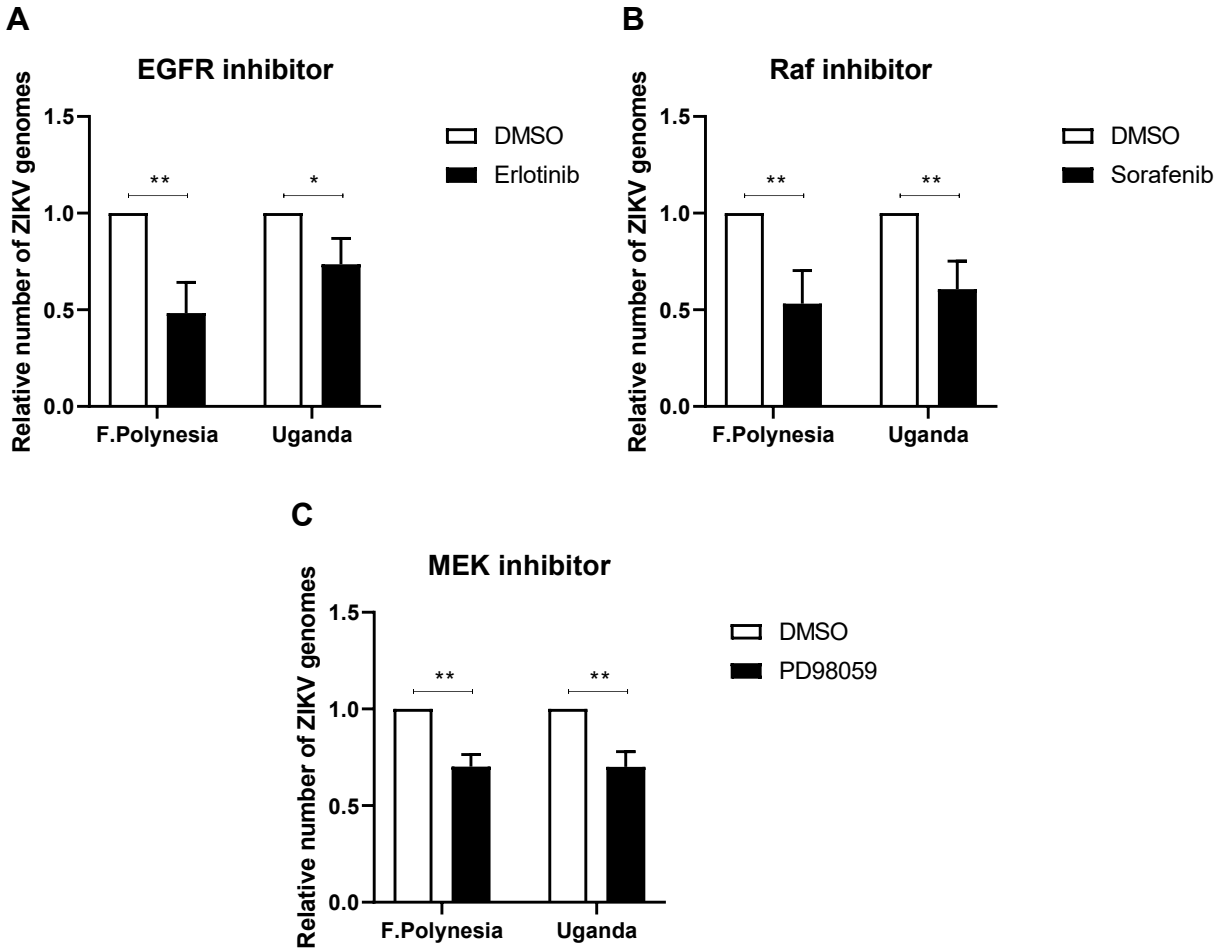

Figure 36 – Selective inhibitors of EGFR and the MAPK/ERK signaling cascade decrease the relative number of ZIKV genomes. (A – C) Relative number of viral genomes of A549 cells pre-treated for 2 h with **(A)** 25 µM Erlotinib, **(B)** 2 µM Sorafenib, and **(C)** 50 µM PD98059 and infected with either the French Polynesia or the Uganda strain with MOI 1. At 4 hpi, attached but not fully internalized viral particles were removed by trypsinization and the number of viral genomes was determined by qPCR at 24 hpi. The compounds were present during the entire experiment. The number of viral genomes was normalized to the number of hRPL27 transcripts. DMSO was used as vehicle control and as control group for the calculation of the fold change. * $p \leq 0.05$; ** $p \leq 0.01$.

To further corroborate these findings, the amount of infectious viral particles was additionally determined by plaque assay. Comparable results could be discerned for the relative amount of infectious viral particles for both ZIKV strains **(Figure 37 A-C)**. These data indicate that selective inhibitors of EGFR and the MAPK/ERK signaling cascade hamper ZIKV infection.

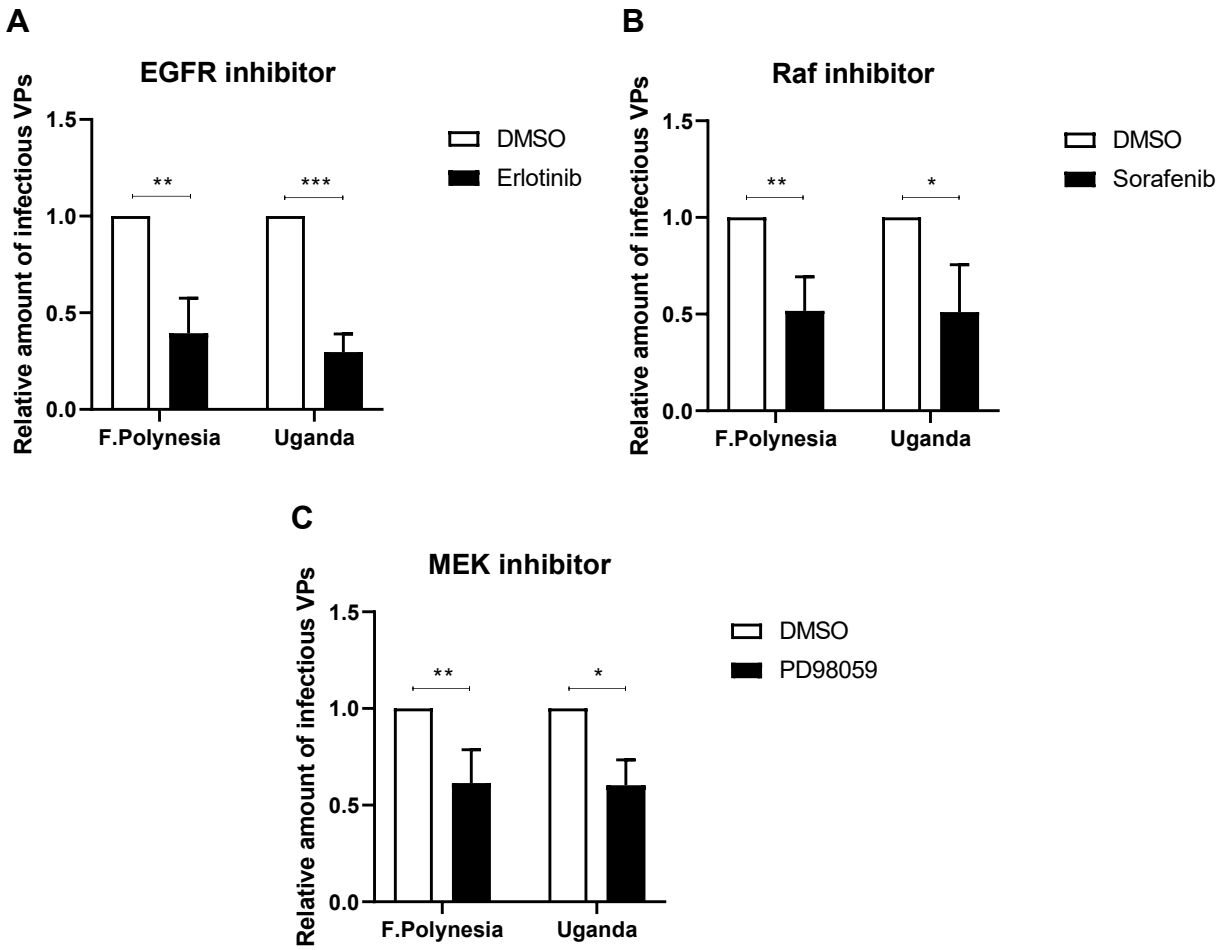

Figure 37 – Selective inhibitors of EGFR and of the MAPK/ERK signaling cascade reduce the relative amount of infectious ZIKV particles. (A – C) Relative amount of infectious viral particles (VPs) of A549 cells pre-treated for 2 h with **(A)** 25 µM Erlotinib, **(B)** 2 µM Sorafenib, and **(C)** 50 µM PD98059 and infected with either the French Polynesia or the Uganda strain with MOI 1. At 4 hpi, attached but not fully internalized viral particles were removed by trypsinization and the amount of infectious viral particles was determined by plaque assay at 24 hpi. The compounds were present during the entire experiment. DMSO was used as vehicle control and as control group for the calculation of the fold change. * $p \leq 0.05$; ** $p \leq 0.01$; *** $p \leq 0.001$.

Moreover, to investigate whether the observed effect on ZIKV infection is due to an impaired viral replication, A549-ZIKVRLuc cells were treated for 24 h under the same conditions as described previously and the luciferase activity was measured by luciferase assay. A minor increase of the relative luciferase activity was detected in Erlotinib-treated cells **(Figure 38 A)**. Nonetheless, no changes could be observed in Sorafenib- and PD98059-treated cells relatively to DMSO-treated cells, rejecting the possibility of the inhibitory effect be on the viral replication **(Figure 38 B and C)**. These findings demonstrate that activation of EGFR and the subsequent MAPK/ERK signaling cascade is essential during the early stages of ZIKV infection, but not for the replication of the viral genome.

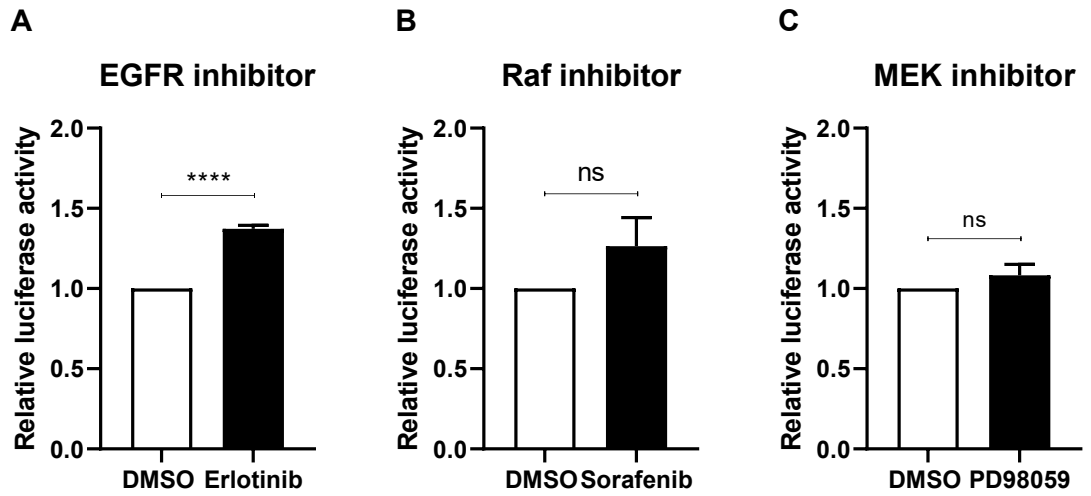

Figure 38 – Selective inhibitors of EGFR and the MAPK/ERK signaling cascade do not diminish the relative luciferase activity. (A – C) Relative luciferase activity of ZIKV-luciferase-replicating A549 cells treated with **(A)** 25 µM Erlotinib, **(B)** 2 µM Sorafenib, and **(C)** 50 µM PD98059 for 24 h. The luciferase activity was determined by luciferase assay. DMSO was used as vehicle control and as control group for the calculation of the fold change. ns = not significant $p>0.05$; **** $p\leq0.0001$.

Due to the lack of impairment in viral replication **(Figure 39)**, the effect of these inhibitors on the viral entry process was investigated. For this purpose, A549 cells were pre-treated with Erlotinib, Sorafenib, and PD98059 for 2 h and subsequently an entry assay was performed. The entry assay revealed a reduction in the relative number of internalized ZIKV genomes determined by qPCR in Erlotinib-treated cells relatively to the DMSO control **(Figure 39 A)**, indicating that the TK activity of EGFR is required for an efficient viral entry. However, no impact could be observed in Sorafenib- and PD98059-treated cells **(Figure 39 and C)**.

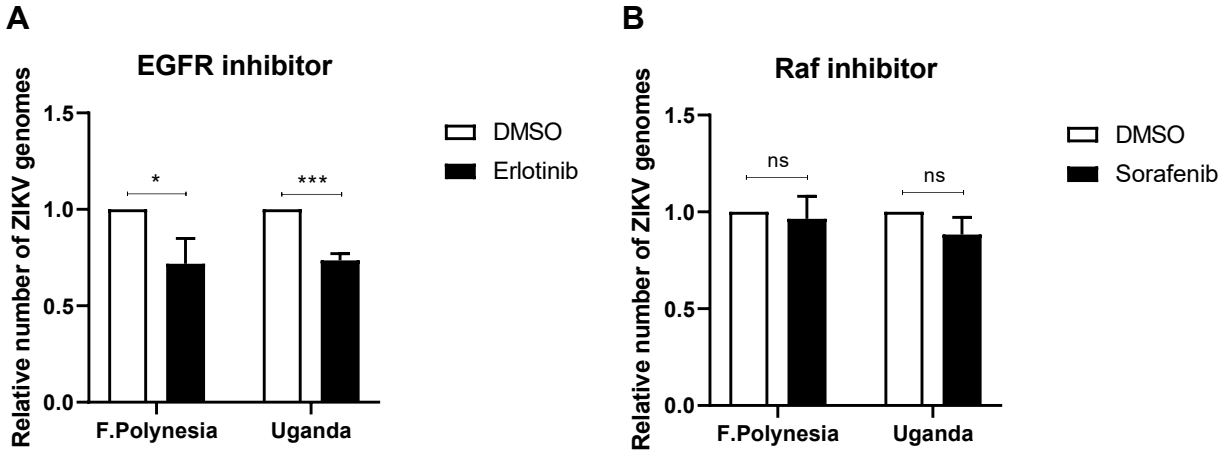

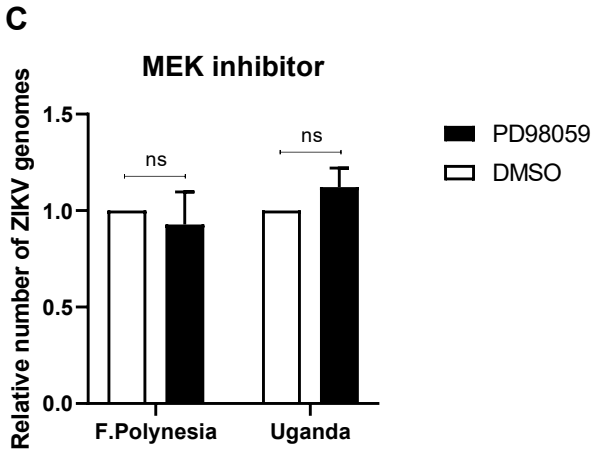

Figure 39 – EGFR selective inhibitor has an impact on viral entry, but not MAPK/ERK signaling cascade inhibitors. (A – C) Relative number of internalized viral genomes of A549 cells pre-treated for 2 h with **(A)** 25 µM Erlotinib, **(B)** 2 µM Sorafenib, and **(C)** 50 µM PD98059 and infected with either the French Polynesia or the Uganda strain with MOI 10. The number of viral genomes was quantified by qPCR and normalized to the number of hRPL27 transcripts after performing an entry assay. The compounds were present during the entire experiment. DMSO was used as vehicle control and as control group for the calculation of the fold change. ns = not significant $p>0.05$; * $p\leq0.05$; *** $p\leq0.001$.

Because of the absent effect of Sorafenib and PD98059 on the ZIKV entry process, the influence of these compounds on EGFR internalization was investigated by CLSM analysis using an EGFR-specific antibody visualized in red. Upon EGF stimulation, only Erlotinib was able to interfere and partially prevent EGFR internalization, indicating that the inhibitory effect of Sorafenib and PD98059 in ZIKV infection is not due to an impaired internalization of EGFR **(Figure 40)**.

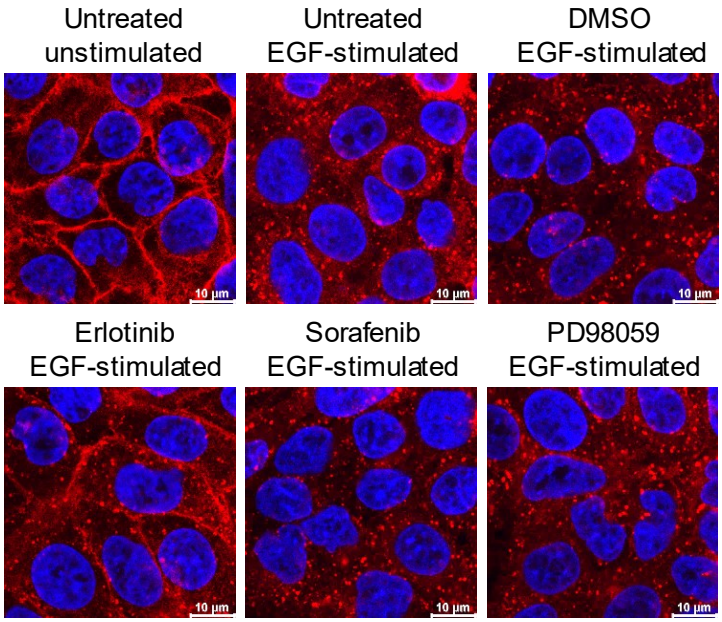

Figure 40 – EGFR selective inhibitor prevents EGFR internalization upon EGF stimulation, but not MAPK/ERK signaling cascade inhibitors. CLSM analysis of A549 cells pre-treated with 25 µM Erlotinib, 2 µM Sorafenib, and 50 µM PD98059 for 2 h and subsequently stimulated with 50 ng/mL of EGF for 30

min. Untreated unstimulated and untreated EGF-stimulated cells were used as negative and positive control for EGF treatment, respectively. DMSO-treated cells were used as vehicle control. Nuclei were stained with DAPI in blue and EGFR was visualized with a specific antibody in red. The scale bar represents 10 µm.

Taken together, these findings indicate that EGFR activation is essential for the ZIKV entry process and the subsequent activation of the MAPK/ERK signaling cascade is relevant to steps of the viral life cycle prior to the onset of viral replication and morphogenesis, but after viral entry.

5.10. Lipid raft disruption affects ZIKV binding and entry

Despite the fact that lipid rafts promote interactions among signaling molecules, previous studies showed that the disruption of lipid rafts results in ligand-independent activation of EGFR and of downstream signaling cascades.[486] To further study the importance of the activation of EGFR and of EGFR-mediated signaling cascades for ZIKV entry and to investigate whether the localization of EGFR in lipid rafts is relevant for ZIKV infection, methyl-β-cyclodextrin (MβCD), a cholesterol-depleting agent, was used to disrupt lipid rafts. To rule out that possible inhibitory effects might derive from cell toxicity, the metabolic activity upon treatment was determined by a cell viability assay. For this purpose, A549 cells were serum-starved for 24 h to lower the cellular cholesterol content, followed by treatment with a wide range of concentrations of MβCD for 1 h. Only the highest concentration (20 µM) affected the cellular metabolic activity **(Figure 41)**. Hence, further experiments were performed with 1, 5, and 10 mM of MβCD.

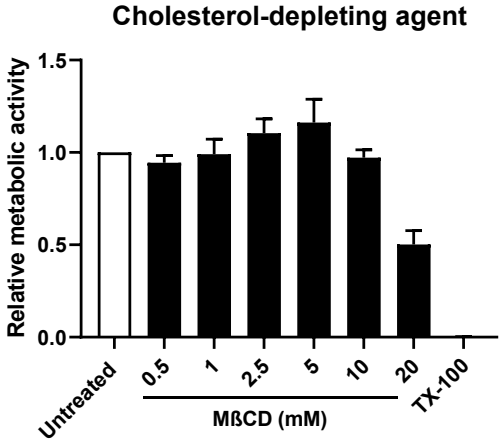

Figure 41 – Cell viability assay after treatment with MβCD. Relative metabolic activity of A549 cells serum-starved for 24 h and treated with MβCD for 1 h. The metabolic activity was determined using the PrestoBlue™ Cell Viability Reagent. Cells treated with 2% Triton X-100 (TX-100) served as positive control. Untreated cells were used as negative control and as control group for the calculation of the fold change.

Following the determination of an optimal range of concentrations, activation of EGFR and the MAPK/ERK signaling cascade upon MβCD treatment was evaluated. In light of this, serum-starved A549 cells were treated with the different concentrations of MβCD, as indicated previously, and the level of phosphorylated EGFR (p-EGFR) and downstream ERK (p-ERK 1/2) was assessed by Western blot analysis. In addition, cells were stimulated with EGF after MβCD treatment. In both unstimulated and EGF-stimulated cells, an increase in the amount of phosphorylated EGFR (p-EGFR) and downstream ERK (p-ERK 1/2) was observed after MβCD treatment **(Figure 42 A-C)**. These data confirm that the chosen concentrations of MβCD activate EGFR and the MAPK/ERK signaling cascade.

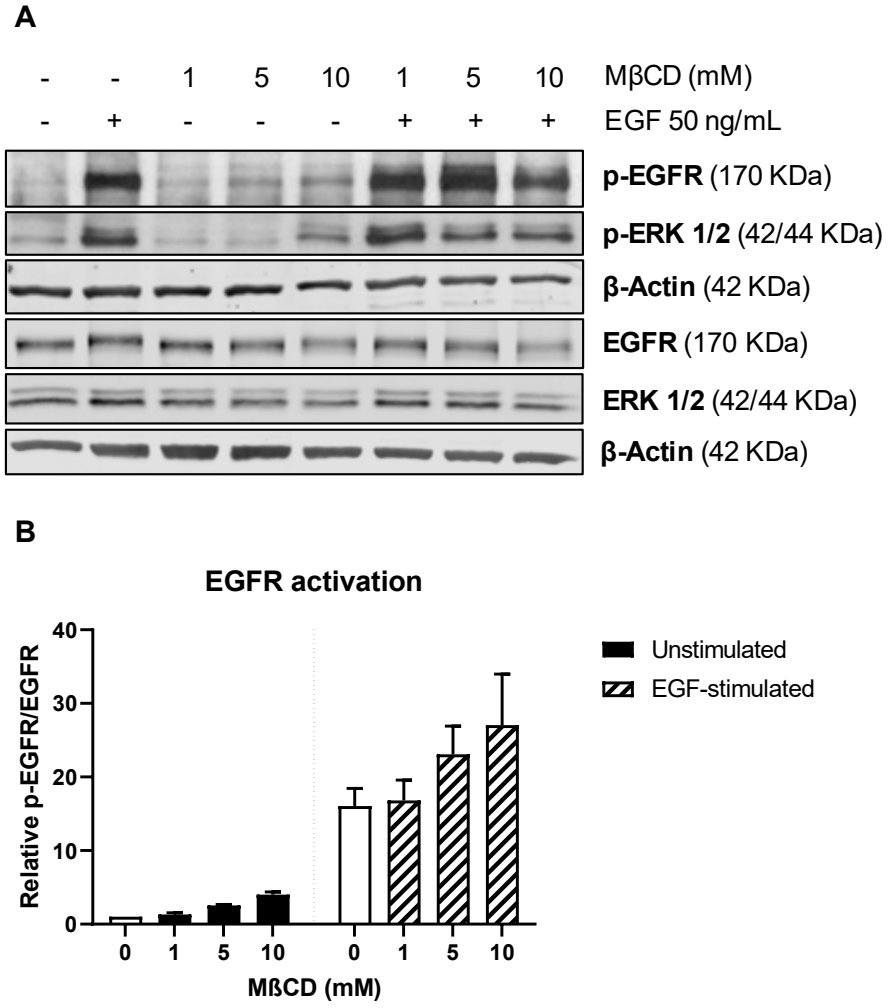

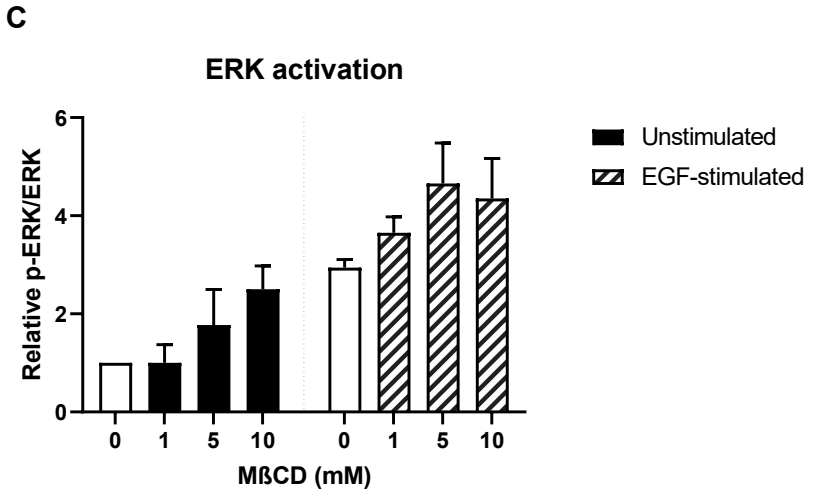

Figure 42 – Activation of EGFR and downstream ERK upon MβCD treatment. (A) Representative Western blot and **(B, C)** respective densitometric quantification of **(B)** p-EGFR/total EGFR and **(C)** p-ERK/total ERK in cell lysates of serum-starved A549 cells treated for 1 h with 1, 5, and 10 mM MβCD and stimulated with EGF (50 ng/mL) for 30 min or left unstimulated. Detection of β-Actin served as loading control. The amounts of p-EGFR and p-ERK were first normalized to the respective amounts of β-Actin, followed by normalization to the total amount of EGFR and ERK, respectively. Unstimulated untreated cells were used as negative control and as control group for the calculation of the fold change.

Ultimately, to investigate the impact of MβCD on the ZIKV entry, serum-starved A549 cells were primarily treated with MβCD for 1 h. After complete removal of this cholesterol-depleting agent to avoid affecting the structure of the viral particles and thus, destroying them, cells were infected with either the French Polynesia or the Uganda strain with MOI 10 for 1 h. Afterwards, binding and entry assays were performed and the number of ZIKV genomes was determined by qPCR. While MβCD showed no effect on the relative number of attached ZIKV genomes in French Polynesia-infected cells, a dose-dependent decline was observed for the Uganda strain **(Figure 43 A)**. Regarding the entry assay, a gradual reduction of the relative number of ZIKV genomes was observed for both strains after treatment **(Figure 43 B)**. These results suggest that lipid raft disruption by MβCD treatment disturbs ZIKV binding and entry.

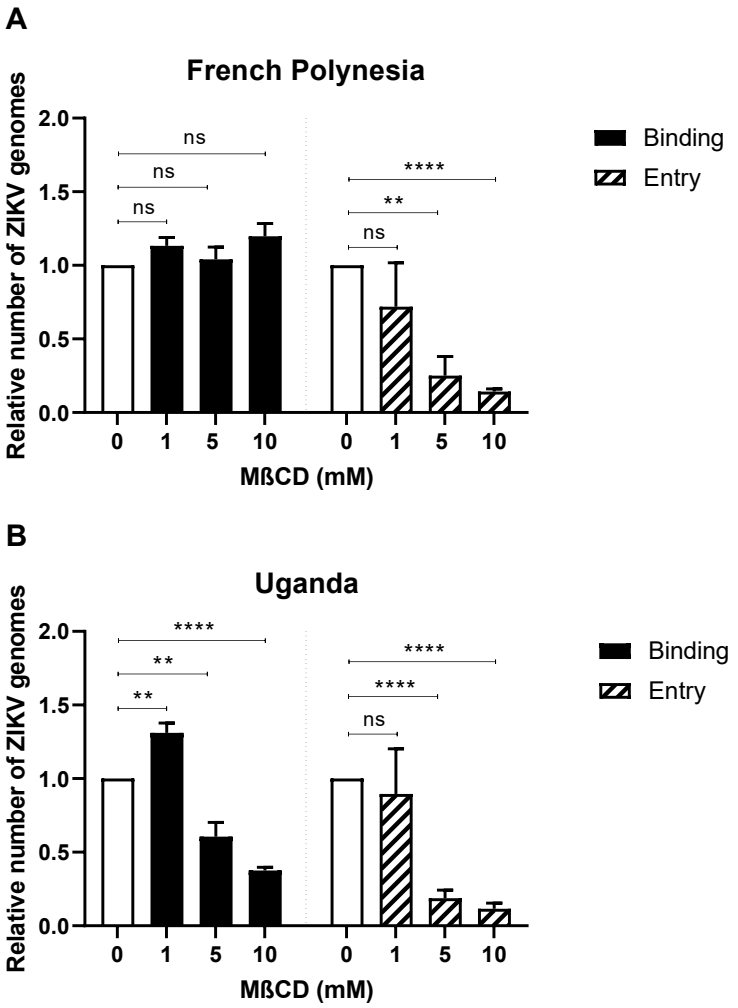

Figure 43 – MβCD treatment disturbs ZIKV binding and entry. (A, B) Relative number of attached and internalized viral genomes of A549 cells serum-starved for 24 h, treated with 1, 5, and 10 mM MβCD and infected with either the French Polynesia or the Uganda strain with MOI 10. The number of genomes was quantified by qPCR and normalized to the number of hRPL27 transcripts after performing a binding and entry assay. Infected untreated cells were used as the control group for the calculation of the fold change. ns = not significant $p > 0.05$; ** $p \leq 0.05$; **** $p \leq 0.0001$.

Regardless of the activation of EGFR and the MAPK/ERK signaling cascade, ZIKV binding and entry were affected upon MβCD treatment. To better understand the effect of MβCD on ZIKV entry and to investigate whether this could be related to hampered EGFR internalization, EGFR subcellular localization was investigated under the same conditions as described above by CLSM analysis using an EGFR-specific antibody visible in red. While in unstimulated cells no impact on the localization of EGFR was noticeable after MβCD treatment, in EGF-stimulated cells higher concentrations of MβCD strongly impaired the amount of internalized EGFR, characterized by the decrease in the number of EGFR dot-like structures **(Figure 44)**.

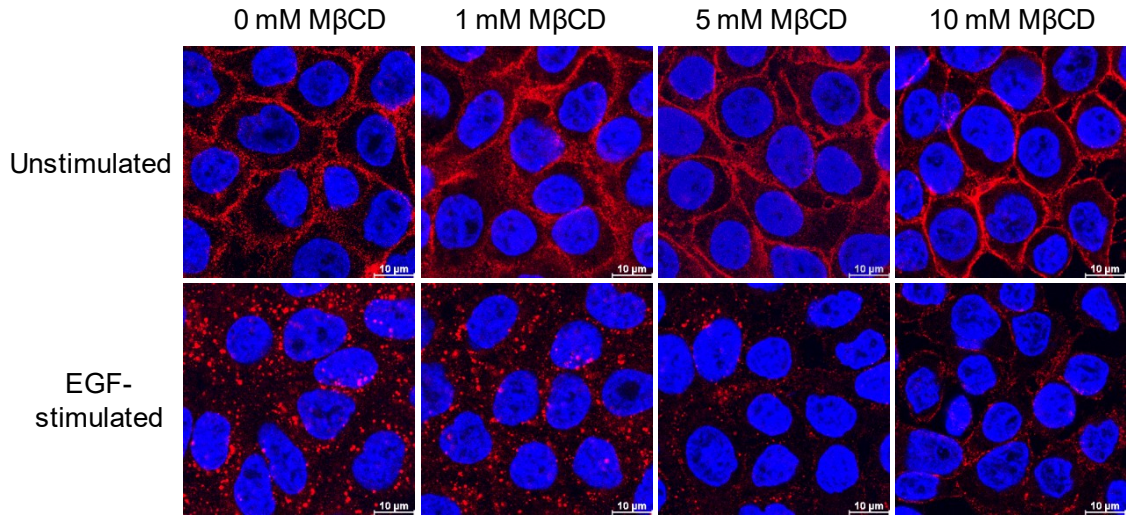

Figure 44 – MβCD treatment affects EGFR internalization upon EGF stimulation. CLSM analysis of serum-starved A549 cells treated with 1, 5, and 10 mM MβCD for 1 h and subsequently stimulated with 50 ng/mL of EGF for 30 min. Untreated unstimulated and untreated EGF-stimulated cells were used as negative and positive control for EGF treatment, respectively. Nuclei were stained with DAPI in blue and EGFR was visualized with a specific antibody in red. The scale bar represents 10 µm.

Taken together, these data indicate that EGFR activation alone is not sufficient for an efficient internalization of ZIKV.

5.11. ZIKV infection is decreased in A549-EGFR KO cells

To validate the relevance of EGFR for ZIKV infection, EGFR was knocked out of A549 cells using the CRISPR/Cas9 system and stable cells were generated by selection with puromycin. Two different cell clones of transfected cells with the PX459 plasmid encoding either one of the EGFR sgRNA sequences were chosen for this study as well as two different cell clones of transfected cells with the PX459 plasmid encoding the off-target sequence. First, the production of monoclonal A549-EGFR KO cells was evaluated by CLSM analysis using an EGFR-specific antibody visible in red. Untransfected A549 cells were used to control possible side effects that originated from the transfection. CLSM analysis revealed a drastic reduction in the EGFR protein and the loss of membrane-associated EGFR level in the PX459-EGFR sgRNA1 or sgRNA 2-transfected cells, demonstrating a successful generation of monoclonal A549-EGFR KO cells **(Figure 45 A)**. Additionally, no major changes in the subcellular localization and protein level of EGFR were discerned between untransfected and off-target cells. The absence of EGFR was further confirmed by Western blot analysis **(Figure 45 B)**.

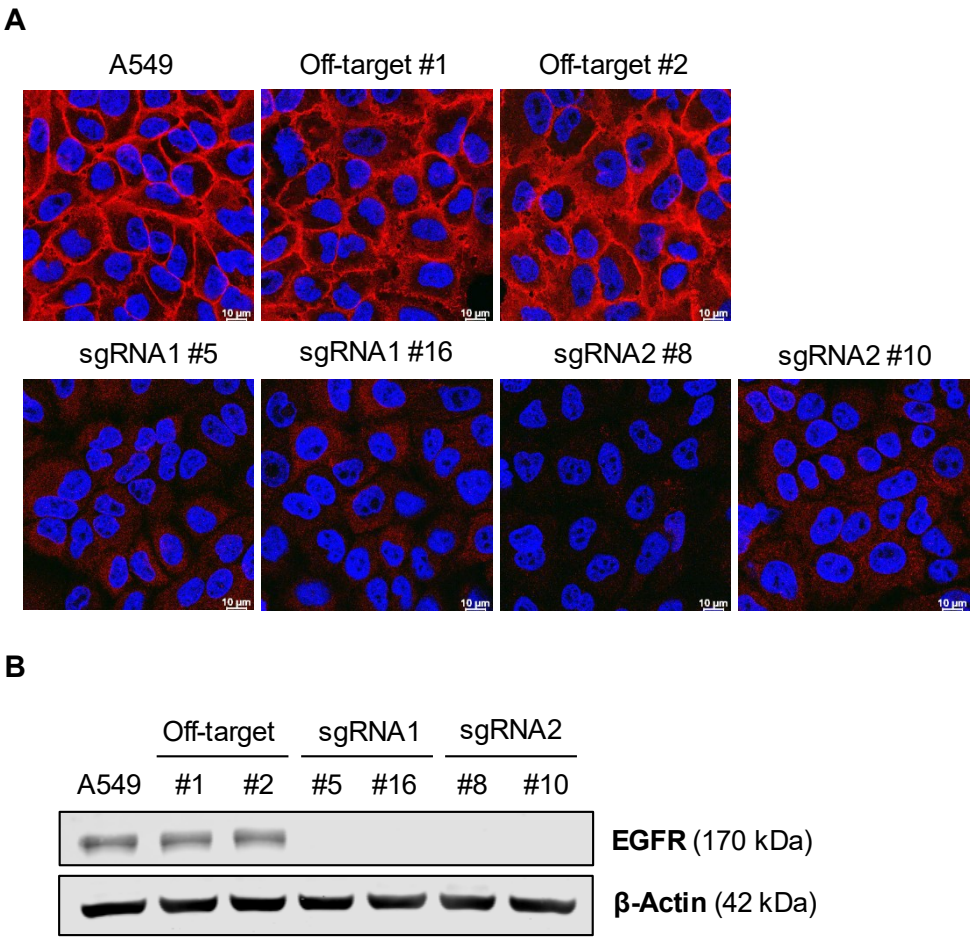

Figure 45 – Successful generation of A549-EGFR KO cells. (A) CLSM analysis of A549-EGFR KO cells generated using the CRISPR/Cas9 system. A549 cells were transfected with the PX459 plasmid containing either one of the EGFR sgRNA sequences. A549 cells transfected with the PX459 plasmid containing the off-target sequence were used as negative control. A549 cells were used as untransfected control. Nuclei were stained with DAPI in blue and EGFR was visualized with a specific antibody in red. The scale bar represents 10 µm. **(B)** Representative Western blot of EGFR in cell lysates of A549-EGFR KO cells generated using the CRISPR/Cas9 system. A549 cells were transfected with the PX459 plasmid containing either one of the EGFR sgRNA sequences. A549 cells transfected with the PX459 plasmid containing the off-target sequence were used as negative control. A549 cells were used as untransfected control. Detection of β-Actin served as loading control.

To validate the lack of EGFR functionality and subsequent activation of the MAPK/ERK signaling cascade, A549-EGFR KO cells were stimulated with EGF for 30 min and the levels of phosphorylation of EGFR and downstream ERK were analyzed by Western blot. Upon EGF stimulation, an increase in the amount of phosphorylated EGFR (p-EGFR) and ERK (p-ERK 1/2) was noticeable in the off-target control cells, but no changes were observed in the A549-EGFR KO cells in comparison to the correspondent unstimulated cells, corroborating the absence of EGFR activity in these cells **(Figure 46)**.

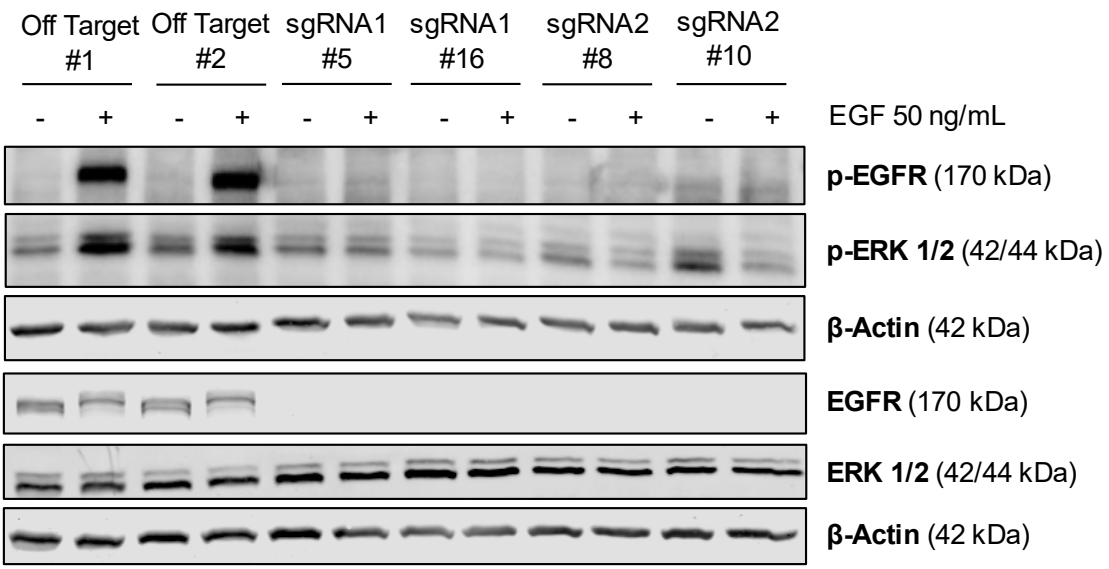

Figure 46 – A549-EGFR KO cells lack EGFR functionality. Representative Western blot of p-EGFR, total EGFR, p-ERK, and total ERK in cell lysates of A549-EGFR KO cells generated using the CRISPR/Cas9 system and stimulated with EGF (50 ng/mL) for 30 min. A549 cells were transfected with the PX459 plasmid containing either one of the EGFR sgRNA sequences. A549 cells transfected with the PX459 plasmid containing the off-target sequence were used as negative control. Unstimulated cells were used as negative control for EGF stimulation. Detection of β-Actin served as loading control.

Following the characterization and confirmation of the successful generation of A549-EGFR KO cells, these cells were infected with either the French Polynesia or the Uganda strain with MOI 1 and the number of ZIKV genomes was determined by qPCR. A considerable reduction of the relative number of ZIKV genomes for both viral strains was detected in A549-EGFR KO cells in comparison to the off-target cells **(Figure 47 A and B)**.

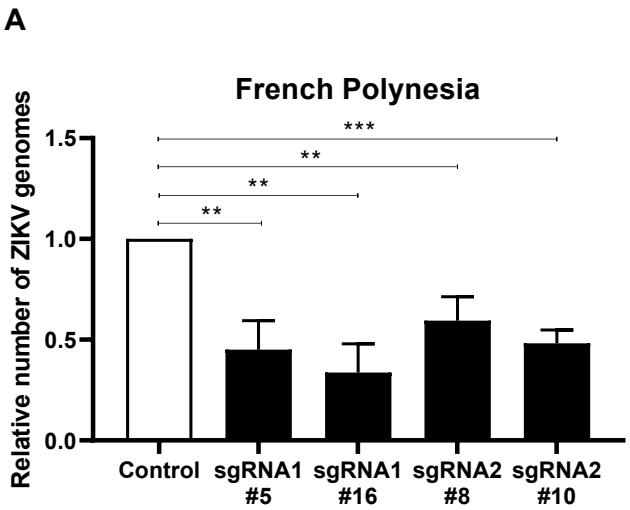

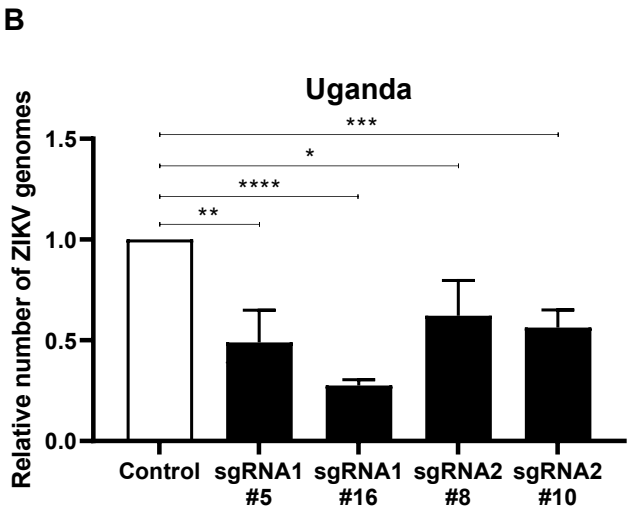

Figure 47 – EGFR KO in A549 cells diminishes the relative number of ZIKV genomes. (A, B) Relative number of viral genomes of A549-EGFR KO cells generated using the CRISPR/Cas9 system and infected with either the **(A)** French Polynesia or the **(B)** Uganda strain with MOI 1. A549 cells were transfected with the PX459 plasmid containing either one of the EGFR sgRNA sequences. A549 cells transfected with the PX459 plasmid containing the off-target sequence were used as negative control. The number of viral genomes was determined at 24 hpi by qPCR and normalized to the number of hRPL27 transcripts. The mean of the viral genomes quantified in the off-target cells was used for the calculation of the fold change. * $p \leq 0.05$; ** $p \leq 0.01$; *** $p \leq 0.001$; **** $p \leq 0.0001$.

To further corroborate these results, the amount of infectious viral particles was determined by plaque assay. A decline in the relative amount of infectious viral particles was perceived as well for both ZIKV strains in the A549-EGFR KO cells **(Figure 48 A and B)**. These data suggest that EGFR KO in A549 cells impairs ZIKV infection.

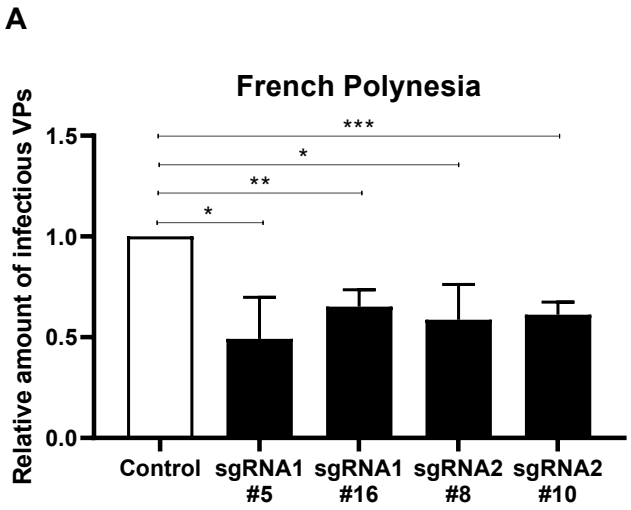

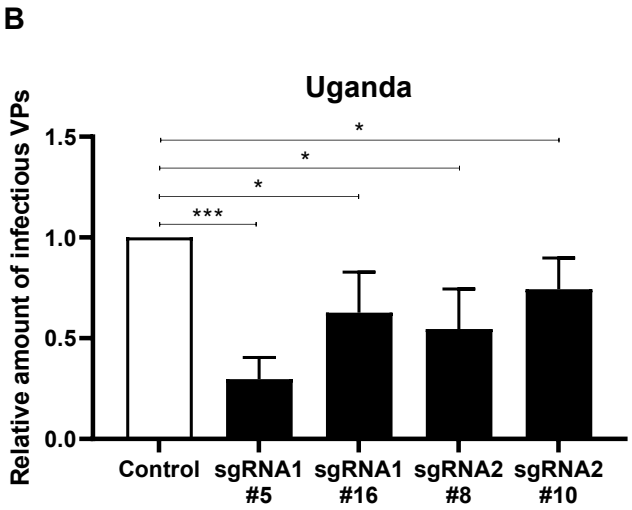

Figure 48 – EGFR KO in A549 cells reduces the relative amount of infectious ZIKV particles. (A, B) Relative amount of infectious viral particles (VPs) of A549-EGFR KO cells generated using the CRISPR/Cas9 system and infected with either the **(A)** French Polynesia or the **(B)** Uganda strain with MOI 1. A549 cells were transfected with the PX459 plasmid containing either one of the EGFR sgRNA sequences. A549 cells transfected with the PX459 plasmid containing the off-target sequence were used as negative control. The amount of infectious viral particles was determined at 24 hpi by plaque assay. The mean of the viral genomes quantified in the off-target cells was used for the calculation of the fold change. * $p \leq 0.05$; ** $p \leq 0.01$; *** $p \leq 0.001$

To further investigate the relevance of EGFR for the ZIKV entry process, A549-EGFR KO cells were infected with either the French Polynesia or the Uganda strain with MOI 10 and subsequently an entry assay was performed. The entry assay revealed a decrease in the relative number of internalized ZIKV genomes determined by qPCR in A549-EGFR KO cells in comparison to the off-target control **(Figure 49)**.

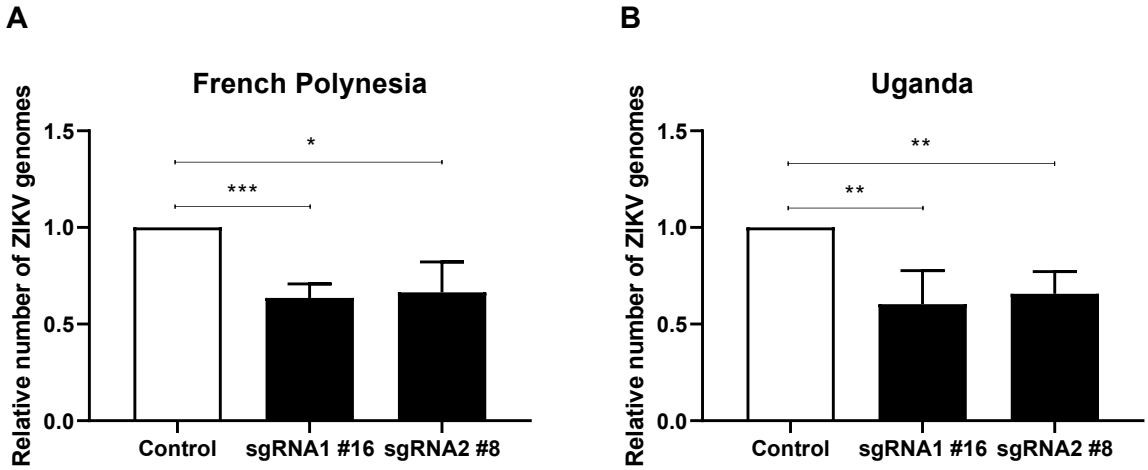

Figure 49 – EGFR KO in A549 cells declines ZIKV entry. (A, B) Relative number of internalized viral genomes of A549-EGFR KO cells generated using the CRISPR/Cas9 system and infected with either the **(A)** French Polynesia or the **(B)** Uganda strain with MOI 10. A549 cells were transfected with the PX459 plasmid containing either one of the EGFR sgRNA sequences. A549 cells transfected with the PX459 plasmid containing the off-target sequence were used as negative control. The number of viral genomes

was quantified by qPCR and normalized to the number of hRPL27 transcripts after performing an entry assay. The mean of the viral genomes quantified in the off-target cells was used for the calculation of the fold change. * $p \leq 0.05$; ** $p \leq 0.01$; *** $p \leq 0.001$.

Taken together, these data show that EGFR KO in A549 cells affects ZIKV entry, indicating that EGFR is a relevant host factor during the early stages of the ZIKV life cycle.

6. Discussion

Even though ZIKV was discovered in 1947, it only caught the interest of the scientific community in the last 10 years due to the outbreak in French Polynesia (2013-2014) and the epidemic in the Americas (2015-2016). These events revealed neurological complications associated with ZIKV infection including microcephaly in newborns and GBS in adults.

Previous research work on the identification of suitable cell culture models to study ZIKV infection unveiled that the CHO cells do not support viral infection.[459] However, it remained unclear which step of the viral life cycle was not sustained in these cells. In light of this, binding, entry, and post-entry assays were performed. In this study, two different ZIKV strains (the French Polynesia H/PF/2013 strain and the Uganda 976 strain) were used to represent the distinct types of pathogenesis observed in the human population. The viral attachment to CHO cells did not significantly vary from A549, a highly ZIKV permissive cell line (Figure 19 A).[225,459] This is not surprising, as elements of the extracellular matrix, such as glycosaminoglycans, have been described as viral attachment factors that concentrate the viral particles on the cell surface before their interaction with primary receptors. More precisely, heparan sulfate and chondroitin sulfate, which are present on the surface of CHO cells, have been shown to be involved in the ZIKV entry process.[271,487] Contrariwise, the entry assay revealed a noteworthy discrepancy between A549 and CHO cells, which was also reflected in the post-entry assay (Figure 19 B and C). These results indicate that ZIKV entry is affected in CHO cells. It is known that the CHO cells lack endogenous EGFR.[482,488] EGFR as an RTK is intimately involved in the regulation of crucial cellular processes such as proliferation, survival, differentiation, and migration. Given the broad range of cellular functions and its localization at the cell surface, several viruses are recognized to interact with EGFR, directly or indirectly through adaptors, and modulate its activity to facilitate their entry into the target cells, to increase viral replication, and even to counteract host antiviral responses.[489] Considering this, the present study aimed to investigate the relevance of EGFR and of EGFR-dependent signaling for the ZIKV life cycle *in vitro* using A549 cells.

Initially, the protein amount of EGFR and AXL, the latter is the initial reported primary receptor, was investigated in ZIKV permissive cell lines. Unlike for AXL, it was possible to detect EGFR on a protein level in all the cell lines studied, except in CHO and HepG2/C3A cells (Figure 20). As previously mentioned, CHO cells do not express endogenous EGFR and the results obtained are in accordance with this. Concerning the HepG2/C3A cells, a subclone of the HepG2 cells, there are contradictory data about EGFR expression.[490,491] Nevertheless, it has been reported that some viruses, including

flaviviruses, are quite promiscuous in their options of host cell receptors and do not rely on a unique molecule to overcome the plasma membrane barrier. [289,492] Thus, it is possible that in this cell line another ErbB receptor or even another RTK might be replacing EGFR and its plausible role on ZIKV infection. This could explain the conflicting data in the literature regarding the relevance of AXL in ZIKV entry as well.[273,279–281] Overall, these data concur with EGFR as a potential host factor relevant for the ZIKV life cycle since it is expressed in the majority of ZIKV permissive cell lines.

As ZIKV entry was found to be compromised in CHO cells, viral infection was investigated in CHO cells stably overexpressing EGFR.[463] EGFR overexpression in CHO cells did not render these cells permissive to ZIKV infection as shown by the absence of ZIKV-infected cells by CLSM analysis (Figure 23). Upon ligand binding, such as EGF, the EGFR tyrosine kinase domain is activated, leading to the phosphorylation of the tyrosine residues in the carboxyl tail of the dimerized receptor and consequently, activating downstream signaling cascades, such as the MAPK/ERK pathway. The functionality of EGFR molecules in CHO cells stably overexpressing EGFR was confirmed by the augmentation of the phosphorylation levels of EGFR and downstream ERK upon EGF stimulation by Western blot analysis (Figure 21) and also by the visualization of internalized EGFR by CLSM analysis (Figure 22). Due to the unsuccessful infection of the CHO cells stably overexpressing EGFR, the permissiveness of these and also of the CHO cells was investigated using a *Renilla* luciferase reporter virus.[464] After transfection by electroporation, no ZIKV-infected cells nor a considerable luciferase activity was obtained in both CHO and CHO cells stably overexpressing EGFR, indicating lack of viral replication (Figure 24). Even though CHO cells are recurrently used in the production of recombinant proteins, they appear to be less permissive to viral infections when compared to other cell lines.[493] Nonetheless, ZIKV entry was analyzed in CHO cells stably overexpressing EGFR and compared to CHO cells by performing an entry assay. Surprisingly, the relative number of internalized ZIKV genomes determined by qPCR was significantly reduced in the EGFR overexpressing cells (Figure 25 A). To better comprehend the outcome of this assay, the viral attachment was determined as well. Similarly, the relative number of attached ZIKV genomes was substantially diminished in the CHO cells stably overexpressing EGFR (Figure 25 B). These data suggest that the overexpression of EGFR severely affects ZIKV binding to the cell surface, explaining the decrease measured in the relative number of internalized viral genomes. Thus, to improve the assessment of ZIKV entry in CHO cells stably overexpressing EGFR, the number of internalized viral genomes was corrected with the correspondent number of attached viral genomes. After this adjustment, a 2-fold increment in the relative number of internalized viral genomes could be perceived in the EGFR overexpressing cells (Figure 25 C). Sole expression of EGFR in CHO cells did

not render these cells permissive to ZIKV infection, but was sufficient to improve viral entry in these cells, indicating that EGFR might be relevant for ZIKV entry. The reason why the CHO cells do not support viral infection remains unclear. As ZIKV can enter CHO cells and CHO-ZIKV-RLuc cells failed to sustain viral infection, the limiting step in CHO cells seems to occur after endosomal fusion and the uncoating of the viral genome. After analysis of the genomic sequence of the CHO cells, Xu *et al.* reported that several human homologous genes are present in these cells, but not expressed.[494] Most likely, one or multiple host factors crucial for viral synthesis and replication are not expressed in CHO cells and thus, they fail to support viral replication analogously to what is described for the vaccinia virus.[495]

Furthermore, CLSM analysis of the EGFR subcellular localization and distribution in ZIKV-infected cells unveiled the appearance of dot-like structures delocalized from the plasma membrane in infected cells. EGFR dot-like structures were most evident at 24 and 48 hpi for both MOI (Figure 29). Moreover, ZIKV-infected cells displayed an elevated degree of colocalization of EGFR dot-like structures with EEA1, an early endosomal marker (Figure 30 A and B), indicating that these structures correspond to intracellular EGFR. The subcellular localization and distribution of EGFR in ZIKV-infected cells were further investigated at the early stages of infection (up to 120 mpi) by CLSM analysis. Intracellular EGFR was exclusively visualized in infected cells at 30 mpi and to a lesser extent at 60 mpi (Figure 31 A), and further corroborated by z-stack imaging (Figure 31 B). These data suggest that ZIKV triggers EGFR internalization shortly after the introduction of the viral inoculum, coinciding with the expected time of ZIKV entry into the host cell.[286,496] As the release of ZIKV genomic RNA into the cytoplasm requires the acidification of the endosomal compartment for membrane fusion, it would not be astonishing that ZIKV might utilize EGFR to enter the target cells by receptor-mediated endocytosis, gaining access to the endosomal system.[225,497] Internalization of EGFR during viral infection is not unusual as many viruses such as HBV, IAV, HSV-1, HCMV, and TGEV exploit its internalization to overcome the plasma membrane barrier.[428,433,438,439,441]

Internalization of EGFR occurs in response to its activation. Since EGFR was found to be internalized in ZIKV-infected cells, EGFR activation and activation of the MAPK/ERK pathway were investigated at the early stages of infection by Western blot analysis. Compared to uninfected cells, increased levels of phosphorylated EGFR and phosphorylated ERK were detectable in infected cells as early as 5 mpi and restored by 30 mpi, except for the ERK phosphorylation level in French Polynesia-infected cells that only reestablished by 60 mpi (Figure 32). EGFR activation induced by ZIKV was further confirmed using the PamChip® Peptide Microarray system where an MOI-dependent

activation was observed (Figure 33). Considering that EGFR internalization in infected cells was visible at 30 mpi, activation of EGFR and ERK and subsequent dephosphorylation within this period is in accordance with this previous observation. Nonetheless, it remains uncertain whether ZIKV particles can directly or indirectly through an interaction partner, activate EGFR and induce its internalization. The direct interaction between ZIKV and EGFR was investigated by co-immunoprecipitation (data not shown). However, no clear results could be obtained from this. In the case of HCV, EGFR activation and internalization are accomplished indirectly through CD81, whereas IAV activates EGFR depending on the interaction with sialic acid.[433,498] In addition, an increase in the level of phosphorylated EGFR was measured at 5-15 mpi in TGEV-, HSV-1-, HCMV-, and JEV-infected cells.[425,428,434,441,499] EGFR is a co-receptor mutual to all these viruses, reinforcing the possibility that EGFR might also participate in ZIKV entry.

Furthermore, inhibition of the activation of EGFR by blocking the tyrosine kinase (TK) activity of EGFR with Erlotinib had a clear impact on the relative number of ZIKV genomes and on the relative amount of infectious viral particles determined by qPCR and plaque assay, respectively (Figure 36 and 37). However, the same trend could not be observed in ZIKV-luciferase-replicating cells by a luciferase assay, suggesting that the inhibitory effect would occur on a step of the viral life cycle before the onset of genome replication and viral morphogenesis (Figure 38). Direct assessment of the influence of Erlotinib on the ZIKV entry by an entry assay showed a decline in the relative number of internalized genomes, demonstrating that the TK activity of EGFR is essential for viral entry (Figure 39). Though, this reduction was only about 0.3-fold in comparison to the vehicle control, which can be derived from the mild inhibitory effect on the internalization of EGFR observed after CLSM analysis (Figure 40). In another study, Erlotinib was also used in ZIKV-infected cells, but no effect could be observed in the amount of infectious viral particles.[500] The reason behind these results, besides the disparity between the cell lines used in both studies, could be because the cells were not pre-incubated with the compound, but rather infected and treated at the same time. Thus, making it highly possible that the viral particles were able to rapidly enter the cells while the inhibitory activity on EGFR was not established. Overall, these data support the hypothesis that EGFR is a relevant host factor for the ZIKV entry process.

When targeting the MAPK/ERK pathway using Sorafenib and PD98059, which inhibit Raf and MEK, a reduction in the relative number of viral genomes and the relative amount of infectious viral particles was detected as well (Figure 36 and 37). These selective inhibitors besides displaying no effect on the viral replication (Figure 38), also showed no impact on the viral entry (Figure 39). While Erlotinib was able to partially hamper EGFR internalization upon EGF stimulation, no effect could be observed in

Sorafenib- and PD98059-treated cells (Figure 40). Contrary to Erlotinib, which directly prevented ZIKV internalization, the inhibitors used in this study to impede the activation of the MAPK/ERK pathway seem to affect the ZIKV life cycle in steps preceding the onset of the viral genome replication and morphogenesis, but after the viral entry. From these results, it can be deduced that hindering the activation of the MAPK/ERK signaling cascade as a consequence of the inhibition of the activation of EGFR by Erlotinib does not influence ZIKV entry. Hence, the effect exhibited by Erlotinib on the ZIKV entry might arise as a result of the impairment of EGFR internalization and without EGFR activation there is no receptor internalization and endocytic sorting. These findings corroborate the proposed premise that EGFR is involved in the ZIKV entry process. Nonetheless, this study could not provide a clear insight into the role of the MAPK/ERK pathway during the early stages of ZIKV infection and requires further investigation. Activation of this pathway leads to the phosphorylation of diverse cytoplasmic proteins and promotes the transcription of several genes linked to crucial cellular functions.[373,387] Since the effect seems to be after viral entry but before the onset of genome replication, it can be speculated that the MAPK/ERK pathway might be essential to the ZIKV-induced reorganization of microtubules required for the formation of the replication factories as ERK 1/2 is responsible for the phosphorylation of microtubule-associated proteins 1, 2, and 4 (MAP1, MAP2, MAP4) that assist in the microtubules redistribution.[501] The reorganization of the microtubules is also involved in protein synthesis and vesicle trafficking and thus, could aid during viral synthesis and trafficking to the replication sites.[502] Alternatively, the MAPK/ERK signaling cascade could be directly involved in the viral translation through the activation of Mnk1 that directly phosphorylates a component of the cap-binding complex eIF4F, eIF4E, and thereby, regulates the translation of the viral genome and formation of the viral polyprotein. [503,504] ERK activation in ZIKV-infected cells was reported by Zhu *et al.* in Müller cells after 3 and 4 days post-infection, but in this cell culture system PD98059 slightly increased the number of ZIKV genomes.[505] As the cells were only subjected to PD98059 treatment 3 days after infection, at this point ZIKV infection was already fully established, the inhibitory effect during the early stages of infection could not be discerned. Moreover, Cheng *et al.* showed that U0126, a MEK inhibitor, displayed no impact on ZIKV infection when HUVEC cells were pre-treated with this inhibitor.[506] On the one hand, as mentioned by the authors, the low concentrations of this inhibitor used in the study might not be sufficient to affect ZIKV infection. On the other hand, these results were normalized to untreated cells and not the appropriate vehicle control (DMSO). As DMSO can alter ZIKV infection, it is plausible that an eventual effect of this compound could not be perceived.[225,504]

To further investigate the importance of EGFR signaling for ZIKV infection, the EGFR protein half-life was investigated by subjecting ZIKV-infected cells simultaneously to EGF and cycloheximide treatment and thereby, targeting EGFR for degradation and inhibiting *de novo* synthesis. According to the literature, the half-life of EGFR is approximately 60 min in EGF-stimulated cells.[507] Similar results were obtained in uninfected and Uganda-infected cells after the analysis of the protein level by Western blot throughout 2 h. However, when cells were infected with the French Polynesia strain, the half-life was prolonged by almost three times (Figure 34 A and B). This delay in EGFR degradation observed uniquely for the French Polynesia strain could reflect an additional necessity for an extended usurpation of the EGFR signaling, as it was observed that EGFR is still active in the endosomes.[508] This can be supported by the fact that the ERK dephosphorylation in French Polynesia-infected cells occurred between 30 and 60 mpi, while in Uganda-infected cells between 15 and 30 mpi. Whether this occurrence could be related to the disparity of the clinical presentation and outcome between both viral strains cannot be concluded from this study and requires further investigation. Higher EGFR half-life was reported in HCV-infected cells as well.[507]

Moreover, by disrupting lipid rafts with MβCD, which selectively depletes cholesterol from the plasma membrane, both ZIKV binding and entry were significantly reduced as quantified by qPCR (Figure 43). Exceptionally, no effect could be observed in the binding assay of French Polynesia-infected cells (Figure 43A). MβCD treatment led to an augmentation of both basal and EGF-stimulated activation of EGFR and the MAPK/ERK signaling cascade analyzed by Western blot (Figure 42). However, a clear inhibition of EGFR internalization in MβCD-treated cells was visible upon EGF stimulation by CLSM analysis (Figure 44). These results suggest that ZIKV does not depend exclusively on the activation of EGFR and the respective signaling cascade for an efficient viral entry. This observation can be corroborated by the absence of an effect on the ZIKV entry displayed by Raf and MEK inhibitors. Whether the lack of EGFR internalization in MβCD-treated cells is the unique reason for the impairment in ZIKV entry in these cells cannot be concluded from this, as additional factors can be affected by the depletion of cholesterol. This could explain the effect that MβCD treatment has on the attachment of ZIKV to the cell surface in the case of the Uganda strain. In the matter of HSV-1 and JEV, MβCD treatment decreased viral entry by disturbing lipid rafts and consequently, affecting the viral-induced activation of EGFR and downstream signaling cascades.[428,434] The ZIKV-induced activation of EGFR and ERK was not investigated in MβCD-treated cells in the present study. Although JEV is closely related to ZIKV, the data in the present study suggest a different mode of action of this compound in ZIKV-infected cells.

For further characterization of the EGFR relevance during ZIKV infection, the mRNA level and the protein amount of EGFR were analyzed throughout 48 hours of infection by qPCR and Western blot analysis, respectively. While the relative number of EGFR specific transcripts continuously increased with ZIKV infection (Figure 27), a reduction of the protein level could be discerned at later times of infection (Figure 28). This increment of the number of EGFR transcripts could be due to ZIKV induction of the EGFR gene expression, as it was reported for HBV and EBV.[450,452] The augment of EGFR gene expression could be a way for ZIKV to increase the number of EGFR molecules at the cell surface and further promote EGFR activation and consequently, stimulate survival signals in ZIKV-infected cells for efficient viral production. This induction might trigger the host cell to restore homeostasis by intensifying EGFR degradation, explaining the decrease of EGFR protein amount. Alternatively, if the internalized EGFR triggered by ZIKV infection is lysosomally degraded, the increment of EGFR gene expression could be a host compensatory mechanism in response to this. Thus, with the existent substantial amount of infectious viral particles at later times of infection, the number of EGFR molecules degraded might not be efficiently compensated by the host cell, leading to a visible decrease of EGFR protein amount. Equivalent EGFR transcriptional levels were reported by Jiang *et al.* at 6 hpi using neuronal progenitor ZIKV-infected cells. However, at 9, 12, and 24 hpi, no significant changes could be observed.[509] As the majority of the changes in the EGFR mRNA level were visible using a higher MOI (MOI 10), the fact that neuronal progenitor cells were infected with MOI 3 and the different cellular background could explain the dissimilarity between both studies. Concerning the EGFR protein level, a 1.24-fold change was reported by Jiang *et al.* at 1-day post-infection (in the present study this should correspond to 24 hpi).[509] Moreover, Sher *et al.* showed a 0.6-fold change of EGFR protein amount at 48 hpi in ZIKV-infected glioblastoma astrocytoma U-251 cells.[510] These data were comparable to the ones in this study.

To directly address the relevance of EGFR for ZIKV infection, EGFR was knocked out in A549 cells using the CRISPR/Cas9 system, and the successful generation of monoclonal EGFR KO cells and the lack of EGFR functionality was confirmed by Western blot and CLSM analyses (Figure 45 and 46). The number of viral genomes and the amount of infectious viral particles were diminished in A549-EGFR KO cells as determined by qPCR and plaque assay, respectively. To assess the impact of EGFR KO in A549 cells on the viral entry, the number of internalized viral genomes was quantified by qPCR after performing an entry assay. The entry assay unveiled a significant decline in the number of internalized viral genomes in A549-EGFR KO cells in comparison to the off-target control, supporting the previous findings that indicate that EGFR is relevant for the ZIKV entry process (Figure 48).

Taken together, this study provides unprecedented evidence that the EGFR and the MAPK/ERK signaling cascade play a role in the ZIKV life cycle, uncovering EGFR as a relevant host factor in the early stages of ZIKV infection *in vitro*. As ZIKV is a re-emerging virus and without a preventive vaccine nor a specific antiviral drug against ZIKV, uncovering and understanding novel virus-host interactions is fundamental for the development of a specific antiviral therapy. EGFR is a well-characterized receptor and due to its role in cancer, several monoclonal antibodies and substances that target EGFR are available and licensed for therapy purposes. Hence, repurposing these compounds could constitute a novel antiviral approach and further studies can be performed to investigate their impact on ZIKV infection *in vivo*. Nevertheless, the crosstalk between ZIKV and EGFR *in vitro* still requires further investigation to elucidate the exact mechanism of their interaction and to deepen the knowledge about the ZIKV entry process.

7. Summary

Zika virus (ZIKV) is a member of the *Flaviviridae* family that received public attention and scientific interest after the outbreak in French Polynesia (2013-2014) and the epidemic in the Americas (2015-2016). Even though only 20% of infected people exhibit clinical manifestations and they are predominantly flu-like symptoms, these events unveiled neurological complications associated with ZIKV infection, such as the Guillain-Barré syndrome in adults and microcephaly in newborns. Lacking a preventive vaccine and a specific antiviral therapy against ZIKV allied to the fact that this pathogen is a re-emerging virus, uncovering and comprehending novel virus-host interactions is crucial to the identification of new antiviral targets and the development of innovative antiviral approaches. Previous research work uncovered that the Chinese hamster ovary (CHO) cells do not support ZIKV infection.[459] As this cell line does not express endogenous epidermal growth factor receptor (EGFR), this study aimed to investigate whether EGFR and EGFR-dependent signaling are relevant for the ZIKV life cycle *in vitro.*

In the first part of the study, viral infection was investigated in CHO cells and compared to A549 cells, a highly ZIKV permissive cell line. After performing binding and entry assays, ZIKV entry, but not the attachment, was significantly decreased in CHO cells in comparison to A549 cells. Additionally, in A549-EGFR KO cells, ZIKV entry was diminished relatively to the off-target control. These results show the clear impact that the absence of EGFR has on viral entry, implicating EGFR during this process. Even though EGFR overexpression in CHO cells could not render these cells permissive to ZIKV infection, as demonstrated by the lack of viral infection after electroporation with *in vitro* transcribed capped ZIKV-*Renilla* luciferase RNA, it was possible to rescue ZIKV entry. These findings suggest that there are additional elements, which are not expressed in CHO cells, required for viral replication.

Furthermore, the impact of ZIKV infection on EGFR mRNA and protein levels as well as on the EGFR subcellular localization and distribution was evaluated. The relative number of EGFR specific transcripts continuously increased with ZIKV infection, whereas the EGFR protein level diminished at later times of infection. Moreover, changes in the subcellular localization of EGFR and its colocalization with the early endosomal marker EEA1 in ZIKV-infected cells revealed that ZIKV triggers EGFR internalization. The relevance of EGFR in the ZIKV entry process was further corroborated by the observation of EGFR internalization at 30 min post-infection (mpi) and to less extent at 60 mpi, which concurs with the expected time of ZIKV entry into the host cells.

In the remaining part of the study, the influence of ZIKV infection in EGFR-dependent signaling as well as the contribution of EGFR and EGFR signaling for viral infection were studied. Activation of EGFR and the MAPK/ERK signaling cascade was detected as early as 5 mpi and ceased within 30 mpi in ZIKV-infected cells. Taking into account that EGFR internalization was observed at 30 mpi in infected cells, the activation of EGFR and ERK and subsequent dephosphorylation within this period go along with this previous observation. *Vice-versa*, inhibition of the activation of EGFR and the MAPK/ERK pathway declines ZIKV infection. On the one hand, inhibition of EGFR activation by Erlotinib affected ZIKV entry, as a consequence of impaired EGFR internalization. On the other hand, Raf and MEK inhibitors reduced ZIKV infection without disturbing viral replication or viral entry. These data suggest that the activation of the MAPK/ERK signaling cascade is necessary for a step of the viral life cycle before the onset of genome replication and morphogenesis and after viral entry. The importance of EGFR signaling was additionally investigated by the determination of EGFR half-life in ZIKV-infected cells upon EGF stimulation. While the EGFR half-life was similar in uninfected and Uganda-infected cells, a delay in EGFR degradation was observed in French Polynesia-infected cells. This observation might indicate an extended usurpation of the EGFR signaling since EGFR seems to still be active in the endosomes. Moreover, disruption of lipid rafts by MβCD, a cholesterol-depleting agent, hampered ZIKV entry. In uninfected cells, MβCD treatment led to the activation of EGFR, but at the same time prevented EGFR internalization, indicating that EGFR activation exclusively is not sufficient for an efficient ZIKV entry and further supporting the importance of EGFR internalization during the ZIKV entry process.

Taken together, this study uncovers EGFR as a relevant host factor in the early stages of ZIKV infection, providing novel insights into the ZIKV entry process. Since numerous monoclonal antibodies and substances that target EGFR are licensed, repurposing these compounds might be a helpful tool for the establishment of an antiviral therapy in case of ZIKV re-emergence.

8. Zusammenfassung

Das Zika-Virus (ZIKV) ist ein hochtransmissives Virus, das zur Gattung *Flavivirus* innerhalb der Familie der *Flaviviridae* gehört. Andere Flaviviren, die eng mit ZIKV verwandt sind, sind Krankheitserreger mit erheblicher Bedrohung für die menschliche Gesundheit, wie unter anderem das Gelbfiebervirus und das Denguevirus. Im April 1947 wurde ZIKV bei einer Gelbfieber-Studie im Zika-Wald in Uganda entdeckt. In den folgenden 60 Jahren verbreitete sich das ZIKV nur gering mit einer niedrigen Anzahl von gemeldeten Fällen, aber erhöhten serologischen Nachweisen. Der erste ZIKV-Ausbruch ereignete sich 2007 auf der Insel Yap in den Föderierten Staaten von Mikronesien und betraf schätzungsweise 75 % der Bevölkerung. Trotz der Entdeckung im Jahr 1947 hat ZIKV aufgrund des Ausbruchs in Französisch-Polynesien (2013-2014) und der Epidemie in Amerika (2015-2016) erst in den letzten 10 Jahren die Aufmerksamkeit der wissenschaftlichen Gemeinschaft auf sich gezogen. Obwohl nur 20 % der Infizierten klinische Manifestationen aufwiesen und es sich überwiegend um grippeähnliche Symptome handelte, zeigten sich auch neurologische Komplikationen im Zusammenhang mit einer ZIKV-Infektion, wie das Guillain-Barré-Syndrom bei Erwachsenen und Mikrozephalie bei Neugeborenen. Als Arbovirus wird ZIKV hauptsächlich durch den Stich einer infizierten Mücke der Gattung Aedes übertragen. Die Übertragung kann jedoch auch direkt von Mensch zu Mensch durch Körperflüssigkeiten erfolgen, einschließlich von einer schwangeren Frau auf den Fötus über die Plazenta, Geschlechtsverkehr und Blutaustausch. Die schnelle weltweite Expansion des ZIKV und die Zunahme der dokumentierten Fälle von Mikrozephalie haben dazu geführt, dass die Weltgesundheitsorganisation im Februar 2016 das ZIKV zum öffentlichen Gesundheitsnotstand von internationaler Bedeutung erklärt hat. Dieser dauerte jedoch aufgrund des drastischen Rückgangs der Zahl der gemeldeten ZIKV-Fälle nur etwa 8 Monate an. In Ermangelung eines präventiven Impfstoffs und einer spezifischen antiviralen Therapie gegen ZIKV und der Tatsache, dass es sich bei diesem Erreger um ein wiederkehrendes Virus handelt, ist das Aufdecken und Verstehen neuer Virus-Wirt-Interaktionen entscheidend für die Identifizierung neuer antiviraler Angriffsziele und die Entwicklung innovativer antiviraler Ansätze.

Wie andere Flaviviren besitzt ZIKV ein einzelsträngiges RNA Genom mit positiver Orientierung und einer Größe von ca. 11 kb. Das virale Genom kodiert für ein einzelnes Polyprotein, das von viralen und Wirtsproteasen in drei strukturelle Proteine – Kapsid (C), Hülle (E) und Vorläufer von Membran/Membran (prM/M) – und sieben nicht-strukturelle Proteine (NS1, NS2A, NS2B, NS3, NS4A, NS4B und NS5) prozessiert wird. Das Viruspartikel besteht aus einem inneren Kern/Nukleokapsid, das von der genomischen RNA und dem C-Protein gebildet wird. Anschließend wird das

Nukleokapsid von einer Lipiddoppelschicht umgeben, die mit E- und M-Proteinen beschichtet ist. Der virale Zyklus ist noch nicht vollständig erforscht. Er beginnt mit der Interaktion des viralen E-Glykoproteins mit mehreren Zelloberflächenmolekülen, um in die Wirtszelle einzudringen. Somit stellt der virale Eintritt ein attraktives Ziel für die Entwicklung antiviraler Strategien dar. Es wurden mehrere Moleküle beschrieben, die den Eintritt von ZIKV in den Wirt vermitteln, einschließlich AXL. Dies ist jedoch immer noch ein rätselhafter Prozess, der nicht vollständig verstanden ist.

Der epidermale Wachstumsfaktorrezeptor (EGFR) ist ein Mitglied der ErbB/HER-Familie innerhalb der Superfamilie der Rezeptortyrosinkinasen (RTKs). EGFR besteht hauptsächlich aus einer extrazellulären Rezeptordomäne, die durch Bindung spezifischer Liganden das Signal in die Zelle weiterleitet. EGFR besitzt eine hydrophobe Transmembrandomäne, eine intrazelluläre Tyrosinkinasedomäne und eine C-terminale regulatorische Schwanzdomäne. Eine beträchtliche Anzahl von EGFR-Molekülen und anderen Rezeptoren ist in Lipid-Rafts lokalisiert, da ihre Funktion bei der Signaltransduktion eng mit der Lokalisierung in diesen Mikrodomänen der Plasmamembran korreliert. Bei der Ligandenbindung dimerisiert ein einzelner Rezeptor mit einem anderen EGFR oder einem anderen Mitglied der ErBb-Familie, wodurch die intrazelluläre Tyrosinkinasedomäne aktiviert wird. Folglich werden die im C-terminalen Schwanz des dimerisierten Rezeptors vorhandenen Tyrosinreste einer Auto- und Trans-Phosphorylierung ausgesetzt, was die Rekrutierung von Adapterproteinen und anderen Effektormolekülen begünstigt. Dies führt zur Aktivierung mehrerer Signalkaskaden, einschließlich der Ras-Raf-MEK-ERK (MAPK/ERK), JAK-STAT und PI3K-AKT-mTOR-Pfade. Um die zellulären Signale herunterzuregulieren und die Homöostase in der Zelle wiederherzustellen, verlässt EGFR die Lipid-Rafts und wird durch Clathrin-vermittelte Endozytose internalisiert. In den endosomalen Kompartimenten kann der internalisierte Rezeptor beim Recycling von Endosomen an die Zelloberfläche zurückgeführt werden oder wird einem lysosomalen Abbau unterzogen. Dieser Schritt ist abhängig von der Art des Liganden und von der Dauer und Intensität des Signals. Aufgrund der zentralen Rolle bei der Zellproliferation, dem Überleben, der Hemmung von Apoptose, Endozytose und dem Umbau des Zytoskeletts manipulieren mehrere Viren, darunter Mitglieder der Familie der *Flaviviridae*, EGFR, um die Plasmamembranbarriere zu überwinden und in den Wirt einzudringen, um Zugang zu den Replikationsstellen zu erhalten und sogar um antivirale Reaktionen des Wirts zu antagonisieren.

In einer früheren Studie wurde berichtet, dass die Ovarialzellen des Chinesischen Hamsters (CHO) die ZIKV-Infektion nicht unterstützen. Es ist bekannt, dass diesen Zellen endogene EGFR fehlt. Vor diesem Hintergrund zielte die vorliegende Studie darauf ab, die Relevanz von EGFR und EGFR-abhängiger Signalübertragung für den ZIKV-Lebenszyklus *in vitro* unter Verwendung von A549-Zellen, einer hoch ZIKV-

permissiven Zelllinie, zu untersuchen. In dieser Arbeit haben wir die Stämme Französisch-Polynesiens und Ugandas verwendet, um die verschiedenen Arten der Pathogenese darzustellen. Während der Uganda-Stamm mit grippeähnlichen Symptomen in Verbindung gebracht wird, wird der Französisch-Polynesien-Stamm mit den bei der menschlichen Bevölkerung beobachteten neurologischen Komplikationen assoziiert.

Im ersten Teil der Studie wurde die virale Infektion in CHO-Zellen untersucht und mit A549-Zellen verglichen. Nach Durchführung von Bindungs- und Eintrittsassays war der ZIKV-Eintritt, aber nicht die Anheftung, in CHO-Zellen im Vergleich zu A549-Zellen signifikant verringert. Diese Reduktion wurde auch nach einem Post-Entry-Assay beobachtet. Außerdem war in A549-EGFR-KO-Zellen der ZIKV-Eintritt relativ zur Off-Target-Kontrolle verringert. Diese Ergebnisse zeigen den klaren Einfluss, den das Fehlen von EGFR auf den Viruseintritt hat. Darüber hinaus ergab die Western-Blot-Analyse, dass EGFR in der Mehrheit der ZIKV-permissiven Zelllinien exprimiert wird, im Gegensatz zu AXL, einem der ersten berichteten ZIKV-Rezeptoren. Das Fehlen von EGFR in HepG2/C3A-Zellen und die Identifizierung mehrerer Moleküle, die am Eintrittsprozess beteiligt sind, legen nahe, dass der ZIKV-Eintritt nicht von einem einzelnen Rezeptor abhängt, sondern mit seinen Interaktionen mit dem Wirt, ähnlich wie bei anderen Flaviviren, eher promiskuitiv ist. Somit ist es möglich, dass in HepG2/C3A ein anderes ErbB oder RTK die EGFR-Funktionen ersetzen könnte. Auch wenn EGFR auf den ersten Blick eine Rolle beim Eintritt von ZIKV zu spielen scheint, konnte eine EGFR-Überexpression in CHO-Zellen diese Zellen nicht für eine ZIKV-Infektion permissiv machen, wie das Fehlen einer Virusinfektion nach Elektroporation mit einem Luciferase-Reportervirus zeigt. Diese Ergebnisse legen nahe, dass zusätzliche Elemente, die in CHO-Zellen nicht exprimiert werden, für die virale Replikation erforderlich sind. Nichtsdestotrotz konnte die EGFR-Überexpression in CHO-Zellen den ZIKV-Eintritt ermöglichen, was die Beteiligung von EGFR an diesem Prozess unterstreicht.

Darüber hinaus enthüllte die konfokale Laser-Scanning-Mikroskopie (CLSM) Analyse der subzellulären EGFR-Lokalisierung und -Verteilung das Auftreten von punktförmigen EGFR-Strukturen, die von der Plasmamembran in ZIKV-infizierten Zellen delokalisiert wurden und einen erhöhten Kolokalisationsgrad mit EEA1 aufwiesen, einem frühen Endosomenmarker. Dies zeigt, dass diese punktförmigen Strukturen dem intrazellulären EGFR entsprechen. Intrazellulärer EGFR wurde in infizierten Zellen 30 min nach der Infektion (mpi) und in geringerem Ausmaß bei 60 mpi beobachtet, was darauf hindeutet, dass ZIKV die EGFR-Internalisierung kurz nach der Einführung des viralen Inokulums auslöst und mit dem erwarteten Zeitpunkt des ZIKV-Eintritts in die Wirtszelle übereinstimmt. Diese Beobachtungen untermauern die Teilnahme von EGFR am ZIKV-Eintrittsprozess weiter.

Die Internalisierung von EGFR erfolgt als Reaktion auf seine Aktivierung. Da festgestellt wurde, dass EGFR in ZIKV-infizierten Zellen internalisiert wird, wurde die EGFR-Aktivierung und die entsprechende nachgeschaltete Aktivierung des MAPK/ERK-Signalwegs in frühen Stadien der Infektion durch Western-Blot-Analyse untersucht. Die Aktivierung von EGFR und der MAPK/ERK-Signalkaskade wurde bereits bei 5 mpi nachgewiesen und kehrte in ZIKV-infizierten Zellen auf basale Werte innerhalb von 30 mpi zurück und war abhängig von der Anzahl infektiöser Viruspartikel, die für die Infektion verwendet wurden. In Anbetracht der Tatsache, dass die EGFR-Internalisierung in infizierten Zellen bei 30 mpi sichtbar war, stimmt die EGFR- und ERK-Aktivierung und die anschließende Herunterregulierung innerhalb dieses Zeitraums mit dieser vorherigen Beobachtung überein. Umgekehrt verringert die Hemmung der Aktivierung von EGFR und des MAPK/ERK-Signalwegs die ZIKV-Infektion. Einerseits beeinflusste die Hemmung der EGFR-Aktivierung durch Erlotinib den ZIKV-Eintritt als Folge einer gestörten EGFR-Internalisierung. Andererseits reduzierten Raf- und MEK-Inhibitoren die ZIKV-Infektion ohne die Virusreplikation oder den Viruseintritt zu stören. Diese Daten legen nahe, dass die Aktivierung der MAPK/ERK-Signalkaskade für einen Schritt im viralen Lebenszyklus vor dem Beginn der Genomreplikation und Morphogenese und nach dem Viruseintritt notwendig ist. Die Bedeutung der EGFR-Signalgebung wurde zusätzlich durch die Bestimmung der EGFR-Halbwertszeit in ZIKV-infizierten Zellen nach EGF-Stimulation untersucht. Während die EGFR-Halbwertszeit in nicht infizierten und mit Uganda infizierten Zellen ähnlich war, wurde in mit Französisch-Polynesien infizierten Zellen eine Verzögerung des EGFR-Abbaus beobachtet. Dies könnte auf eine zusätzliche Notwendigkeit für eine erweiterte Usurpation der EGFR-Signalgebung hindeuten, da beobachtet wurde, dass EGFR in den Endosomen immer noch aktiv ist. Dies kann durch die Tatsache unterstützt werden, dass die ERK-Dephosphorylierung in mit Französisch-Polynesien infizierten Zellen bei 30 bis 60 mpi auftrat, während sie in mit Uganda infizierten Zellen bei 15 bis 30 mpi stattfand. Ob dieses Auftreten mit der Ungleichheit der klinischen Präsentation und des Outcomes zwischen beiden Virusstämmen zusammenhängen könnte, lässt sich aus dieser Studie nicht ableiten und bedarf weiterer Untersuchungen. Darüber hinaus behinderte die Zerstörung von Lipid-Rafts mit Methyl-β-Cyclodextrin (MβCD), einem cholesterinsenkenden Mittel, den Eintritt von ZIKV. In nicht infizierten Zellen führte die MβCD-Behandlung zur Aktivierung von EGFR, verhinderte aber gleichzeitig die EGFR-Internalisierung, was darauf hindeutet, dass die ausschließliche EGFR-Aktivierung für einen effizienten ZIKV-Eintritt nicht ausreicht und die Bedeutung von EGFR während des ZIKV-Eintrittsprozesses weiter unterstützt.

Die Auswirkungen einer ZIKV-Infektion auf die EGFR-mRNA- und -Proteinspiegel wurden ebenfalls bewertet. Während die relative Zahl der EGFR-spezifischen Transkripte mit der ZIKV-Infektion kontinuierlich zunahm, konnte zu späteren

Zeitpunkten der Infektion eine Verringerung des Proteinspiegels festgestellt werden. Die Erhöhung der EGFR-Genexpression könnte für ZIKV eine Möglichkeit sein, die Anzahl der EGFR-Moleküle an der Zelloberfläche zu erhöhen und die EGFR-Aktivierung weiter zu fördern und folglich Überlebenssignale in ZIKV-infizierten Zellen für eine effiziente Virusproduktion zu stimulieren. Diese Induktion könnte die Wirtszelle veranlassen, die Homöostase wiederherzustellen, indem sie den EGFR-Abbau intensiviert, was die Abnahme der EGFR-Proteinmenge erklärt. Wenn alternativ der durch eine ZIKV-Infektion ausgelöste internalisierte EGFR lysosomal abgebaut wird, könnte die Zunahme der EGFR-Genexpression ein kompensatorischer Mechanismus des Wirts als Reaktion darauf sein. Bei der vorhandenen erheblichen Menge an infektiösen Viruspartikeln zu späteren Zeitpunkten der Infektion wird die Anzahl der abgebauten EGFR-Moleküle daher möglicherweise nicht effizient von der Wirtszelle kompensiert, was zu einer sichtbaren Abnahme der EGFR-Proteinmenge führt.

Zusammenfassend liefert diese Studie beispiellose Beweise dafür, dass EGFR und die MAPK/ERK-Signalkaskade eine Rolle im ZIKV-Lebenszyklus spielen, und deckt EGFR als relevanten Wirtsfaktor in den frühen Stadien der ZIKV-Infektion *in vitro* auf. EGFR ist ein gut charakterisierter Rezeptor und mehrere monoklonale Antikörper und Substanzen, die auf EGFR abzielen, sind verfügbar und zugelassen. Daher könnte die Wiederverwendung dieser Verbindungen einen neuen antiviralen Ansatz darstellen und weitere Studien können durchgeführt werden, um ihren Einfluss auf die ZIKV-Infektion *in vivo* zu untersuchen. Dennoch bedarf der Crosstalk zwischen ZIKV und EGFR *in vitro* noch weiterer Untersuchungen, um den genauen Mechanismus ihrer Interaktion aufzuklären und das Wissen über den ZIKV-Eintrittsprozess zu vertiefen.

9. References

1. Simmonds, P. *et al.* ICTV Virus Taxonomy Profile: Flaviviridae. *Journal of General Virology* **98**, 2–3 (2017).

2. Payne, S. Family Flaviviridae. in *Viruses* 129–139 (Elsevier, 2017).

3. Kuno, G., Chang, G.-J. J., Tsuchiya, K. R., Karabatsos, N. & Cropp, C. B. Phylogeny of the Genus Flavivirus. *Journal of Virology* **72**, 73–83 (1998).

4. Cook, S. & Holmes, E. C. A multigene analysis of the phylogenetic relationships among the flaviviruses (Family: Flaviviridae) and the evolution of vector transmission. *Archives of Virology* **151**, 309–325 (2006).

5. Cook, S. *et al.* Molecular evolution of the insect-specific flaviviruses. *Journal of General Virology* **93**, 223–234 (2012).

6. Pierson, T. C. & Diamond, M. S. *Fields Virology*. vol. 1 (Lippincott Williams & Wilkins, 2013).

7. Heinz, F. X. & Stiasny, K. The Antigenic Structure of Zika Virus and Its Relation to Other Flaviviruses: Implications for Infection and Immunoprophylaxis. *Microbiology and Molecular Biology Reviews* **81**, (2017).

8. Dick, G. W. A. Paper: Epidemiological notes on some viruses isolated in Uganda (Yellow fever, Rift Valley fever, Bwamba fever, West Nile, Mengo, Semliki forest, Bunyamwera, Ntaya, Uganda S and Zika viruses). *Transactions of the Royal Society of Tropical Medicine and Hygiene* **47**, 13–48 (1953).

9. Dick, G. W. A., Kitchen, S. F. & Haddow, A. J. Zika Virus (I). Isolations and serological specificity. *Transactions of the Royal Society of Tropical Medicine and Hygiene* **46**, 509–520 (1952).

10. Dick, G. W. A. Pathogenicity and Physical Properties. *Transactions of the Royal Society of Tropical Medicine and Hygiene* **46**, 521–534 (1952).

11. Smithburn, K. C. Neutralizing Antibodies Against Certain Recently Isolated Viruses in the Sera of Human Beings Residing in East Africa. *The Journal of Immunology* **69**, (1952).

12. Smithburn, K. C. Neutralizing antibodies against arthropod-borne viruses in the sera of long-time residents of Malaya and Borneo. *American Journal of Hygiene* **59**, 157–63 (1954).

13. Simpson, D. I. H. Zika virus infection in man. *Transactions of the Royal Society of Tropical Medicine and Hygiene* **58**, (1964).

14. Moore, D. L. *et al.* Arthropod-borne viral infections of man in nigeria, 1964-1970. *Annals of Tropical Medicine and Parasitology* **69**, 49–64 (1975).

15. Boorman, J. P. T. & Draper, C. C. Isolations of arboviruses in the Lagos area of Nigeria, and a survey of antibodies to them in man and animals. *Transactions of the Royal Society of Tropical Medicine and Hygiene* **62**, (1968).

16. Marchette, N., Garcia, R. & Rudnick, A. Isolation of Zika virus from Aedes aegypti mosquitoes in Malaysia. *Am J Trop Med Hyg* **18**, 411–415 (1969).

17. Olson, J. G., Ksiazek, T. G., Suhandiman & Triwibowo. Zika virus, a cause of fever in Central Java, Indonesia. *Transactions of the Royal Society of Tropical Medicine and Hygiene* **75**, 389–393 (1981).

18. Smithburn, K. C., Kerr, J. A. & Gatne, P. B. Neutralizing Antibodies Against Certain Viruses in the Sera of Residents of India. *The Journal of Immunology* **72**, (1954).

19. Hammon, W. M., Schrack, W. D. & Sather, G. E. Serological survey for a arthropod-borne virus infections in the Philippines. *The American journal of tropical medicine and hygiene* **7**, 323–328 (1958).

20. Pond, W. L. Arthropod-borne virus antibodies in sera from residents of South-East Asia. *Transactions of the Royal Society of Tropical Medicine and Hygiene* **57**, 364–371 (1963).

21. Lanciotti, R. S. *et al.* Genetic and serologic properties of Zika virus associated with an epidemic, Yap State, Micronesia, 2007. *Emerging Infectious Diseases* **14**, 1232–1239 (2008).

22. ProMED. Zika virus outbreak - Micronesia (Yap) (02): confirmed. https://promedmail.org/promed-posts/ (2007).

23. Cao-Lormeau, V. M. *et al.* Zika virus, French Polynesia, South Pacific, 2013. *Emerging Infectious Diseases* vol. 20 1085–1086 (2014).

24. Oehler, E. *et al.* Zika virus infection complicated by Guillain-Barré syndrome - a case report, French Polynesia, December 2013. *Eurosurveillance* **19**, 20720 (2014).

25. Cao-Lormeau, V. M. *et al.* Guillain-Barré Syndrome outbreak associated with Zika virus infection in French Polynesia: A case-control study. *The Lancet* **387**, 1531–1539 (2016).

26. Mallet, H.-P., Vial, A.-L. & Musso, D. Assessment of the Zika virus outbreak in French Polynesia between October 2013 and March 2014 - From the description of the outbreak to knowledge gained subsequently. *Bulletin épidémiologique hebdomadaire* (2016).

27. European Centre for Disease Prevention and Control. Rapid risk assessment: Zika virus infection outbreak, French Polynesia. https://www.ecdc.europa.eu/en/publications-data/rapid-risk-assessment-zika-virus-infection-outbreak-french-polynesia.

28. Dupont-Rouzeyrol, M. *et al.* Co-infection with zika and dengue viruses in 2 patients, New Caledonia, 2014. *Emerging Infectious Diseases* vol. 21 381–382 (2015).

29. Tognarelli, J. *et al.* A report on the outbreak of Zika virus on Easter Island, South Pacific, 2014. *Archives of Virology* **161**, 665–668 (2016).

30. European Center for Disease Prevention and Control. Rapid risk assessment: Zika virus infection outbreak, Brazil and the Pacific region. https://www.ecdc.europa.eu/en/publications-data/rapid-risk-assessment-zika-virus-infection-outbreak-brazil-and-pacific-region-26 (2015).

31. Cardoso, C. W. *et al.* Outbreak of Exanthematous Illness associated with Zika, Chikungunya, and Dengue viruses, Salvador, Brazil. *Emerging Infectious Diseases* vol. 21 2274–2276 (2015).

32. ProMED. Undiagnosed illness - Brazil: (Northeast, RJ) Zika virus suspected. https://promedmail.org/promed-posts/ (2015).

33. Zanluca, C. *et al.* First report of autochthonous transmission of Zika virus in Brazil. *Memorias do Instituto Oswaldo Cruz* **110**, 569–572 (2015).

34. Campos, G. S., Bandeira, A. C. & Sardi, S. I. Zika virus outbreak, Bahia, Brazil. *Emerging Infectious Diseases* vol. 21 1885–1886 (2015).

35. PAHO/WHO. 1 December 2015: Neurological syndrome, congenital malformations, and Zika virus infection. Implications for public health in the Americas - Epidemiological Alert. https://www.paho.org/hq/index.php?option=com_content&view=article&id=11484:1-december-2015-neurological-syndrome-zika-virus-infection-americas-epidemiological-alert&Itemid=42346&lang=en.

36. European Centre for Disease Prevention and Control. Rapid risk assessment: Zika virus epidemic in the Americas: potential association with microcephaly and Guillain-Barré syndrome - 4th update, 10 December 2015. https://www.ecdc.europa.eu/en/publications-data/rapid-risk-assessment-zika-virus-epidemic-americas-potential-association (2015).

37. European Centre for Disease Prevention and Control. Rapid Risk Assessment: Zika virus disease epidemic: potential association with microcephaly and Guillain-

Barré syndrome (first update). https://www.ecdc.europa.eu/en/publications-data/rapid-risk-assessment-zika-virus-disease-epidemic-potential-association.

38. Kindhauser, M. K., Allen, T., Frank, V., Santhana, R. S. & Dye, C. Zika: the origin and spread of a mosquito-borne virus. *Bulletin of the World Health Organization* **94**, 675-686C (2016).

39. World Health Organization. Zika situation report. http://www.who.int/emergencies/zika-virus/situation-report/19-february-2016/en/ (2016).

40. Centers for Disease Control and Prevention. Case Counts in the US | Zika Virus. https://www.cdc.gov/zika/reporting/2016-case-counts.html (2016).

41. Government of Canada. Zika virus: For health professionals - Canada.ca. https://www.canada.ca/en/public-health/services/diseases/zika-virus/health-professionals.html#_Zika_virus_around.

42. Kutsuna, S. Zika virus infection: Clinical overview with a summary of Japanese cases. *Clinical and Experimental Neuroimmunology* **8**, 192–198 (2017).

43. Yin, Y. *et al.* Epidemiologic investigation of a family cluster of imported ZIKV cases in Guangdong, China: probable human-to-human transmission. *https://doi.org/10.1038/emi.2016.100* **5**, 100 (2019).

44. Pyke, A. T. , *et al.* Isolation of Zika Virus Imported from Tonga into Australia. *PLoS currents* **8**, (2016).

45. Harrower, J. *et al.* Sexual Transmission of Zika Virus and Persistence in Semen, New Zealand, 2016. *Emerging Infectious Diseases* **22**, 1855–1857 (2016).

46. Duijster, J. W. *et al.* Zika virus infection in 18 travellers returning from Surinam and the Dominican Republic, The Netherlands, November 2015–March 2016. *Infection 2016 44:6* **44**, 797–802 (2016).

47. Gyurech, D. *et al.* False positive dengue NS1 antigen test in a traveller with an acute Zika virus infection imported into Switzerland. *Swiss Medical Weekly* (2016).

48. Díaz-Menéndez, M. *et al.* Initial experience with imported Zika virus infection in Spain. *Enfermedades infecciosas y microbiologia clinica (English ed.)* **36**, 4–8 (2018).

49. Zé-Zé, L. *et al.* Zika virus infections imported from Brazil to Portugal, 2015. *IDCases* **4**, 46–49 (2016).

50. Nicastri, E. *et al.* Three cases of Zika virus imported in Italy: need for a clinical awareness and evidence-based knowledge. *BMC Infectious Diseases 2016 16:1* **16**, 1–4 (2016).

51. Maria, A. T. *et al.* Zika virus infections in three travellers returning from South America and the Caribbean respectively, to Montpellier, France, December 2015 to January 2016. *Eurosurveillance* **21**, 30131 (2016).

52. de Smet, B. *et al.* Confirmed Zika virus infection in a Belgian traveler returning from Guatemala, and the diagnostic challenges of imported cases into Europe. *Journal of Clinical Virology* **80**, 8–11 (2016).

53. Araújo, T. V. B. de *et al.* Association between Zika virus infection and microcephaly in Brazil, January to May, 2016: preliminary report of a case-control study. *The Lancet Infectious Diseases* **16**, 1356–1363 (2016).

54. Rocha, S. G. M. O. *et al.* Zika Virus Infection and Microcephaly: A Case-Control Study in Brazil. *Annals of Global Health* **85**, (2019).

55. Cauchemez, S. *et al.* Association between Zika virus and microcephaly in French Polynesia, 2013-15: A retrospective study. *The Lancet* **387**, 2125–2132 (2016).

56. World Health Organization. WHO statement on the first meeting of the International Health Regulations (2005) (IHR 2005) Emergency Committee on Zika virus and observed increase in neurological disorders and neonatal malformations. https://www.who.int/news/item/01-02-2016-who-statement-on-the-first-meeting-of-the-international-health-regulations-(2005)-(ihr-2005)-emergency-committee-on-zika-virus-and-observed-increase-in-neurological-disorders-and-neonatal-malformations.

57. World Health Organization. Fifth meeting of the Emergency Committee under the International Health Regulations (2005) regarding microcephaly, other neurological disorders and Zika virus. https://www.who.int/news/item/18-11-2016-fifth-meeting-of-the-emergency-committee-under-the-international-health-regulations-(2005)-regarding-microcephaly-other-neurological-disorders-and-zika-virus (2005).

58. Hill, S. C. *et al.* Emergence of the Asian lineage of Zika virus in Angola: an outbreak investigation. *The Lancet Infectious Diseases* **19**, 1138–1147 (2019).

59. Yadav, P. D. *et al.* Zika virus outbreak in Rajasthan, India in 2018 was caused by a virus endemic to Asia. *Infection, Genetics and Evolution* **69**, 199–202 (2019).

60. Grubaugh, N. D. *et al.* Travel Surveillance and Genomics Uncover a Hidden Zika Outbreak during the Waning Epidemic. *Cell* **178**, 1057-1071.e11 (2019).

61. Public Health Landscape. A History of Zika Virus in Brazil. https://publichealthlandscape.com/volume-26-april-2016/a-history-of-zika-virus-in-brazil/.

62. Haby, M. M., Pinart, M., Elias, V. & Reveiz, L. Systematic reviews Prevalence of asymptomatic Zika virus infection: a systematic review. *Bull World Health Organ* **96**, 402–413 (2018).

63. Aubry, M. *et al.* Zika Virus Seroprevalence, French Polynesia, 2014–2015. *Emerging Infectious Diseases* **23**, 669 (2017).

64. Halani, S. *et al.* Clinical manifestations and health outcomes associated with Zika virus infections in adults: A systematic review. *PLOS Neglected Tropical Diseases* **15**, e0009516 (2021).

65. World Health Organization. Zika virus: Factsheet. https://www.who.int/news-room/fact-sheets/detail/zika-virus (2018).

66. van Doorn, P. A. Diagnosis, treatment and prognosis of Guillain-Barré syndrome (GBS). *La Presse Médicale* **42**, e193–e201 (2013).

67. Willison, H. J., Jacobs, B. C. & Doorn, P. A. van. Guillain-Barré syndrome. *The Lancet* **388**, 717–727 (2016).

68. van den Berg, B., Bunschoten, C., van Doorn, P. & Jacobs, B. Mortality in Guillain-Barre syndrome. *Neurology* **80**, 1650–1654 (2013).

69. Domínguez-Moreno, R. *et al.* Mortality associated with a diagnosis of Guillain-Barré syndrome in adults of Mexican health institutions. *Revista de Neurologia* **58**, 4–10 (2014).

70. Carteaux, G. *et al.* Zika Virus Associated with Meningoencephalitis. *The New England Journal of Medicine* **374**, 1595–1596 (2016).

71. Mécharles, S. *et al.* Acute myelitis due to Zika virus infection. *The Lancet* **387**, 1481 (2016).

72. Meaney-Delman, D. Zika Virus Infection Among U.S. Pregnant Travelers — August 2015–February 2016. *MMWR. Morbidity and Mortality Weekly Report* **65**, (2019).

73. Brasil, P. *et al.* Zika Virus Infection in Pregnant Women in Rio de Janeiro. *The New England Journal of Medicine* **375**, 2321–2334 (2016).

74. Ventura, C. v, Maia, M., Dias, N., Ventura, L. O. & Belfort, R. Zika: neurological and ocular findings in infant without microcephaly. *The Lancet* **387**, 2502 (2016).

75. Freitas, D. A. *et al.* Congenital Zika syndrome: A systematic review. *PLoS ONE* **15**, (2020).

76. W, K. de O. *et al.* Increase in Reported Prevalence of Microcephaly in Infants Born to Women Living in Areas with Confirmed Zika Virus Transmission During the First Trimester of Pregnancy - Brazil, 2015. *MMWR. Morbidity and mortality weekly report* **65**, 242–247 (2016).

77. S, P., AM, K. & A, V. Microcephaly. *Handbook of clinical neurology* **111**, 129–141 (2013).

78. M, von der H. *et al.* Diagnostic approach to microcephaly in childhood: a two-center study and review of the literature. *Developmental medicine and child neurology* **56**, 732–741 (2014).

79. Secretaria de Vigilância em Saúde - Ministério da Saúde. *Boletim Epidemiológico: Monitoramento dos casos de dengue, febre de chikungunya e febre pelo vírus Zika até a Semana Epidemiológica 16, 2016*. (2016).

80. Dirlikov, E. Update: Ongoing Zika Virus Transmission — Puerto Rico, November 1, 2015–April 14, 2016. *MMWR. Morbidity and Mortality Weekly Report* **65**, 451–455 (2019).

81. Arzuza-Ortega, L. *et al.* Fatal Sickle Cell Disease and Zika Virus Infection in Girl from Colombia. *Emerging Infectious Diseases* **22**, 925 (2016).

82. Sarmiento-Ospina, A., Vásquez-Serna, H., Jimenez-Canizales, C. E., Villamil-Gómez, W. E. & Rodriguez-Morales, A. J. Zika virus associated deaths in Colombia. *The Lancet Infectious Diseases* **16**, 523–524 (2016).

83. Petersen, L. R., Jamieson, D. J., Powers, A. M. & Honein, M. A. Zika Virus. *New England Journal of Medicine* **374**, 1552–1563 (2016).

84. Haddow, A. D. *et al.* Genetic Characterization of Zika Virus Strains: Geographic Expansion of the Asian Lineage. *PLOS Neglected Tropical Diseases* **6**, e1477 (2012).

85. Alera, M. T. *et al.* Zika Virus Infection, Philippines, 2012. *Emerging Infectious Diseases* **21**, 722–724 (2015).

86. Faye, O. *et al.* Molecular Evolution of Zika Virus during Its Emergence in the 20th Century. *PLoS Neglected Tropical Diseases* **8**, 36 (2014).

87. Lanciotti, R. S., Lambert, A. J., Holodniy, M., Saavedra, S. & Signor, L. del C. C. Phylogeny of Zika Virus in Western Hemisphere, 2015. *Emerging Infectious Diseases* **22**, 933–935 (2016).

88. Wang, L. *et al.* From Mosquitos to Humans: Genetic Evolution of Zika Virus. *Cell Host & Microbe* **19**, 561–565 (2016).

89. Smith, D. R. *et al.* African and Asian Zika Virus Isolates Display Phenotypic Differences Both In Vitro and In Vivo. *The American Journal of Tropical Medicine and Hygiene* **98**, 432 (2018).

90. H-O Pettersson, J. *et al.* How Did Zika Virus Emerge in the Pacific Islands and Latin America? *mBio* **7**, (2016).

91. Liu, Y. *et al.* Evolutionary enhancement of Zika virus infectivity in Aedes aegypti mosquitoes. *Nature* **545**, 482–486 (2017).

92. Aubry, F. *et al.* Recent African strains of Zika virus display higher transmissibility and fetal pathogenicity than Asian strains. *Nature Communications 2021 12:1* **12**, 1–14 (2021).

93. Weaver, S. C. Emergence of epidemic zika virus transmission and congenital zika syndrome: Are recently evolved traits to blame? *mBio* **8**, (2017).

94. Vermillion, M. S. *et al.* Intrauterine Zika virus infection of pregnant immunocompetent mice models transplacental transmission and adverse perinatal outcomes. *Nature Communications 2017 8:1* **8**, 1–14 (2017).

95. Jaeger, A. S. *et al.* Zika viruses of African and Asian lineages cause fetal harm in a mouse model of vertical transmission. *PLoS Neglected Tropical Diseases* **13**, (2019).

96. Tripathi, S. *et al.* A novel Zika virus mouse model reveals strain specific differences in virus pathogenesis and host inflammatory immune responses. *PLOS Pathogens* **13**, e1006258 (2017).

97. Kramer, L. D. & Ciota, A. T. Dissecting vectorial capacity for mosquito-borne viruses. *Current Opinion in Virology* vol. 15 112–118 (2015).

98. Azar, S. R. & Weaver, S. C. Vector competence: What has Zika virus taught us? *Viruses* vol. 11 867 (2019).

99. Chouin-Carneiro, T. *et al.* Differential Susceptibilities of Aedes aegypti and Aedes albopictus from the Americas to Zika Virus. *PLoS Neglected Tropical Diseases* **10**, (2016).

100. Kraemer, M. U. G. *et al.* The global distribution of the arbovirus vectors Aedes aegypti and Ae. Albopictus. *eLife* **4**, (2015).

101. Gutiérrez-Bugallo, G. *et al.* Vector-borne transmission and evolution of Zika virus. *Nature Ecology and Evolution* vol. 3 561–569 (2019).

102. Vazeille, M. *et al.* Zika virus threshold determines transmission by European Aedes albopictus mosquitoes. *Emerging Microbes and Infections* **8**, 1668–1678 (2019).

103. Ledermann, J. P. *et al.* Aedes hensilli as a Potential Vector of Chikungunya and Zika Viruses. *PLoS Neglected Tropical Diseases* **8**, (2014).

104. Musso, D., Nilles, E. J. & Cao-Lormeau, V. M. Rapid spread of emerging Zika virus in the Pacific area. *Clinical Microbiology and Infection* **20**, O595–O596 (2014).

105. Calvez, E. *et al.* Zika virus outbreak in the Pacific: Vector competence of regional vectors. *PLoS Neglected Tropical Diseases* **12**, e0006637 (2018).

106. Oliveira Melo, A. S. *et al.* Zika virus intrauterine infection causes fetal brain abnormality and microcephaly: Tip of the iceberg? *Ultrasound in Obstetrics and Gynecology* vol. 47 6–7 (2016).

107. de Oliveira Melo, A. S. *et al.* Congenital Zika virus infection: Beyond neonatal microcephaly. *JAMA Neurology* **73**, 1407–1416 (2016).

108. Besnard, M., Lastère, S., Teissier, A., Cao-Lormeau, V. M. & Musso, D. Evidence of perinatal transmission of Zika virus, French Polynesia, December 2013 and February 2014. *Eurosurveillance* **19**, 20751 (2014).

109. Dupont-Rouzeyrol, M., Biron, A., O'Connor, O., Huguon, E. & Descloux, E. Infectious Zika viral particles in breastmilk. *The Lancet* vol. 387 1051 (2016).

110. Musso, D. *et al.* Potential sexual transmission of zika virus. *Emerging Infectious Diseases* **21**, 359–361 (2015).

111. Foy, B. D. *et al.* Probable Non-Vector-borne Transmission of Zika Virus, Colorado, USA. *Emerging Infectious Diseases* **17**, 880–882 (2011).

112. D'Ortenzio, E., Matheron, S. & Yazdanpanah, Y. Evidence of sexual transmission of Zika Virus. *New England Journal of Medicine* vol. 374 2195–2198 (2016).

113. Hills, S. L. *et al.* Transmission of Zika Virus Through Sexual Contact with Travelers to Areas of Ongoing Transmission — Continental United States, 2016. *MMWR. Morbidity and Mortality Weekly Report* **65**, (2016).

114. Paz-Bailey, G. *et al.* Persistence of Zika Virus in Body Fluids — Final Report. *New England Journal of Medicine* **379**, 1234–1243 (2018).

115. Musso, D. *et al.* Potential for Zika virus transmission through blood transfusion demonstrated during an outbreak in French Polynesia, November 2013 to February 2014. *Eurosurveillance* **19**, (2014).

116. Aubry, M. *et al.* Seroprevalence of arboviruses among blood donors in French Polynesia, 2011-2013. *International Journal of Infectious Diseases* **41**, 11–12 (2015).

117. Gallian, P. *et al.* Zika virus in asymptomatic blood donors in Martinique. *Blood* vol. 129 263–266 (2017).

118. Nogueira, M. L. *et al.* Zika Virus Infection and Solid Organ Transplantation: A New Challenge. *American Journal of Transplantation* **17**, 791–795 (2017).

119. Schwartzmann, P. v. *et al.* Zika Virus Meningoencephalitis in an Immunocompromised Patient. *Mayo Clinic Proceedings* **92**, 460–466 (2017).

120. Filipe, A. R., Martins, C. M. V. & Rocha, H. Laboratory infection with Zika virus after vaccination against yellow fever. *Archiv für die gesamte Virusforschung* **43**, 315–319 (1973).

121. Leung, G. H., Baird, R. W., Druce, J. & Anstey, N. M. *Zika virus infection in Australia following a monkey bite in Indonesia*. *J trop Med public health* vol. 460 (2015).

122. Rather, I. A., Lone, J. B., Bajpai, V. K., Paek, W. K. & Lim, J. Zika virus: An emerging worldwide threat. *Frontiers in Microbiology* **8**, 1417 (2017).

123. European Centre for Disease Prevention and Control. Factsheet about Zika virus disease. https://www.ecdc.europa.eu/en/zika-virus-infection/facts/factsheet.

124. Faye, O. *et al.* One-step RT-PCR for detection of Zika virus. *Journal of Clinical Virology* **43**, 96–101 (2008).

125. Faye, O. *et al.* Quantitative real-time PCR detection of Zika virus and evaluation with field-caught Mosquitoes. *Virology Journal* **10**, 311 (2013).

126. Balm, M. N. D. *et al.* A diagnostic polymerase chain reaction assay for Zika virus. *Journal of Medical Virology* **84**, 1501–1505 (2012).

127. Centers for Disease Control and Prevention. *Comparison of Test Results for Zika Virus RNA in Urine, Serum, and Saliva Specimens from Persons with Travel-Associated Zika Virus Disease-Florida, 2016*. http://www.cdc.gov/mmwr.

128. Gourinat, A. C., O'Connor, O., Calvez, E., Goarant, C. & Dupont-Rouzeyrol, M. Detection of zika virus in urine. *Emerging Infectious Diseases* **21**, 84–86 (2015).

129. Musso, D. *et al.* Detection of Zika virus in saliva. *Journal of Clinical Virology* **68**, 53–55 (2015).

130. Eppes, C. *et al.* Testing for Zika virus infection in pregnancy: key concepts to deal with an emerging epidemic. *American Journal of Obstetrics and Gynecology* vol. 216 209–225 (2017).

131. Driggers, R. W. *et al.* Zika virus infection with prolonged maternal viremia and fetal brain abnormalities. *New England Journal of Medicine* **374**, 2142–2151 (2016).

132. Besnard, M., Lastère, S., Teissier, A., Cao-Lormeau, V. M. & Musso, D. Evidence of perinatal transmission of zika virus, French Polynesia, December 2013 and February 2014. *Eurosurveillance* **19**, (2014).

133. Calvet, G. *et al.* Detection and sequencing of Zika virus from amniotic fluid of fetuses with microcephaly in Brazil: a case study. *The Lancet Infectious Diseases* **16**, 653–660 (2016).

134. Colt, S. *et al.* Transmission of Zika virus through breast milk and other breastfeeding-related bodily-fluids: A systematic review. *PLoS Neglected Tropical Diseases* **11**, (2017).

135. Poland, J. D., Calisher, C. H., Monath, T. P., Downs, W. G. & Murphy, K. Persistence of neutralizing antibody 30-35 years after immunization with 17D yellow fever vaccine. *Bulletin of the World Health Organization* **59**, 895–900 (1981).

136. Cao-Lormeau, V.-M. *et al.* Guillain-Barré Syndrome outbreak associated with Zika virus infection in French Polynesia: a case-control study. *The Lancet* **387**, 1531–1539 (2016).

137. Fonseca, K. *et al.* Case Report: First Case of Zika Virus Infection in a Returning Canadian Traveler. *Am. J. Trop. Med. Hyg* **91**, 1035–1038 (2014).

138. Jorge, F. A. *et al.* Evolutions and upcoming on Zika virus diagnosis through an outbreak: A systematic review. *Reviews in Medical Virology* vol. 30 (2020).

139. Keasey, S. L. *et al.* Antibody Responses to Zika Virus Infections in Environments of Flavivirus Endemicity. *Naval Medical Research Unit* (2017).

140. Ribeiro, M. R. C. *et al.* Plaque reduction neutralization test (PRNT) in the congenital zika syndrome: Positivity and associations with laboratory, clinical, and imaging characteristics. *Viruses* **12**, (2020).

141. Sornjai, W., Jaratsittisin, J., Auewarakul, P., Wikan, N. & Smith, D. R. Analysis of Zika virus neutralizing antibodies in normal healthy Thais. *Scientific Reports 2018 8:1* **8**, 1–6 (2018).

142. Chua, A., Prat, I., Nuebling, C. M., Wood, D. & Moussy, F. Update on Zika Diagnostic Tests and WHO's Related Activities. *PLoS Neglected Tropical Diseases* **11**, (2017).

143. Rabe, I. B. Interim Guidance for Interpretation of Zika Virus Antibody Test Results. *MMWR. Morbidity and Mortality Weekly Report* **65**, 543–546 (2019).

144. Centers for Disease Control and Prevention. Treatment | Zika virus. https://www.cdc.gov/zika/symptoms/treatment.html.

145. World Health Organization. *Assessment and management of Guillain-Barré syndrome in the context of Zika virus infection Interim guidance update*. (2016).

146. Xu, M. *et al.* Identification of small-molecule inhibitors of Zika virus infection and induced neural cell death via a drug repurposing screen. *Nature Medicine* **22**, 1101–1107 (2016).

147. Barrows, N. J. *et al.* A Screen of FDA-Approved Drugs for Inhibitors of Zika Virus Infection. *Cell Host & Microbe* **20**, 259–270 (2016).

148. Retallack, H. *et al.* Zika virus cell tropism in the developing human brain and inhibition by azithromycin. *Proceedings of the National Academy of Sciences* **113**, 14408–14413 (2016).

149. Li, Z. *et al.* Existing drugs as broad-spectrum and potent inhibitors for Zika virus by targeting NS2B-NS3 interaction. *Cell Research 2017 27:8* **27**, 1046–1064 (2017).

150. Delvecchio, R. *et al.* Chloroquine, an endocytosis blocking agent, inhibits zika virus infection in different cell models. *Viruses* **8**, (2016).

151. Yang, S. *et al.* Emetine inhibits Zika and Ebola virus infections through two molecular mechanisms: inhibiting viral replication and decreasing viral entry. *Cell Discovery 2018 4:1* **4**, 1–14 (2018).

152. Kim, J.-A., Seong, R.-K., Kumar, M. & Shin, O. S. Favipiravir and Ribavirin Inhibit Replication of Asian and African Strains of Zika Virus in Different Cell Models. *Viruses* **10**, (2018).

153. Lee, J. le, Loe, M. W. C., Lee, R. C. H. & Chu, J. J. H. Antiviral activity of pinocembrin against Zika virus replication. *Antiviral Research* **167**, 13–24 (2019).

154. Julander, J. G. *et al.* Efficacy of the broad-spectrum antiviral compound BCX4430 against Zika virus in cell culture and in a mouse model. *Antiviral Research* **137**, 14–22 (2017).

155. Simanjuntak, Y. *et al.* Ebselen alleviates testicular pathology in mice with Zika virus infection and prevents its sexual transmission. *PLoS Pathogens* **14**, (2018).

156. Merino-Ramos, T., Oya, N. J. de, Saiz, J.-C. & Martín-Acebes, M. A. Antiviral Activity of Nordihydroguaiaretic Acid and Its Derivative Tetra-O-Methyl Nordihydroguaiaretic Acid against West Nile Virus and Zika Virus. *Antimicrobial Agents and Chemotherapy* **61**, (2017).

157. Deng, Y.-Q. *et al.* Adenosine Analog NITD008 Is a Potent Inhibitor of Zika Virus. *Open Forum Infectious Diseases* **3**, (2016).

158. Zmurko, J. *et al.* The Viral Polymerase Inhibitor 7-Deaza-2′-C-Methyladenosine Is a Potent Inhibitor of In Vitro Zika Virus Replication and Delays Disease Progression in a Robust Mouse Infection Model. *PLOS Neglected Tropical Diseases* **10**, e0004695 (2016).

159. BioCryst Pharmaceuticals. *Galidesivir Stops Zika Viral Replication in Primate Model*. www.BioCryst.com. (2020).

160. Mwaliko, C. *et al.* Zika virus pathogenesis and current therapeutic advances. *Pathogens and Global Health* vol. 115 21–39 (2021).

161. Han, Y. & Mesplède, T. Investigational drugs for the treatment of Zika virus infection: a preclinical and clinical update. *Expert Opinion on Investigational Drugs* **27**, 951–962 (2018).

162. Pan American Health Organization. *Zika virus infection. 7 May 2015*. https://iris.paho.org/handle/10665.2/34232 (2015).

163. Staples, J. E. *et al.* Interim Guidelines for the Evaluation and Testing of Infants with Possible Congenital Zika Virus Infection — United States, 2016. *MMWR. Morbidity and Mortality Weekly Report* **65**, 63–67 (2016).

164. Centers for Disease Control and Prevention. Sexual Transmission and Prevention | Zika Virus. https://www.cdc.gov/zika/prevention/sexual-transmission-prevention.html.

165. Centers for Disease Control and Prevention. Pregnant Women and Zika. https://www.cdc.gov/pregnancy/zika/protect-yourself.html.

166. Halstead, S. B., Chow, J. S. & Marchette, N. J. Immunological enhancement of dengue virus replication. *Nature New Biology* **243**, 24–5 (1973).

167. Halstead, S. & O'Rourke, E. Dengue viruses and mononuclear phagocytes. I. Infection enhancement by non-neutralizing antibody. *Journal of Experimental Medicine* **146**, 201–217 (1977).

168. Littaua, R., Kurane, I. & Ennis, F. A. Human IgG Fc receptor II mediates antibody-dependent enhancement of dengue virus infection. *The Journal of Immunology* **144**, (1990).

169. Rodrigo, W. W. S. I., Jin, X., Blackley, S. D., Rose, R. C. & Schlesinger, J. J. Differential Enhancement of Dengue Virus Immune Complex Infectivity Mediated by Signaling-Competent and Signaling-Incompetent Human FcγRIA (CD64) or FcγRIIA (CD32). *Journal of Virology* **80**, 10128–10138 (2006).

170. Wang, T. T. *et al.* IgG antibodies to dengue enhanced for FcγRIIIA binding determine disease severity. *Science (New York, N.Y.)* **355**, 395–398 (2017).

171. Miner, J. J. & Diamond, M. S. Dengue Antibodies, then Zika: A Fatal Sequence in Mice. *Immunity* **46**, 771–773 (2017).

172. National Institutes of Health. Zika - Clinical trials. https://clinicaltrials.gov/ct2/results?cond=zika&term=&cntry=&state=&city=&dist=.

173. Gaudinski, M. R. *et al.* Safety, tolerability, and immunogenicity of two Zika virus DNA vaccine candidates in healthy adults: randomised, open-label, phase 1 clinical trials. *The Lancet* **391**, 552–562 (2018).

174. Modjarrad, K. *et al.* Safety and immunogenicity of a purified inactivated Zika virus vaccine candidate: preliminary aggregate results from three phase 1a randomized, double-blind, placebo controlled clinical trials. *Lancet (London, England)* **391**, 563 (2018).

175. Tebas, P. *et al.* Safety and Immunogenicity of an Anti–Zika Virus DNA Vaccine. *The New England Journal of Medicine* **385**, e35 (2017).

176. National Institutes of Health. NCBI Virus. https://www.ncbi.nlm.nih.gov/labs/virus/vssi/#/virus?VirusLineage_ss=Zika%20virus,%20taxid:64320&SeqType_s=Nucleotide&Completeness_s=complete.

177. Kuno, G. & Chang, G. J. J. Full-length sequencing and genomic characterization of Bagaza, Kedougou, and Zika viruses. *Archives of Virology* **152**, 687–696 (2007).

178. Baronti, C. *et al.* Complete coding sequence of Zika virus from a French Polynesia outbreak in 2013. *Genome Announcements* **2**, 500–514 (2014).

179. Lindenbach, B. D. & Rice, C. M. Molecular biology of flaviviruses. in *Advances in virus research* vol. 59 23–61 (2003).

180. Shatkin, A. Capping of eucaryotic mRNAs. *Cell* **9**, 645–653 (1976).

181. Darnell, J. E. Transcription Units for mRNA Production in Eukaryotic Cells and Their DNA Viruses. in *Progress in nucleic acid research and molecular biology* vol. 22 327–353 (1979).

182. Muthukrishnan, S., Both, G. W., Furuichi, Y. & Shatkin, A. J. 5′-Terminal 7-methylguanosine in eukaryotic mRNA is required for translation. *Nature 1975 255:5503* **255**, 33–37 (1975).

183. Filipowicz, W. *et al.* A protein binding the methylated 5′-terminal sequence, m7GpppN, of eukaryotic messenger RNA. *Proceedings of the National Academy of Sciences* **73**, 1559–1563 (1976).

184. Schibler, U. & Perry, R. P. The 5′-termini of heterogeneous nuclear RNA: a comparison among molecules of different sizes and ages. *Nucleic Acids Research* **4**, 4133–4150 (1977).

185. Coutard, B. *et al.* Zika Virus Methyltransferase: Structure and Functions for Drug Design Perspectives. *Journal of Virology* **91**, (2017).

186. Daffis, S. *et al.* 2′-O methylation of the viral mRNA cap evades host restriction by IFIT family members. *Nature* **468**, 452–456 (2010).

187. Züst, R. *et al.* Ribose 2′-O-methylation provides a molecular signature for the distinction of self and non-self mRNA dependent on the RNA sensor Mda5. *Nature Immunology* **12**, 137–143 (2011).

188. Brinton, M. A. & Dispoto, J. H. Sequence and secondary structure analysis of the 5′-terminal region of flavivirus genome RNA. *Virology* **162**, 290–299 (1988).

189. Lodeiro, M. F., Filomatori, C. v. & Gamarnik, A. v. Structural and Functional Studies of the Promoter Element for Dengue Virus RNA Replication. *Journal of Virology* **83**, 993–1008 (2009).

190. Bujalowski, P. J., Bujalowski, W. & Choi, K. H. Identification of the viral RNA promoter stem loop A (SLA)-binding site on Zika virus polymerase NS5. *Scientific Reports 2020 10:1* **10**, 1–13 (2020).

191. Filomatori, C. v. A 5′ RNA element promotes dengue virus RNA synthesis on a circular genome. *Genes & Development* **20**, 2238–2249 (2006).

192. Dong, H. *et al.* Distinct RNA Elements Confer Specificity to Flavivirus RNA Cap Methylation Events. *Journal of Virology* **81**, 4412–4421 (2007).

193. Alvarez, D. E., Lodeiro, M. F., Ludueña, S. J., Pietrasanta, L. I. & Gamarnik, A. v. Long-Range RNA-RNA Interactions Circularize the Dengue Virus Genome. *Journal of Virology* **79**, 6631 (2005).

194. Lodeiro, M. F., Filomatori, C. v. & Gamarnik, A. v. Structural and Functional Studies of the Promoter Element for Dengue Virus RNA Replication. *Journal of Virology* **83**, 993–1008 (2009).

195. Clyde, K. & Harris, E. RNA Secondary Structure in the Coding Region of Dengue Virus Type 2 Directs Translation Start Codon Selection and Is Required for Viral Replication. *Journal of Virology* **80**, 2170–2182 (2006).

196. Clyde, K., Barrera, J. & Harris, E. The capsid-coding region hairpin element (cHP) is a critical determinant of dengue virus and West Nile virus RNA synthesis. *Virology* **379**, 314–323 (2008).

197. Wengler, G., Wengler, G. & Gross, H. J. Studies on virus-specific nucleic acids synthesized in vertebrate and mosquito cells infected with flaviviruses. *Virology* **89**, 423–437 (1978).

198. Wengler, G. & Wengler, G. Terminal sequences of the genome and replicatioe-form RNA of the flavivirus west nile virus: absence of poly(A) and possible role in RNA replication. *Virology* **113**, 544–555 (1981).

199. Zhu, Z. *et al.* Comparative genomic analysis of pre-epidemic and epidemic Zika virus strains for virological factors potentially associated with the rapidly expanding epidemic. *Emerging Microbes & Infections* **5**, 1–12 (2016).

200. Polacek, C., Friebe, P. & Harris, E. Poly(A)-binding protein binds to the non-polyadenylated 3′ untranslated region of dengue virus and modulates translation efficiency. *Journal of General Virology* **90**, 687–692 (2009).

201. Villordo, S. M., Alvarez, D. E. & Gamarnik, A. v. A balance between circular and linear forms of the dengue virus genome is crucial for viral replication. *RNA* **16**, 2325 (2010).

202. Davis, W. G., Basu, M., Elrod, E. J., Germann, M. W. & Brinton, M. A. Identification of cis-Acting Nucleotides and a Structural Feature in West Nile Virus 3′-Terminus RNA That Facilitate Viral Minus Strand RNA Synthesis. *Journal of Virology* **87**, 7622–7636 (2013).

203. Pijlman, G. P. *et al.* A Highly Structured, Nuclease-Resistant, Noncoding RNA Produced by Flaviviruses Is Required for Pathogenicity. *Cell Host & Microbe* **4**, 579–591 (2008).

204. Akiyama, B. M. *et al.* Zika virus produces noncoding RNAs using a multi-pseudoknot structure that confounds a cellular exonuclease. *Science* **354**, 1148–1152 (2016).

205. Donald, C. L. *et al.* Full Genome Sequence and sfRNA Interferon Antagonist Activity of Zika Virus from Recife, Brazil. *PLOS Neglected Tropical Diseases* **10**, e0005048 (2016).

206. Pallarés, H. M. *et al.* Zika Virus Subgenomic Flavivirus RNA Generation Requires Cooperativity between Duplicated RNA Structures That Are Essential for Productive Infection in Human Cells. *Journal of Virology* **94**, (2020).

207. Li, X.-D., Deng, C.-L., Yuan, Z.-M., Ye, H.-Q. & Zhang, B. Different Degrees of 5′-to-3′ DAR Interactions Modulate Zika Virus Genome Cyclization and Host-Specific Replication. *Journal of Virology* **94**, (2020).

208. Zhang, B., Dong, H., Ye, H., Tilgner, M. & Shi, P.-Y. Genetic analysis of West Nile virus containing a complete 3′CSI RNA deletion. *Virology* **408**, 138–145 (2010).

209. Annamalai, A. S. *et al.* Zika Virus Encoding Nonglycosylated Envelope Protein Is Attenuated and Defective in Neuroinvasion. *Journal of Virology* **91**, (2017).

210. Lindenbach, B. D., Thiel, H.-J. & Rice, C. M. Flaviviridae: The Viruses and Their Replication. in *Fields Virology* (eds. Knipe, D. M. & Howley, P. M.) 1101–1152 (Lippincott-Raven, 2007).

211. Tan, T. Y. *et al.* Capsid protein structure in Zika virus reveals the flavivirus assembly process. *Nature Communications 2020 11:1* **11**, 1–13 (2020).

212. Shang, Z., Song, H., Shi, Y., Qi, J. & Gao, G. F. Crystal Structure of the Capsid Protein from Zika Virus. *Journal of Molecular Biology* **430**, 948–962 (2018).

213. Morando, M. A., Barbosa, G. M., Cruz-Oliveira, C., da Poian, A. T. & Almeida, F. C. L. Dynamics of Zika Virus Capsid Protein in Solution: The Properties and Exposure of the Hydrophobic Cleft Are Controlled by the α-Helix 1 Sequence. *Biochemistry* **58**, 2488–2498 (2019).

214. Hou, S. *et al.* Zika Virus Hijacks Stress Granule Proteins and Modulates the Host Stress Response. *Journal of Virology* **91**, (2017).

215. Fontaine, K. A. *et al.* The Cellular NMD Pathway Restricts Zika Virus Infection and Is Targeted by the Viral Capsid Protein. *mBio* **9**, (2018).

216. Zeng, J. *et al.* The Zika Virus Capsid Disrupts Corticogenesis by Suppressing Dicer Activity and miRNA Biogenesis. *Cell Stem Cell* **27**, 618-632.e9 (2020).

217. Wengler, G. & Wengler, G. Cell-associated West Nile flavivirus is covered with E+pre-M protein heterodimers which are destroyed and reorganized by proteolytic cleavage during virus release. *Journal of Virology* **63**, 2521–2526 (1989).

218. Konishi, E. & Mason, P. W. Proper maturation of the Japanese encephalitis virus envelope glycoprotein requires cosynthesis with the premembrane protein. *Journal of Virology* **67**, 1672–1675 (1993).

219. Lorenz, I. C., Allison, S. L., Heinz, F. X. & Helenius, A. Folding and Dimerization of Tick-Borne Encephalitis Virus Envelope Proteins prM and E in the Endoplasmic Reticulum. *Journal of Virology* **76**, 5480–5491 (2002).

220. Beeck, A. op de *et al.* Role of the Transmembrane Domains of prM and E Proteins in the Formation of Yellow Fever Virus Envelope. *Journal of Virology* **77**, 813 (2003).

221. Beeck, A. op de, Rouillé, Y., Caron, M., Duvet, S. & Dubuisson, J. The Transmembrane Domains of the prM and E Proteins of Yellow Fever Virus Are

Endoplasmic Reticulum Localization Signals. *Journal of Virology* **78**, 12591 (2004).

222. Lin, Y.-J. & Wu, S.-C. Histidine at Residue 99 and the Transmembrane Region of the Precursor Membrane prM Protein Are Important for the prM-E Heterodimeric Complex Formation of Japanese Encephalitis Virus. *Journal of Virology* **79**, 8535–8544 (2005).

223. Heinz, F. X. *et al.* Structural Changes and Functional Control of the Tick-Borne Encephalitis Virus Glycoprotein E by the Heterodimeric Association with Protein prM. *Virology* **198**, 109–117 (1994).

224. Yu, I.-M. *et al.* Structure of the Immature Dengue Virus at Low pH Primes Proteolytic Maturation. *Science* **319**, 1834–1837 (2008).

225. Sabino, C. *et al.* Bafilomycin A1 and U18666A efficiently impair ZIKV infection. *Viruses* **11**, (2019).

226. Fontes-Garfias, C. R. *et al.* Functional Analysis of Glycosylation of Zika Virus Envelope Protein. *Cell Reports* **21**, 1180–1190 (2017).

227. Dai, L. *et al.* Structures of the Zika Virus Envelope Protein and Its Complex with a Flavivirus Broadly Protective Antibody. *Cell Host & Microbe* **19**, 696–704 (2016).

228. Rey, F. A., Heinz, F. X., Mandl, C., Kunz, C. & Harrison, S. C. The envelope glycoprotein from tick-borne encephalitis virus at 2 Å resolution. *Nature* **375**, 291–298 (1995).

229. Kostyuchenko, V. A. *et al.* Structure of the thermally stable Zika virus. *Nature* **533**, 425–428 (2016).

230. Allison, S. L., Stiasny, K., Stadler, K., Mandl, C. W. & Heinz, F. X. Mapping of Functional Elements in the Stem-Anchor Region of Tick-Borne Encephalitis Virus Envelope Protein E. *Journal of Virology* **73**, 5605–5612 (1999).

231. Gallichotte, E. N. *et al.* Role of Zika Virus Envelope Protein Domain III as a Target of Human Neutralizing Antibodies. *mBio* **10**, (2019).

232. Ci, Y. *et al.* Zika NS1–induced ER remodeling is essential for viral replication. *Journal of Cell Biology* **219**, (2020).

233. Youn, S. *et al.* Evidence for a Genetic and Physical Interaction between Nonstructural Proteins NS1 and NS4B That Modulates Replication of West Nile Virus. *Journal of Virology* **86**, 7360–7371 (2012).

234. Wu, Y. *et al.* Zika virus evades interferon-mediated antiviral response through the co-operation of multiple nonstructural proteins in vitro. *Cell Discovery* **3**, 17006 (2017).

235. Xia, H. *et al.* An evolutionary NS1 mutation enhances Zika virus evasion of host interferon induction. *Nature Communications 2018 9:1* **9**, 1–13 (2018).

236. Zheng, Y. *et al.* Zika virus elicits inflammation to evade antiviral response by cleaving cGAS via NS1-caspase-1 axis. *The EMBO Journal* **37**, (2018).

237. Brown, W. C. *et al.* Extended surface for membrane association in Zika virus NS1 structure. *Nature Structural & Molecular Biology 2016 23:9* **23**, 865–867 (2016).

238. Song, H., Qi, J., Haywood, J., Shi, Y. & Gao, G. F. Zika virus NS1 structure reveals diversity of electrostatic surfaces among flaviviruses. *Nature Structural & Molecular Biology 2016 23:5* **23**, 456–458 (2016).

239. Flamand, M. *et al.* Dengue Virus Type 1 Nonstructural Glycoprotein NS1 Is Secreted from Mammalian Cells as a Soluble Hexamer in a Glycosylation-Dependent Fashion. *Journal of Virology* **73**, 6104–6110 (1999).

240. Kam, Y.-W. *et al.* ZIKV-Specific NS1 Epitopes as Serological Markers of Acute Zika Virus Infection. *The Journal of Infectious Diseases* **220**, 203–212 (2019).

241. Márquez-Jurado, S. *et al.* An Alanine-to-Valine Substitution in the Residue 175 of Zika Virus NS2A Protein Affects Viral RNA Synthesis and Attenuates the Virus In Vivo. *Viruses* **10**, 547 (2018).

242. Zhang, X. *et al.* Zika Virus NS2A-Mediated Virion Assembly. *mBio* **10**, (2019).

243. Ngueyen, T. T. N., Kim, S.-J., Lee, J. Y. & Myoung, J. Zika Virus Proteins NS2A and NS4A Are Major Antagonists that Reduce IFN-β Promoter Activity Induced by the MDA5/RIG-I Signaling Pathway. *Journal of Microbiology and Biotechnology* **29**, 1665–1674 (2019).

244. Yoon, K.-J. *et al.* Zika-Virus-Encoded NS2A Disrupts Mammalian Cortical Neurogenesis by Degrading Adherens Junction Proteins. *Cell Stem Cell* **21**, 349-358.e6 (2017).

245. Li, Y. *et al.* Structural Insights into the Inhibition of Zika Virus NS2B-NS3 Protease by a Small-Molecule Inhibitor. *Structure* **26**, 555-564.e3 (2018).

246. Phoo, W. W. *et al.* Structure of the NS2B-NS3 protease from Zika virus after self-cleavage. *Nature Communications 2016 7:1* **7**, 1–8 (2016).

247. Xing, H. *et al.* Zika NS2B is a crucial factor recruiting NS3 to the ER and activating its protease activity. *Virus Research* **275**, 197793 (2020).

248. Wu, Y. *et al.* Zika virus evades interferon-mediated antiviral response through the co-operation of multiple nonstructural proteins in vitro. *Cell Discovery* **3**, 17006 (2017).

249. Lei, J. *et al.* Crystal structure of Zika virus NS2B-NS3 protease in complex with a boronate inhibitor. *Science* **353**, 503–505 (2016).

250. Xu, S. *et al.* Zika virus NS3 is a canonical RNA helicase stimulated by NS5 RNA polymerase. *Nucleic Acids Research* **47**, 8693–8707 (2019).

251. Ding, Q. *et al.* Species-specific disruption of STING-dependent antiviral cellular defenses by the Zika virus NS2B3 protease. *Proceedings of the National Academy of Sciences* **115**, E6310–E6318 (2018).

252. Li, H. *et al.* Zika Virus Protease Cleavage of Host Protein Septin-2 Mediates Mitotic Defects in Neural Progenitors. *Neuron* **101**, 1089-1098.e4 (2019).

253. Chen, W. *et al.* Zika virus NS3 protease induces bone morphogenetic protein-dependent brain calcification in human fetuses. *Nature Microbiology* **6**, 455–466 (2021).

254. Kumar, A., Kumar, P. & Giri, R. Zika virus NS4A cytosolic region (residues 1–48) is an intrinsically disordered domain and folds upon binding to lipids. *Virology* **550**, 27–36 (2020).

255. Liang, Q. *et al.* Zika Virus NS4A and NS4B Proteins Deregulate Akt-mTOR Signaling in Human Fetal Neural Stem Cells to Inhibit Neurogenesis and Induce Autophagy. *Cell Stem Cell* **19**, 663–671 (2016).

256. Ma, J. *et al.* Zika Virus Non-structural Protein 4A Blocks the RLR-MAVS Signaling. *Frontiers in Microbiology* **0**, 1350 (2018).

257. Hu, Y. *et al.* Zika virus antagonizes interferon response in patients and disrupts RIG-I–MAVS interaction through its CARD-TM domains. *Cell & Bioscience 2019 9:1* **9**, 1–15 (2019).

258. Zhao, B. *et al.* Structure and function of the Zika virus full-length NS5 protein. *Nature Communications 2017 8:1* **8**, 1–9 (2017).

259. Ferrero, D. S. *et al.* Supramolecular arrangement of the full-length Zika virus NS5. *PLOS Pathogens* **15**, e1007656 (2019).

260. Grant, A. *et al.* Zika Virus Targets Human STAT2 to Inhibit Type I Interferon Signaling. *Cell Host & Microbe* **19**, 882–890 (2016).

261. Hertzog, J. *et al.* Infection with a Brazilian isolate of Zika virus generates RIG-I stimulatory RNA and the viral NS5 protein blocks type I IFN induction and signaling. *European Journal of Immunology* **48**, 1120–1136 (2018).

262. Lin, S. *et al.* Zika virus NS5 protein antagonizes type I interferon production via blocking TBK1 activation. *Virology* **527**, 180–187 (2019).

263. Ji, W. & Luo, G. Zika virus NS5 nuclear accumulation is protective of protein degradation and is required for viral RNA replication. *Virology* **541**, 124–135 (2020).

264. Expansy. Zika virus. https://viralzone.expasy.org/6756.

265. Barreto-Vieira, D. F. *et al.* Ultrastructure of Zika virus particles in cell cultures. *Memorias do Instituto Oswaldo Cruz* **111**, 532 (2016).

266. Sirohi, D. *et al.* The 3.8 Å resolution cryo-EM structure of Zika virus. *Science* **352**, 467–470 (2016).

267. Prasad, V. M. *et al.* Structure of the immature Zika virus at 9 A resolution. *Nature Structural and Molecular Biology* **24**, 184–186 (2017).

268. Bell, T. M., Field, E. J. & Narang, H. K. Zika virus infection of the central nervous system of mice. *Archiv für die gesamte Virusforschung* **35**, 183–193 (1971).

269. Heinz, F. X. & Stiasny, K. The Antigenic Structure of Zika Virus and Its Relation to Other Flaviviruses: Implications for Infection and Immunoprophylaxis. *Microbiology and Molecular Biology Reviews* **81**, (2017).

270. Y, C. *et al.* Dengue virus infectivity depends on envelope protein binding to target cell heparan sulfate. *Nature medicine* **3**, 866–871 (1997).

271. Kim, S. Y. *et al.* Interaction of Zika Virus Envelope Protein with Glycosaminoglycans. *Biochemistry* **56**, 1151–1162 (2017).

272. H, G. *et al.* Role of heparan sulfate in the Zika virus entry, replication, and cell death. *Virology* **529**, 91–100 (2019).

273. Hamel, R. *et al.* Biology of Zika Virus Infection in Human Skin Cells. *Journal of Virology* **89**, 8880–8896 (2015).

274. Stitt, T. N. *et al.* The anticoagulation factor protein S and its relative, Gas6, are ligands for the Tyro 3/Axl family of receptor tyrosine kinases. *Cell* **80**, 661–670 (1995).

275. Meertens, L. *et al.* Axl Mediates ZIKA Virus Entry in Human Glial Cells and Modulates Innate Immune Responses. *Cell Reports* **18**, 324–333 (2017).

276. Richard, A. S. *et al.* AXL-dependent infection of human fetal endothelial cells distinguishes Zika virus from other pathogenic flaviviruses. *Proceedings of the National Academy of Sciences* **114**, 2024–2029 (2017).

277. Liu, S., DeLalio, L. J., Isakson, B. E. & Wang, T. T. AXL-Mediated Productive Infection of Human Endothelial Cells by Zika Virus. *Circulation Research* **119**, 1183–1189 (2016).

278. Wells, M. F. *et al.* Genetic Ablation of AXL Does Not Protect Human Neural Progenitor Cells and Cerebral Organoids from Zika Virus Infection. *Cell Stem Cell* **19**, 703–708 (2016).

279. Hastings, A. K. *et al.* TAM Receptors Are Not Required for Zika Virus Infection in Mice. *Cell Reports* **19**, 558–568 (2017).

280. Li, F. *et al.* AXL is not essential for Zika virus infection in the mouse brain. *Emerging Microbes & Infections* **6**, 1–2 (2017).

281. Wang, Z. Y. *et al.* Axl is not an indispensable factor for zika virus infection in mice. *Journal of General Virology* **98**, 2061–2068 (2017).

282. Miner, J. J. *et al.* Zika Virus Infection in Mice Causes Panuveitis with Shedding of Virus in Tears. *Cell Reports* **16**, 3208–3218 (2016).

283. Tan, C. W. *et al.* Cell surface α2,3-linked sialic acid facilitates Zika virus internalization. *Emerging Microbes and Infections* **8**, 426–437 (2019).

284. Pujhari, S. *et al.* Heat shock protein 70 (Hsp70) mediates Zika virus entry, replication, and egress from host cells. *Emerging Microbes & Infections* **8**, 8–16 (2019).

285. Wang, S. *et al.* Integrin αvβ5 Internalizes Zika Virus during Neural Stem Cells Infection and Provides a Promising Target for Antiviral Therapy. *Cell Reports* **30**, 969-983.e4 (2020).

286. Srivastava, M. *et al.* Chemical proteomics tracks virus entry and uncovers NCAM1 as Zika virus receptor. *Nature Communications* **11**, (2020).

287. Khongwichit, S. *et al.* A functional interaction between GRP78 and Zika virus E protein. *Scientific Reports* **11**, 393 (2021).

288. Baron, S., Fons, M. & Albrecht, T. Viral Pathogenesis. *Encyclopedia of Virology* 314–319 (1996).

289. Ebel, G. D. Promiscuous viruses – how do viruses survive multiple unrelated hosts? *Current opinion in virology* **23**, 125 (2017).

290. Owczarek, K. *et al.* Zika virus: mapping and reprogramming the entry. *Cell Communication and Signaling 2019 17:1* **17**, 1–19 (2019).

291. Li, M. *et al.* Characterization of Zika Virus Endocytic Pathways in Human Glioblastoma Cells. *Frontiers in Microbiology* **11**, (2020).

292. Rawle, R. J., Webster, E. R., Jelen, M., Kasson, P. M. & Boxer, S. G. pH Dependence of Zika Membrane Fusion Kinetics Reveals an Off-Pathway State. *ACS Central Science* **4**, 1503–1510 (2018).

293. Song, Y., Mugavero, J., Stauft, C. B. & Wimmer, E. Dengue and Zika Virus 5′ Untranslated Regions Harbor Internal Ribosomal Entry Site Functions. *mBio* **10**, (2019).

294. Rana, J. *et al.* Role of Capsid Anchor in the Morphogenesis of Zika Virus. *Journal of Virology* **92**, (2018).

295. Cortese, M. *et al.* Ultrastructural Characterization of Zika Virus Replication Factories. *Cell Reports* **18**, 2113–2123 (2017).

296. Överby, A. K., Popov, V. L., Niedrig, M. & Weber, F. Tick-Borne Encephalitis Virus Delays Interferon Induction and Hides Its Double-Stranded RNA in Intracellular Membrane Vesicles. *Journal of Virology* **84**, 8470–8483 (2010).

297. Hoenen, A., Liu, W., Kochs, G., Khromykh, A. A. & Mackenzie, J. M. West Nile virus-induced cytoplasmic membrane structures provide partial protection against the interferon-induced antiviral MxA protein. *Journal of General Virology* **88**, 3013–3017 (2007).

298. Klema, V. J., Padmanabhan, R. & Choi, K. H. Flaviviral Replication Complex: Coordination between RNA Synthesis and 5′-RNA Capping. *Viruses 2015, Vol. 7, Pages 4640-4656* **7**, 4640–4656 (2015).

299. Rossignol, E. D., Peters, K. N., Connor, J. H. & Bullitt, E. Zika virus induced cellular remodelling. *Cellular Microbiology* **19**, e12740 (2017).

300. Stadler, K., Allison, S. L., Schalich, J. & Heinz, F. X. Proteolytic activation of tick-borne encephalitis virus by furin. *Journal of virology* **71**, 8475–8481 (1997).

301. Pierson, T. C. & Diamond, M. S. Degrees of maturity: the complex structure and biology of flaviviruses. *Current Opinion in Virology* **2**, 168–175 (2012).

302. Muller, D. A. & Young, P. R. The flavivirus NS1 protein: molecular and structural biology, immunology, role in pathogenesis and application as a diagnostic biomarker. *Antiviral research* **98**, 192–208 (2013).

303. Carpenter, G., King, L. & Cohen, S. Epidermal growth factor stimulates phosphorylation in membrane preparations in vitro. *Nature* vol. 276 409–410 (1978).

304. Cohens, S., Ushiro, H., Stoscheckg, C. & Chinkers, M. A Native 170,000 Epidermal Growth Factor Receptor-Kinase Complex from Shed Plasma Membrane Vesicles*. *The Journal of Biological Chemistry* **257**, 1523–1531 (1982).

305. Hayman, M. J. *et al.* Identification and characterization of the avian erythroblastosis virus erbB gene product as a membrane glycoprotein. *Cell* **32**, 579–588 (1983).

306. Privalsky, M. L., Sealy, L., Michael Bishop, J., McGrath, J. P. & Levinson, A. D. The product of the avian erythroblastosis virus erbB locus is a glycoprotein. *Cell* **32**, 1257–1267 (1983).

307. Semba, K., Kamata, N., Toyoshima, K. & Yamamoto, T. A v-erbB-related protooncogene, c-erbB-2, is distinct from the c-erbB-1/epidermal growth factor-receptor gene and is amplified in a human salivary gland adenocarcinoma. *Proceedings of the National Academy of Sciences of the United States of America* **82**, 6497–6501 (1985).

308. Kraus, M. H., Issing, W., Miki, T., Popescu, N. P. & Aaronson, S. A. Isolation and characterization of ERBB3, a third member of the ERBB/epidermal growth factor receptor family: Evidence for overexpression in a subset of human mammary tumors. *Proceedings of the National Academy of Sciences of the United States of America* **86**, 9193–9197 (1989).

309. Plowman, G. D. *et al.* Ligand-specific activation of HER4/p180erbB4, a fourth member of the epidermal growth factor receptor family. *Proceedings of the National Academy of Sciences of the United States of America* **90**, 1746–1750 (1993).

310. Reiter, J. L. *et al.* Comparative genomic sequence analysis and isolation of human and mouse alternative EGFR transcripts encoding truncated receptor isoforms. *Genomics* **71**, 1–20 (2001).

311. Ullrich, A. *et al.* Human epidermal growth factor receptor cDNA sequence and aberrant expression of the amplified gene in A431 epidermoid carcinoma cells. *Nature* **309**, 418–425 (1984).

312. Bajaj, M., Waterfield, M. D., Schlessinger, J., Taylor, W. R. & Blundell, T. On the tertiary structure of the extracellular domains of the epidermal growth factor and insulin receptors. *Biochimica et Biophysica Acta (BBA) - Protein Structure and Molecular Enzymology* **916**, 220–226 (1987).

313. Welsh, J. B., Gill, G. N., Rosenfeld, M. G. & Wells, A. A negative feedback loop attenuates EGF-induced morphological changes. *Journal of Cell Biology* **114**, 533–543 (1991).

314. Chen, P., Xie, H. & Wells, A. Mitogenic signaling from the EGF receptor is attenuated by a phospholipase C-γ/protein kinase C feedback mechanism. *Molecular Biology of the Cell* **7**, 871–881 (1996).

315. Martín-Nieto, J. & Villalobo, A. The human epidermal growth factor receptor contains a juxtamembrane calmodulin-binding site. *Biochemistry* **37**, 227–236 (1998).

316. Tebar, F. *et al.* Calmodulin regulates intracellular trafficking of epidermal growth factor receptor and the MAPK signaling pathway. *Molecular Biology of the Cell* **13**, 2057–2068 (2002).

317. Segatto, O. *et al.* The juxtamembrane regions of the epidermal growth factor receptor and gp185erbB-2 determine the specificity of signal transduction. *Molecular and Cellular Biology* **11**, 3191–3202 (1991).

318. Aifa, S. *et al.* Interactions between the juxtamembrane domain of the EGFR and calmodulin measured by surface plasmon resonance. *Cellular Signalling* **14**, 1005–1013 (2002).

319. Poppleton, H. M., Wiepz, G. J., Bertics, P. J. & Patel, T. B. Modulation of the protein tyrosine kinase activity and autophosphorylation of the epidermal growth factor receptor by its juxtamembrane region. *Archives of Biochemistry and Biophysics* **363**, 227–236 (1999).

320. Aifa, S. *et al.* A basic peptide within the juxtamembrane region is required for EGF receptor dimerization.

321. Heisermann, G. J. *et al.* Mutational removal of the Thr669 and Ser671 phosphorylation sites alters substrate specificity and ligand-induced internalization of the epidermal growth factor receptor. *Journal of Biological Chemistry* **265**, 12820–12827 (1990).

322. Stamos, J., Sliwkowski, M. X. & Eigenbrot, C. Structure of the Epidermal Growth Factor Receptor Kinase Domain Alone and in Complex with a 4-Anilinoquinazoline Inhibitor *. *Journal of Biological Chemistry* **277**, 46265–46272 (2002).

323. Knighton, D. R. *et al.* Crystal Structure of the Catalytic Subunit of Cyclic Adenosine Monophosphate-Dependent Protein Kinase. *Science* **253**, 407–414 (1991).

324. Nolen, B., Taylor, S. & Ghosh, G. Regulation of Protein Kinases: Controlling Activity through Activation Segment Conformation. *Molecular Cell* **15**, 661–675 (2004).

325. Downward, J., Parker, P. & Waterfield, M. D. Autophosphorylation sites on the epidermal growth factor receptor. *Nature* **311**, 483–485 (1984).

326. Margolis, B. L. *et al.* All Autophosphorylation Sites of Epidermal Growth Factor (EGF) Receptor and HER2/neu Are Located in Their Carboxyl-terminal Tails. *The Journal of Biological Chemistry* **264**, 10667–10671 (1989).

327. Dankort, D. L., Wang, Z., Blackmore, V., Moran, M. F. & Muller, W. J. Distinct Tyrosine Autophosphorylation Sites Negatively and Positively Modulate Neu-Mediated Transformation. *Molecular and Cellular Biology* **17**, 5410–5425 (1997).

328. Pines, G., Huang, P. H., Zwang, Y., White, F. M. & Yarden, Y. EGFRvIV: a previously uncharacterized oncogenic mutant reveals a kinase autoinhibitory mechanism. *Oncogene* **29**, 5850 (2010).

329. Sorkin, A., Mazzotti, M., Sorkina, T., Scotto, L. & Beguinot, L. Epidermal growth factor receptor interaction with clathrin adaptors is mediated by the Tyr974-containing internalization motif. *The Journal of biological chemistry* **271**, 13377–13384 (1996).

330. Huang, Y., Kim, S. O., Jiang, J. & Frank, S. J. Growth hormone-induced phosphorylation of epidermal growth factor (EGF) receptor in 3T3-F442A cells. Modulation of EGF-induced trafficking and signaling. *The Journal of biological chemistry* **278**, 18902–18913 (2003).

331. Huang, Y. *et al.* Molecular basis for multimerization in the activation of the epidermal growth factor receptor. *eLife* **5**, (2016).

332. Cohen, S. & Carpenter, G. Human epidermal growth factor: isolation and chemical and biological properties. *Proceedings of the National Academy of Sciences of the United States of America* **72**, 1317–1321 (1975).

333. Derynck, R., Roberts, A. B., Winkler, M. E., Chen, E. Y. & Goeddel, D. v. Human transforming growth factor-alpha: precursor structure and expression in E. coli. *Cell* **38**, 287–297 (1984).

334. Shoyab, M., Plowman, G. D., McDonald, V. L., Bradley, J. G. & Todaro, G. J. Structure and function of human amphiregulin: a member of the epidermal growth factor family. *Science (New York, N.Y.)* **243**, 1074–1076 (1989).

335. Strachan, L. *et al.* Cloning and biological activity of epigen, a novel member of the epidermal growth factor superfamily. *The Journal of biological chemistry* **276**, 18265–18271 (2001).

336. Higashiyama, S., Abraham, J. A., Miller, J., Fiddes, J. C. & Klagsbrun, M. A heparin-binding growth factor secreted by macrophage-like cells that is related to EGF. *Science (New York, N.Y.)* **251**, 936–939 (1991).

337. Sasada, R. *et al.* Cloning and expression of cDNA encoding human betacellulin, a new member of the EGF family. *Biochemical and biophysical research communications* **190**, 1173–1179 (1993).

338. Komurasaki, T., Toyoda, H., Uchida, D. & Morimoto, S. Epiregulin binds to epidermal growth factor receptor and ErbB-4 and induces tyrosine phosphorylation of epidermal growth factor receptor, ErbB-2, ErbB-3 and ErbB-4. *Oncogene* **15**, 2841–2848 (1997).

339. Carraway, K. L. *et al.* Neuregulin-2, a new ligand of ErbB3/ErbB4-receptor tyrosine kinases. *Nature* **387**, 512–516 (1997).

340. Zhang, D. *et al.* Neuregulin-3 (NRG3): a novel neural tissue-enriched protein that binds and activates ErbB4. *Proceedings of the National Academy of Sciences of the United States of America* **94**, 9562–9567 (1997).

341. Harari, D. *et al.* Neuregulin-4: a novel growth factor that acts through the ErbB-4 receptor tyrosine kinase. *Oncogene* **18**, 2681–2689 (1999).

342. Rayego-Mateos, S. *et al.* Connective tissue growth factor is a new ligand of epidermal growth factor receptor. *Journal of Molecular Cell Biology* **5**, 323–335 (2013).

343. Wang, Y. N. *et al.* Angiogenin/Ribonuclease 5 Is an EGFR Ligand and a Serum Biomarker for Erlotinib Sensitivity in Pancreatic Cancer. *Cancer Cell* **33**, 752-769.e8 (2018).

344. Yang, L., Li, Y. & Zhang, Y. Identification of prolidase as a high affinity ligand of the ErbB2 receptor and its regulation of ErbB2 signaling and cell growth. *Cell Death & Disease 2014 5:5* **5**, e1211–e1211 (2014).

345. Massagué, J. & Pandiella, A. Membrane-anchored growth factors. *Annual review of biochemistry* **62**, 515–541 (1993).

346. Sanderson, M. P., Dempsey, P. J. & Dunbar, A. J. Control of ErbB signaling through metalloprotease mediated ectodomain shedding of EGF-like factors. *Growth factors (Chur, Switzerland)* **24**, 121–136 (2006).

347. Davis, C. G. The many faces of epidermal growth factor repeats. *The New Biologist* **2**, 410–419 (1990).

348. Lax, I. *et al.* Localization of a major receptor-binding domain for epidermal growth factor by affinity labeling. *Molecular and Cellular Biology* **8**, 1831 (1988).

349. Pike, L. J., Han, X. & Gross, R. W. Epidermal growth factor receptors are localized to lipid rafts that contain a balance of inner and outer leaflet lipids: A shotgun lipidomics study. *Journal of Biological Chemistry* **280**, 26796–26804 (2005).

350. Klausner, R. D., Kleinfeld, A. M., Hoover, R. L. & Karnovsky, M. J. Lipid Domains in Membranes. Evidence derived from structural perturbations induced by free fatty acids and lifetime heterogeneity analyis. *Journal of Biological Chemistry* **255**, 1286–1295 (1980).

351. Yu, X., Sharma, K. D., Takahashi, T., Iwamoto, R. & Mekada, E. Ligand-independent Dimer Formation of Epidermal Growth Factor Receptor (EGFR) Is a Step

Separable from Ligand-induced EGFR Signaling. *Molecular Biology of the Cell* **13**, 2547 (2002).

352. Chung, I. *et al.* Spatial control of EGF receptor activation by reversible dimerization on living cells. *Nature* **464**, 783–787 (2010).

353. Ferguson, K. M. *et al.* EGF Activates Its Receptor by Removing Interactions that Autoinhibit Ectodomain Dimerization. *Molecular Cell* **11**, 507–517 (2003).

354. Lemmon, M. A. *et al.* Two EGF molecules contribute additively to stabilization of the EGFR dimer. *The EMBO Journal* **16**, 281 (1997).

355. Ogiso, H. *et al.* Crystal structure of the complex of human epidermal growth factor and receptor extracellular domains. *Cell* **110**, 775–787 (2002).

356. Tzahar, E. *et al.* A hierarchical network of interreceptor interactions determines signal transduction by Neu differentiation factor/neuregulin and epidermal growth factor. *Molecular and cellular biology* **16**, 5276–5287 (1996).

357. Graus-Porta, D., Beerli, R. R., Daly, J. M. & Hynes, N. E. ErbB-2, the preferred heterodimerization partner of all ErbB receptors, is a mediator of lateral signaling. *The EMBO Journal* **16**, 1647 (1997).

358. Dawson, J. P. *et al.* Epidermal growth factor receptor dimerization and activation require ligand-induced conformational changes in the dimer interface. *Molecular and cellular biology* **25**, 7734–7742 (2005).

359. Moriki, T., Maruyama, H. & Maruyama, I. N. Activation of preformed EGF receptor dimers by ligand-induced rotation of the transmembrane domain. *Journal of molecular biology* **311**, 1011–1026 (2001).

360. Zhang, X., Gureasko, J., Shen, K., Cole, P. A. & Kuriyan, J. An allosteric mechanism for activation of the kinase domain of epidermal growth factor receptor. *Cell* **125**, 1137–1149 (2006).

361. Jura, N. *et al.* Mechanism for activation of the EGF receptor catalytic domain by the juxtamembrane segment. *Cell* **137**, 1293–1307 (2009).

362. Red Brewer, M. *et al.* The juxtamembrane region of the EGF receptor functions as an activation domain. *Molecular cell* **34**, 641–651 (2009).

363. Honegger, A. M., Kris, R. M., Ullrich, A. & Schlessinger, J. Evidence that autophosphorylation of solubilized receptors for epidermal growth factor is mediated by intermolecular cross-phosphorylation. *Proceedings of the National Academy of Sciences of the United States of America* **86**, 925 (1989).

364. Margolis, B. L. *et al.* All Autophosphorylation Sites of Epidermal Growth Factor (EGF) Receptor and HER2/neu Are Located in Their Carboxyl-terminal Tails. *The Journal of Biological Chemistry* **264**, 10667–10671 (1989).

365. Stover, D. R., Becker, M., Liebetanz, J. & Lydon, N. B. Src Phosphorylation of the Epidermal Growth Factor Receptor at Novel Sites Mediates Receptor Interaction with Src and P85α (∗). *Journal of Biological Chemistry* **270**, 15591–15597 (1995).

366. Hunter, T., Ling, N. & Cooper, J. A. Protein kinase C phosphorylation of the EGF receptor at a threonine residue close to the cytoplasmic face of the plasma membrane. *Nature 1984 311:5985* **311**, 480–483 (1984).

367. Sadowski, I., Stone, J. C. & Pawson, T. A noncatalytic domain conserved among cytoplasmic protein-tyrosine kinases modifies the kinase function and transforming activity of Fujinami sarcoma virus P130gag-fps. *Molecular and cellular biology* **6**, 4396–4408 (1986).

368. Kavanaugh, W. M. & Williams, L. T. An alternative to SH2 domains for binding tyrosine-phosphorylated proteins. *Science (New York, N.Y.)* **266**, 1862–1865 (1994).

369. Anderson, D. *et al.* Binding of SH2 domains of phospholipase C gamma 1, GAP, and Src to activated growth factor receptors. *Science (New York, N.Y.)* **250**, 979–982 (1990).

370. Mineo, C., James, G. L., Smart, E. J. & Anderson, R. G. W. Localization of epidermal growth factor-stimulated Ras/Raf-1 interaction to caveolae membrane. *The Journal of biological chemistry* **271**, 11930–11935 (1996).

371. Couet, J., Sargiacomo, M. & Lisanti, M. P. Interaction of a receptor tyrosine kinase, EGF-R, with caveolins. Caveolin binding negatively regulates tyrosine and serine/threonine kinase activities. *The Journal of biological chemistry* **272**, 30429–30438 (1997).

372. Mineo, C., Gill, G. N. & Anderson, R. G. W. Regulated migration of epidermal growth factor receptor from caveolae. *The Journal of biological chemistry* **274**, 30636–30643 (1999).

373. Yoon, S. & Seger, R. The extracellular signal-regulated kinase: Multiple substrates regulate diverse cellular functions. *Growth Factors* **24**, 21–44 (2009).

374. Manning, B. D. & Cantley, L. C. AKT/PKB Signaling: Navigating Downstream. *Cell* **129**, 1261 (2007).

375. Nakashima, S. Protein kinase C alpha (PKC alpha): regulation and biological function. *Journal of biochemistry* **132**, 669–675 (2002).

376. Horvath, C. M. STAT proteins and transcriptional responses to extracellular signals. *Trends in biochemical sciences* **25**, 496–502 (2000).

377. Quesnelle, K. M., Boehm, A. L. & Grandis, J. R. STAT-mediated EGFR signaling in cancer. *Journal of cellular biochemistry* **102**, 311–319 (2007).

378. Pelicci, G. *et al.* A novel transforming protein (SHC) with an SH2 domain is implicated in mitogenic signal transduction. *Cell* **70**, 93–104 (1992).

379. Batzer, A. G., Rotin, D., Ureña, J. M., Skolnik, E. Y. & Schlessinger, J. Hierarchy of binding sites for Grb2 and Shc on the epidermal growth factor receptor. *Molecular and cellular biology* **14**, 5192–5201 (1994).

380. Hu, Y. & Bowtell, D. Sos1 rapidly associates with Grb2 and is hypophosphorylated when complexed with the EGF receptor after EGF stimulation. *Oncogene* (1996).

381. Lowenstein, E. J. *et al.* The SH2 and SH3 domain-containing protein GRB2 links receptor tyrosine kinases to ras signaling. *Cell* **70**, 431–442 (1992).

382. Rozakis-Adcock, M. *et al.* Association of the Shc and Grb2/Sem5 SH2-containing proteins is implicated in activation of the Ras pathway by tyrosine kinases. *Nature* **360**, 689–692 (1992).

383. Howe, L. R. *et al.* Activation of the MAP kinase pathway by the protein kinase raf. *Cell* **71**, 335–342 (1992).

384. Leevers, S. J., Paterson, H. F. & Marshall, C. J. Requirement for Ras in Raf activation is overcome by targeting Raf to the plasma membrane. *Nature 1994 369:6479* **369**, 411–414 (1994).

385. Boulton, T. G. *et al.* ERKs: A family of protein-serine/threonine kinases that are activated and tyrosine phosphorylated in response to insulin and NGF. *Cell* **65**, 663–675 (1991).

386. Zhang, W., Dziak, R. M. & Aletta, J. M. EGF-mediated phosphorylation of extracellular signal-regulated kinases in osteoblastic cells. *Journal of cellular physiology* **162**, 348–358 (1995).

387. Schulze, A., Lehmann, K., Jefferies, H. B. J., McMahon, M. & Downward, J. Analysis of the transcriptional program induced by Raf in epithelial cells. *Genes & Development* **15**, 981 (2001).

388. Lock, L. S., Royal, I., Naujokas, M. A. & Park, M. Identification of an atypical Grb2 carboxyl-terminal SH3 domain binding site in Gab docking proteins reveals Grb2-dependent and -independent recruitment of Gab1 to receptor tyrosine kinases. *The Journal of biological chemistry* **275**, 31536–31545 (2000).

389. Mattoon, D. R., Lamothe, B., Lax, I. & Schlessinger, J. The docking protein Gab1 is the primary mediator of EGF-stimulated activation of the PI-3K/Akt cell survival pathway. *BMC biology* **2**, (2004).

390. Carpenter, C. L. *et al.* Purification and characterization of phosphoinositide 3-kinase from rat liver. *Journal of Biological Chemistry* **265**, 19704–19711 (1990).

391. Sjolander, A., Yamamoto, K., Huber, B. E. & Lapetina, E. G. Association of p21ras with phosphatidylinositol 3-kinase. *Proceedings of the National Academy of Sciences of the United States of America* **88**, 7908–7912 (1991).

392. Rodriguez-Viciana, P., Warne, P. H., Vanhaesebroeck, B., Waterfield, M. D. & Downward, J. Activation of phosphoinositide 3-kinase by interaction with Ras and by point mutation. *The EMBO Journal* **15**, 2442 (1996).

393. Whitman, M., Downes, C. P., Keeler, M., Keller, T. & Cantley, L. Type I phosphatidylinositol kinase makes a novel inositol phospholipid, phosphatidylinositol-3-phosphate. *Nature 1988 332:6165* **332**, 644–646 (1988).

394. Auger, K. R., Serunian, L. A., Soltoff, S. P., Libby, P. & Cantley, L. C. PDGF-dependent tyrosine phosphorylation stimulates production of novel polyphosphoinositides in intact cells. *Cell* **57**, 167–175 (1989).

395. Franke, T. F., Kaplan, D. R., Cantley, L. C. & Toker, A. Direct regulation of the Akt proto-oncogene product by phosphatidylinositol-3,4-bisphosphate. *Science (New York, N.Y.)* **275**, 665–668 (1997).

396. Alessi, D. R. *et al.* Characterization of a 3-phosphoinositide-dependent protein kinase which phosphorylates and activates protein kinase Balpha. *Current biology : CB* **7**, 261–269 (1997).

397. Chattopadhyay, A., Vecchi, M., Ji, Q. S., Mernaugh, R. & Carpenter, G. The role of individual SH2 domains in mediating association of phospholipase C-gamma1 with the activated EGF receptor. *The Journal of biological chemistry* **274**, 26091–26097 (1999).

398. Berridge, M. J. Inositol Trisphosphate and Diacylglycerol as Intracellular Second Messengers. *Mechanisms of Receptor Regulation* 111–130 (1985) doi:10.1007/978-1-4613-2131-6_8.

399. Berridge, M. J. Inositol trisphosphate and calcium signalling. *Nature* **361**, 315–325 (1993).

400. Huang, K. P. The mechanism of protein kinase C activation. *Trends in Neurosciences* **12**, 425–432 (1989).

401. Coffer, P. J. & Kruijer, W. EGF receptor deletions define a region specifically mediating STAT transcription factor activation. *Biochemical and biophysical research communications* **210**, 74–81 (1995).

402. Xia, L. *et al.* Identification of both positive and negative domains within the epidermal growth factor receptor COOH-terminal region for signal transducer and activator of transcription (STAT) activation. *The Journal of biological chemistry* **277**, 30716–30723 (2002).

403. Olayioye, M. A., Beuvink, I., Horsch, K., Daly, J. M. & Hynes, N. E. ErbB receptor-induced activation of stat transcription factors is mediated by Src tyrosine kinases. *The Journal of biological chemistry* **274**, 17209–17218 (1999).

404. Andl, C. D. *et al.* EGFR-induced cell migration is mediated predominantly by the JAK-STAT pathway in primary esophageal keratinocytes. *American journal of physiology. Gastrointestinal and liver physiology* **287**, (2004).

405. Shostak, K. & Chariot, A. EGFR and NF-κB: partners in cancer. *Trends in Molecular Medicine* **21**, 385–393 (2015).

406. West, M. A., Bretscher, M. S. & Watts, C. Distinct endocytotic pathways in epidermal growth factor-stimulated human carcinoma A431 cells. *The Journal of cell biology* **109**, 2731–2739 (1989).

407. Lund, K. A., Opresko, L. K., Starbuck, C., Walsh, B. J. & Steven Wiley4, H. Quantitative Analysis of the Endocytic System Involved in Hormone-induced Receptor Internalization*. *The Journal of Biological Chemistry* **265**, 15713–15723 (1990).

408. Hanover, J. A., Willingham, M. C. & Pastan, I. Kinetics of transit of transferrin and epidermal growth factor through clathrin-coated membranes. *Cell* **39**, 283–293 (1984).

409. Sorkin, A. & Carpenter, G. Interaction of activated EGF receptors with coated pit adaptins. *Science (New York, N.Y.)* **261**, 612–615 (1993).

410. Huang, F., Jiang, X. & Sorkin, A. Tyrosine phosphorylation of the beta2 subunit of clathrin adaptor complex AP-2 reveals the role of a di-leucine motif in the epidermal growth factor receptor trafficking. *The Journal of biological chemistry* **278**, 43411–43417 (2003).

411. Sigismund, S. *et al.* Clathrin-independent endocytosis of ubiquitinated cargos. *Proceedings of the National Academy of Sciences of the United States of America* **102**, 2760–2765 (2005).

412. Umebayashi, K., Stenmark, H. & Yoshimori, T. Ubc4/5 and c-Cbl continue to ubiquitinate EGF receptor after internalization to facilitate polyubiquitination and degradation. *Molecular Biology of the Cell* **19**, 3454–3462 (2008).

413. Grøvdal, L. M., Stang, E., Sorkin, A. & Madshus, I. H. Direct interaction of Cbl with pTyr 1045 of the EGF receptor (EGFR) is required to sort the EGFR to lysosomes for degradation. *Experimental cell research* **300**, 388–395 (2004).

414. Huang, F., Kirkpatrick, D., Jiang, X., Gygi, S. & Sorkin, A. Differential regulation of EGF receptor internalization and degradation by multiubiquitination within the kinase domain. *Molecular cell* **21**, 737–748 (2006).

415. Sigismund, S. *et al.* Threshold-controlled ubiquitination of the EGFR directs receptor fate. *The EMBO journal* **32**, 2140–2157 (2013).

416. Bache, K. G., Raiborg, C., Mehlum, A. & Stenmark, H. STAM and Hrs are subunits of a multivalent ubiquitin-binding complex on early endosomes. *The Journal of biological chemistry* **278**, 12513–12521 (2003).

417. Miller, K., Beardmore, J., Kanety, H., Schlessinger, J. & Hopkins, C. R. Localization of the epidermal growth factor (EGF) receptor within the endosome of EGF-stimulated epidermoid carcinoma (A431) cells. *The Journal of cell biology* **102**, 500–509 (1986).

418. Sorkin, A. *et al.* Recycling of Epidermal Growth Factor-Receptor Complexes in A431 Cells: Identification of Dual Pathways. *The Journal of Cell Biology* **112**, (1991).

419. Sigismund, S. *et al.* Clathrin-mediated internalization is essential for sustained EGFR signaling but dispensable for degradation. *Developmental cell* **15**, 209–219 (2008).

420. Flint, A. J., Tiganis, T., Barford, D. & Tonks, N. K. Development of "substrate-trapping" mutants to identify physiological substrates of protein tyrosine phosphatases. *Proceedings of the National Academy of Sciences* **94**, 1680–1685 (1997).

421. Haj, F. G., Verveer, P. J., Squire, A., Neel, B. G. & Bastiaens, P. I. H. Imaging sites of receptor dephosphorylation by PTP1B on the surface of the endoplasmic reticulum. *Science* **295**, 1708–1711 (2002).

422. French, A. R., Tadaki, D. K., Niyogi, S. K. & Lauffenburger, D. A. Intracellular trafficking of epidermal growth factor family ligands is directly influenced by the pH sensitivity of the receptor/ligand interaction. *The Journal of biological chemistry* **270**, 4334–4340 (1995).

423. Roepstorff, K. *et al.* Differential Effects of EGFR Ligands on Endocytic Sorting of the Receptor. *Traffic (Copenhagen, Denmark)* **10**, 1115 (2009).

424. Conte, A. & Sigismund, S. Chapter Six - The Ubiquitin Network in the Control of EGFR Endocytosis and Signaling. *Progress in Molecular Biology and Translational Science* **141**, 225–276 (2016).

425. Wang, X., Huong, S. M., Chiu, M. L., Raab-Traub, N. & Huang, E. S. Epidermal growth factor receptor is a cellular receptor for human cytomegalovirus. *Nature* **424**, 456–461 (2003).

426. Kim, J. H., Collins-McMillen, D., Buehler, J. C., Goodrum, F. D. & Yurochko, A. D. Human Cytomegalovirus Requires Epidermal Growth Factor Receptor Signaling To Enter and Initiate the Early Steps in the Establishment of Latency in CD34 + Human Progenitor Cells. *Journal of virology* **91**, (2017).

427. Fulkerson, H. L. *et al.* HCMV-induced signaling through gB-EGFR engagement is required for viral trafficking and nuclear translocation in primary human monocytes. *Proceedings of the National Academy of Sciences of the United States of America* **117**, 19507–19516 (2020).

428. Zheng, K. *et al.* Epidermal Growth Factor Receptor-PI3K Signaling Controls Cofilin Activity To Facilitate Herpes Simplex Virus 1 Entry into Neuronal Cells. *mBio* (2014).

429. Dawson, C. W., Tramountanis, G., Eliopoulos, A. G. & Young, L. S. Epstein-Barr virus latent membrane protein 1 (LMP1) activates the phosphatidylinositol 3-kinase/Akt pathway to promote cell survival and induce actin filament remodeling. *The Journal of biological chemistry* **278**, 3694–3704 (2003).

430. Kung, C.-P., Meckes, D. G. & Raab-Traub, N. Epstein-Barr virus LMP1 activates EGFR, STAT3, and ERK through effects on PKCdelta. *Journal of virology* **85**, 4399–4408 (2011).

431. Pöhlmann, S. & Simmons, G. *Viral Entry into Host Cells*. vol. 790 (Springer New York, 2013).

432. Diao, J. *et al.* Hepatitis C Virus Induces Epidermal Growth Factor Receptor Activation via CD81 Binding for Viral Internalization and Entry. *Journal of Virology* **86**, 10935–10949 (2012).

433. Eierhoff, T., Hrincius, E. R., Rescher, U., Ludwig, S. & Ehrhardt, C. The epidermal growth factor receptor (EGFR) promotes uptake of influenza a viruses (IAV) into host cells. *PLoS Pathogens* **6**, (2010).

434. Xu, Q. *et al.* Caveolin-1-mediated Japanese encephalitis virus entry requires a two-step regulation of actin reorganization. *Future Microbiology* **11**, 1227–1248 (2016).

435. Surviladze, Z., Sterk, R. T., DeHaro, S. A. & Ozbun, M. A. Cellular Entry of Human Papillomavirus Type 16 Involves Activation of the Phosphatidylinositol 3-Kinase/Akt/mTOR Pathway and Inhibition of Autophagy. *Journal of Virology* **87**, 2508 (2013).

436. Mercer, J. *et al.* Vaccinia virus strains use distinct forms of macropinocytosis for host-cell entry. *Proceedings of the National Academy of Sciences of the United States of America* **107**, 9346–9351 (2010).

437. Krzyzaniak, M. A., Zumstein, M. T., Gerez, J. A., Picotti, P. & Helenius, A. Host cell entry of respiratory syncytial virus involves macropinocytosis followed by proteolytic activation of the F protein. *PLoS pathogens* **9**, (2013).

438. Iwamoto, M. *et al.* Epidermal growth factor receptor is a host-entry cofactor triggering hepatitis B virus internalization. *Proceedings of the National Academy of Sciences of the United States of America* **116**, 8487–8492 (2019).

439. Hu, W., Zhang, S., Shen, Y. & Yang, Q. Epidermal growth factor receptor is a co-factor for transmissible gastroenteritis virus entry. *Virology* **521**, 33–43 (2018).

440. Weller, M. L. *et al.* Epidermal growth factor receptor is a co-receptor for adeno-associated virus serotype 6. *Nature Medicine 2010 16:6* **16**, 662–664 (2010).

441. Chan, G., Nogalski, M. T. & Yurochko, A. D. Activation of EGFR on monocytes is required for human cytomegalovirus entry and mediates cellular motility. *Proceedings of the National Academy of Sciences* **106**, 22369–22374 (2009).

442. Liu, D. *et al.* p17 from HIV induces brain endothelial cell angiogenesis through EGFR-1-mediated cell signalling activation. *Laboratory Investigation 2018 99:2* **99**, 180–190 (2018).

443. Venkataraman, T., Coleman, C. M. & Frieman, M. B. Overactive Epidermal Growth Factor Receptor Signaling Leads to Increased Fibrosis after Severe Acute Respiratory Syndrome Coronavirus Infection. (2017).

444. Klann, K., Bojkova, D., Tascher, G. & Ciesek, S. Growth Factor Receptor Signaling Inhibition Prevents SARS-CoV-2 Replication. *Molecular Cell* (2020).

445. Ueki, I. F. *et al.* Respiratory virus–induced EGFR activation suppresses IRF1-dependent interferon λ and antiviral defense in airway epithelium. *Journal of Experimental Medicine* **210**, 1929–1936 (2013).

446. Gong, G., Waris, G., Tanveer, R. & Siddiqui, A. Human hepatitis C virus NS5A protein alters intracellular calcium levels, induces oxidative stress, and activates STAT-3 and NF-κB. *Proceedings of the National Academy of Sciences* **98**, 9599–9604 (2001).

447. Benkheil, M. *et al.* HCV-induced EGFR-ERK signaling promotes a pro-inflammatory and pro-angiogenic signature contributing to liver cancer pathogenesis. *Biochemical Pharmacology* **155**, 305–315 (2018).

448. Kalinowski, A. *et al.* Respiratory syncytial virus activates epidermal growth factor receptor to suppress interferon regulatory factor 1-dependent interferon-lambda and antiviral defense in airway epithelium. *Mucosal immunology* **11**, 958 (2018).

449. Groepper, C. *et al.* HCV modifies EGF signalling and upregulates production of CXCR2 ligands: Role in inflammation and antiviral immune response. *Journal of hepatology* **69**, 594–602 (2018).

450. Ochi, M., Otsuka, M., Maruyama, R. & Koike, K. HBx increases EGFR expression by inhibiting miR129–5p function. *Biochemical and Biophysical Research Communications* **529**, 198–203 (2020).

451. Prudenziati, M., Sirito, M., Dam, H. van & Ravazzolo, R. Adenovirus E1A down-regulates the EGF receptor via repression of its promoter. *International Journal of Cancer* (2000).

452. Miller, W. E., Shelton Earp, H. & Raab-Traub, N. The Epstein-Barr virus latent membrane protein 1 induces expression of the epidermal growth factor receptor. *Journal of Virology* **69**, 4390–4398 (1995).

453. Jafferji, I., Bain, M., King, C. & Sinclair, J. H. Inhibition of epidermal growth factor receptor (EGFR) expression by human cytomegalovirus correlates with an increase in the expression and binding of Wilms' Tumour 1 protein to the EGFR promoter. *The Journal of general virology* **90**, 1569–1574 (2009).

454. Valiathan, R. R. & Resh, M. D. Expression of human immunodeficiency virus type 1 gag modulates ligand-induced downregulation of EGF receptor. *Journal of virology* **78**, 12386–12394 (2004).

455. Zhang, B., Srirangam, A., Potter, D. A. & Roman, A. HPV16 E5 protein disrupts the c-Cbl–EGFR interaction and EGFR ubiquitination in human foreskin keratinocytes. *Oncogene* **24**, 2585 (2005).

456. Igloi, Z. *et al.* Hepatitis C virus NS5A protein blocks epidermal growth factor receptor degradation via a proline motif- dependent interaction. *The Journal of general virology* **96**, 2133–2144 (2015).

457. Hoffman, P. & Carlin, C. Adenovirus E3 protein causes constitutively internalized epidermal growth factor receptors to accumulate in a prelysosomal compartment, resulting in enhanced degradation. *Molecular and Cellular Biology* **14**, 3695–3706 (1994).

458. Liang, Y., Kurakin, A. & Roizman, B. Herpes simplex virus 1 infected cell protein 0 forms a complex with CIN85 and Cbl and mediates the degradation of EGF receptor from cell surfaces. *Proceedings of the National Academy of Sciences of the United States of America* **102**, 5838–5843 (2005).

459. Himmelsbach, K. & Hildt, E. Identification of various cell culture models for the study of Zika virus. *World Journal of Virology* **7**, 10–20 (2018).

460. Giard, D. J. *et al.* In Vitro Cultivation of Human Tumors: Establishment of Cell Lines Derived From a Series of Solid Tumors2. *JNCI: Journal of the National Cancer Institute* **51**, 1417–1423 (1973).

461. Kao, F. T. & Puck, T. T. Genetics of somatic mammalian cells, VII. Induction and isolation of nutritional mutants in Chinese hamster cells. *Proceedings of the National Academy of Sciences of the United States of America* **60**, 1275–1281 (1968).

462. Yasumura, Y. & Kawakita, Y. Studies on SV40 in tissue culture - preliminary step for cancer research in vitro. *Nihon Rinsho* **21**, 1201–1215 (1963).

463. Friedrich, K. *et al.* DARPin-targeting of measles virus: Unique bispecificity, effective oncolysis, and enhanced safety. *Molecular Therapy* **21**, 849–859 (2013).

464. Shan, C. *et al.* An Infectious cDNA Clone of Zika Virus to Study Viral Virulence, Mosquito Transmission, and Antiviral Inhibitors. *Cell Host and Microbe* **19**, 891–900 (2016).

465. Ran, F. A. *et al.* Genome engineering using the CRISPR-Cas9 system. *Nature Protocols* **8**, 2281–2308 (2013).

466. Akhras, S., Herrlein, M. L., Elgner, F., Holzhauser, T. & Hildt, E. Zikv envelope domain-specific antibodies: Production, purification and characterization. *Viruses* **11**, (2019).

467. Rhim, J. S., Schell, K., Creasy, B. & Case, W. Biological Characteristics and Viral Susceptibility of an African Green Monkey Kidney Cell Line (Vero). *Proceedings of the Society for Experimental Biology and Medicine* **132**, 670–678 (1969).

468. Desmyter, J., Melnick, J. L. & Rawls, W. E. Defectiveness of Interferon Production and of Rubella Virus Interference in a Line of African Green Monkey Kidney Cells (Vero). *Journal of Virology* **2**, (1968).

469. Graham, F. L. & van der Eb, A. J. A new technique for the assay of infectivity of human adenovirus 5 DNA. *Virology* **52**, 456–467 (1973).

470. Bimboim, H. C. & Doly, J. A rapid alkaline extraction procedure for screening recombinant plasmid DNA. *Nucleic Acids Research* **7**, 1513–1523 (1979).

471. Swinehart, D. F. The Beer-Lambert Law. *Journal of Chemical Education* **39**, 333–335 (1962).

472. Sharp, P. A., Sugden, B. & Sambrook, J. Detection of two restriction endonuclease activities in Haemophilus parainfluenzae using analytical agarose--ethidium bromide electrophoresis. *Biochemistry* **12**, 3055–3063 (1973).

473. Chomczynski, P. & Sacchi, N. Single-step method of RNA isolation by acid guanidinium thiocyanate-phenol-chloroform extraction. *Analytical Biochemistry* **162**, 156–159 (1987).

474. Ponchel, F. *et al.* Real-time PCR based on SYBR-Green I fluorescence: An alternative to the TaqMan assay for a relative quantification of gene rearrangements, gene amplifications and micro gene deletions. *BMC Biotechnology* **3**, 18 (2003).

475. Livak, K. J. & Schmittgen, T. D. Analysis of relative gene expression data using real-time quantitative PCR and the 2(-Delta Delta C(T)) Method. *Methods (San Diego, Calif.)* **25**, 402–408 (2001).

476. GenScript. Genome-wide gRNA database of validated gRNA sequences. https://www.genscript.com/gRNA-database.html.

477. MM, B. A rapid and sensitive method for the quantitation of microgram quantities of protein utilizing the principle of protein-dye binding. *Analytical biochemistry* **72**, 248–254 (1976).

478. Walker, J. M. The Bicinchoninic Acid (BCA) Assay for Protein Quantitation. *The Protein Protocols Handbook* 11–14 (1996).

479. Laemmli, U. K. Cleavage of Structural Proteins during the Assembly of the Head of Bacteriophage T4. *Nature 1970 227:5259* **227**, 680–685 (1970).

480. Towbin, H. & Gordon, J. Immunoblotting and dot immunobinding--current status and outlook. *Journal of immunological methods* **72**, 313–340 (1984).

481. Thorpe, G. H. G. & Kricka, L. J. Enhanced chemiluminescent reactions catalyzed by horseradish peroxidase. *Methods in enzymology* **133**, 331–353 (1986).

482. AW, K. *et al.* Human epidermal growth factor receptor-1 expression renders Chinese hamster ovary cells sensitive to alternative aldosterone signaling. *The Journal of biological chemistry* **277**, 45892–45897 (2002).

483. Zhang, F. *et al.* Quantification of epidermal growth factor receptor expression level and binding kinetics on cell surfaces by surface plasmon resonance imaging. *Analytical chemistry* **87**, 9960–9965 (2015).

484. Yonesaka, K. *et al.* The pan-HER family tyrosine kinase inhibitor afatinib overcomes HER3 ligand heregulin-mediated resistance to EGFR inhibitors in non-small cell lung cancer. *Oncotarget* **6**, 33602–33611 (2015).

485. Cerioni, L., Palomba, L. & Cantoni, O. The Raf/MEK inhibitor PD98059 enhances ERK1/2 phosphorylation mediated by peroxynitrite via enforced mitochondrial formation of reactive oxygen species. *FEBS Letters* **547**, 92–96 (2003).

486. Lambert, S., Vind-Kezunovic, D., Karvinen, S. & Gniadecki, R. Ligand-independent activation of the EGFR by lipid raft disruption. *Journal of Investigative Dermatology* **126**, 954–962 (2006).

487. H, K., SL, A., FX, H. & CW, M. Role of heparan sulfate for attachment and entry of tick-borne encephalitis virus. *Virology* **308**, 92–100 (2003).

488. TS, B., PB, L. & R, D. Different transforming growth factor-alpha species are derived from a glycosylated and palmitoylated transmembrane precursor. *Cell* **48**, 429–440 (1987).

489. K, Z., K, K. & Y, W. Viruses exploit the function of epidermal growth factor receptor. *Reviews in medical virology* **24**, 274–286 (2014).

490. C, D. *et al.* Novel recombinant immunotoxin of EGFR specific nanobody fused with cucurmosin, construction and antitumor efficiency in vitro. *Oncotarget* **8**, 38568–38580 (2017).

491. Zhao, P. *et al.* Molecular imaging of hepatocellular carcinoma xenografts with epidermal growth factor receptor targeted affibody probes. *BioMed Research International* **2013**, (2013).

492. Cabrera-Hernandez, A. & Smith, D. R. Mammalian Dengue Virus Receptors. *Dengue Bulletin* **29**, (2005).

493. A, B., MR, F. & TR, K. Virus susceptibility of Chinese hamster ovary (CHO) cells and detection of viral contaminations by adventitious agent testing. *Biotechnology and bioengineering* **106**, 598–607 (2010).

494. Xu, X. *et al.* The genomic sequence of the Chinese hamster ovary (CHO)-K1 cell line. *Nature Biotechnology* **29**, 735–741 (2011).

495. D, S., S, G., R, D. & A, K. A cowpox virus gene required for multiplication in Chinese hamster ovary cells. *Journal of virology* **62**, 1297–1304 (1988).

496. Schaar, H. M. van der *et al.* Dissecting the Cell Entry Pathway of Dengue Virus by Single-Particle Tracking in Living Cells. *PLOS Pathogens* **4**, e1000244 (2008).

497. Li, M. *et al.* Characterization of Zika Virus Endocytic Pathways in Human Glioblastoma Cells. *Frontiers in Microbiology* **11**, (2020).

498. Sieben, C., Sezgin, E., Eggeling, C. & Manley, S. Influenza A viruses use multivalent sialic acid clusters for cell binding and receptor activation. *PLoS pathogens* **16**, (2020).

499. Hu, W., Zhu, L., Yang, X., Lin, J. & Yang, Q. The epidermal growth factor receptor regulates cofilin activity and promotes transmissible gastroenteritis virus entry into intestinal epithelial cells. *Oncotarget* **7**, 12206–12221 (2016).

500. Chuang, F. K. *et al.* Antiviral activity of compound I3 against dengue and zika viruses in vitro and in vivo. *International Journal of Molecular Sciences* **21**, 1–13 (2020).

501. MH, N. & D, W. Microtubule Regulation and Function during Virus Infection. *Journal of virology* **91**, (2017).

502. YJ, G. *et al.* ERK/MAPK signalling pathway and tumorigenesis. *Experimental and therapeutic medicine* **19**, (2020).

503. S, P. Phosphorylation of the cap-binding protein eIF4E by the MAPK-activated protein kinase Mnk1. *Biochemical pharmacology* **60**, 1237–1243 (2000).

504. Elgner, F. *et al.* Inhibition of zika virus replication by silvestrol. *Viruses* **10**, (2018).

505. Zhu, S. *et al.* p38MAPK plays a critical role in induction of a pro-inflammatory phenotype of retinal Müller cells following Zika virus infection. *Antiviral research* **145**, 70 (2017).

506. F, C., S, R. da S., IC, H., JU, J. & SJ, G. Suppression of Zika Virus Infection and Replication in Endothelial Cells and Astrocytes by PKA Inhibitor PKI 14-22. *Journal of virology* **92**, (2018).

507. Wozniak, A. L., Long, A., Jones-Jamtgaard, K. N. & Weinman, S. A. Hepatitis C virus promotes virion secretion through cleavage of the Rab7 adaptor protein RILP. **113**, (2016).

508. Burke, P., Schooler, K. & Wiley, H. S. Regulation of Epidermal Growth Factor Receptor Signaling by Endocytosis and Intracellular Trafficking. *Molecular Biology of the Cell* **12**, 1897–1910 (2001).

509. Jiang, X. *et al.* Proteomic Analysis of Zika Virus Infected Primary Human Fetal Neural Progenitors Suggests a Role for Doublecortin in the Pathological

Consequences of Infection in the Cortex. *Frontiers in Microbiology* **9**, 1067 (2018).

510. Sher, A. A., Glover, K. K. M. & Coombs, K. M. Zika virus infection disrupts astrocytic proteins involved in synapse control and axon guidance. *Frontiers in Microbiology* **10**, 596 (2019).

511. Sabino, C., Bender, D., Herrlein, M.-L. & Hildt, E. The Epidermal Growth Factor Receptor Is a Relevant Host Factor in the Early Stages of The Zika Virus Life Cycle In Vitro. *Journal of virology* **95**, (2021).

10. Publications

Peer-reviewed publications

Herrlein, M. L., Schmanke, P., Elgner, F., Sabino, C., Akhras, S., Bender, D., Glitscher, M., Tabari, D., Scholl, C., Stingl, J., & Hildt, E. (2021). Catch me if you can - the crosstalk of ZIKV and the restriction factor Tetherin. Journal of virology, jvi0211721. Advance online publication. DOI: 10.1128/jvi.02117-21

Sabino, C., Bender, D., Herrlein, M. L., & Hildt, E. (2021). The Epidermal Growth Factor Receptor Is a Relevant Host Factor in the Early Stages of The Zika Virus Life Cycle In Vitro. Journal of virology, 95(20), e0119521. DOI: 10.1128/JVI.01195-21

Tabari, D., Scholl, C., Steffens, M., Weickhardt, S., Elgner, F., Bender, D., Herrlein, M. L., Sabino, C., Semkova, V., Peitz, M., Till, A., Brüstle, O., Hildt, E., & Stingl, J. (2020). Impact of Zika Virus Infection on Human Neural Stem Cell MicroRNA Signatures. Viruses, 12(11), 1219. DOI: 10.3390/v12111219

Basic, M., Elgner, F., Bender, D., Sabino, C., Herrlein, M. L., Roth, H., Glitscher, M., Fath, A., Kerl, T., Schmalz, H. G., & Hildt, E. (2019). A synthetic derivative of houttuynoid B prevents cell entry of Zika virus. Antiviral research, 172, 104644. DOI: 10.1016/j.antiviral.2019.104644

Sabino, C., Basic, M., Bender, D., Elgner, F., Himmelsbach, K., & Hildt, E. (2019). Bafilomycin A1 and U18666A Efficiently Impair ZIKV Infection. Viruses, 11(6), 524. DOI: 10.3390/v11060524

Elgner, F., Sabino, C., Basic, M., Ploen, D., Grünweller, A., & Hildt, E. (2018). Inhibition of Zika Virus Replication by Silvestrol. Viruses, 10(4), 149. DOI: 10.3390/v10040149

Oral presentations

14th Annual Meeting, Retreat on Biomedical Research, 2020, Ronneburg, Germany.
Catarina Sabino, Daniela Bender, Marie-Luise Herrlein, and Eberhard Hildt.
Interactions between ZIKV and the host.

Poster presentations

30th Annual Meeting of the Society of Virology, 2021, digital.
"Interactions between ZIKV and the host"

29th Annual Meeting of the Society of Virology, 2019, Düsseldorf, Germany.
"Interactions between ZIKV and the host"

13th Annual Meeting, Retreat on Biomedical Research, 2019, Ronneburg, Germany.
"Interactions between ZIKV and the host" – **1st prize award**

28th Annual Meeting of the Society of Virology, 2019, Würzburg, Germany.
"Bafilomycin A1 efficiently inhibits infection by ZIKV"

12th Annual Meeting, Retreat on Biomedical Research, 2018, Ronneburg, Germany.
"Bafilomycin A1 efficiently inhibits infection by ZIKV" – **3rd prize award**